Investigating the Expression of Topoisomerase II Beta in Aged Neurons: Development of a Murine Cell Line and *Drosophila* Model

Callum S. Bainbridge

PhD

2020

Investigating the Expression of Topoisomerase II Beta in Aged Neurons: Development of a Murine Cell Line and *Drosophila* Model

Callum S. Bainbridge

A thesis submitted in partial fulfilment of the requirements of the University of Northumbria at Newcastle for the degree of Doctor of Philosophy

2020

Abstract

The enzyme Topoisomerase II Beta (Top2B) has previously been shown to be a crucial component of neuronal differentiation and development in mammals. It is also expressed in adult neuronal tissue where it plays important roles in facilitating transcription of long genes and early response genes and may also be involved in DNA repair. To date, studies investigating age-related changes in Top2B expression in neuronal tissue are limited and the importance of Top2B in the maintenance of neuronal function and integrity during ageing has not yet been fully elucidated, thus this study aimed to further investigate Top2B during the ageing process.

The development of an *in vitro* murine model of neuronal ageing was successfully achieved using the Cath.a-differentiated (CAD) cell line. A neuronal-like phenotype in CAD cells was achieved through serum starvation and cells were then chronologically aged. Levels of Top2B mRNA and protein were seen to decline significantly during ageing of the cells in RT-qPCR and western blotting experiments, respectively. Concomitant increases in protein levels of the tumour suppressor gene p21 were also observed as well as a significant accumulation of double strand breaks as shown by γH2AX assays. In addition, preliminary *in vivo* experiments also revealed age-related declines of Top2B in mouse hippocampus. The development of an equivalent human *in vitro* model using the human neuroblastoma cell line SH-SY5Y was unsuccessful.

Further *in vivo* experiments using *Drosophila* brain tissue also revealed significant age-related declines in Topoisomerase II (Top2) protein levels with ageing in both males and females, which was accompanied by a decline in locomotor function and increases in advanced glycation end-products (AGEs) in females. Interestingly, in *Drosophila* this was not accompanied by a reduction in Top2 mRNA levels.

Reduction in the levels of mouse Top2B and *Drosophila* Top2 with age may have profound effects on transcription and the ability of cells to repair DNA damage and may result in increased vulnerability to oxidative stress, ultimately having detrimental effects on longevity and normal ageing. Thus, these models offer an opportunity to further elucidate the functional effect of this loss, its causes and potential pharmaceutical interventions to reverse these effects. Importantly, they also illustrate the need for such research to be carried out in human neuronal cells and brain tissues.

Table of Contents

1. Introduction **1**

1.1 Effects of ageing 1

1.2 Cellular senescence 2

1.2.1 Oxidative stress and DNA damage in neurons 5

1.2.2 DNA repair in neurons 6

1.3 Topoisomerase family 8

1.3.1 Topoisomerase classification 8

1.3.2 Catalytic cycle of topoisomerase II 10

1.3.3 Structure of type II topoisomerases 13

1.3.4 Topoisomerase II isoforms 14

1.3.5 Homology of mammalian topoisomerase II isoforms 15

1.3.6 C-terminal divergence of mammalian topoisomerase II isoforms 15

1.3.7 Subcellular location of topoisomerase II 16

1.4 Top2A 17

1.4.1 Role of Top2A in replication 17

1.4.2 Role of Top2A in chromosome segregation 19

1.4.3 Roles of Top2A in transcription 20

1.5 Top2B 21

1.5.1 Role of Top2B in transcription 21

1.5.2 Top2B in neuronal development 25

1.5.3 Expression levels and patterns of Top2B during development 27

1.5.4 Regulation of Top2B expression 27

1.5.5 Top2B in neuronal ageing 29

1.5.6 Top2B and repair 31

1.6 Aims 32

2. Materials and methods **33**

2.1 Materials 33
2.1.1 Antibodies 33
2.1.2 RT-qPCR 34
2.1.3 Reagents 35
2.1.4 Cell culture reagents 36
2.1.5 Special consumables 37
2.1.6 Commercially available kits and products 38
2.1.7 Buffers and solutions 38
2.1.8 Cell lines 40
2.2 Methods 41
2.2.1 *Drosophila* work 41
2.2.2 Mammalian cell culture 48
2.2.3 Western blotting 55
2.2.4 RNA work 57
2.2.5 RT-qPCR 58
2.2.6 Mouse work 58
2.2.7 Statistical analysis 61
3. Development of an ageing *Drosophila* model to investigate changes in Top2 expression 62
3.1 Introduction 62
3.2 Developing a *Drosophila* model of ageing 65
3.2.1 Longevity of *Drosophila* 65
3.2.2 Locomotor activity of ageing *Drosophila* 67
3.2.3 Advanced glycation end-products as a biomarker of ageing in *Drosophila* 72
3.3 Quantification of Top2 protein in *Drosophila* brains 74
3.3.1 Optimising protein extraction and western blotting methods 74
3.4 Quantification of Top2 mRNA in *Drosophila* brains 79
3.4.1 Selection of RT-qPCR reference genes 79

3.4.2 Optimisation of Top2, Cyp1 and eIF-1A for RT-qPCR 80

3.4.3 Analysis of Top2 mRNA in male and female *Drosophila* aged 5, 30 and 50 days old 83

3.5 Immunofluorescent analysis of Top2 in *Drosophila* brains 84

3.6 Discussion 86

3.6.1 Sex differences in lifespan 86

3.6.2 Advanced glycation end-products 88

3.6.3 Top2 mRNA levels in ageing 90

3.6.4 Top2 protein levels in ageing 91

3.6.5 Consequences of declining Top2 levels 94

4. Development of a cell line model of ageing using the human neuroblastoma cell line SH-SY5Y to investigate changes in Top2B expression 97

4.1 Introduction 97

4.2 Hydrogen peroxide induced cellular senescence of undifferentiated SH-SY5Y 100

4.3 Hydrogen peroxide induced cellular senescence of retinoic acid treated SH-SY5Y cells 106

4.3.1 Retinoic acid-induced differentiation-like phenotype in SH-SY5Y cells ... 106

4.3.2 Quantification of topoisomerase II protein during SH-SY5Y differentiation 110

4.3.3 Hydrogen peroxide-induced cellular senescence of RA treated SH-SY5Y cells 113

4.4 Discussion 117

5. Development of murine models of ageing to investigate changes in Top2B expression 123

5.1 Introduction 123

5.1.1 CAD neuronal cell line model 123

5.1.2 Mouse model of ageing 124

5.2 Differentiation of CAD cell line through serum starvation 125

5.3 Semi-quantification of Top2B during CAD differentiation 128

5.3.1 Semi-quantification of Top2B protein during CAD differentiation 128

5.3.2 Semi-quantification of Top2B mRNA during CAD differentiation 130

5.4 Hydrogen peroxide-induced cellular senescence of serum-free treated CAD cells 134

5.5 Semi-quantification of Top2B in serum-free treated CAD cells over six weeks of ageing 137

5.5.1 Semi-quantification of Top2B protein in serum-free treated CAD cells over six weeks of ageing 137

5.5.2 Semi-quantification of Top2B mRNA in serum-free treated CAD cells over six weeks of ageing 143

5.6 Immunohistochemical analysis of Top2B in mouse hippocampal tissue 146

5.7 Discussion 151

5.7.1 Reductions of Top2B mRNA 152

5.7.2 Implications of reductions of Top2B 153

5.7.3 The use of the CAD cell line as a differentiated neuronal model of ageing 156

5.7.4 Declines of Top2B in hippocampal tissue 160

6. The DNA damage response of differentiated CAD cells during ageing 161

6.1 Introduction 161

6.2 Do DSBs accumulate in serum-free treated CAD cells when chronologically aged *in vitro*? 163

6.2.1 Quantification of DNA damage in serum-free treated CAD cells 164

6.3 Discussion 169

6.3.1 Why do DSBs accumulate during ageing? 170

6.3.2 DNA damage as measured by the alkaline Comet assay 174

7. Final discussion and future work 176

7.1 Top2 during *Drosophila* ageing 176

7.2 Developing senescence in the SH-SY5Y cell line 178

7.3 Top2B in the CAD cell line and mouse hippocampal tissue during ageing 180

7.4 Increases of DNA damage during ageing 183

7.5 Conclusion 184

8. References **187**

Appendices **235**

Appendix A 235

Appendix B 240

Appendix C 241

Appendix D 243

Appendix E 251

List of Figures

Figure 1.1 Diagrammatical representations of the actions of type 2 topoisomerases on DNA topology 10

Figure 1.2 Structural domains of Topoisomerase II 11

Figure 1.3 Diagrammatical representation of the mechanisms of topoisomerase II isoforms 12

Figure 1.4 Homology of amino acid sequences in type II topoisomerases 13

Figure 1.5 Diagrammatical representation of topological changes caused by advancing replication machinery 18

Figure 1.6 Diagrammatical representation of supercoil formation during transcription through the actions of RNA polymerase 22

Figure 2.1 CO_2 apparatus used for *Drosophila* anaesthetisation 42

Figure 2.2 Differences in male and female *Drosophila* anatomy 43

Figure 3.1 Diagrammatical representation of the *Drosophila* brain 63

Figure 3.2 Longevity of mixed populations, male and female *Drosophila* 66

Figure 3.3 Climbing assays of male and female *Drosophila* at 5, 30 and 50 days old 69

Figure 3.4 Comparison of locomotor activity between male and female *Drosophila* at 5, 30 and 50 days old 70

Figure 3.5 AGE products of male and female *Drosophila* aged 5, 30 and 50 days old 73

Figure 3.6 Example standard curve of BSA 75

Figure 3.7 Optimisation of *Drosophila* protein extraction and western blot analysis of Top2..... 76

Figure 3.8 Optimisation of protein extraction and western blotting using *Drosophila* brains 77

Figure 3.9 Semi-quantification of Top2 in male and female *Drosophila* aged 5, 30 and 50 days old 78

Figure 3.10 Amplification curves for primer efficiency of Top2, Cyp1 and eIF-1A . 81

Figure 3.11 Variance of Cyp1 and eIF-1A reference genes across all *Drosophila* samples tested 82

Figure 3.12 Analysis of RT-qPCR data comparing relative Top2 mRNA expression in male and female *Drosophila* aged 5, 30 and 50 days old 83

Figure 3.13 Immunofluorescent staining of Top2 in *Drosophila* brain 84-85

Figure 4.1 Proliferation of SH-SY5Y cells treated with a 1 hour pulse of a range of H_2O_2 concentrations and grown for 24, 48 or 72 hours 101

Figure 4.2 Proliferation of SH-SY5Y cells over 24 and 48 hours after a 1 hour pulse with a range of H_2O_2 concentrations 104

Figure 4.3 β-galactosidase assay of SH-SY5Y cells 48 hours after a 1 hour exposure to 10 µM H_2O_2..... 105

Figure 4.4 The effects of all-trans retinoic acid on SH-SY5Y proliferation 108

Figure 4.5 Morphological changes of SH-SY5Y after 10 µM RA treatment 109

Figure 4.6 Semi-quantitation of Top2A over 72 hours of RA-induced differentiation of the SH-SY5Y cell line 111

Figure 4.7 Semi-quantitation of Top2B over 72 hours of RA-induced differentiation of the SH-SY5Y cell line 112

Figure 4.8 Proliferation of untreated and RA treated SH-SY5Y cells after treatment with H_2O_2..... 114

Figure 4.9 β-galactosidase assay of RA treated SH-SY5Y cells treated with or without 100 µM H_2O_2..... 116

Figure 5.1 The effects of serum starvation on CAD proliferation 126

Figure 5.2 The effects of serum starvation on CAD morphology 127

Figure 5.3 Semi-quantification of Top2B over 72 hours of serum starvation-induced differentiation of the CAD cell line 129

Figure 5.4 Amplification curves for primer efficiency of Top2B, GAPDH and β-actin 131

Figure 5.5 Variance of β-actin and GAPDH reference genes from all CAD 72 hour differentiation experiments 132

Figure 5.6 Analysis of RT-qPCR data comparing relative Top2B expression in CAD cells during the first 72 hours of differentiation in serum-free media 133

Figure 5.7 β-galactosidase assay of differentiated CAD cells treated with a range of H_2O_2 concentrations 135

Figure 5.8 Semi-quantification of p21 in CAD cells grown in serum-free (-) or complete (+) media treated with or without a 24 hour pulse of H_2O_2 136

Figure 5.9 Semi-quantification of Top2B protein levels in CAD cells during six weeks of ageing in serum-free media 138

Figure 5.10 Semi-quantification of p21 in serum-free treated CAD cells during six weeks of ageing 140

Figure 5.11 Proliferation of CAD cells over 30 days in serum-free media and neurite length over 6 weeks in serum-free media 142

Figure 5.12 Variance of β-actin and GAPDH reference genes from all 6 week CAD experiments 144

Figure 5.13 Semi-quantification of Top2B mRNA in serum-free treated CAD cells during six weeks of ageing 145

Figure 5.14 Immunofluorescent analysis of Top2B in hippocampal tissue of a 29.5 month old C57BL/6 male mouse 147

Figure 5.15 DAB immunoperoxidase staining of Top2B in the hippocampus of 4 and 31 month old C57BL/6 male mice 149-150

Figure 6.1 γH2AX foci analysis over 6 weeks in serum-free treated CAD cells 165

Figure 6.2 Manual scoring analysis of Comet assay over 6 weeks in serum-free treated CAD cells 167

Figure 6.3 Variability of OpenComet image analysis of serum-free treated CAD cells 168

Figure A.1 Calculating statistical significance using the log-rank test 235

Figure A.2 Optimisation of *Drosophila* brain protein extraction and western blot analysis of Top2 236

Figure A.3 Calculating the efficiency of primers 236

Figure A.4 Representative melt curves from RT-qPCR of primers used in *Drosophila* experiments 237

Figure A.5 Analysing qPCR results with two reference genes 238

Figure A.6 Example calculation of the coefficient of variance of qPCR primers using Ct data. 239

Figure C.1 Representative melt curves from RT-qPCR of primers used in CAD experiments 241

Figure C.2 Analysing qPCR results with one reference gene 242

List of Tables

Table 1.1 Classification of Type I and II topoisomerases 9

Table 2.1 Antibodies for western blotting 33

Table 2.2 Antibodies for immunohistochemistry applications 34

Table 2.3 Primers for RT-qPCR 34

Table 2.4 Reagents 35

Table 2.5 Reagents used in cell culture 36

Table 2.6 Special consumables 37

Table 2.7 Commercially available kits and products 38

Table 2.8 Buffers and solutions 38

Table 2.9 Cell lines 40

Table B.1 p values from Figure 4.1B 240

Table B.2 p values from Figure 4.2B 240

Table C.1 p values from Figure 6.1 242

List of abbreviations

AP-1	Activating protein 1
AGE	Advanced Glycation End-product
ALE	Advanced Lipoxidation End-products
RA	all-trans-Retinoic acid
APS	Ammonium persulfate
ATM	Ataxia Telangiectasia Mutated
ASD	Autism Spectrum Disorder
BER	Base Excision Repair
β-gal	β-galactosidase
BSA	Bovine Serum Albumin
BDNF	Brain-Derived Neurotrophic Factor
CAD	Cath. a-differentiated
CAP	Catabolite Activator Protein
CTCF	CCCTC-binding factor
CNS	Central Nervous System
CGN	Cerebellar Granule Neuron
CHK1	Checkpoint Kinase 1
CHK2	Checkpoint Kinase 2
ACF	Chromatin Assembly Factor
ChIP	Chromatin Immunoprecipitation
CisPt	Cisplatin
CtIP	C-terminal binding protein-interacting protein
Cyp1	Cyclophilin 1
DNase	Deoxyribonuclease I
DAB	Diaminobenzidine

8-oxoG	Dihydro-8-oxoguanine
DMSO	Dimethyl Sulfoxide
DNA-PK	DNA-dependent protein kinase
DSB	Double Strand Break
ECL	Enhanced Chemiluminescence
EDTA	Ethylenediaminetetra-acetic acid
eIF-1A	Eukaryotic Initiation Factor 1A
FBS	Foetal Bovine Serum
GHKL	Gyrase, HSP90, histidine Kinase, MutL
HMGB1/2	High Mobility Group B 1/2
HDAC	Histone Deacetylase
HR	Homologous Recombination
H_2O_2	Hydrogen Peroxide
IL-6	Interleukin-6
MDA	Malondialdehyde
MDC1	Mediator of DNA Damage Checkpoint 1
MMS	Methyl-Methanesulfonate
MMR	Mismatch Repair
NKT	Neuroketal
TEMED	N,N,N',N'-Tetramethylethylenediamine
NHEJ	Non-Homologous End Joining
NDS	Normal Donkey Serum
NGS	Normal Goat serum
NTC	No-template control
Nrf2	Nuclear factor erythroid 2-related factor
NF-κB	Nuclear factor kappa B

NF-Y	Nuclear Factor-Y
NURR1	Nuclear Receptor Related 1 protein
NER	Nucleotide Excision Repair
ERα	Oestrogen Receptor-α
PSN	Peripheral Nervous System
PMSF	Phenylmethanesulfonyl Fluoride
PBS	Phosphate Buffered Saline
γH2AX	Phosphorylated H2A histone family member X
PAGE	Polyacrylamide Gel Electrophoresis
PARP-1	Poly (ADP-ribose) Polymerase 1
P53BP1	p53-binding protein 1
ROS	Reactive Oxygen Species
RT-qPCR	Real-time reverse transcription quantitative polymerase chain reaction
RAR	Retinoic Acid Receptor
RARα	Retinoic Acid Receptor α
RARE	Retinoic Acid Response Element
RXR	Retinoid X Receptors
SASP	Senescence-Associated Secretory Phenotype
SSB	Single Strand Break
SUMO	Small Ubiquitin-related Modifier
SDS	Sodium Dodecyl Sulphate
Sp1	Specificity protein 1
Ct	Threshold cycle
Top2A	Topoisomerase II alpha
Top2B	Topoisomerase II beta
Toprim	Topoisomerase-primase

TARDIS	Trapped in Agarose DNA Immunostaining Assay
TBS	Tris Buffered Saline
TE	Tris/EDTA
Ube3a	Ubiquitin protein ligase E3A
UPR	Unfolded Protein Response
WHD	Winged Helix Domain

Acknowledgements

Without a doubt, the last four years have been my most challenging so far, both in and out of the lab. As a person who is typically very chilled out, this PhD has finally made me understand what it truly means to be stressed out. However, given the chance, I would do it all over again due to the brilliant people who have helped, supported and encouraged me during this time.

Firstly and most importantly I would like to thank my supervisor, Dr Kay Padget. I will be forever grateful for the opportunity she has given me and could not have asked for a better person to guide me through the last four years. Not only is she the hardest working person I have ever met but she also happens to be one of the most kind and lovely people as well. Everyone should have a Kay in their life.

I would like to thank Dr Rachel Ranson for her help and expertise on the immunohistochemical elements of my mouse studies and also Dr Tora Smulders-Srinivasan for her help getting me started with my *Drosophila* studies. I would also like to acknowledge and thank Northumbria University for funding this project.

To the members of the lab and the PGR office, I am also extremely grateful. The friendships I have made with this lovely bunch of people are a highlight of my time at Northumbria. Their encouragement, support and great sense of humour made going to work every day so much more enjoyable.

I would also like to thank my Mum and Dad. Due to the one-page limit for the acknowledgements section I cannot write anywhere near as much as I would like to for this particular section and I have already wasted crucial space writing this sentence, so I will limit myself to acknowledging only the most important points. First and foremost, I would like to thank them for feeding me such delicious food on such a regular basis. Secondly, I want to thank them for their constant love and support with everything I have chosen to do and for never putting pressure on me to do anything other than to try my best. I would also like to thank my brother, James, for his support throughout my PhD (and for having a garden, which provided much needed respite during the final months of writing).

Finally, I would like to say thank you to my girlfriend and fellow PhD student, Libby. Writing a thesis is tricky at the best of times, never mind being trapped writing a thesis in a one-bed flat during a global pandemic whilst your partner is trying to do the exact same thing. Her love and support over the last four years has made difficult times just that little bit easier. I hope she realises how important she is.

This thesis is dedicated to the thousands of fruit flies that laid down their lives for this research.

Declaration

I declare that the work contained in this thesis has not been submitted for any other award and that it is all my own work. I also confirm that this work fully acknowledges opinions, ideas and contributions from the work of others. When necessary, permission was requested for the reuse of figures in the printed and electronic copies of this thesis that are subject to copyright. This project has had full ethical approval (Project reference: BMS53UNNCBKP2016) and any work carried out on mouse tissue was in conjunction with Dr Ranson under ethics licensing BMS37UNNRNR2015.

The word count of this thesis is 46,556 words.

Name: Callum Bainbridge

Signature: 

Date: 06/10/2020

1. Introduction

1.1 Effects of ageing

Ageing is a gradual, continuous process that is characterised by an aggregation of biological changes that leads to functional decline in humans resulting ultimately in death (Liguori *et al*., 2018). Losses in regenerative potential, decreases in genomic stability and alterations to metabolism are all key molecular features of cellular ageing and can be driven by biological processes such as cellular senescence and oxidative stress-induced DNA damage (Kubben & Misteli, 2017). Ageing is not determined and caused by any single event, but rather a whole host of biological and environmental factors that influence and affect the rate at which biological ageing occurs (Partridge, 2010). Age-related declines in function not only give rise to mental and physical impairments, such as problems with language comprehension, memory loss, reductions in grip strength and increases in hip fractures (Haigh, 1993; Harada *et al*., 2013; Kubben & Misteli, 2017) but also susceptibility to developing diseases, such as diabetes and cancer, as well as other conditions affecting cardiovascular and musculoskeletal health (McPhee *et al*., 2016; Houck *et al*., 2018).

Neurodegeneration is a common problem associated with ageing (Kritsilis *et al*., 2018). The nervous system, consisting of the central nervous system (CNS) and the peripheral nervous system (PSN), is a group of complex and specialised cells that interact and coordinate bodily responses to sensory information through the transmission of electrochemical signals via neural pathways to create somatic and autonomic outputs (Llinas, 1988; Monje, 2018). Normally, neuronal cells transmit these electrochemical signals and relay information between afferent and efferent neurons, which allows the body to maintain homeostatic regulation of all systems (Ramocki & Zoghbi, 2008). Cellular metabolism and other fundamental processes experience reductions in efficiency with age and can lead to a number of neurodegenerative diseases, such as Alzheimer's disease and Parkinson's disease, which typically manifest in the elderly. Thus, ageing is a major risk factor for neurodegeneration (Kritsilis *et al*., 2018). Autopsy analysis of aged brains that have not been diagnosed with neurological conditions consistently show synaptic dystrophy, a loss of neurons and brain volume as well as the accumulation of Lewy bodies, amyloid plaques and TAR DNA-binding protein 43 (TDP-43) when compared to younger brains (Chen-Plotkin *et al*., 2010; Wyss-Coray, 2016). Alzheimer's disease, which is characterised by progressive declines

in memory, language, problem solving and other cognitive functions (Venkataraman *et al*., 2013), and Parkinson's disease, which is a progressive nervous system disorder that affects movement, show significant increases in a number of these proteins, which suggests an important overlap between ageing and neurodegeneration (Elobeid *et al*., 2016). Numerous factors including genetic mutations, environmental toxins and components of the diet may bring about neuronal cell death in ageing and neurodegenerative diseases (Hutchins & Barger, 1998; Castelli *et al*., 2019). These potential triggers can cause initiating factors to promote alterations to cellular functions, including energy and calcium homeostasis changes, increased oxygen radical production and apoptotic cascade activation. These cellular alterations, occurring in conjunction to age-related increases of oxidative stress, dysregulation of energy and ion homeostasis and decreases in DNA stability, can challenge neuronal integrity and cause disruptions to synaptic function and promote cell death (Mattson & Magnus, 2006).

1.2 Cellular senescence

Cellular senescence is a homeostatic response that aims to prevent an accumulation of damaged cells and development of pro-carcinogenic mutations through a phenotype typically characterised by irreversible cell cycle arrest (Moreno-Blas *et al*., 2019). Unlike necrosis and apoptosis, senescent cells remain metabolically active and can be divided into acute and chronically senescent cells (Martínez-Cué & Rueda, 2020). Acute senescence occurs during biological processes in embryonic development and tissue repair, whereas chronic senescence is induced over prolonged periods of stress. Cellular senescence primarily has roles in anti-tumour responses but evidence has shown that the loss of function associated with ageing and age related diseases can partly be accredited to chronic cellular senescence (Martínez-Cué & Rueda, 2020). Different categories of chronic cellular senescence have been identified and are used to describe the way in which a cell becomes senescent. Primarily, senescence is caused through replicative senescence or stress-induced premature senescence (Jurk *et al*., 2012). Replicative senescence occurs over prolonged periods of time during normal cell division. After each division telomeres become shorter. The shortening of telomeres reduces the protection available to the end of a chromosome and can leave them exposed to DNA damage, which in turn triggers a DNA damage response. If DNA repair pathways cannot repair the damage, chronic DNA damage response signalling can initiate other pathways, including cell death by apoptosis or induction of cell cycle

arrest via replicative senescence, both of which possess potential anti-cancer functions (Campisi, 1997; Herranz & Gil, 2018). Stress-induced premature senescence is described as the early onset of senescence in cells resulting from prolonged or repeated exposure to sub-cytotoxic concentrations of cellular stressors, such as oxidative stress (Kuilman *et al*., 2010). The increase of cells displaying this phenotype occurs during healthy ageing but also contributes to functional alterations associated with neurodegenerative diseases (Fielder *et al*., 2017).

Cellular senescence is not just limited to a phenotype of cell cycle arrest but a range of changes in protein expression and secretion, which ultimately causes a cell to develop a senescence-associated secretory phenotype (SASP) (Coppé *et al*., 2010). Persistent DNA damage signalling causes the synthesis and release of inflammatory cytokines, chemokines, growth factors and secreted insoluble proteins/extracellular matrix components and are all characteristics of SASP (Chen *et al*., 2015). Both endogenous and exogenous stresses are regulated by complex signalling pathways. Persistent DNA damage response signalling proteins Ataxia Telangiectasia Mutated (ATM) and checkpoint kinase-2 (CHK2) have been shown to be essential for the secretion of senescence-associated cytokines, such as interleukin-6 (IL-6) and tumour necrosis factors (Raghuram & Mishra, 2014). IL-6 expression in senescent cells has been shown to directly affect neighbouring cells and subsequently cause progressive expression of the transcription factor nuclear factor kappa B (NF-κB). The expression of the proinflammatory NF-κB signalling system is thought to be the crucial pathway that induces SASP and inflammatory responses in cellular senescence (Salminen *et al*., 2012). Mitochondrial dysfunction, which is predominantly caused by oxidative stress, is one of the leading triggers of senescence (Chapman *et al*., 2019). Dysfunction of mitochondria alters cell signalling and subsequently causes SASP (Vizioli *et al*., 2020). Molecules that are secreted by SASP have been seen to have both beneficial and deleterious roles to play throughout different life stages (Coppé *et al*., 2008). Senescence is thought to follow the antagonistic pleiotropic theory of ageing, which proposes that age-related declines in function are partly due to genetic programs that are pleiotropic. The theory suggests that genes that are beneficial to reproduction in early life are favoured by natural selection despite any negative effects that these genes might have in later life (Williams, 1957; Austad & Hoffman, 2018). Senescence-induced cell cycle arrest has beneficial properties as it can prevent neoplastic malignancies from developing. However, an accumulation of non-proliferating senescent cells can reduce

the ability of renewable tissues to repair or regenerate (Pérez-Garijo & Steller, 2014). Cytokine network components of SASP contribute to the maintenance of senescence cell-cycle arrest. It is also suggested that numerous components of SASP contribute to tissue repair and regeneration by signalling and initiating DNA damage responses (Kritsilis *et al*., 2018). However, as more senescent cells develop through life, persistent signalling of these molecules contributes to a chronic inflammatory status, which is a pervasive characteristic of ageing and a key driving force of age-related dysfunction (Coppé *et al*., 2008). DNA damage signalling is known to activate the tumour suppressor gene p53 (Ungewitter & Scrable, 2009). p53 activities can determine the fate of damaged cells, i.e. whether they enter apoptosis or senescence. p53 possesses regulatory effects on the SASP through transcriptional regulation of its target genes and has been shown to actively restrain it, thus preventing the development of a proinflammatory environment (Beauséjour *et al*., 2003). Age-related declines in p53 expression causes a quick increase in cells developing SASP (Feng *et al*., 2007). The age-related accumulation of senescent cells with inflammatory characteristics have been seen to be a driving force of cancer with many proteases secreted by senescent cells overlapping with those found in malignant tumours (Coppé *et al*., 2010).

No individual marker of senescence can be measured or monitored to confirm if a cell is senescent. However, a number of common features of senescent cells can be observed to suggest a senescent phenotype: Senescence-associated β-galactosidase is a lysosomal enzyme most commonly used as a senescence biomarker (Dimri *et al*., 1995). A common feature of senescent cells is a persistent DNA damage response, which can be detected through analysis of phosphorylated H2A histone family member X (γH2AX) foci (Redona *et al*., 2002), which become elevated in senescent cells at the sites of DNA double strand breaks (DSBs). Expression of the cyclin-dependent kinase inhibitors $p21^{WAF1/CIP1}$ and $p16^{INK4A}$ increase during senescence and are also used as biomarkers (Caliò *et al*., 2015). An accumulation of the nondegradable oxidation product lipofuscin can also be seen commonly in aged post-mitotic cells (Moreno-García *et al*., 2018).

Although fully-differentiated neuronal cells are post-mitotic and do not display typical senescence-associated cell cycle arrest, they have been shown to express other key features of senescent cells and develop a senescence-like state (Fielder *et al*., 2017). The cell cycle arrest of proliferating cells, which is conventionally seen as the defining hallmark of mitotic cellular senescence, has been suggested to be just one of many phenotypic changes that occur due to the downstream effects of signalling pathways of

the DNA damage response. Therefore, senescence is not exclusive to proliferating cells and can be used to describe senescence-like states of post-mitotic cells such as neurons (Jurk *et al*., 2012). An increase in oxidative stress has been shown to be associated with increased activity of the tumour suppressor gene p21 and senescence-associated β-galactosidase in the neurons of mice (Jurk *et al*., 2012). This is a phenotype that has been shown to become more prominent with ageing as the efficiency of DNA repair mechanisms, such as non-homologous end joining, declines with age, thus contributing to increased genomic instability and incidence of neurodegeneration (Vaidya *et al*., 2014).

1.2.1 Oxidative stress and DNA damage in neurons

During normal ageing neuronal cells develop an accumulation of damaged proteins, whilst experiencing increased levels of oxidative stress. This can cause mutations in nucleic acids and disrupt normal energy homeostasis (Castelli *et al*., 2019). The effects of normal ageing are amplified in neurodegenerative diseases (Mattson & Magnus, 2006). Numerous neurodegenerative diseases are linked to increases in oxidative stress and subsequent DNA damage including: Parkinson's disease, Alzheimer's disease, multiple sclerosis, motor neurone disease, Huntington's disease, mild cognitive impairment and cerebral ischemia (Venkataraman *et al*., 2013).

The balance between reactive oxygen species (ROS) and the antioxidant system is crucial for the maintenance of structural and functional qualities of neurons and subsequently the brain. The point at which cellular antioxidant defences are no longer able to keep ROS below the threshold for toxicity describes the state of 'oxidative stress' (Schulz *et al*., 2001). ROS are the main source of oxidative stress in living organisms and include oxygen-derived molecules such as hydrogen peroxide, superoxide and hydroxyl radicals that are highly reactive towards biomolecules (Aguiar *et al*., 2013). Glutathione is one of the most abundant small molecule antioxidant thiols and is heavily involved in the modulation of ROS and is a key component of the oxidative stress response. Age-related declines of intracellular glutathione concentrations have been demonstrated in murine brain models (Sasaki *et al*., 2001; Wang *et al*., 2003). In response to an increase of ROS, the transcription factor nuclear factor erythroid 2-related factor (Nrf2) becomes active. Activation of the Nrf2 pathway causes the expression of numerous endogenous antioxidants to increase, which helps to counteract ROS accumulation. The activation of Nrf2 has also been shown to decline in an age-related manner (Duan *et al*., 2009). Reductions in glutathione and reduced

activation of Nrf2 transcription factors contribute to the overall increase of oxidative stress throughout the ageing process.

Excess levels of ROS contribute to adverse modifications of cellular components and can amplify the development of damage to DNA, lipids and proteins and can induce apoptosis and necrosis (Lundgren *et al*., 2018). The formation of DNA base lesions is one of the most deleterious consequences of oxidative stress. When bases become oxidised the base excision repair (BER) pathway typically recognises the damage and repairs it. However, when bases become simultaneously oxidised on opposing strands of DNA, attempted repair through BER can lead to double strand breaks in which sites on both strands of the DNA helix are broken on the sugar phosphate backbone (Srinivas *et al*., 2019). Closely spaced transversion mutations can lead to lesions such as this and can be severely genotoxic if left unrepaired. The low redox potential of guanine makes it the most vulnerable base to oxidative stress, with 7,8-dihydro-8-oxoguanine (8-oxoG) being the predominant product of guanine oxidation. As guanine is the most vulnerable base, 8-oxoG is subsequently the most common base lesion caused by ROS (Aguiar *et al*., 2013). 8-oxoG is considered one of the predominant endogenous mutagens that contribute greatly to spontaneous cell transformations if left unrepaired. During replication 8-oxoG frequently mispairs with adenine as it is functionally able to mimic thymine. Consequently, this can lead to an increase in the number of G:C to T:A transversion mutations, which are among the most common somatic mutations seen in human cancers (Nakabeppu, 2014).

The lipid content of neurons is high and makes them particularly susceptible to lipid peroxidation, the process by which electrons are removed from lipids by ROS and, in turn, cause damage to the membrane structure of a cell. The predominant source of endogenous ROS originates from the oxidative metabolism of mitochondria as by-products in the forms of superoxide anions and hydrogen peroxide, which are produced through the action of the electron transport chain (Votyakova & Reynolds, 2001).

1.2.2 DNA repair in neurons

The proper repair of DNA damage is vital for the preservation of genomic integrity. In neurons the majority of DNA damage is caused by oxidative stress. As previously stated, one of the DNA repair pathways responsible for repairing this damage and maintaining genomic integrity is the base excision repair pathway (BER) (Fleming *et al*., 2017). Bases that become oxidatively damaged, deaminated cytidines and adenines

and single strand breaks (SSBs) are primarily repaired through BER (Yang *et al*., 2019). In addition to this, there are two main repair pathways that repair DSBs, non-homologous end joining (NHEJ) and homologous recombination (HR) (Brandsma & Gent, 2012). The error-prone NHEJ pathway is the predominant DSB repair pathway in neurons (Vyjayanti & Rao, 2006) with NHEJ activity seen in both developing and post-mitotic neurons (Oka *et al*., 2000; Kanungo, 2012). It had been assumed that the NHEJ pathway was the only pathway utilised in post-mitotic neurons to repair DSBs associated with oxidative damage as HR typically requires a sister chromatid template, which is not present in non-replicating neuronal cells. However, recent studies have discovered RNA-templated HR repair mechanisms of DSBs in terminally differentiated post-mitotic neurons at active transcription sites. The HR repair protein RAD52 has been shown to be recruited to DSB sites and has demonstrated an HR repair mechanism in these cells (Welty *et al*., 2018). In addition to BER, NHEJ and HR, other repair pathways have shown to be of importance in response to DNA damage such as nucleotide excision repair (NER) and mismatch repair (MMR). NER is the main repair pathway used by mammals to remove bulky DNA lesions, which can be caused by numerous factors including ROS (Schärer, 2013). Lesions such as this can cause large disruptions to transcription and replication. Although mismatch repair recognises and repairs incorrectly paired nucleotides predominantly in replicating cells, studies in differentiated neuroblastoma SH-SY5Y cells suggest that neurons possess MMR activity and that it is triggered following oxidative stress (Fishel *et al*., 2007).

With important roles in a number of cellular processes such as DNA replication, transcription, recombination, chromosome organization and segregation as well as being a pivotal enzyme during neuronal development, it has been suggested that the enzyme Topoisomerase II beta (Top2B) may be involved in DNA repair processes (Emmons *et al*., 2006; Gupta *et al*., 2012; Morotomi-Yano *et al*., 2018). Top2B is a member of a larger family of enzymes that possess the ability to regulate DNA topology in all cells (Woessner *et al*., 1991; Adachi *et al*., 1997; Vávrová & Šimůnek, 2012; Pommier *et al*., 2016).

1.3 Topoisomerase family

1.3.1 Topoisomerase classification

The topology of the double helix structure of DNA, i.e., the way in which it tightly twists and coils to remain compact, can cause numerous issues for biological processes such as transcription, replication, recombination and repair where strand separation and access to single strands of DNA is required. Discovered during the 1970s (Wang, 1971), DNA topoisomerases are a family of enzymes that control the topological state of DNA by catalysing transient SSBs or DSBs and allowing an intact single strand of DNA or a DNA duplex to pass through the break, respectively. The enzyme then reseals the break (Nitiss, 2009).

Topoisomerases are divided into a number of classes depending on their structural and biological functions. Primarily topoisomerases are divided into type 1 and type 2 variants. Topoisomerases that cleave and reseal only one single strand of DNA are classified as type 1 topoisomerases. Type 1 topoisomerases can be further classified into subfamilies, which include those that link to a 5' phosphate in the cleaved DNA (Type IA) and those that link to a 3' phosphate in the cleaved DNA (Type 1B) (Champoux, 2001). Topoisomerases that cleave both strands of DNA to create a double strand DNA break prior to religation are described as being type 2 topoisomerases (Harkin *et al*., 2015) with any further divisions of the subfamilies being due to structural differences (Table 1.1). Type 2 topoisomerases are classified as either Type IIA or Type IIB. They share homologous B subunits (N-terminal domains) but their A subunits (central domains) share neither sequence or structural homology, so are therefore classified accordingly (Gadelle *et al*., 2014).

Table 1.1 Classification of Type I and II topoisomerases (Champoux, 2001)

Topoisomerase	**Subfamily Type**
Eubacterial DNA topoisomerase I & III	IA
Yeast DNA topoisomerase III	IA
Mammalian DNA topoisomerase III α & β	IA
Eubacterial and archaeal reverse DNA gyrase	IA
Eukaryotic DNA topoisomerase I	IB
Poxvirus DNA topoisomerase	IB
Eubacterial DNA topoisomerase V	IB
Eubacterial DNA gyrase	IIA
Eubacterial DNA topoisomerase IV	IIA
Yeast/*Drosophila* DNA topoisomerase II	IIA
Mammalian DNA topoisomerase II alpha	IIA
Mammalian DNA topoisomerase II beta	IIA
Archaeal DNA topoisomerase VI	IIB

1.3.2 Catalytic cycle of topoisomerase II

The overall reaction strategy of eukaryotic type 2 topoisomerases is the generation of a transient double strand break in one DNA duplex and passing an unbroken DNA duplex through it, before resealing the break in order to relax torsional stress and resolve knots and tangles such as supercoils and catenanes (Figure 1.1).

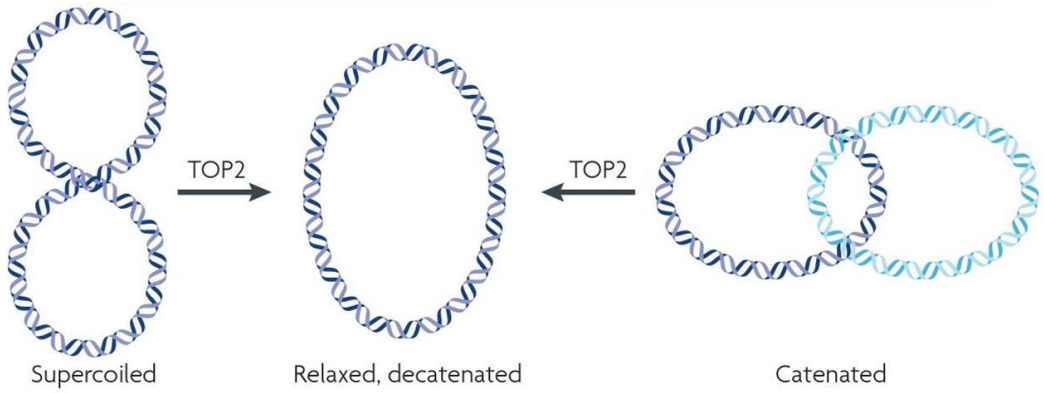

Figure 1.1 Diagrammatical representation of the actions of type 2 topoisomerases on DNA topology (Nitiss, 2009).

The catalytic domains of topoisomerase II include an N-terminal domain, a central domain and a C-terminal domain (Figure 1.2) (Burden & Osheroff, 1998). The catalytic cycle of eukaryotic topoisomerase II is initiated by the binding of the enzyme to its DNA substrate. Initially, prior to nucleotide binding, the highly conserved N-terminal domain, which contains the ATPase domain, is in an open conformation. This allows one DNA duplex (termed the G-segment) to bind to the gated region of the central domain, which resides in the interior of the enzyme (Laponagov *et al.*, 2013). The segment of DNA to be transported and passed through the G-segment, known as the T-segment, then travels through the open region of the N-terminal. The binding of ATP molecules then causes a 90° movement of the domains such that they dimerize and capture the T-segment in its interior, creating a closed clamp conformation (Schmidt *et al.*, 2012; Laponogov *et al.*, 2013) (Figure 1.3).

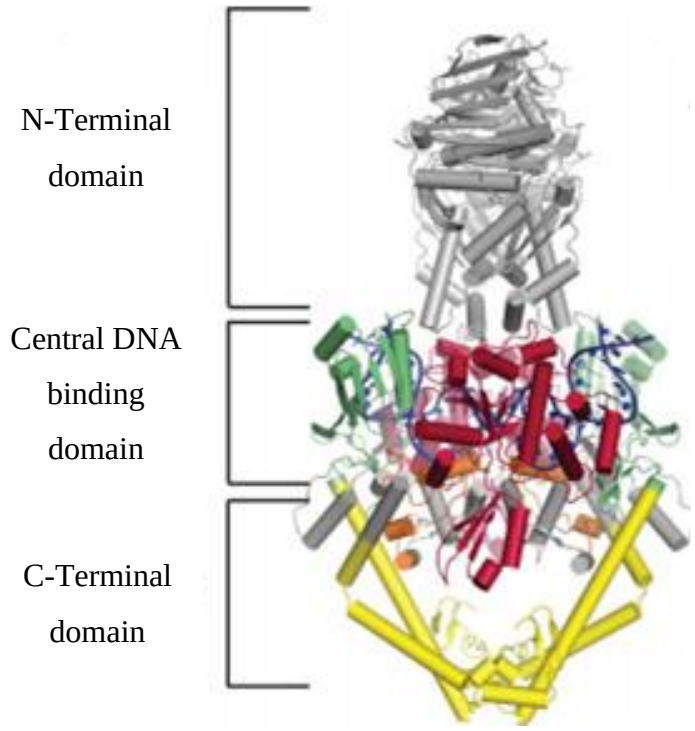

Figure 1.2 Structural domains of topoisomerase II.

The three structural domains of topoisomerase II shown as the N-terminal domain, the central DNA binding domain, which is divided into the Toprim (topoisomerase-primase) domain (red), Winged Helix domain (WHD)/ catabolite activation protein (CAP) (orange) and the tower domain (green), and the C-terminal domain (C-gate coloured yellow) (Riccio *et al*., 2019).

The ATPase region initiates significant conformational changes to the enzyme, which ultimately leads to the cleavage of the G-segment of DNA through the actions of the Toprim and WHD/CAP subdomains forming a G-gate (Aravind *et al*., 1998). These domains transiently cleave a pair of opposing phosphodiester bonds four base pairs apart in the G-segment of DNA, in the presence of Mg^{2+}, which generates a staggered topoisomerase II-DNA cleavage complex (Wu *et al*., 2011). This is achieved by a transesterification reaction mediated by a conserved tyrosine residue in both subunits of the enzyme. As a result, the active site tyrosines (Residue 821) become transiently covalently linked to the 5' ends phosphoryl groups via covalent phosphotyrosine bonds (Deweese & Osheroff, 2009). Simultaneously, events in the ATPase domain also prompt the opening of the G-gate through which the T-segment can be passed (Berger *et al*., 1996). Once the T-segment reaches the lower cavity of the enzyme next to the C-gate, the G-gate closes and is resealed via a transesterification reaction between the hydroxyl groups of the G-segments 3' ends and the phosphotyrosyl linkages (Berger *et al*., 1996). The T-segment is then released via the opening and closure of the C-gate at the bottom of the enzyme. ATP hydrolysis starts during transportation of the T-segment

through the G-gate and concludes to allow the N-gate to reopen, allowing further catalytic cycles to take place (Figure 1.3) (Burden & Osheroff, 1998; Champoux, 2001).

The mechanism of DNA cleavage utilised by topoisomerase II provides a number of advantages. The nature of the covalent complexes that are created between topoisomerase II and the G-segment are mostly freely reversible. This helps to protect the integrity of the cleaved DNA strands as no rearrangement or recombination of the DNA occurs during religation (Nitiss, 2009). This reversible covalent bond also allows religation to occur quickly and efficiently.

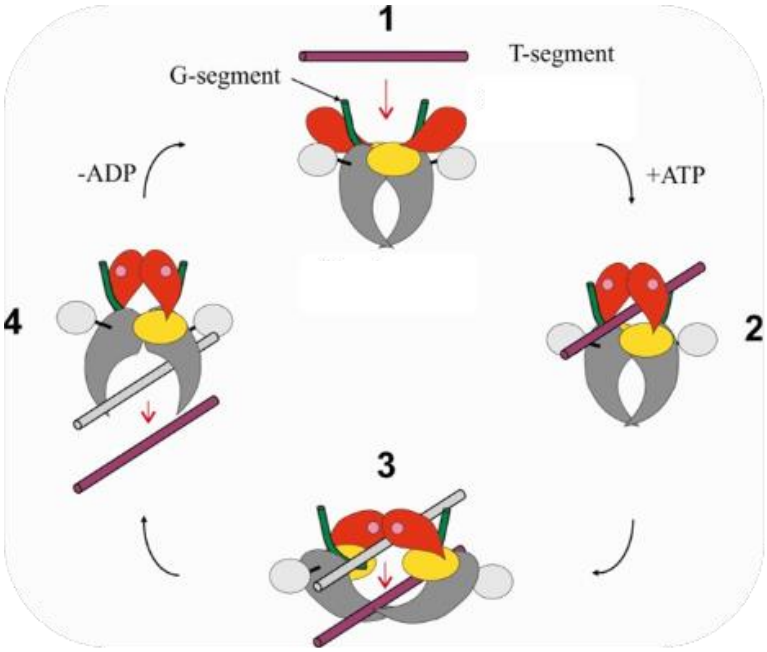

Figure 1.3 Diagrammatical representation of the mechanism of topoisomerase II isoforms. Adapted from Laponogov *et al*. (2013).

Topoisomerase II resembles the shape of an open clamp prior to interaction with DNA. The section of DNA to be cleaved (G-segment) binds to a gated region in the central domain of topoisomerase II known as the DNA gate (1). The T-segment approaches and moves through the gate region of the N-terminal and subsequent binding of ATP causes this gate to close behind the DNA segment (2) (Laponogov *et al*., 2013). The G-segment is then cleaved to form the G-gate by transesterification reactions, which results in the 5' ends of the strands becoming linked to tyrosine residues through covalent phosphotyrosyl bonds. Hydrolysis of the first ATP to ADP + P_i allows the T-segment to be transported through the G-gate (3). The G-gate is then resealed and the T segment is released via the C-gate (4). The closing of the C-gate through hydrolysis of the second ATP and subsequent release of ADP + P*i* resets the ATPase domains back to the open conformation (the N-terminal domain reopens) allowing further catalytic cycles to take place (Champoux, 2001).

1.3.3 Structure of type II topoisomerases

Eukaryotic type 2 topoisomerases function as homodimeric enzymes and when aligning amino acid sequences to that of the Type II topoisomerase found in bacteria, DNA gyrase (Figure 1.4), three distinct functional domains that are linked by flexible hinge regions are identifiable (Champoux, 2001). Eukaryotic topoisomerase II isoforms share up to 65% homology with DNA gyrase. DNA gyrase was the first type 2 topoisomerase to be described when it was isolated from *E.coli* (Gellert *et al*., 1976).

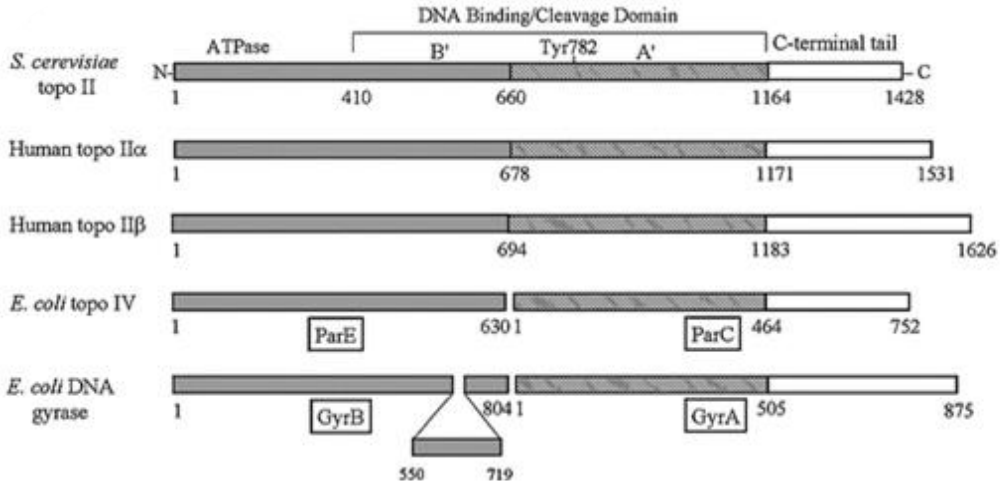

Figure 1.4 Homology of amino acid sequences in type II topoisomerases.

Type 2 topoisomerase amino acid sequence homology compared to bacterial DNA gyrase. N-terminal domains of eukaryotic topoisomerase II (B'), *E.coli* topo IV (ParE) and *E.coli* DNA gyrase (GyrB) are shaded grey. Central domains A', ParC and GyrA are shown with grey diagonal shading and C-terminal domains are coloured white (Champoux, 2001).

The catalytic domains of topoisomerase II include an N-terminal domain, a central domain and a C-terminal domain (Figure 1.2) (Burden & Osheroff, 1998). The N-terminal domain, which approximately spans the first 660 amino acids of type 2 topoisomerases and is the most conserved domain within the family, is homologous to the B subunit of DNA gyrase and contains the active site for ATP binding (Corbett & Berger, 2004; Burden & Osheroff, 1998). This region can be divided into two subdomains, which include the GHKL (gyrase, HSP90, histidine kinase, MutL) ATP binding domain and a transducer domain, which forms a gated region known as the N-Gate (Schmidt *et al*., 2012). The A subunit of DNA gyrase, which extends to

approximately amino acid 1200, is homologous to the central domain of topoisomerase II and is the domain responsible for DNA binding through an active site tyrosine residue (Laponogov *et al*., 2013). The central domain has a large central cavity and can be divided into three subdomains, which together form the DNA-gate region of the enzyme. These include the Winged Helix Domain (WHD) (sometimes referred to as catabolite activator protein [CAP] domains), which contains the conserved catalytic tyrosine, the Toprim (topoisomerase-primase) domain, which contains the acidic triad DXD motif involved in metal binding, and the tower domain (Nitiss, 2009; Bedez *et al*., 2018). The Toprim domain contains a cluster of conserved acidic residues that are thought to form binding sites for Mg^{2+} ions, which are a crucial cofactor essential to complete catalytic function (Corbett & Berger, 2004). The C-terminal of topoisomerase II is the most variable domain and contains no regions of amino acid sequence homology with DNA gyrase (Sengupta *et al*., 2003). The C-terminal domain of topoisomerase II plays roles in the regulation of cellular functions including key nuclear localisation signalling and many post-translational modifications including phosphorylation, acetylation, sumoylation and ubiquitination (Adachi *et al*., 1997; Linka *et al*., 2007).

1.3.4 Topoisomerase II isoforms

First discovered in the 1970s (Wang, 1971; Gellert *et al*., 1976), DNA gyrase isolated from *E.coli* was the first type 2 topoisomerase to be identified. In mammals, research from Drake *et al*. (1987) showed that analysis of purified topoisomerase II from the P388 leukaemia cell line by SDS-PAGE gave two protein bands for topoisomerase II; one band at 170 KDa and one band at 180 KDa. *Staphylococcus* V8 protease cleavage patterns of the two proteins showed distinct differences between them (Drake *et al*., 1987). They were individually purified and antibodies were raised against each of the two proteins. After western blot analysis the antibodies specifically recognised the 170 KDa protein and the 180 KDa protein, respectively, further supporting the distinct identities of the two proteins (Austin *et al*., 2018). The 170 KDa isoform later became known as Topoisomerase II alpha (Top2A) and the 180 KDa isoform became known as Topoisomerase II beta (Top2B). Nucleotide sequence analysis of the two proteins mapped Top2A to chromosome 17 and Top2B to chromosome 3 (Tan *et al*., 1992). Although Top2A and Top2B share large portions of sequence homology, this study confirmed that Top2A and Top2B were different isoforms rather than Top2B being a spliced variant of Top2A. Although similar in structure, Top2A and Top2B demonstrate

clear differences genetically, biochemically and immunologically (Wendorff *et al*., 2012).

Non-vertebrate eukaryotes such as *Drosophila* and yeast possess just a single 164 KDa topoisomerase II enzyme, Top2 (Hohl *et al*., 2012). Both *Drosophila* Top2 and each of the human topoisomerase isoforms, Top2A and Top2B, can rescue the phenotype of yeast Top2 mutants, which highlights the strong functional conservation of type II topoisomerases between species (Wyckoff & Hsieh, 1988; Jensen *et al*., 1996). Although these type 2 topoisomerases are highly conserved, it has been suggested that only the chromosomes of *Drosophila* are morphologically comparable to chromosomes of vertebrates (Mengoli *et al*., 2014). In this organism, Top2 has been shown to be expressed in mitotically active cells but has also been found to be stably expressed bound to chromatin in non-dividing cells. Based on this expression, indications might be made for homologous roles between *Drosophila* Top2 and mammalian Top2A and Top2B (Lee & Berger, 2019).

1.3.5 Homology of mammalian topoisomerase II isoforms

Top2A and Top2B are paralogues and share large portions of homology (Figure 1.4). Both isoforms have an ATPase N-terminal domain, a central DNA binding domain and a C-terminal domain (Austin *et al*., 1993; Riccio *et al*., 2019). Analysis of the amino acid sequence shows Top2A and Top2B share 68% homology. However, the homology of individual domains shows significant differences (Wendorff *et al*., 2012). The most conserved domain, the N-terminal domain, shares 78% amino acid homology between the two isoforms, whereas the least conserved domain, the C-terminal domain, is only 34% homologous between Top2A and Top2B (Austin *et al*., 2018). The difference in size and amino acid sequence of the C-terminal domain between the two isoforms suggests that Top2A and Top2B may have distinct roles in the cell (Linka *et al*., 2007).

1.3.6 C-terminal divergence of mammalian topoisomerase II isoforms

Both mammalian isoforms of topoisomerase II mechanistically function by passing strands of DNA through one another to relieve the torsional stress caused by DNA supercoiling. However, the divergence of amino acid sequence seen the in the C-terminal domain between the two isoforms could explain their differential roles both *in vivo* and *in vitro* (Schoeffler & Berger, 2008). The C-terminal has been shown to be dispensable for the catalytic activity of both isoforms of the enzyme (Adachi *et al*., 1997) but it is necessary for the nuclear localisation of each isoform (Linka *et al*.,

2007). The production of C-terminally truncated recombinant chimeric type 2 topoisomerases demonstrated the cell cycle-dependent roles for each of the two isoforms (Linka *et al*., 2007; Meczes *et al*., 2008). All chimeric proteins carrying a Top2A C-terminal domain were firmly associated with chromosomes during metaphase of mitosis and were able to support cell proliferation. However, chimeric proteins carrying a Top2B C-terminal domain were only able to support proliferation with minimal affect when expressed in high levels and they were not bound to chromosomes during metaphase in human cells (Linka *et al*., 2007). In addition to this, *in vitro* studies using C-terminally truncated recombinant chimeric proteins demonstrated that although the removal of the C-terminal domain does not have detrimental effects on the catalytic activity of either Top2A or Top2B, loss of the C-terminal did cause considerable increases in the binding of Top2B to DNA. Loss of the C-terminal in Top2A had no effect on the binding of Top2A to DNA but the chimeric protein of Top2A with β C-terminal caused significant inhibition of the enzymes catalytic function, whereas the chimeric Top2B protein with α C-terminal caused a slight increase in the catalytic activity of Top2B (Meczes *et al*., 2008). These studies suggest that the specific cell cycle-dependent characteristics displayed by Top2A and Top2B are determined by the diverse amino acid sequence of their C-terminal domain (Madabhushi, 2018).

1.3.7 Subcellular location of Topoisomerase II

Type 2 topoisomerases are predominantly nuclear enzymes with the C-terminal domains of both Top2A and Top2B containing nuclear localisation signals. However, the specific interphase nuclear location of Top2B has been reported differently in a number of different studies. A study by Meyer *et al*. (1997) suggested that Top2B was completely excluded from the nucleoli, whereas research by Zini *et al*. (1992) suggested that Top2B was nucleolar. In addition to this, Top2B has also been reported to be expressed in both the nucleolus and the nucleoplasm, whilst being frequently associated with heterochromatin (Petrov *et al*., 1993). A study by Chaly & Brown (1996) reported that the interphase distribution of Top2B was quite variable and that both methodology and antibodies used can affect the results. They show that Top2B is predominantly nucleoplasmic but small amounts are also seen to be associated with intranucleolar chromatin. In addition to this, Cowell *et al*. (2011) demonstrated that Top2B is concentrated in heterochromatic regions in the nucleus of mouse C127I cells and that inhibition of the enzyme histone deacetylase by trichostatin A resulted in Top2B being redistributed to euchromatic regions with a more pan-nuclear distribution. Interestingly,

work by Onoda *et al*. (2014) demonstrated that the subcellular location of Top2B correlates to it endogenous activities. Activity attenuation experiments in conjunction with nuclear localisation data suggested that Top2B shuttles between the nucleoplasm and the nucleolus. Their data suggests that Top2B is active in the nucleoplasm and becomes quiescent in the nucleolus. In addition to the nuclear functions of Top2B, mass spectroscopy has identified the presence of a truncated form of Top2B in mitochondria, which has shown to be important for mitochondrial DNA maintenance (Low *et al*., 2003; Zhang *et al*., 2014). The apparent diversity in subcellular locations of Top2B may be attributed to a number of factors. As stated by Chaly & Brown (1996), differences in methodology within their own experiment caused variability of results, which could go some way to explaining the discrepancies seen between different studies. The variability of species, cell cultures, methodological techniques and antibodies used may all have contributed to differences seen in Top2B subcellular distribution.

1.4 Top2A

1.4.1 Role of Top2A in replication

The unwinding of DNA and the subsequent copying of each strand of DNA that occurs during semi-conservative replication can lead to topological issues in the absence of topoisomerase (Nitiss, 2009). Unwinding of the parental DNA duplex and subsequent movement of the replication machinery along the double helix causes superhelical strain to build up around the elongating replication fork resulting in the formation of positive supercoils ahead of the replication fork and precatenanes behind it (Figure 1.5) (McClendon *et al*., 2005).

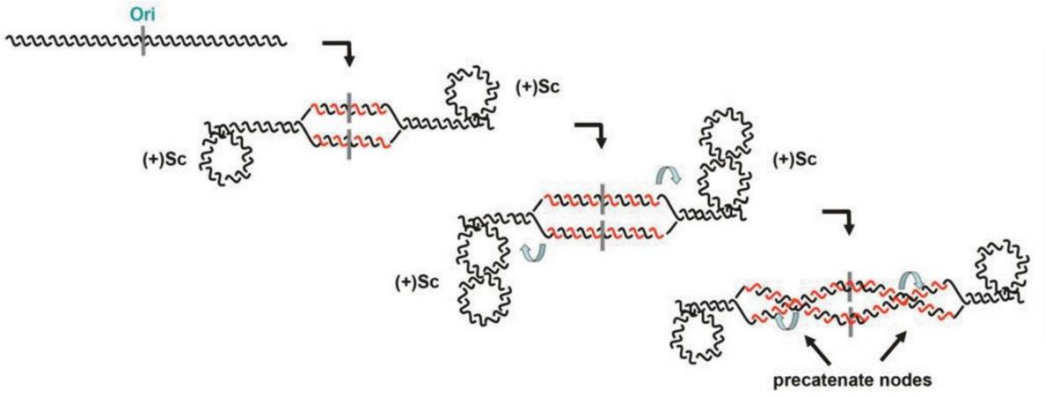

Figure 1.5 Diagrammatical representation of topological changes caused by advancing replication machinery.

The enzyme helicase unwinds and opens up the DNA double helix to create two Y-shaped structures at the origin of replication and are called replication forks. As replication machinery advances, the replication forks are extended bi-directionally creating positive supercoils [(+)Sc] ahead of the replication machinery. Compensatory replication fork rotation creates precatenanes behind the replication fork from the newly synthesised DNA (Bermejo *et al*., 2007).

The term ‘supercoil’ is often used in the context of DNA topology. It is a fundamental property of DNA and describes the overwound (positive supercoil) or underwound (negative supercoil) state of DNA (Gilbert & Allan, 2014). The overwinding of DNA ahead of the replication fork and subsequent accumulation of positive supercoils results in a compensatory underwinding of DNA behind the replication machinery through rotation of the replication fork. Underwinding of DNA behind the replication machinery causes daughter duplexes to become intertwined, thus forming structures known as precatenanes (Postow *et al*., 2001). Supercoils and precatenanes pose significant obstacles to the progression of replication. Supercoiling makes the separation of a DNA duplex into its individual strands difficult and an accumulation of supercoils can prevent the replication machinery from progressing (Heintzman *et al*., 2019). If precatenanes are left unresolved they can form catenated duplex daughter chromosomes, which can result in topological issues in replication termination if left unresolved. The relaxation of supercoils through the actions of topoisomerase is essential for the progression of the

replication machinery and the removal of precatenated/catenated DNA is essential to allow chromosomes to separate during mitosis (Gonzalez *et al*., 2011).

The modulation and resolution of these topological issues are accredited to topoisomerases. Both type 1 and type 2 topoisomerases have been shown to remove and relax positive supercoiling. However, only type 2 topoisomerases can remove precatenanes efficiently, hence most models have postulated that type 1 topoisomerases act ahead of the replication fork and type 2 topoisomerases act behind it (Postow *et al*., 2001). In addition to this, analysis of the two mammalian isoforms of type 2 topoisomerases has shown that Top2A preferentially removes positive supercoils from DNA. Human Top2A has been seen to remove positive supercoils >10-fold faster than negatively supercoiled DNA whereas Top2B, which is not required for replication, does not show any preference, which suggests that Top2A may also work in front of the replication fork, which goes against previous suggestions (McClendon *et al*., 2005).

Previous studies have shown that the simultaneous knockdown of mammalian Top2A and Top2B does not affect transcription initiation or elongation. However, cells with depleted type 2 topoisomerases displayed increases in cell cycle and mitosis duration with disruptions causing dysfunction to chromosome condensation and sister chromatid segregation. This eventually led to cell death or permanent cell cycle arrest, which suggests the actions of type 2 topoisomerases are required for functional DNA replication (Gonzalez *et al*., 2011). Similarly, the inactivation of Top2 in budding yeast cells has been seen to prevent decatenation during S-phase of the cell cycle, which in turn caused extensive chromosome missegregation resulting ultimately in dysfunctional cytokinesis and cell death (Baxter & Diffley, 2008).

1.4.2 Role of Top2A in chromosome segregation

A specific and unique role for type 2 topoisomerases was proposed for the segregation of daughter chromatids after DNA replication. More specifically, it is the actions of Top2A that are essential for this process (Pommier *et al*., 2016). Top2A protein levels show significant variability depending on the stage of the cell cycle in proliferating cells, which is in contrast to Top2B and type 1 topoisomerases that do not show any significant fluctuations in expression throughout the cell cycle (Cortés *et al*., 2003). mRNA levels of Top2A have been seen to peak during late S and G2/M phases of the cell cycle with levels increasing 2-3 fold (Bower *et al*., 2010). These increases seen during G2/M phases and subsequent decreases as cells become differentiated support

the suggestion that Top2A is primarily required during the final stages of DNA replication in order to aid chromosome untangling and segregation (Woessner *et al*., 1991; Chen *et al*., 2015). The importance of Top2A in chromosome segregation has been highlighted in previous studies in which topoisomerase II poisons and catalytic inhibitors of the enzyme have been used. Top2A malfunction/inhibition prevents daughter chromosome separation towards the cell poles during anaphase and results in the production of polyploid cells (Cortés *et al*., 2003). This has been supported by another study carried out in the human cell line HTETOP, which demonstrated phenotypic cell cycle arrest and cell death with a significant number of cells developing combinations of enlarged, distorted and polyploid nuclei in response to the absence of Top2A (Carpenter & Porter, 2004). In addition to this, Akimitsu *et al.* (2003) demonstrated incomplete nuclear division followed by enforced cytokinesis in Top2A knockout mouse models with embryos terminating at the 4 to 8 cell stage with chromosome defects. Reports in *Drosophila*, amphibians and mammals all show this conserved role for type 2 topoisomerases (Shamu & Murray, 1992; Christensen *et al*., 2002; Mengoli *et al*., 2014). Although these cells are able to continue through the cell cycle up to a point, eventually they die, which is one of the primary reasons topoisomerase II poisons that target Top2A are utilised to treat a wide range of cancers (Jain *et al*., 2013; Chen, *et al*., 2015).

1.4.3 Role of Top2A in transcription

As well as having roles in chromosome segregation and untangling chromosomes during mitosis, Top2A has also been found to be required in the RNA polymerase II-dependent transcription of chromatin bound DNA. Mondal *et al*. (2003) showed that elongation of RNA polymerase II during transcription on chromatin templates causes increasing tension in DNA due to the accumulation of positive supercoils in front of RNA polymerase, which inhibits further elongation and subsequently transcription of RNA transcripts over 200 nucleotides in the absence of topoisomerase. In addition to this, Top2A has shown to be a component of an initiation-competent RNA polymerase Iβ complex and directly interacts with RNA polymerase I-associated transcription factor RRN3 through its specific C-terminal, which in turn interacts with the promotor-bound SL1 transcription factor in U2OS and HTETOP cell lines. Absence of Top2A has been seen to influence assembly and stability of this pre-initiation complex, thus highlighting its role in facilitating its formation (Ray *et al*., 2013).

1.5 Top2B

Discovered in 1987, Top2B has been reported to play key roles in transcriptional regulation and genome organisation with particular activity seen during neuronal development and in post-mitotic cells (Drake *et al*., 1987). Although Top2B is expressed throughout the cell cycle in all mammalian cells, it is significantly upregulated when cells enter a state of terminal differentiation (Tsutsui *et al*., 1993; Tiwari *et al*., 2012; Harkin *et al*., 2015; Austin *et al*., 2018).

1.5.1 Role of Top2B in transcription

The actions of RNA polymerase during transcription introduces axial rotation in DNA, which results in positively supercoiled DNA forming in front of the enzyme and negatively supercoiled DNA behind the enzyme (Figure 1.6), thus increasing torsional stress, whilst also displacing nucleosomes in the process (Björkegren & Baranello, 2018). The increase of positive supercoils and subsequent torsional stress can inhibit RNA polymerase activities and disrupt transcription. The roles of topoisomerase in relieving torsional stress are essential to maintaining DNA templates in a transcriptionally competent state (Gilbert & Allan, 2014).

The initiation of transcription is highly influenced by the presence of supercoiled DNA. The controlled action of topoisomerases and their ability to make alterations to DNA topology facilitates protein interactions with DNA and allows key biological processes to take place (Durand-Dubief *et al*., 2011). It has been suggested that topoisomerase I activity is mainly responsible for the resolution of supercoiling that has been generated by transcription but topoisomerase II activity is required for the most highly expressed genes (Kouzine *et al*., 2013; Naughton *et al*., 2013).

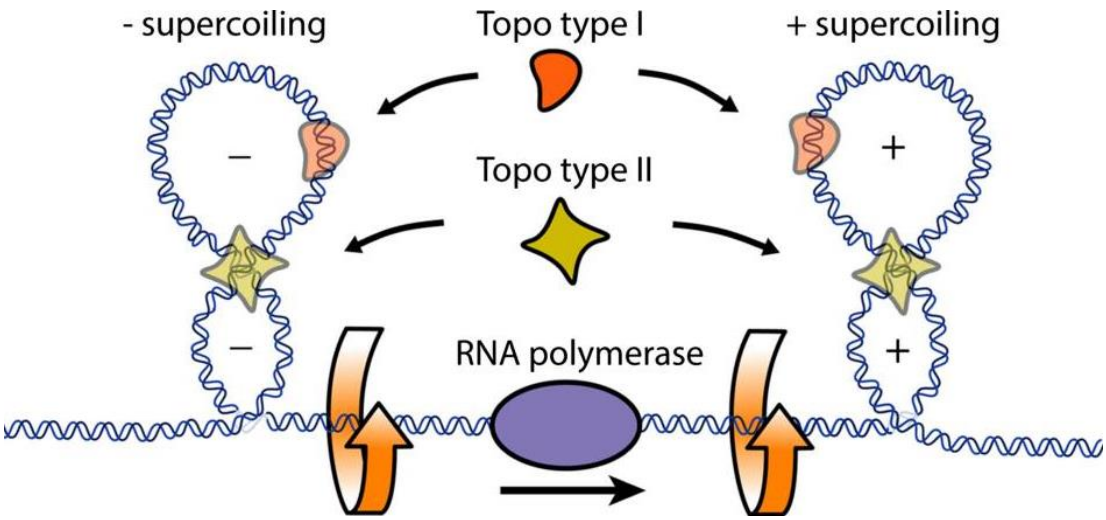

Figure 1.6 Diagrammatical representation of supercoil formation during transcription through the actions of RNA polymerase.

As RNA polymerase tracks along DNA it is unable to turn around the helical shape of DNA. Instead, segments of DNA turn around its helical axis to allow the transcription machinery to proceed. However, the process of DNA unwinding and the tracking of RNA polymerase subsequently introduces torsional stress in the DNA that results in the formation of supercoils. As RNA tacks along a segment of DNA, positive supercoils are formed ahead of the enzyme and negative supercoils form behind it (Ma & Wang, 2016). The actions of topoisomerase relieve the torsional stress caused by supercoiling (Liu & Wang, 1987).

A role for Top2B in transcriptional regulation has also been observed through the formation of stimulus-induced DSBs. Nucleosome-specific recruitment of Top2B has been seen to activate transcription by generating a break in double-stranded DNA, allowing subsequent relaxation of chromatin, and driving gene expression. Top2B-mediated cleavage of DSBs has been seen to be essential for the expression of oestrogen receptor-α (ERα) target genes. Through the use of chromatin immunoprecipitation (ChIP), analysis of the oestrogen-responsive promoter gene *pS2* has been examined in 17β-estradiol (E_2)–treated Michigan Cancer Foundation (MCF)–7 cells with rapid increases in Top2B recruitment seen after E_2 treatment, resulting in the formation of

transient DSBs within the promoter (Ju *et al*., 2006). Subsequent increases in the recruitment of DNA DSB repair machinery, including DNA-dependent protein kinase (DNA-PK), Ku86, Ku70 and Poly [ADP-ribose] polymerase 1 (PARP-1) was also seen. Type 2 topoisomerases typically create transient DSBs and reseal them immediately after resolving torsional stress, without needing DNA repair factors (Morimoto *et al*., 2019), but it is hypothesised that these proteins are in the locality to repair any incorrectly repaired Top2B mediated DBSs (Haffner *et al*., 2011). This particular role during promoter gene activation implies a mode of type 2 topoisomerase activity in addition to removing supercoils. After E_2 treatment histone H1 was replaced by high mobility group B 1/2 (HMGB1/2) on the nucleosome containing the oestrogen receptor binding site and is thought to be part of the ERα-mediated transcriptional activation of the *pS2* gene. The inhibition of either Top2B or PARP-1 prevented the exchange of histone H1 for HMGB1/2, which resulted in the suppression of the *pS2* gene suggesting mechanistic cooperation between Top2B and components of the DNA damage response machinery during regulation of gene transcription. Although numerous important repair proteins are recruited to the site of the DSB, they do not appear to be required to repair the Top2B induced DSB. Instead, it appears that Top2B is recruited to the promoter as part of a larger complex, which also includes proteins from DNA repair pathways (Nitiss, 2009). In addition to its roles regarding ERα-dependent promoters, Top2B has also been reported to have analogous roles in retinoic acid receptor, androgen receptor, thyroid receptor, and activating protein 1 (AP-1)–dependent transcriptional activation, which all utilise Top2B-mediated DNA DSB activities and subsequent activation of PARP-1 and histone H1-HMGB1/2 exchange (Ju *et al*., 2006). In addition to this, Top2B is thought to play an important role in the development of adaptive responses and the formation of long-lasting memories by facilitating the transcription of genes that allow alteration in the morphology and connectivity of neural circuits in the brain. The initiation of new gene transcription programmes is crucial for this and occurs in two phases, early and late. It is thought that Top2B-induced DSBs in promoter regions of the neuronal early response genes *Fos*, *Npas4* and *Egr1* is needed to induce their expression as knockdown of Top2B attenuates both DSB formation and early response gene expression (Madabhushi *et al*., 2015). The activities of Top2B have not only been seen to upregulate genes but may also be responsible for repression of gene expression and silencing. Studies by Huang *et al*. (2011) demonstrated that inhibition of Top2B can cause unsilencing of the paternal allele of ubiquitin protein ligase E3A (*Ube3a*) in *Ube3a-Yellow Fluorescent Protein* knock-in mouse models suggesting that

topoisomerase inhibitors can potentially rescue cellular, molecular and behavioural deficits that are observed with a loss of *Ube3a*. In addition to this, expression of *Ube3a* was also seen to be upregulated in Top2B knockout mice providing further support that *Ube3a* expression is regulated by topoisomerases (Huang *et al*., 2011). Studies by McNamara *et al*. (2008) suggested that Top2B negatively modulates expression of retinoic acid receptor α (RARα). Knockdown of Top2B in NB4 cells was seen to upregulate retinoic acid gene expression, whilst overexpression of Top2B caused a reduction in retinoic acid-induced expression of target genes and differentiation. Therefore, it may be postulated that the down-regulation of Top2B may lead to unsilencing and activation of numerous genes.

Top2B activity has been seen to facilitate the formation of a favourable chromatin environment that allows transcription initiation. Top2B co-purifies with ATP-dependent chromatin assembly factor (ACF), which is a chromatin remodeler that regulates nucleosome spacing, whereas Top2A does not (Madabhushi, 2018). In addition to this, CCCTC-binding factor (CTCF), a transcription factor that also acts as a transcriptional activator, is a key player in the regulation of chromatin structure and gene regulation and has been shown to be enriched at Top2B binding sites (Barutcu *et al*., 2017). CTCF forms chromatin loops and can attract numerous transcription factors to chromatin, including transcriptional activators, repressors, cohesin and RNA polymerase II (Racko *et al*., 2018). A study demonstrated that approximately half of all CTCF/cohesin-bound regions in primary mouse liver cells were also occupied by Top2B, using chromatin immunoprecipitation analysis followed by DNA sequencing, and suggested that activity of Top2B could regulate supercoiling at CTCF binding sites (Uusküla-Reimand *et al*., 2016). Further studies also demonstrated that Top2B is co-localised at sites that are occupied by CTCF and cohesin but also suggested that Top2B exerts its actions primarily at the anchors of chromatin loops (Canela *et al*., 2017). Together, these studies suggested that chromatin architecture and organisation could have major implications in DNA topology and could be a source of topological stress. The resolution of topological stress that is caused during chromatin looping is thought to be carried out by Top2B and therefore considered an important component in the maintenance of chromatin architecture (Uusküla-Reimand *et al*., 2016; Canela *et al*., 2017).

1.5.2 Top2B in neuronal development

At early embryonic stages Top2A is prominent in areas concomitant with proliferating neurons i.e., within the ventricular zones and in the external granular layer of the cerebellum (Harkin *et al*., 2016). In contrast, Top2B is observed to be distributed throughout the brain both in mice, rats and in the human foetus (Harkin *et al*., 2016). In addition, post-mitotic granule cells in the external granular layer of the cerebellum in rats have displayed a transition in expression of Top2 isoforms from Top2A to Top2B during development (Tiwari *et al*., 2012).

Thus, it is clear that Top2B is important in neuronal development, illustrated by the genetic deletion of Top2B in mice, which has been seen to cause neuronal defects during development (Lyu & Wang, 2003). Mice lacking Top2B display defective embryonic brain development and die shortly after birth due to respiratory failure. Perinatal death phenotypes have also been observed in Top2B null mutant mouse models (Yang *et al*., 2000), with analysis of mutant embryos revealing an inability of motor neurons to innervate muscles of the diaphragm, which further supports the important role that Top2B plays in neuronal development. In addition to this, defects in corticogenesis, including abnormal lamination patterns in the developing cerebral cortex, have also been observed in brain-specific Top2B knockout mice models (Lyu & Wang, 2003). Further work by Lyu *et al*. (2006) carried out transcriptional profiling analysis of gene profiles in the brains of wild-type mouse embryos in comparison to Top2B null mouse embryos at three developmental stages. Genes responsible for encoding cell growth functions and early differentiation markers were not affected by the absence of Top2B and Top2B was shown to only be required for the expression of a small subset of Top2B-sensitive genes during embryonic development of the brain. However, 30% of the subset of developmentally regulated genes were affected as a result of Top2B being knocked out, suggesting that Top2B may regulate the expression of developmentally regulated genes at later stages of differentiation.

Work by Tiwari *et al*. (2012) demonstrated that during neural maturation Top2B binds preferentially to regions containing H3K4 methylation, a feature of euchromatin, and that Top2B is particularly enriched at promoters at times when neurons exit the cell cycle. Also in their study they found that knockdown of Top2B caused an upregulation in a small set of Top2B bound genes. They hypothesised that these genes are actively repressed and that the mode of repression is dependent on the structure of the chromatin (as it is the case for gene activation above) and that Top2B is required for this

maintenance. One such repressed gene is *Ngfr* p75, which increases when Top2B is knocked down. *Ngfr* p75 is a member of the tumour necrosis factor receptor superfamily and during neuronal development *Ngfr* p75 plays an important role in central and peripheral nervous system cell death and becomes down-regulated in adults (Chan & Tahan, 2010). Expression of *Ngfr* p75 has been shown to only increase in adults in a response to injury with higher levels seen in neurodegeneration-related cell death (Miller & Kaplan, 2001). In the absence of Top2B, *Ngfr* p75 becomes upregulated, which does not hinder cellular processes during the early stages of neuronal differentiation but causes phenotypic premature cell death in post-mitotic neurons. Top2B knockout neurons displayed a delay in death of cells that had depleted *Ngfr* p75. In addition to this, *Ngfr* p75 knockout neurons also displayed significant reductions in cell death when compared to wild-type neurons after Top2B had been chemically inhibited by ICRF-193. This study suggests a role for Top2B in the regulation of target genes that are responsible for controlling programmed cell death during neuronal differentiation.

Further supporting the roles of Top2B in the regulation of developmentally regulated gene expression, research by King *et al*. (2013) also suggests important developmental roles for Top2B in establishing correct neural circuitry for proper brain function. Mutations in topoisomerases have been seen in neurodevelopmental disorders such as autism spectrum disorder (ASD) (Neale *et al*., 2012). The gene ubiquitin protein ligase E3A (*Ube3a*) plays a critical role in the normal development and function of the nervous system and has been associated with neurodevelopmental disorders. Topoisomerases have been implicated in *Ube3a* expression. *Ube3a* is a long gene and Top2B has been shown to be crucial in facilitating the expression of long genes, including numerous long ASD candidate genes that are thought to contribute to ASD pathology (Lam *et al*., 2017). Inhibition of Top2B has been shown to cause reductions in expression of long genes, suggesting that higher order structure constrains short and long genes differentially. This indicates a mechanistic link between transcriptional elongation and expression of numerous long genes with findings suggesting chemical and genetic mutations that cause topoisomerase impairment may have the potential to contribute to length-dependent impairments of gene transcription in neurons during development, thus contributing to neurodevelopmental disorders such as ASD (King *et al*., 2013).

1.5.3 Expression levels and patterns of Top2B during development

Northern blot analysis of Top2A and Top2B using specific probes has shown differential expression patterns of RNA transcripts in the two isoforms in various murine tissues from embryonic, new-born and adult tissue samples. During early embryogenesis both isoforms are expressed highly with post-natal increases of Top2B expression seen in the brain. More than a 6-fold increase in Top2B expression was seen in new-borns compared to embryos, adding to the increasing evidence that Top2B is important for neuronal development. Differential expression of Top2A and Top2B has also been reported in rats, human foetal tissues and the developing human telencephalon (Tsutsui *et al*., 1993; Zandvliet *et al*., 1996; Harkin *et al*., 2015). Previous studies by Tsutsui *et al*. (1993) have shown that Top2A is highly expressed in the embryonic brain and in the cerebellum of two day old rats followed by a sudden decrease in expression and undetectable levels at four weeks old. The cells within the cerebellum expressing Top2A were strictly confined to the proliferative outer mitotic region of the external granular layer. This differs to Top2B, which is expressed throughout embryonic and post-natal stages and is not limited to the outer mitotic region of the external granular layer of the cerebellum but is expressed throughout the entire cortical region (Tsutsui *et al*., 1993; Watanabe *et al*., 1994). Further studies by Kondapi *et al*. (2004) have also reported high levels of Top2B in the cerebellum of young rats (<10 days), but in addition to this claimed Top2B was only found in cerebellar regions. Their studies indicated that levels of Top2B in the cerebral cortex and mid-brain were negligible with analysis of hippocampal regions similarly showing negative results. High levels of Top2B were seen in the cerebellar region during the early post-natal period suggesting roles in development. This contradicts findings by Maeda *et al*. (2000), which suggest that not only is Top2B expressed in the hippocampus, but is expressed differently across the CA1, CA2 and CA3 regions of the hippocampus. Positive expression of Top2B was observed in both immunohistochemistry and immunoblotting experiments in hippocampal tissue in early post-natal rats. In addition to this Top2B expression was also seen in the neocortex (a component of the cerebral cortex) and in tissue of the olfactory bulb. The conflicting results from these studies suggest that regional differences of Top2B expression in the brain are yet to be fully elucidated.

1.5.4 Regulation of Top2B expression

Guo *et al*. (2014) suggested a role for the transcription factor specificity protein 1 (Sp1) in the regulation of Top2B expression during neuronal differentiation. Sp1 was one of

the first transcription factors to be identified and previous research suggests that Sp1 plays key roles in gene expression, particularly in embryonic development and early foetal development of neural tissue (Saffer *et al*., 1991; Marin *et al*., 1997). However, activity of Sp1 has been seen in a number of cellular processes including cell differentiation, cell growth, chromatin remodelling, immune responses, responses to DNA damage and apoptosis by binding to the GC and GT box sequences of gene promoters (Gory *et al*., 1997). Results showed an increase in Top2B expression at both the mRNA and protein level during retinoic acid-induced neuronal differentiation of the neuroblastoma cell line SH-SY5Y over a five day period (Guo *et al*., 2014). These results were similarly reported in mouse embryonic stem cells that were also undergoing differentiation (Tiwari *et al*., 2012). Alongside increases in Top2B expression, Sp1 levels of expression were also seen to increase over five days of cellular differentiation at the mRNA and protein level. Previous studies have provided functional analysis of the gene structure of Top2B through isolation, cloning and sequencing of the 1.3 kb 5'-flanking region of the gene to help understand Top2B promoter activity. A region within the Top2B promoter sequence between -533 and -481 has been shown to be responsible for approximately 80% of the promoters' activity (Lok *et al*., 2002). Analysis within this region identified two inverted CCAAT boxes that bind the transcription factor nuclear factor-Y (NF-Y), and a GC box in close proximity to the inverted CCAAT box that binds Sp1. Mutation of these binding sites causes significant reductions in Top2B promoter activity, which suggests a synergy between the two binding sites and indicates key roles for these sites in Top2B transcription and subsequent expression regulation (Lok *et al*., 2002). In addition to this, interference of Sp1 binding to GC-rich DNA sequences through treatment with the compound mithramycin A (MIT) resulted in a decrease in expression of Top2B at both the mRNA and protein level, further suggesting that Sp1 might regulate Top2B expression by binding to its GC box in the promoter region (Guo *et al*., 2014).

Other regulators of Top2B expression include nuclear receptor related 1 protein (NURR1). NURR1 is a transcription factor and binds to specific DNA binding sites in the promoters of regulated target genes as a monomer, homodimer or heterodimer (Decressac *et al*., 2013). Studies suggest that NURR1 influences the development and differentiation of mesencephalic dopaminergic neurons through axon genesis regulation (Heng *et al*., 2012). It is also seen to have essential roles in maintenance of function in dopaminergic neurons and provide neuroprotection as well as being identified as having

a distinctive role in Parkinson's disease pathology (Eells *et al*., 2002). Previous studies show that Top2B plays significant roles in axon genesis and neurite outgrowth (Nur-E-Kamal *et al*., 2007). ChIP assays have identified a region on the Top2B promoter that NURR1 directly binds to suggesting its importance in Top2B expression and axon genesis in dopaminergic neurons. Double immunofluorescent staining of coronal brain sections of mice showed co-expression of NURR1 and Top2B in the nuclei of ventral mesencephalon neurons and cells of the hippocampus and cerebral cortex. In addition to this, Top2B expression was seen to significantly reduce in NURR1 knockout mouse brain sections, whilst Top2B null mice showed significant loss of dopaminergic neurons in the substantia nigra and lack of neurites along the nigrostriatal pathway. Inhibition of Top2B caused dopaminergic neurons to exhibit shortened neurites in ventral mesencephalon neurons isolated from 13.5-day-old mouse pups. However, over-expression of Top2B in SH-SY5Y cells rescued NURR1 deficiency-induced neurite impairments. In addition to this, using a Top2B silenced neurally-differentiated human mesenchymal (hMSC) cell line and cerebellar granule neurons (CGNs) it was shown that Top2B is necessary for effective NURR1 expression and normal axonal length in differentiated cells (Terzioglu-Usak *et al*., 2017). As two functional NURR1 binding sites in the proximal Top2B promoter have been identified, it has been proposed that NURR1 may influence axon genesis in dopaminergic neurons by recruiting Top2B, hence suggesting that NURR1 can directly regulate Top2B expression and interactions between NURR1 and Top2B both *in vitro* and *in vivo* are important for the regulation of mesencephalic dopaminergic neuronal development, differentiation and maintenance (Heng *et al*., 2012).

1.5.5 Top2B in neuronal ageing

The activities of Top2B appears to peak during neuronal differentiation and development in a number of neuronal cells, including purkinje and cerebellar granule cells, before decreasing, as demonstrated in work by Tsutsui *et al*. (2000). After neuronal differentiation Top2B expression decreased by approximately half of the maximum peak but it continued to be expressed at this level into adulthood, which suggests other roles for Top2B outside of neuronal differentiation. The expression of Top2B can be observed in most adult tissues (Capranico *et al*., 1992).

The importance of Top2B in differentiation and development of neuronal cells has been well published but age-related changes in Top2B expression is yet to be fully elucidated. Age-dependent decreases of Top2B activity in the brains of rats and in cell

cultures have been reported in a very limited number of studies. Decreases of Top2B expression have been seen in the cerebellum of rats (Kondapi *et al*., 2004), with cell cultures of cerebellar granule neurons similarly showing a decrease with age (Bhanu *et al*., 2010). Kondapi *et al*. (2004) attempted to determine the regional distribution of Top2B and identify any age-dependent changes in Top2B expression. They suggested that Top2B is only expressed in cerebellar tissue and that expression is high in young rats, moderate in adults and low in old rat cerebellar regions. As described previously, data from Maeda *et al*. (2000) contradicts findings by Kondapi *et al*. (2004) as they indicate Top2B is present in rat hippocampal tissue. However, this data does not analyse Top2B expression throughout the ageing process and looks at developmental levels of expression in post-natal rats compared to adults. Further studies incorporating aged rats would be required to elucidate Top2B expression in hippocampal tissue throughout the ageing process. As the numbers of studies in this area are so limited, it isn't possible to confirm the roles, regulation and expression of Top2B throughout the ageing process.

Top2B associates with chromatin and has been shown to be fundamentally important for chromatin architecture (Uusküla-Reimand *et al*., 2016). During the ageing process epigenetic changes, including histone modifications and specific changes in DNA methylation occur (Armstrong *et al*., 2019). These age-related changes in DNA methylation and histone modifications can alter and disrupt chromatin architecture, which in turn is associated with the neuropathology and progression of numerous neurodegenerative diseases (Berson *et al*., 2018). In the early stages of neurodegenerative diseases epigenetic modifications, such as those previously described, can affect specific gene expression and correlates with the presence of misfolded proteins in specific regions of the brain (Martínez-Cué & Rueda, 2020). Altered proteostasis is a common feature of senescent cells with increases in unfolded protein response (UPR) frequently seen and, as stated previously, numbers of senescent cells increase with age. In neurodegenerative diseases, such as Alzheimer's disease, dysregulation of histone modifications and DNA methylation have been seen to be prominent features (Prasad & Jho, 2019). As Top2B plays an important role in maintaining neuronal function and is associated with maintaining chromatin architecture, it is possible that age related declines that have been previously reported in Top2B expression (Kondapi *et al*., 2004; Bhanu *et al*., 2010) may influence the progression of neurodegenerative diseases. In addition to this, the histone code hypothesis describes the idea that gene regulation depends partly on histone

modifications. Post-translational modifications to histones act like a molecular code and can be recognised by non-histone proteins to modulate specific chromatin functions (Rando, 2012). Altered/aberrant histone modification and DNA methylation themselves may be responsible for changes in Top2B expression.

1.5.6 Top2B and repair

Top2B has been reported by a number of studies to be involved in DNA repair. Gupta *et al*. (2012) suggested an indirect but significant role of Top2B in regulating BER capacity in neurons and suggested it is an important component in the promotion of DNA break repair through the BER pathway in cerebellar granule neurons. DNA damage induced by ROS in these cell types can cause abasic sites, which are commonly repaired by BER (Maynard *et al*., 2009). In addition to ROS induced damage, abasic sites are also formed at the initial stage of BER as a processed intermediate. Abasic sites are highly mutagenic, so efficient repair of these sites is critical. Interestingly, the presence of abasic sites, such as methoxyamine-bound abasic sites, within the vicinity of Top2B cleavage sites have been seen to act as endogenous topoisomerase II poisons and significantly stimulate Top2B-mediated cleavage. Gupta *et al*. (2012) reported that the activities of Top2B at abasic sites suggested a possible overlap of Top2B in BER processing regions, thus implicating Top2B activity in the regulation of BER pathway intermediates. In addition to abasic sites, crosslinks have been shown to interfere with cellular metabolism, causing DNA replication and transcription dysfunction, leading to cell death (Hashimoto *et al*., 2016). Work by Emmons *et al*. (2006) suggested that levels of Top2B are a determinant of melphalan-induced crosslinks. In the study Emmons *et al*. (2006) demonstrated that knocking down Top2B inhibited the repair of melphalan-induced crosslinks in K562 cells, which indicated that Top2B participates in the repair of alkylating agent-induced DNA damage. Furthermore, Top2B was seen to dynamically respond to DNA damage and rapid recruitment of Top2B to DSB sites has been demonstrated. Inhibition of Top2B reduced the enzymes mobility and prevented recruitment to DSB sites. In addition to this, Top2B knockout cells displayed increased sensitivity to the DNA damaging agent bleomycin and subsequently caused decreases in HR-mediated DSB repair, thus implicating the role of Top2B in DSB repair pathways (Morotomi-Yano *et al*., 2018). Indeed, if Top2B does decline with age as suggested by Kondapi *et al*. (2004) and Bhanu *et al*. (2010), this may have subsequent consequences for DNA repair pathways such as BER and HR and could lead to an accumulation of DNA damage, resulting in neuronal malfunction and cell death.

1.6 Aims

Top2B has been shown to be a critical component of neuronal differentiation and development with the expression of developmentally regulated genes relying on its activities (Guo *et al*., 2014; Tiwari *et al*., 2012). Active regulatory regions of the genome that are responsible for transcriptional modulation of target genes essential to neuronal differentiation are occupied by Top2B (Tiwari *et al*., 2012). However, the roles and regulation of Top2B in neurons throughout the ageing process are yet to be elucidated with a very limited number of studies in this area of research.

The main focus of this project was to investigate the expression of Top2B in aged neurons through the development of suitable models.

Different models of ageing, including cell culture and animal models were utilised to accomplish this aim. Research focussed on the development of a reliable model of ageing in a differentiated neuronal cell culture and in chronologically aged *Drosophila*.

Levels of Top2B protein and mRNA were investigated in differentiated neuronal cell cultures and *Drosophila* brain tissue over time. The ageing process was carried out through chronological ageing of differentiated neuronal cell lines and chronological ageing of wild-type *Drosophila*.

The DNA damage response of neuronal cell lines was investigated during chronological ageing by analysing γH2AX foci and carrying out Comet assays.

Immunohistochemical techniques were used to attempt to investigate Top2B expression in young versus aged mouse hippocampal tissue.

2. Materials and methods

2.1 Materials

The following section lists all the materials used for experiments in this thesis.

2.1.1 Antibodies

Table 2.1 Antibodies for western blotting

Name	Host	Supplier and product number	Dilution
Anti-Top2A	Mouse	Santa Cruz Biotechnology: sc-166934	1/500
Anti-Top2A	Mouse	BD biosciences: 611326	1/500
Anti-Tob2B	Mouse	BD Bioscience: 611493	1/500
Anti-Top2B	Rabbit	Novus Biologicals: NBP1-89527	1/500
Anti-Top2B	Mouse	Santa Cruz Biotechnology: sc-365071	1/250
Anti-Top2	Mouse	Santa Cruz Biotechnology: sc-65742	1/200
Anti-Top2	Mouse	Santa Cruz Biotechnology: sc-65743	1/200
Anti-β-Actin	Mouse	Santa Cruz Biotechnology: sc-47778	1/500
Anti-β-Actin	Mouse	Thermo Fisher: AM4302	1/1000
Anti-α-Tubulin	Mouse	Santa Cruz Biotechnology: sc-8035	1/200
Anti-α-Tubulin	Mouse	Cell signaling: 3873s	1/100
Anti-p21	Mouse	Santa Cruz Biotechnology: sc-6246	1/250
Anti-p21	Mouse	Novus Biologicals: NBP2-29463	1/500
Anti-GAPDH	Mouse	Santa Cruz Biotechnology: sc-47724	1/200
Anti-β-Tubulin	Mouse	Santa Cruz Biotechnology: sc-365791	1/200
Anti-Actin	Mouse	Developmental Studies Hybridoma Bank (JLA20)	1/80
Rabbit anti-mouse immunoglobulins HRP	Rabbit	Dako: P0260	1/1000
Donkey anti-rabbit IgG HRP	Donkey	Novus Biologicals: NB7185	1/5000

Table 2.2 Antibodies for immunohistochemistry applications

Name	Host	Supplier and product number	Dilution
Anti-Top2B	Rabbit	Novus Biologicals: NBP1-89527	1/500
Anti-Top2	Mouse	Santa Cruz Biotechnology: sc-65742	1/200
Rabbit IgG isotype control	Rabbit	Novus Biologicals: AB-105-C	1/500
Alexa Fluor 488 anti-H2A.X	Mouse	Biolegend: 613406	1/100
Goat anti-rabbit IgG FITC	Goat	Novus Biologicals: NBP2-30342	1/100
Alexa Fluor 488 Goat anti-rabbit IgG	Goat	Jackson Immuno Research: 111-545-003	1/200
Alexa Fluor 488 Goat anti-mouse IgG	Goat	Thermo Fisher: A32723	1/100
Goat anti-mouse IgG FITC	Goat	Sigma-Aldrich: F0257	1/200

2.1.2 RT-qPCR

Table 2.3 Primers for RT-qPCR

Primer	Supplier	Sequence
Drosophila Top2	Eurofins	Forward: AGACACCACCGTTCGCTTTG Reverse: ACAGCGTCGTGGTAAGTTG
Drosophila Cyp1	Eurofins	Forward: TCAGCGTGCAGTGTGAATAGG Reverse: GTTGTCGGCGGTCATATCAAA
Drosophila eIF-1A	Eurofins	Forward: AAGAATCGTCGTCGTGGTAAGA Reverse: CTGCGCGTACTCCTGTTGG

Mouse Top2B	Eurofins	Forward: TGGGTGAACAATGCTACAAA Reverse: TGTATGTATCAGGACGAAGGA
Mouse β-Actin	Eurofins	Forward: GCTCTTTTCCAGCCTTCCTT Reverse: CGGATGTCAACGTCACACTT
Mouse GAPDH	Eurofins	Forward: CACATTGGGGGTAGGAACAC Reverse: AACTTTGGCATTGTGGAAGG

2.1.3 Reagents

Table 2.4 Reagents

Name	**Supplier and product code**
PrecisionPLUS qPCR master mix with SYBR green	Primer Design: PPLUS-SY
Precision Plus Protein Dual Colour Standards	Bio-rad: 1610374
PCR water: Ultra-pure 18.2MΩ DNase/RNase-free H_2O	Bioline: BIO-37080
Bradford reagent	Sigma-Aldrich: B6916
Agarose, low melting point, analytical	Promega: V2111
Tris Base	Thermo Fisher: BP152
p-Coumaric acid	Sigma-Aldrich: C9008
Luminol	Sigma-Aldrich: A8511
Phenylmethanesulfonyl fluoride solution (PMSF)	Sigma-Aldrich: 93482
Acetic Acid	Thermo-Fisher: 10171460
Hydrogen peroxide solution 30 % (w/w) in H2O	Sigma-Aldrich: H1009
Deoxyribonuclease I from bovine pancreas (DNase)	Sigma-Aldrich: D4263-5VL
Acrylamide/Bisacrylamide 30% solution	Sigma-Aldrich: A3699
Triton X-100	Sigma-Aldrich: T8787
Sodium chloride	Sigma-Aldrich: S7653
Glycerol	Melford: G22020
Glycine	Sigma-Aldrich: G8898
Agarose	Melford: A20090
N,N,N',N'-Tetramethylethylenediamine (TEMED)	Melford: T18000
Paraformaldehyde	Sigma-Aldrich: P6148
Fluoroshield with DAPI	Sigma-Aldrich: F6057

Ethylenediaminetetra-acetic acid (EDTA), disodium salt dehydrate	Melford: E57020
Sodium Dodecyl Sulphate (SDS)	Melford: B2008
Potassium ferricyanide (III)	Sigma-Aldrich: 702587
Potassium ferrocyanide	Sigma-Aldrich: P3289
β-Mercaptoethanol	Sigma-Aldrich: M-6250
Bovine serum albumin	Sigma-Aldrich: A2153-50G
Bromophenol blue	Sigma-Aldrich: 11439
Methanol	Thermo Fisher: M/4000/PC17
Ethanol	Thermo Fisher: M/4450/15
Ammonium persulfate (APS)	Thermo Fisher: 17874
Citric acid	Sigma-Aldrich: 251275
Brilliant Blue R	Sigma-Aldrich: B7920
Sodium phosphate dibasic	Sigma-Aldrich: S7907
Sodium hydroxide	Thermo Fisher: 10502731
Magnesium chloride	Sigma-Aldrich: M8266
X-Gal	Thermo Fisher: R0404

2.1.4 Cell culture reagents

Table 2.5 Reagents used in cell culture

Name	**Supplier and product code**
DMEM GlutaMAX	Gibco: 21885-025
DMEM/F12 GlutaMAX	Gibco: 2113894
Foetal Bovine Serum (FBS)	Gibco: 10500-064
Trypan Blue Solution, 0.4%	Gibco: 15250061
Penicillin-Streptomycin (5000 U/mL-5000 μg/mL)	Gibco: 15070063
Trypsin-EDTA (0.5%)	Gibco: 15400054
Dimethyl Sulfoxide (DMSO)	Sigma-Aldrich: D8418
all-trans-Retinoic acid (RA)	Thermo Fisher: 207341000

2.1.5 Special consumables

Table 2.6 Special consumables

Name	Supplier and product code
T25 culture flask	Greiner Bio-One: 690175
T75 culture flask	Greiner Bio-One: 658175
6 well plate	Greiner Bio-One: 657160
12 well plate	Greiner Bio-One: 665180
24 well plate	Greiner Bio-One: 662160
96 well plate	Greiner Bio-One: 655180
5 ml graduated pipette	Greiner Bio-One: 606180
10 ml graduated pipette	Greiner Bio-One: 607180
25 ml graduated pipette	Greiner Bio-One: 760180
Colourcoat adhesion positively charged microscope slides	Cellpath: MDB-0106
Histobond+ slides	Marienfeld Superior: 0810721
Thin blot paper filter paper	Bio-Rad: 1620118
0.45 µm Nitrocellulose blotting membrane	Amersham protran: 10600002
10 µl Manual Filter Tips Featuring Chem-Resin	Biotix: M-0009-9FC
20 µl Manual Filter Tips Featuring Chem-Resin	Biotix: M-0021-9FC
1250 µl Manual Filter Tips Featuring Chem-Resin	Biotix: M-1251-9FC
Cryospray	Cellpath: KNA-0173-00A
Eppendorf DNA/RNA LoBIND S/L tubes 1.5 ml	Sigma-Aldrich: Z666548

2.1.6 Commercially available kits and products

Table 2.7 Commercially available kits and products

Name	Supplier and product code
Avidin/Biotin blocking kit	Vector: SP-2001
Peroxidase substrate kit DAB	Vector: SK-4100
Vectastain ABC kit peroxidase IgG	Vector: PK-4001
Mini protean 3 system glass plates	Bio-Rad: 1653312
Mini Trans-Blot Electrophoretic Transfer Cell	Bio-Rad: 170-3930
Aurum^{TM} Total RNA mini kit	Bio-Rad: 7326820
qPCRBIO cDNA synthesis kit	PCR Biosystems: PB30.11-10
Senescence Cells Histochemical Staining Kit	Sigma-Aldrich: CS0030

2.1.7 Buffers and solutions

All buffers and solutions were made up in H_2O unless stated otherwise.

Table 2.8 Buffers and solutions

Name	Composition
10x Phosphate buffered saline (PBS)	1.37 M NaCl, 27 mM KCl, 0.1 M Na_2HPO_4, 18 mM NaH_2PO_4.
4x SDS-PAGE Loading buffer	20% (v/v) glycerol, 4% (w/v) SDS, 25% (v/v) stacking gel buffer, 10% (v/v) βmercaptoethanol, 5% (v/v) H_2O, trace bromophenol blue.
10x SDS-PAGE running buffer	250 mM Tris, 1.92 M Glycine, 1% (w/v) SDS.
SDS-PAGE stacking gel buffer	0.25 M Tris-HCl pH 6.8.
SDS-PAGE stacking gel solution	6 ml stacking gel buffer, 3.7 ml H_2O, 2 ml 30% acrylamide, 120 µl 10% SDS, 120 µl 10% APS, 60 µl TEMED.
SDS-PAGE separating buffer	0.75 M Tris-HCl pH 8.8.

7.5 % SDS-PAGE separating gel solution	7.5 ml separating buffer, 3.75 ml 30% acrylamide, 3.45 ml H_2O, 150 µl 10% SDS, 100 µl 10% APS, 50 µl TEMED.
1x Wet western transfer buffer	25 mM Tris-HCl pH 8.3, 192 mM glycine, 20% (v/v) Methanol, 0.1% (w/v) SDS.
Enhanced chemiluminescence (ECL) solution	45 µl coumaric acid (1.5% w/v in DMSO), 100 µl luminol (4.4% w/v in DMSO) in 10 ml 100 mM Tris-HCL pH 8.5 combined with 6 µl H_2O_2 in 10 ml 100 mM Tris-HCl pH 8.5.
5x Tris Buffered Saline (TBS)	100 mM Tris-HCl pH 7.5, 2.5 M NaCl.
TBST	1x TBS, 0.05% (v/v) Tween20.
Deoxyribonuclease I, standardised vial containing 2,000 Kunitz units of DNase I (Sigma-Aldrich)	500 µl 0.15 M NaCl, 500 µl glycerol (store at -20°C).
Buffer I	111 mM Tris-HCl pH 7.4, 0.56% (w/v) SDS, 22.2 mM $MgCl_2$.
Whole Cell Extraction Buffer	50% (v/v) DNase I, 45.2% (v/v) Buffer I, 50 µg/ml RNase, 2 µg/ml pepstatin, 2 µg/ml leupeptin, 1 mM dithiothreitol (DTT), 1 mM benzamidine, 1 mM phenylmethylsulfonyl fluoride (PMSF).
Mild stripping buffer	200 mM glycine, 0.1% SDS (w/v), 1% Tween20, adjusted to pH 2.2.
Drosophila lysis buffer (1)	1% (v/v) Triton X-100, 2 µg/ml pepstatin, 2 µg/ml leupeptin, 1 mM DTT, 1 mM benzamidine, 1 mM PMSF, made up in 10 ml PBS.
Drosophila lysis buffer (2)	50 mM Tris-HCl pH 7.5, 1.5 mM MgCl, 125 mM NaCl, 0.5% (v/v) Triton X-100, 5% (v/v) glycerol, 2 µg/ml pepstatin, 2 µg/ml leupeptin, 1 mM DTT, 1 mM benzamidine, 1 mM PMSF.

10x Tris/acetic acid/ EDTA buffer (TAE)	0.4 M Tris-HCl, 1.142% (v/v) glacial acetic acid, 10 mM EDTA pH 8.0.
Coomassie Blue Stain	45% (v/v) Methanol, 45 % (v/v) H_2O, 10% (v/v) glacial acetic acid, 0.004% (w/v) Brilliant Blue R.
Coomassie Blue de-stain	45% (v/v) Methanol, 45% (v/v) H2O, 10% (v/v) glacial acetic acid.
Tris/EDTA buffer (TE)	10 mM Tris-HCl pH 8.0, 1 mM EDTA pH 8.0.
Comet lysis buffer	2.5 M NaCl, 0.1 M EDTA, 10 mM Tris-HCl, adjust to pH 10.0. 1ml Triton X-100 added immediately before use.
Comet electrophoresis buffer	0.3 M NaOH, 1 mM EDTA.
Comet neutralising buffer	0.4 M Tris-HCl pH 7.5.
Senescence-associated β-galactosidase staining solution	1 mg/ml X-Gal, 40 mM citric acid, 40 mM sodium phosphate dibasic, 5 mM potassium ferrocyanide pH 6.0, 5 mM potassium ferricyanide pH 6.0, 150 mM NaCl, 2 mM $MgCl_2$.
PTN buffer	0.1M Sodium Phosphate pH 7.2, 0.1% Triton-X-100
KCM+T	120 mM KCl, 20 mM NaCl, 10 mM Tris-HCL pH 8.0, 1 mM EDTA, 0.1% Triton X-100.

2.1.8 Cell lines

Table 2.9 Cell lines

Name	**Obtained from**
SH-SY5Y. Human neuroblastoma.	Newcastle University
CAD (cath. a-differentiated). Murine catecholaminergic neuronal tumour.	Durham University

2.2 Methods

2.2.1 *Drosophila* work

2.2.1.1 Preparing food vials

2 g of Plain White Medium (*Drosophila* quick mix 173202 Blades biological Ltd) was added to a *Drosophila* vial (Regina industries drosophila vials P1014). 8 ml of H_2O (food vials can be prepared using laboratory tap water) was pipetted into the vial. The vial was gently tapped on the lab bench to prevent air pockets from forming in the food mix and was then left for 30-60 seconds to set before placing a stopper in the vial.

2.2.1.2 Transferring *Drosophila* to new vials

Drosophila (Dahomey strain) that needed to be transferred to new vials containing fresh food were selected. *Drosophila* were tapped to the bottom of their current vial, the stopper was removed quickly and both index and middle fingers were placed over the open vial to prevent *Drosophila* escaping. *Drosophila* were tapped to the bottom of the vial once again and a new vial containing fresh food was inverted and quickly placed on top of the opening of the vial containing *Drosophila*. The vials were held together and inverted so that the new vial was now on the bottom. The vials were tapped on the lab bench to transfer *Drosophila* from the old vial into the new vial containing fresh food and then a stopper was quickly placed in the vial.

2.2.1.3 Environmental conditions

Drosophila were housed in a Percival AR36L3 Environmental Chamber on a 12 hour light/dark cycle at 24°C with 60% relative humidity.

2.2.1.4 Anaesthetising *Drosophila*

It was necessary to anaesthetise *Drosophila* to aid physical manipulation of individual flies. In order to do this two methods were used. *Drosophila* were anaesthetised using either CO_2 or ice.

2.2.1.4.1 Carbon Dioxide anaesthetisation

A vial containing *Drosophila* was selected and tapped to move flies towards the stopper. This was done to prevent flies from getting stuck in the food once they were anaesthetised. A blunt fill needle, which was attached to a CO_2 cylinder via a flexible plastic tube (Figure 2.1A), was inserted between the rim of the vial and the stopper. CO_2 was then released into the vial for 5-10 seconds to anaesthetise the flies. Once fully anaesthetised, flies were tipped out of the vial onto a CO_2 pad (Figure 2.1B) and could

subsequently be processed. *Drosophila* were kept under CO_2 anaesthesia for no longer than 30 minutes to prevent any longer lasting side effects (Bartholomew *et al*., 2015).

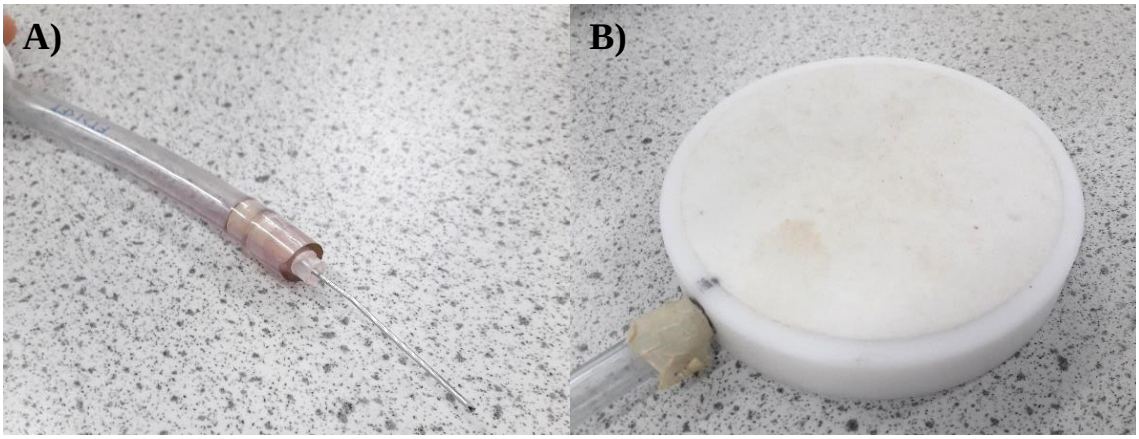

Figure 2.1 CO_2 apparatus used for *Drosophila* anaesthetisation.

(A) A blunt fill needle was attached to a CO_2 cylinder via a flexible plastic tube. (B) CO_2 pad composed of a semi-permeable plastic that allowed *Drosophila* to be physically manipulated while anaesthetised.

2.2.1.4.2 Ice anaesthetisation

Alternatively, flies were anaesthetised by cooling. *Drosophila* were transferred to an empty vial containing no food and a stopper was added. The vial was then placed in crushed ice and after approximately 1 minute *Drosophila* became incapacitated. Once incapacitated, *Drosophila* were processed.

2.2.1.5 Sexing *Drosophila*

Where experiments were carried out on male and female D*rosophila* separately, male and female flies were identified and reared in separate vials.

Vials of flies were selected and anaesthetised using CO_2 as described previously (2.2.1.4.1). Flies were viewed under a stereomicroscope (GXM-XTL3101) and then picked up using fine forceps and sorted into male and female groups. *Drosophila* have a number of observable features that make this possible. Males are typically smaller than females and possess a more rounded abdomen. The colouration of *Drosophila* also distinguishes them. On the dorsal side of the abdomen females display a dark narrow band on each abdominal segment, whereas males display uniformly dark colouration on

their rearmost abdominal sections. Males also have dark, rounded genitalia that are visible ventrally, compared to females that have pale, pointed genitalia (Figure 2.2).

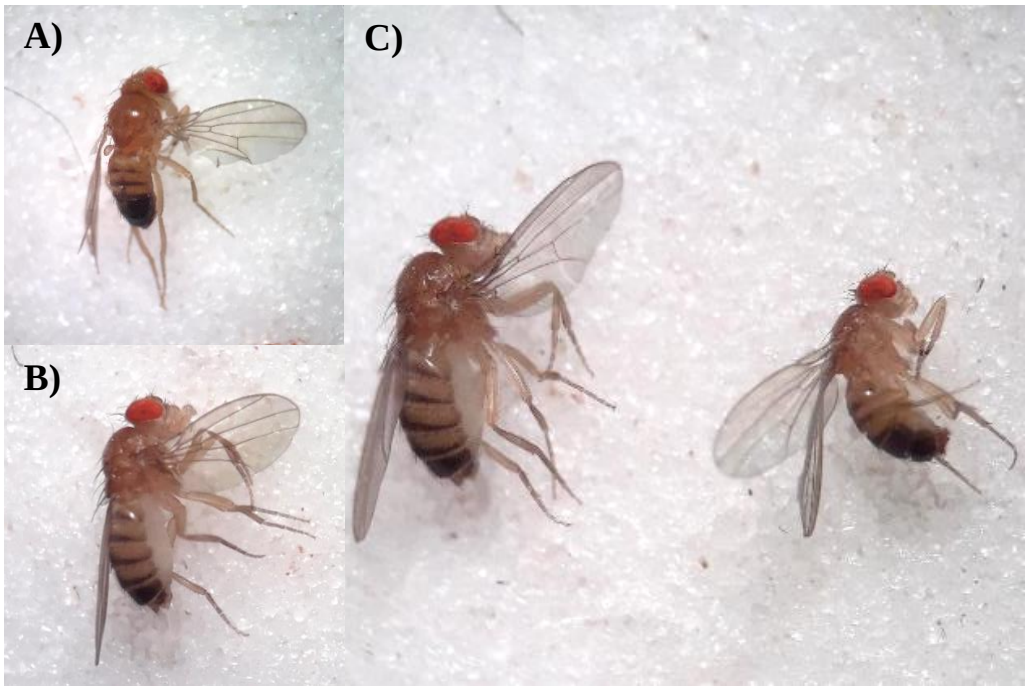

Figure 2.2 Differences in male and female *Drosophila* anatomy.

(A) Adult male fly displaying uniformly dark patterning of lower abdomen. (B) Adult female fly displaying dark narrow banding pattern on lower abdomen. (C) Comparison of male (Right) and female (Left) *Drosophila*.

2.2.1.6 Ageing *Drosophila*

Mixed populations of *Drosophila* were kept in vials for 1-3 days to allow flies to mate and eggs to be laid. Flies were then removed after this period and vials were placed back in the incubator. *Drosophila* eclose between 12-14 days. New progeny were collected within 24 hours of eclosion and placed in a new vial containing fresh food. After 24 hours flies were sorted into male and female groups as stated in 2.2.1.5 and placed into new vials. Flies were transferred into new food vials (2.2.1.2) every week to avoid food from becoming dehydrated but to also help prevent food from becoming contaminated and affecting the population within a vial. Female D*rosophila* store sperm after mating and continue to lay eggs long after physical separation from male flies. It is therefore important to transfer female flies to new vials regularly to prevent new progeny from eclosing and spoiling the ageing uniformity of the population. Flies were

aged in this manner until they were required for experimentation. The age of the flies was recorded in days and was accurate within 24 hours (day of initial collection after eclosion was recorded as day 1).

2.2.1.7 *Drosophila* head dissection

A vial of flies were selected and anaesthetised on ice (2.2.1.4.2). An area of crushed ice within the ice box was flattened down for a petri dish to be placed. The petri dish was left for 1 minute on the ice to cool down before anaesthetised flies were tipped into it. One hand was used to hold an individual fly steady by closing fine forceps around the fly's thorax while the other hand was used to remove the head by cutting at the neck using a scalpel. Heads were transferred to a microfuge tube containing 1 ml phosphate buffered saline (PBS) with protease inhibitors (2 µg/ml pepstatin, 2 µg/ml leupeptin, 1 mM DTT, 1 mM benzamidine, 1 mM PMSF) and then either used immediately for experimentation or stored in a -80°C freezer for later use. Heads were stored at -80℃ for no longer than 1 month to preserve protein integrity.

2.2.1.8 *Drosophila* brain dissection

A vial of flies were selected and anaesthetised on ice (2.2.1.4.2). Flies were then transferred and submerged in a dish containing 70% ethanol (v/v) for approximately 30 seconds. This dewaxes the cuticle of the flies and prevents air bubbles from adhering to them once they have been immersed in PBS dissecting solution. After ethanol submersion, flies were dabbed onto a paper towel to remove excess ethanol before being placed in a petri dish containing ice chilled 1x PBS under a stereomicroscope (GXM-XTL3101). Using a set of fine forceps in each hand a fly was selected and held at the thorax using one hand, whilst the other hand removed the head from the body by grasping the neck and pulling the head away from the body. All dissection work was performed while keeping the fly fully submerged in PBS. Once the head had been removed the rest of the body was discarded. To maintain brain integrity it was important to not release the head and allow it to float to the surface of the petri dish. This can make grasping the head difficult without damaging the brain. After this, the second set of forceps was used to grasp the base of the proboscis and remove it. The head was then pinned to the bottom of the petri dish using the forceps, being careful not to damage the brain. When the proboscis is removed, a small hole is visible. Using this hole the medial edge of one of the eyes was grasped and gently pulled laterally until the eye was removed. Care was taken to avoid damaging the optic lobe. This was then repeated for the remaining eye. After this step it was relatively simple to remove the brain from the

remaining structures of the head by gently grasping and peeling back the frons to expose the brain. Any remaining pieces of the retina were removed from the optic lobes once the brain had been removed. Removing any visible trachea was also important during dissection as these structures can fill with air and cause the brain to float, which can impair any subsequent immunostaining procedures. Once fully dissected, brains were transferred to a microfuge tube containing PBS with protease inhibitors (2 µg/ml pepstatin, 2 µg/ml leupeptin, 1 mM DTT, 1 mM benzamidine, 1 mM PMSF) using a P20 pipette. PBS was drawn up and down the pipette tip to coat the surface of the tip prior to transferring the brain. This prevents the brain from sticking to the inner surface of the pipette tip. Brains were either used immediately for subsequent immunohistochemical experiments or pooled together and frozen down at -80°C in PBS with protease inhibitors to be used at a later date for protein extractions. Brains were stored at -80°C for no longer than 1 month to preserve protein integrity.

2.2.1.9 Protein extraction from *Drosophila*

Whole flies, heads or brains were placed into a 1.5 ml microfuge tube. In microfuge tubes of *Drosophila* heads and brains that had previously been pooled and frozen at -80°C, the tubes were thawed and as much of the PBS with protease inhibitors was removed prior to protein extraction.

Either *Drosophila* lysis buffer 1 or 2 was added to a microfuge tube containing whole flies, heads or brains. The volume of lysis buffer added to the microfuge tube varied depending on the number of whole flies, heads or brains. Enough volume was added so that flies could be crushed easily. After the addition of lysis buffer, *Drosophila* tissue was crushed and homogenised using a pellet pestle (Sigma Z359947) for approximately 10 seconds. To aid lysis, samples were freeze/thawed in liquid nitrogen. Samples were added to liquid nitrogen for 30 seconds before being removed and crushed once again using a pellet pestle. Samples were freeze/thawed 3 times before being centrifuged at 16000 g for 5 minutes at room temperature. After centrifugation, the supernatant was transferred to a new microfuge tube and either used immediately for downstream experiments or frozen at -80°C for no longer than 1 month.

2.2.1.10 Immunofluorescent staining of *Drosophila* brains

Drosophila brains were immunofluorescently stained using two methods;

1. *Drosophila* brains were dissected (2.2.1.8) and pooled in groups of 5-10 in 1.5 ml microfuge tubes. Isolated brains were fixed in 4% paraformaldehyde/PBS for 30 minutes at room temperature. Samples were quickly washed 3 times in wash solution (PBS, 0.1% Triton X-100, 0.1% Tween 20) and then blocked for 1 hour at room temperature in blocking solution (0.1 M Tris·Cl pH 7.5, 0.15 M NaCl, 0.1% Triton X-100, 10% heat-inactivated FBS). Blocking solution was removed and brains were incubated in primary antibody diluted in blocking solution at 4°C overnight. Brains were quickly washed again 3 times in wash solution and incubated in fluorescent secondary antibody for 1 hour at room temperature. Microfuge tubes containing brains were wrapped in tin foil to protect the samples from light and prevent photo-bleaching. Brains were again washed 3 times before being mounted on microscope slides with DAPI-containing mounting medium (Vectashield). Brains were transferred from microfuge tube to a microscope slide using a P200 pipette. Once on the microscope slide, a paper towel was used to carefully dab away excess wash solution from around the brains. Using a set of fine forceps the brains were moved and positioned in a grid pattern. A drop of DAPI-containing mounting media was then added to the centre of the microscope slide before a cover slip was gently lowered and placed over the brains. The edge of the cover slip was then sealed with clear fingernail polish and the brains were viewed using fluorescence microscopy.
2. *Drosophila* brains were dissected (2.2.1.8) and pooled in groups of 5-10 in 1.5 ml microfuge tubes. Isolated brains were fixed in 4% paraformaldehyde/PTN for 30 minutes at room temperature with gentle rocking. Samples were quickly washed 2 times in PTN buffer and then washed 3 times for 20 minutes in PTN buffer with gentle rocking. After the final wash, brains were blocked for 30 minutes in blocking solution (0.1M Sodium Phosphate, pH 7.2, 0.1% Triton-X-100, 5% Normal Goat Serum) at room temperature with gentle rocking. Blocking solution was removed and brains were incubated in primary antibody diluted in blocking solution at 4°C with gentle rocking for 72 hours. Brains were quickly washed again 2 times in wash solution and then washed 3 times for 20 minutes at room temperature with gentle rocking. The wash solution was removed and the brains were incubated in fluorescent secondary antibody for 3

hours at room temperature with gentle rocking. After the addition of the fluorescent secondary antibody, microfuge tubes containing brains were wrapped in tin foil to protect the samples from light and prevent photo-bleaching. After incubation with the secondary antibody the brains were quickly washed 2 times in wash solution and then washed 3 times for 20 minutes at room temperature with gentle rocking. After the final wash, brains were mounted on microscope slides as described in the first method.

2.2.1.11 Fluorescence microscopy

Whole D*rosophila* brains were imaged using a Leica DM500 fluorescence microscope. Images were captured under A filter cube (320 nm-380 nm excitation filter and 425 nm emission filter) and I3 filter cube (450 nm-490 nm excitation and 515 nm emission filter) settings to show respective antibody staining. Both individual and overlay images were acquired.

2.2.1.12 Measuring *Drosophila* longevity

To measure *Drosophila* longevity flies were added to food vials within 24 hours of eclosion, 20 flies per vial. Male, female and mixed populations of flies were added to vials respectively. Every 3 days the vials were monitored and the number of flies that had died was recorded. Vials were analysed like this until all flies had died. Flies were transferred to new food vials twice every week. Survivorship was calculated by dividing the number of living flies at each time point by the total number of flies used in the experiment.

2.2.1.13 Measuring Advanced Glycation End-Products (AGEs)

Male and female flies were aged up to 5, 30 and 50 days old, respectively. 20 flies from each group were anaesthetised on ice and then transferred to 1.5 ml microfuge tubes. 1 ml of PBS containing 5 mg/ml trypsin and 10 mM EDTA was added to each microfuge tube and flies were quickly crushed using a pellet pestle until homogenised. The microfuge tubes of fly homogenate were wrapped in tin foil and incubated at 37°C for 24 hours. After 24 hours homogenates were centrifuged at 11000 g for 5 minutes. The supernatant was removed and transferred to a new microfuge tube before being centrifuged at 11000 g for a further 5 minutes to remove as much chitin and debris as possible. The supernatant was transferred to a new 1.5 ml microfuge tube and then diluted to an absorbance between 0.02-0.05 at 365 nm (Cecil CE 1011

spectrophotometer). This dilution step is important to ensure that the sample stays within the linear range of fluorescence, which helps to prevent any quantification problems that may occur due to the inner-filter effect. Diluted homogenate was aliquoted into a 96-well plate (200 µl per well) and fluorescence was measured at excitation and emission wavelengths of 365 nm and 440 nm respectively using a Tecan Spark 10M multimode microplate reader.

2.2.1.14 *Drosophila* climbing assays

Locomotor function of *Drosophila* was analysed using climbing assays. Flies were grouped into males and females aged 5, 30 and 50 days old, respectively. 20 flies from each group were anesthetised on ice and then transferred to a 250 ml graduated cylinder. The opening of the cylinder was sealed with parafilm and the flies were then left for half an hour to wake up and acclimatise. Target lines were marked on the cylinder 10 cm and 17 cm from the bottom. Flies were tapped to the bottom of the cylinder and then a timer was started. The number of flies that crossed each target line was recorded every 10 seconds for 2 minutes.

2.2.2 Mammalian cell culture

2.2.2.1 General culturing procedure

All cells were incubated and grown at 37°C with 95 % (v/v) air, 5 % (v/v) CO_2 and >93% relative humidity (Thermo Scientific Heracell VIOS 160i). All cell culture procedures were performed in a Class II cell culture hood under sterile conditions. Before and after each use of the culture hood 70% (v/v) ethanol was used to sterilise all interior surfaces. All equipment entering the hood was also sterilised with 70% (v/v) ethanol.

2.2.2.2 Reviving cryopreserved cells

Frozen stocks of cell lines stored in cryovials at -150°C were revived by thawing rapidly in a 37°C water bath. The thawed cells were added to 5 ml of pre-warmed culture media and mixed. Cells were then centrifuged (Thermo Scientific, Heraeus Megafuge 16) at 1500 rpm for 3 minutes to pellet the cells. The supernatant was then removed and the cell pellet was resuspended in 12 ml of fresh culture media and then pipetted into a T75 culture flask and incubated, as above, to allow the cells to proliferate.

2.2.2.3 Subculturing cells

For the SH-SY5Y cell line, the method of subculturing cells was as follows;

Once a flask of cells had reached 80-90% confluency, the media was removed from the culture flask and discarded. Cells were then washed with PBS. Enough PBS was added to cover the surface of the tissue culture flask before gently rocking the flask. The PBS was removed before the addition of trypsin-EDTA to the flask. Again, enough trypsin-EDTA was added to ensure that the cells were covered. The flask was then placed in the 37°C incubator. The time taken to optimally trypsinise each cell line was determined empirically as both the cell line and confluency of the flask can implicate the time taken for adherent cell lines to detach from the bottom of a cell culture flask. Flasks were initially checked after 2 minutes of incubation to see if cells had detached and then every 30 seconds after that. The side of the flasks were hit with the palm of the hand to encourage detachment from the surface of the flask. When the majority of cells had detached, the flask was returned to the cell culture hood and fresh media was added to halt trypsinisation. When using T25 culture flasks, 5 ml of fresh media was added and when using T75 culture flasks, 10 ml of fresh media was added. The resuspended cells were pipetted into a falcon tube and centrifuged at 1500 rpm for 3 minutes. The supernatant was removed and cells were resuspended in fresh media and diluted 1 in 5 before being added to new cell culture flasks and returned to the 37°C incubator.

A trypsinisation step was not necessary for the CAD cell line as they were weakly adherent to the surface of the cell culture flask. Instead, they detached simply by removing media from the flask and forcefully pipetting fresh media onto the surface of the culture flask. Media was pipetted up and down to ensure the majority of cells were detached. Resuspended cells were diluted 1 in 5 and then added to new cell culture flasks.

2.2.2.4 Cryopreservation

A T75 flask of cells was grown until it had reached ≥80% confluency. Cells were then detached from the surface of the culture flask using the previously described subculturing method (2.2.2.3) and centrifuged to create a cell pellet. The supernatant was discarded and a freezing medium was prepared containing 90% (v/v) fresh cell culture media and 10% (v/v) DMSO. 4 ml of freezing medium was added to cells harvested from a T75 culture flask and resuspended to yield a concentration of ~ 1 x 10^6 cells/ml. The cell suspension was aliquoted into cryogenic storage vials, adding 1 ml to

each. The cryovials were then placed in a Mr Frosty freezing container (Thermo Fisher Scientific, catalogue 5100-0001). These containers slow down the freezing process to -1°C/min when placed in a -80°C freezer. The Mr Frosty freezing container was placed in a -80°C freezer for 24 hours. After 24 hours the cryovials were removed from the -80°C freezer and transferred to a -150°C freezer for long term storage.

2.2.2.5 Culturing SH-SH5Y

SH-SY5Y cells were cultured in complete DMEM that contained media supplemented with 10% (v/v) FBS, 45 U/ml of penicillin and 45 U/ml of streptomycin. SH-SY5Y cells were subcultured twice per week.

2.2.2.6 Culturing CAD cells

CAD cells were cultured in complete DMEM/F12 that contained media supplemented with 10% (v/v) FBS, 45 U/ml of penicillin and 45 U/ml of streptomycin. CAD cells were subcultured twice per week.

2.2.2.7 Differentiating cells

2.2.2.7.1 Differentiating SH-SY5Y cells

SH-SY5Y cells were differentiated through exposure to all-*trans* retinoic acid (RA). Two different techniques were used to induce differentiation;

1. Culture flasks were seeded at 1 x 10^5 cells/ml in complete DMEM and incubated for 24 hours. Media was removed and replaced with fresh complete DMEM containing 0.5 µM or 1 µM RA and incubated for 72 hours.
2. Culture flasks were seeded at 1 x 10^5 cells/ml in complete DMEM and incubated for 24 hours. Media was removed and replaced with fresh complete DMEM containing 10 µM RA and incubated for 24 hours. Media was removed and replaced with fresh complete DMEM containing 10 µM RA and incubated for further 48 hours.

2.2.2.7.2 Differentiating CAD cells

CAD cells were seeded at 2.5 x 10^4 cells/ml in a T25 or T75 culture flask in complete DMEM/F12 and incubated for 24 hours. After 24 hours media was removed and replaced with media minus FBS. The media was removed and replenished every 3-4 days.

2.2.2.8 Cell counting

Prior to seeding culture flasks or well-plates, cells were counted using the Trypan blue exclusion method. Cells were harvested and centrifuged at 1500 rpm for 3 minutes to create a cell pellet. The pellet was then resuspended in 1 ml of media. 8 µl of cell culture was mixed in a 1:1 ratio with 8 µl of 0.4% Trypan blue and incubated for 1 minute at room temperature. Both chambers of a glass haemocytometer were then filled with the cell culture/trypan blue solution. The haemocytometer was viewed under an inverted light microscope and the cells within one set of 16 squares were counted utilising the north-west rule. Only unstained cells were counted. The cells within the three remaining sets of 16 squares were then counted.

The following calculation was then used;

$$\frac{(\text{Number of unstained cells} \times 2)}{4} \times 10000 = \text{Number of cells/ml of cell culture.}$$

2.2.2.9 Whole cell extraction

A culture flask of cells was selected and the media was removed and discarded. Cells were harvested and centrifuged at 1500 rpm for 3 minutes to create a cell pellet. The supernatant was removed and the cells were resuspended in 1 ml phosphate buffered saline (PBS) with protease inhibitors (2 µg/ml pepstatin, 2 µg/ml leupeptin, 1 mM DTT, 1 mM benzamidine, 1 mM PMSF) and transferred to a microfuge tube. Cells were centrifuged once more and the supernatant was removed. Harvested cells were then resuspended in whole cell extraction buffer. After resuspension the microfuge tube was placed on ice for 1 hour, after which, the lysate was used immediately for experimentation or frozen down at -80°C to be used at a later date.

2.2.2.10 Protein quantification

Protein from lysates was quantified using the Bradford assay. A standard curve of proteins with a known concentration was created alongside sample analysis. Bradford reagent was aliquoted into a falcon tube and allowed to reach room temperature. Bovine serum albumin (BSA) protein standards were created, ranging from 0-1.4 mg/ml dissolved in H_2O. 5 µl of protein standard or protein sample was pipetted into an individual well of a 96-well plate alongside a blank composed of water for the protein

standard and extraction buffer for the protein sample. 250 µl of Bradford reagent was added to each well and mixed well by pipetting up and down. The 96-well plate was then incubated at room temperature for 10 minutes. After the incubation period, the absorbance of the samples was then read on a plate reader at 595 nm. A standard curve was created by plotting the net absorbance against the protein concentration of each standard used. The protein concentration of the unknown sample was then determined by comparing the net absorbance against the standard curve.

2.2.2.11 WST-1 assay

Cells were seeded in a 96-well plate in culture media at a density of 1 x 10^5 cells/ml with 100 µl added to each well. The cells were then incubated for 48 hours at 37°C, 5% CO_2. 10 µl of Cell Proliferation Reagent WST-1 (Roche- 05015944001) was then added to each well and incubated for 2 hours. The absorbance of the samples was then measured at 450 nm on a plate reader. The absorbance of the sample wells were measured against background control wells containing only culture media.

2.2.2.12 Oxidative stress induced senescence of SH-SY5Y cells

SH-SY5Y cells were subjected to hydrogen peroxide (H_2O_2) oxidative stress in order to induce senescence. Both differentiated and undifferentiated cells were exposed to a range of H_2O_2 concentrations from 10 µM to 2 mM (in complete media) to empirically determine the optimum concentration to induce senescence. Undifferentiated cells were seeded for 48 hours prior to H_2O_2 exposure and differentiated cells were exposed to H_2O_2 after following the differentiation protocol. Cells were incubated from 1-24 hours at varying H_2O_2 concentrations to determine optimum incubation times to cause cell cycle arrest and induce senescence. After each dose, media was replaced with fresh complete media. Cells were also subjected to a different number of doses ranging from a single dose up to a dose every day for 5 days.

2.2.2.13 SA-β-galactosidase staining assay

Cells were stained for β-galactosidase using two methods.

1. Cells were stained using Sigma Senescence Cells Histochemical Staining Kit (CS0030). Cells were grown in 6-well plates prior to staining. Media was removed and cells were briefly washed twice with 1 ml of PBS per well. PBS was removed carefully to ensure that the cells did not become detached. 1.5 ml of fixation buffer (F1797) was added to each well for 6-7 minutes at room

temperature. Cells were briefly washed 3 times with PBS. 1 ml of staining mixture was added to each well (1ml staining solution [S5818], 125 µl Reagent B [R5272], 125 µl Reagent C [R5147], 250 µl X-gal solution [X3753], 8.5 ml ultrapure H_2O) and incubated overnight at 37°C without CO_2. The 6-well plate was wrapped in parafilm to prevent wells from drying out. Cells were viewed under a bright field microscope and the total number of blue-stained cells was counted against total cells and the percentage of senescent (blue-stained) cells was calculated.

2. The second method used a similar protocol to the one previously described but differed in the following ways;

Kit reagents were replaced with lab-made reagents;

-Cells were fixed in 2% paraformaldehyde in PBS.

-Staining mixture consisted of 8.5 ml SA-β-galactosidase solution (150 mM NaCl, 2 mM $MgCl_2$, 40 mM citric acid, 12 mM Na_2HPO_4 in H_2O at pH 6), 1, 2, 3 or 4 mg/ml X-Gal and 1 ml of solution consisting of 50 mM potassium ferrocyanide and 50 mM potassium ferricyanide.

2.2.2.14 γH2AX assay

Differentiated CAD cells were aged to specific time points in T25 flasks prior to γH2AX assay. A sterilised 24 x 24 mm coverslip was placed in each of the wells of a 6-well plate. Differentiated CAD cells were then seeded into the 6-well plate at a density of 5 x 10^4 cells/ml (2 ml per well) and incubated at 37°C, 5% CO_2 for 24 hours. Media was removed and discarded and wells were gently washed with 0.5 ml cold PBS. PBS was removed and cells were fixed in 0.5 ml methanol at -20°C for 5 minutes. Methanol was discarded and cells were rehydrated in 3 changes of PBS (10 minutes per wash at room temperature). The final PBS wash was discarded and 0.5 ml of KCM+T buffer was added to each well for 15 minutes to permeabilise the cells. KCM+T buffer was removed and 1 ml of blocking buffer (KCM+T, 2% BSA, 10% skimmed milk powder) was added to each well for 1 hour 30 minutes at room temperature or overnight at 4°C. Blocking buffer was removed and cells were incubated in 0.5 ml anti-γH2AX antibody (1:100 dilution in blocking buffer) overnight at 4°C, ensuring the 6-well flask was wrapped in tin foil to protect the light-sensitive antibody. Cells were gently washed 3 times for 10 minutes in KCM+T buffer in reduced light conditions. A drop of Vectashield mounting media containing DAPI was placed onto a microscope slide. A

coverslip from one of the wells of the 6-well plate was placed face down onto the microscope slide. Coverslips were fixed in place with nail varnish and slides were stored in the dark at 4°C until required for analysis.

2.2.2.14.1 Imaging and analysis

Slides were viewed under a Leica DM500 fluorescence microscope and images were captured under A filter cube (320 nm-380 nm excitation filter and 425 nm emission filter) and I3 filter cube (450 nm-490 nm excitation and 515 nm emission filter) to collect images displaying both γH2AX foci and DAPI staining. Images were imported to the image processing program ImageJ. Images displaying γH2AX foci were stacked with the corresponding DAPI image and were converted to greyscale. Using the multipoint tool, γH2AX foci were counted in each individual cell. Cells were analysed based on number of γH2AX foci visible.

2.2.2.15 Comet assay

Differentiated CAD cells were aged to specific time points in T25 flasks prior to carrying out Comet assays. Microscope slides were dipped into coplin jars containing 1% standard agarose to pre-coat the slide. Excess agarose was drained off and the back of each slide was wiped clean before being dried in a warming oven.

4 x 10^4 cells were harvested and centrifuged (1500 rpm for 3 minutes) to create a pellet. The supernatant was removed and cells were washed in PBS before being centrifuged once more. The supernatant was removed and 140 µl of 1% low melting point agarose in PBS was quickly added to the cells at 37°C and pipetted up and down to thoroughly disperse cells. Two drops of cells were placed onto a pre-coated microscope slide and 18 x 18 mm coverslips were placed over each drop. The slide was refrigerated at 4°C for 5 minutes to set the agarose. 100 ml of pre-chilled Comet lysis solution was added to a coplin jar with 1 ml of Triton X-100. Coverslips were removed from the microscope slide, which was then placed into the lysis solution and incubated at 4°C for 1 hour. The slide was removed from the lysis solution and rinsed twice in dH_2O. Slides were placed in a Comet assay electrophoresis tank (CSL-COM20 5055323200281) at 4°C and the tank was gently filled with pre-chilled Comet electrophoresis buffer until the slides became submerged. Slides were incubated in this alkaline buffer for 40 minutes to allow DNA to unwind and denature, after which, the tank was run at a constant voltage setting of 21 V for 40 minutes. Slides were removed from the tank and were washed 3 times for 5 minutes in Comet neutralising buffer at 4°C before being left to air dry at room

temperature. Slides were stained with 20 µl of DAPI (1 µg/ml) and were covered with an 18 x 18 mm coverslip before viewing under a microscope.

2.2.2.15.1 Imaging and analysis.

Slides were viewed under a Leica DM500 fluorescence microscope and images were captured under A filter cube (320 nm-380 nm excitation filter and 425 nm emission filter) settings. Images were collected and processed in two ways;

- Cells were analysed manually and were sorted into one of five classes ranging from 0-4 depending on tail intensity as described by Collins *et al*. (1995). Cells with no DNA damage were given a score of 0 and cells that were highly damaged were given a score of 4.

- Images were uploaded and analysed using the automated plugin OpenComet on the image processing program ImageJ. DNA damage was analysed through comparison of tail DNA percentages.

2.2.3 Western blotting

2.2.3.1 Sample preparation

Following protein quantification samples were diluted in H_2O for each western blot experiment to ensure all samples had an equal protein concentration prior to loading on an SDS-PAGE gel. Once diluted, 12.5 µl of 4x SDS loading buffer was added to 37.5 µl of protein sample and pipetted up and down to mix thoroughly. Samples were then heated at 68°C for 5 minutes before being centrifuged at 12000 g for ~10 seconds to ensure that the entire sample had collected at the bottom of the microfuge tube.

2.2.3.2 SDS-PAGE

SDS-PAGE gels were cast using spacer plates with 1.5 mm integrated spacers (Mini-PROTEAN® 1653312). Spacer plates and short plates were placed together and clamped into a casting frame and then placed into a casting stand (Mini-PROTEAN Tetra Cell 1658007). Separation gel solution was carefully pipetted into the casting plates, avoiding bubbles. H_2O was then pipetted on top of the separation gel to help remove any remaining bubbles and to create a level surface. Once set (15-20 minutes), the H_2O was poured off the separating gel and any residual liquid was dabbed away with a paper towel. The stacking gel was then pipetted directly on top of the separating gel and a 10-well comb was slotted into position. Once set (10-15 minutes), the newly cast gel was

placed into an electrophoresis unit (Bio-Rad). The buffer atriums of the unit were filled with 1x SDS-PAGE running buffer and the 10-well comb was removed from the SDS gel. The wells in the SDS gel were flushed with running buffer using a 50 µl Hamilton syringe to remove any residual acrylamide from the well. Using the Hamilton syringe 50 µl of prepared protein sample was loaded into each well alongside 4 µl of pre-stained molecular weight markers (Bio-rad: 1610374). Gels were run at 100 V for 90-120 minutes until the bromophenol blue dye from the loading buffer had run out from the bottom of the gel.

2.2.3.3 Electrophoretic transfer of proteins

The transfer of proteins from an SDS-PAGE gel to nitrocellulose blotting membrane was carried out using a Mini Trans-Blot Electrophoretic Transfer Cell (Bio-Rad 170-3930). Prior to usage, the fibre pads of the assembly were soaked in 1x wet western transfer buffer for ~10 minutes along with two pieces of filter paper (Bio- Rad 1620118) and one piece of nitrocellulose blotting membrane (Amersham Protran 0.45 µm 10600002) that had been cut to the size of the SDS gel. Once an SDS gel had been run it was carefully removed from the two glass plates. The pre-soaked nitrocellulose blotting membrane was placed over the gel, ensuring no air pockets were present between the surface of the gel and the membrane. This was then placed between the two pre-soaked pieces of filter paper, which in turn was placed in between the two pre-soaked fibre pads. This ‘sandwich’ was placed in a gel holder cassette and slotted into the electrode module within the buffer tank. An ice pack was placed in the buffer tank, which was fully filled with refrigerator-cooled wet western transfer buffer. A current and voltage of 500 mA/100 V was applied to the electrophoretic transfer cell for 1 hour. The assembly was taken apart and the nitrocellulose membrane was carefully removed.

2.2.3.4 Immunoassay probing of nitrocellulose membrane

Nitrocellulose membranes were blocked in TBST with 3% (w/v) skimmed milk powder overnight at 4°C or 60 minutes at room temperature. The blocking solution was poured off the membrane, which was then washed three times in TBST for 10 minutes per wash at room temperature with gentle rocking. Primary antibodies were added to TBST with 3% (w/v) skimmed milk powder at optimal concentrations that were empirically determined. Nitrocellulose membranes were incubated in primary antibody solution for 2 hours at room temperature with gentle rocking. Primary antibody solution was poured off and the membrane was then washed 3 times in TBST for 5-10 minutes per wash at

room temperature with gentle rocking. Secondary antibodies were added to TBST with 3% (w/v) skimmed milk powder. Membranes were incubated in secondary antibody solution for 2 hours at room temperature with gentle rocking. The secondary antibody solution was poured off and the membrane was washed a further 3 times in TBST for 5-10 minutes.

2.2.3.5 Protein detection

Proteins on nitrocellulose membranes were detected using enhanced chemiluminescence (ECL). Membranes were submerged in ECL reagent for 1 minute and then exposed and imaged using a G-box chemiluminescent detection system (Synegene G-box chemi XX6). Analysis of blot densitometry was carried out using GeneTools (Syngene).

2.2.4 RNA work

2.2.4.1 RNA extraction

RNA was isolated using Aurum^{TM} Total RNA Mini Kit using the spin protocol. This kit was used to extract RNA from both *Drosophila* tissue and mammalian cell cultures. Samples of *Drosophila* tissue and mammalian cell culture were processed using the manufacturer's instructions apart from the sample preparation for *Drosophila* tissue.

2.2.4.1.1 *Drosophila* sample preparation

Drosophila tissue was placed in an RNase/DNase-free 1.5 ml microfuge tube. Quantities of whole flies, heads and brains required for optimal RNA isolation was determined empirically. The microfuge tube was placed in liquid nitrogen for ~30 seconds until the entire contents had frozen. The microfuge tube was removed from the liquid nitrogen and the *Drosophila* tissue was crushed using a pellet pestle (Sigma Z359947). This process was repeated a further two times to help breakdown the tissue. After the final freezing/crushing step the tissue was left to thaw. 350 µl of lysis solution was added to the microfuge tube and pipetted up and down to aid in sample disruption. The microfuge tube was then centrifuged at 12000 g for 3 minutes and the supernatant was transferred to a 2 ml capped microfuge tube. 350 µl of 60% ethanol was added to the supernatant and thoroughly mixed to ensure that no bilayer was visible.

2.2.4.2 RNA quantification

The quality and quantity of isolated RNA samples was analysed on a NanoDrop ND-1000 spectrophotometer.

2.2.4.3 cDNA synthesis

Isolated RNA samples were reverse transcribed using PCR Biosystems qPCRBIO cDNA synthesis kit (PB30.11). 4 µl of 5x cDNA Synthesis Mix, 1 µl of 20x RTase and 0.4 µg of total RNA was added to an RNase/DNase-free microfuge tube. PCR grade dH_2O (Bioline BIO-37080) was added to the microfuge tube to bring the total volume up to 20 µl and pipetted up and down to ensure all components were fully mixed. The microfuge tube was incubated at 42°C for 30 minutes followed by 10 minutes incubation at 85°C to denature the RTase. After cDNA synthesis, samples were either used immediately in downstream qPCR applications or stored at -20°C for later use.

2.2.5 RT-qPCR

All RT-qPCR experiments were carried out using a BIO RAD C1000 Thermal cycler (CFX96 Real-Time system). Each PCR reaction was pipetted into a well of a white PCR 96-well plate and comprised of 10 µl Precision PLUS qPCR Master Mix (Primer design PPLUS-SY), 0.6 µl forward primer (300 nM working concentration), 0.6 µl reverse primer (300 nM working concentration), 2 µl cDNA and 6.8 µl PCR grade H_2O. PCR reactions were run alongside a no-template control (NTC). The amplification protocol included a 2 minute enzyme activation (hot-start) at 95°C followed by 40 cycles at 95°C for 10 seconds and a 60 second data collection step at 60°C. Melt curve data were recorded and analysed to confirm the presence of a single PCR product after each run. Ct values were recorded and fold-change was calculated to determine relative gene expression (Pfaffl., 2001).

2.2.6 Mouse work

2.2.6.1 Animal collection and tissue preparation

Animal licensing was held by Dr R. N. Ranson (UK Home Office personal licence). C57BL/6 male mice samples were transported to Northumbria University for immunofluorescence labelling and microscopy analysis. See Appendix E for letter detailing ethical approval.

2.2.6.2 Tissue preparation and brain sectioning

Sections of mouse brain tissue were cut using a cryostat (Bright Instrument OTF/AS Cryostat) or a vibrating blade microtome (Leica VT1000S vibratome). Cryostat sectioning was utilised when cutting thin 12 µm sections, whereas vibratome sectioning was utilised when cutting thicker 30 µm sections.

2.2.6.2.1 Cryostat sectioning

Prior to cryostat sectioning, brain tissue was placed in a solution of PBS with 30% sucrose for 1 week at 4°C to cryopreserve tissue samples. 12 µm sections of mouse brain tissue were cut using a Bright Instrument OTF/AS Cryostat. Sections were cut sequentially and placed on Histobond+ slides (0810721), left to dry and then stored at 4°C in a cardboard microscope slide storage box to be used when needed.

2.2.6.2.2 Vibrating blade microtome sectioning

30 µm sections of mouse brain tissue were cut using a Leica VT1000S vibratome and were placed sequentially into wells of a 24-well plate containing PBS. Sections were processed immediately when using this method of sectioning.

2.2.6.3 Immunohistochemistry of brain tissue

A Histobond+ slide of cryostat-cut mouse brain sections was selected and a thin hydrophobic barrier was drawn around the brain sections using a PAP (peroxidase-antiperoxidase) pen. The sections were washed 3 times (5 minutes per wash) with 250 µl PBS per slide. Slides were covered during 5 minute washes to ensure sections did not become dehydrated. The final wash was drained off and primary blocking solution (10% normal donkey serum [NDS] in PBS) was added to the slide for 1 hour 30 minutes (250 µl per slide). The blocking solution was drained off and the edge of the slide was dabbed dry with a paper towel. The primary antibody (primary antibody, diluted in PBS with 1% NDS) was added to the sections at specified concentrations. 1% NDS in PBS was added to control slides and an isotype control (isotype control, diluted in PBS with 1% NDS) was added to another slide of sections. The slides were incubated overnight at 4°C in an incubation tray covered in tin foil. Cotton wool moistened with PBS was added to the inside edge of the tray to maintain a humid environment to prevent sections from drying out. The primary antibody was drained off and sections were washed 3 times for 5 minutes in PBS. The final wash was drained off and secondary antibody (made up in PBS) was added for 2 hours, after which the sections

were washed 3 times for 5 minutes in PBS. Autofluorescence blocking solution (2 mM copper sulphate, 50 mM ammonium acetate in dH_2O) was added to the sections for 10 minutes before being washed 4 times for 5 minutes in PBS. The final PBS wash was drained off the slide and the edges were dabbed dry with a paper towel. A drop of Vectashield containing DAPI was added onto each section and a coverslip was placed over the sections. The edges of the coverslip were sealed with nail varnish and the slides were viewed under a Leica DM500 fluorescence microscope.

2.2.6.4 Peroxidase staining of brain tissue

2.2.6.4.1 Peroxidase staining of cryostat sections

All peroxidase staining used a Vectastain ABC peroxidase rabbit IgG PK-4001 kit. A Histobond+ slide of cryostat-cut mouse brain sections was selected and a hydrophobic barrier was drawn around the brain sections using a PAP pen. Sections were briefly washed in dH_2O. A blocking solution of 0.3% H_2O_2 in methanol was added to the sections for 15 minutes to block endogenous peroxidases. Sections were washed 3 times for 5 minutes in PBS. Normal Goat serum (NGS) (3 drops pk-4001 in 10 ml of PBS) was added to sections for 1 hour 30 minutes at room temperature. Sections were then washed for 5 minutes in PBS. Avidin and biotin were blocked using Vector Avidin/Biotin Blocking Kit SP-2001. Sections were treated for 15 minutes with Avidin blocking solution and then washed for 5 minutes in PBS followed by a 15 minute treatment with Biotin blocking solution and another 5 minute wash in PBS. Primary antibody (Primary antibody, diluted in PBS with 1% NGS) was added to the sections and was incubated overnight at 4°C. Sections were washed 3 times for 5 minutes in PBS. Secondary antibody (Secondary antibody from Vectastain ABC kit) was added to the sections for 3 hours at room temperature. Sections were washed 3 times for 5 minutes in PBS. The ABC complex from the kit was added to the sections for 1 hour. Sections were washed 3 times for 5 minutes in PBS. The sections were treated with a diaminobenzidine (DAB) peroxidase substrate kit (Vector peroxidase substrate kit DAB SK-4100) following manufacturer instructions. The sections were quickly washed in dH_2O and then air dried for 48 hours. Sections were counterstained in 1% neutral red solution for 10 minutes and then washed briefly in dH_2O. Sections were dehydrated in an alcohol series (70% ethanol 5 minutes, 95% ethanol 5 minutes, 2 times 100% ethanol 5 minutes, 2 times histoclear 10-15 minutes) and then mounted in DPX. Slides were viewed under a Leica DM500 fluorescence microscope using bright field.

2.2.6.4.2 Peroxidase staining of vibratome sections

Sections from paraformaldehyde-fixed mouse brains were cut using a Leica VT1000S vibratome and were placed sequentially into wells of a 24-well plate containing PBS. Vectastain ABC peroxidase rabbit IgG PK-4001 kit and methodology from 2.2.6.4.1 was utilised apart from the following;

-Staining of sections was carried out in a 24-well plate until counterstaining step.

-Prior to counter staining, sections were mounted onto glass microscope slides and air dried for 48 hours. Counterstaining and all steps afterwards were carried out as described in 2.2.6.4.1.

2.2.7 Statistical analysis

Data in this study are presented as mean results and standard errors of the mean. ANOVA, f-tests and Student's t-tests (two-tailed) were carried out using Microsoft Excel to determine p value significance. Other methods used in this study include; log-rank tests (example calculation Appendix Figure A.1), calculating primer efficiencies (example calculation Appendix Figure A.3), calculating coefficient of variance (example calculation Appendix Figure A.6) and analysing qPCR data with one or two reference genes (example calculation Appendix Figure C.2 and Figure A.5).

3. Development of an ageing *Drosophila* model to investigate changes in Top2 expression

3.1 Introduction

Investigations into the levels of topoisomerase II in multicellular organisms throughout the ageing process is incredibly limited, with age-dependent decreases of Top2B activity in rat brains and cultures of cerebellar granule neurons reported in a limited number of studies (Kondapi *et al*., 2004; Bhanu *et al*., 2010). The focus of this chapter was to develop a model of ageing in *Drosophila* and to investigate protein and mRNA levels of Top2 throughout the ageing process. Unlike mammals, *Drosophila melanogaster* possess a single isoform of topoisomerase II (Top2) but have chromosomes that are morphologically comparable to those of vertebrates (Mengoli *et al*., 2014).

Drosophila melanogaster are one of the longest serving models of ageing with some of the first ageing experiments using *Drosophila* taking place over 100 hundred years ago (Hyde, 1913). The simplest model of ageing is an old organism and *Drosophila* possesses numerous attributes that make it an effective model of ageing. Many tissues in *Drosophila* are equivalent to those found in mammals and 77% of human genes associated with ageing-related diseases have equivalent counterparts found in tissues of *Drosophila* (Piper & Partridge, 2018). In addition to possessing a high proportion of gene homology to humans, the relatively short life span and high reproductive ability of *Drosophila* allows a continuous supply of tissue samples to be obtained to produce increased experimental output in comparison to other animal models of ageing. Adult female *Drosophila* lay up to 100 eggs every 24 hours and an adult fly emerges between 9-10 days after fertilisation (Fernández-Moreno *et al*., 2007). The life span of *Drosophila* typically ranges from 60 to 80 days depending on culturing conditions (Jennings, 2011). This short life span of *Drosophila* allows aged samples to be obtained at a much quicker rate and lower cost compared to other animal models (Piper & Partridge, 2018).

Although adult *Drosophila* only possess 100,000-150,000 neurons in their brain (Huang *et al*., 2019) compared to ~86 billion neurons found in the human brain (Herculano-Houzel, 2009), *Drosophila* are often utilised in neuroscience studies as they possess a number of neuronal structures that are equivalent to brain structures found in humans. For example, the mushroom bodies of *Drosophila,* that consist of ~2,500 neurons, are

responsible for associative learning and memory of olfactory stimuli (Akalal *et al*., 2006) and represent the equivalent brain structure to the hippocampus, which is a brain region that has major roles in learning and memory formation in humans (Figure 3.1) (Barnstedt *et al*., 2016). These brain structures make *Drosophila* suitable for studying neurodegenerative diseases such as Alzheimer's disease, which is associated with declines in memory formation and reductions in cognitive ability with particular vulnerability seen in the hippocampus at early stages of the disease (Mu & Gage, 2011). Ageing phenotypes seen in humans have similarly been observed in *Drosophila* with previous studies showing intermediate and long term memory impairments with increasing age (Tonoki & Davis, 2015). In addition to this, *Drosophila* also display reductions in locomotor ability with increasing age and have been frequently used, alongside *Drosophila* possessing mutant genes, to study Parkinson's disease. The degeneration of dopaminergic neurons is thought to play a key role in the development of Parkinson's disease (Mamelak, 2018) and *Drosophila* have been shown to possess distinct dopaminergic neurons that innervate different areas of the *Drosophila* brain (Mao & Davis, 2009) making it a versatile model when studying ageing and age-related neurodegenerative diseases (Xiong & Yu, 2018).

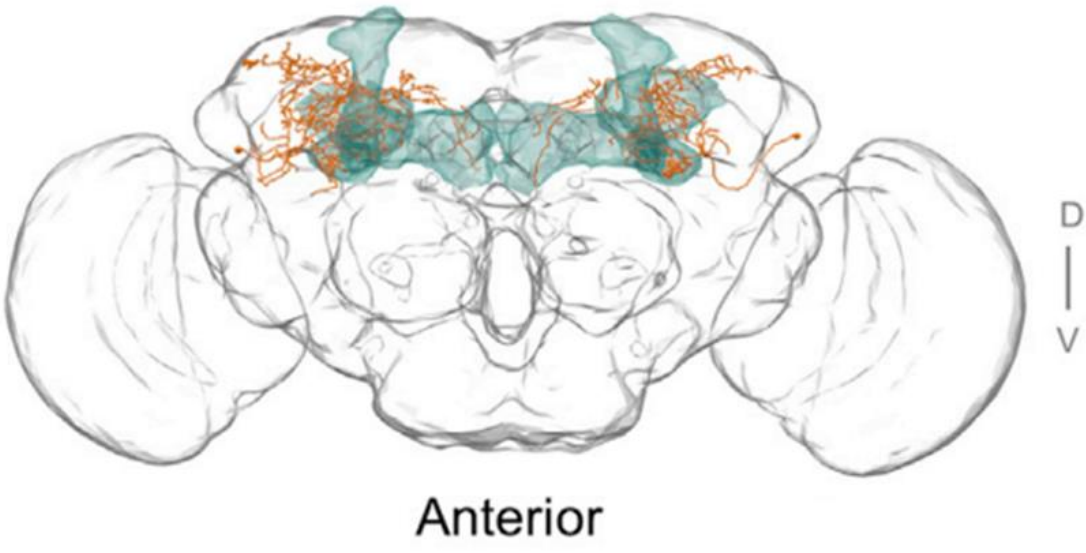

Figure 3.1 Diagrammatical representation of the *Drosophila* brain.

Anterior view of the whole *Drosophila* brain with mushroom body structures coloured green (Zheng *et al*., 2018).

As previously stated, *Drosophila* possess a single isoform of topoisomerase II but it has been shown to play very similar roles as mammalian isoforms to control the topological state of DNA by catalysing transient DSBs and allowing an intact DNA duplex to pass through the break (Hohl *et al*., 2012; Mengoli *et al*., 2014). In mammals Top2A and Top2B have been shown to demonstrate clear and distinct roles between the two isoforms (Nitiss, 2009). Unlike Top2A, the expression of *Drosophila* Top2 has not been observed to be cell-cycle dependent (Whalen *et al*., 1991). Whalen reported fluctuations of Top2 mRNA and protein throughout embryogenesis and development, whilst establishing the presence of Top2 in non-proliferating cells by carrying out immunocytochemical analysis of adult head cryosections that found Top2 to be present in all identifiable nuclei. Thus, suggesting that *Drosophila* Top2 may not be a useful marker for the proliferative state. As the presence of Top2 is not dependent on proliferation, it may suggest that the single Top2 isoform performs the roles of both Top2A and Top2B (Lee & Berger, 2019). It is thought that the single Top2 isoform in *Drosophila* is able to perform several functions through post-translational modifications such as phosphorylation (Chen *et al*., 2016). Phosphorylation has been shown to modulate interactions between Top2 and its nucleic acid substrates in *Drosophila* (Ackerman *et al*., 1985). An observed effect of Top2 modification by casein kinase II-induced phosphorylation is the considerable stimulation of its decatenation activity. As Top2 is seen to be active in mitotic cells, the cell cycle control of chromosome condensation may require phosphorylation of Top2, especially since the enzyme is seen to be more highly phosphorylated in metaphase than in G1 (Gasser *et al*., 1992). *In vitro* studies on *Drosophila* Top2 have demonstrated an enhanced ATP turnover through casein kinase II phosphorylation (Nakazawa *et al*., 2019). In addition, phosphorylation of *Drosophila* Top2 *in vitro* has been reported to enhance enzyme activity (Li *et al*., 2008). However, eliminating phosphorylation of human Top2A by casein kinase II has been seen to have no effect on catalytic activity of the enzyme (Escargueil *et al*., 2000). Top2 phosphorylation events are generally more frequent during S phase through mitosis. However, the highly divergent C-terminals of topoisomerase II enzymes are the site for many phosphorylation events. Due to this divergence it is likely there are species-specific and site-specific effects of phosphorylation on enzyme activity (Lee & Berger, 2019). The C-terminal of Top2 has also been shown to be subjected to other post-translational modifications, including sumoylation. The small ubiquitin-related modifier (SUMO) pathway has emerged as an important determinant of Top2 function with its actions shown to be important for allowing Top2 to accumulate at mitotic

centromeres. It is suggested that sumoylation promotes the final step in decatenation, allowing chromatids to disjoin efficiently (Lee & Bachant, 2009).

During *Drosophila* embryogenesis Top2 protein and mRNA levels have not been shown to be strictly correlated (Whalen *et al*., 1991). Gemkow *et al*. (2001) reported a strong correlation between Top2 mRNA transcription levels and mitotically active cells. However, an absence of Top2 mRNA in cells arrested for DNA replication was reported, whilst non-proliferating endoreplicating tissues were shown to express Top2 at a much lower level. Interestingly, it was also reported that Top2 protein levels persist in non-dividing cells, suggesting Top2 protein and mRNA levels are not directly comparable. In addition to this, Top2 protein has been detected throughout embryonic development in all regions and tissues with stable levels of chromatin-bound Top2 protein seen from the beginning of cycle 15 to the end of embryogenesis in non-replicating cells (Gemokow *et al*., 2001).

Although *Drosophila* has been extensively used in ageing and neuroscience studies, the expression of Top2 throughout the adult lifespan of *Drosophila* has not been studied to the best of our knowledge. This chapter focussed on developing a *Drosophila* model to investigate the changes in Top2 protein and mRNA levels and *Drosophila* activity through the ageing process.

3.2 Developing a *Drosophila* model of ageing

3.2.1 Longevity of *Drosophila*

To investigate Top2 expression throughout the adult lifespan of *Drosophila*, an appropriate model of ageing was required. The literature suggests that *Drosophila* have a mean lifespan between 2-3 months (Linford *et al*., 2013; Sun *et al*., 2013; Piper & Partridge, 2018). However, in order to select appropriate age groups for this study, longevity studies were carried out to determine survivorship of both male and female *Drosophila*, as well as mixed populations, under laboratory conditions. Survivorship curves are utilised most commonly to present longevity data and display the probability that an individual will survive to a given age (Linford *et al*., 2013). Results of male, female and mixed populations of *Drosophila* survivorship are shown in figure 3.2.

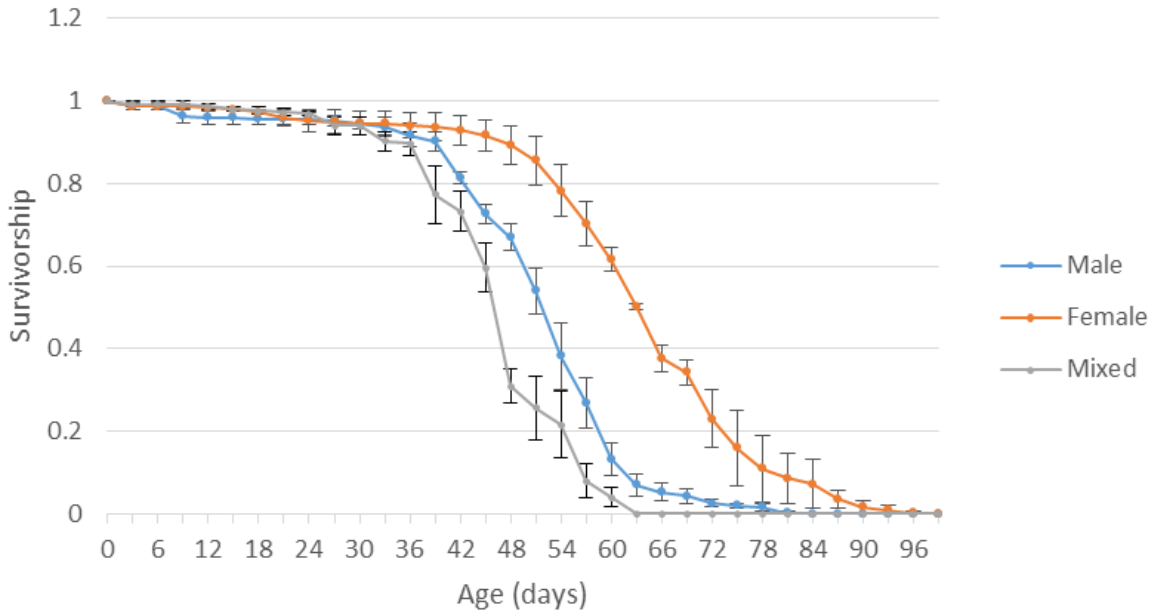

Figure 3.2 Longevity of male, female and mixed populations of *Drosophila*.

Survivorship of *Drosophila* maintained on Plain (white) *Drosophila* Medium (DTS 077) at 24°C was calculated for male, female and mixed populations of *Drosophila*. Male and female *Drosophila* were collected within 24 hours of eclosion and placed into vials (20 male/female flies per vial or 10 of each sex for mixed populations) with a total of 5 vials used for each group. All longevity assays were carried out in triplicate and are presented as the mean survivorship ± standard error. Survivorship was calculated as described in methods (2.2.1.12) and log-rank tests were carried out (see Appendix Figure A.1).

Although ageing in *Drosophila* has been extensively studied, there are relatively few studies investigating sex differences in ageing. The most extensive study focusing on sex differences in longevity demonstrated that longevity can be complex and is highly dependent on genotype, mating status and female fecundity (Malick & Kidwell, 1966). However, survivorship curves from Figure 3.2 show that under the environmental conditions described in 2.2.1.3, females can be seen to have a greater probability of surviving to an older age than male and mixed flies. Log-rank tests were carried out on the data set to compare the entire survival experience between groups and demonstrated significant differences between all three populations of *Drosophila*. Female *Drosophila* displayed the highest overall survivorship with differences between females-males and females-mixed seen to be statistically significant ($p<0.001$). Males displayed the second

highest overall survivorship and were also significantly different to the mixed population of flies ($p<0.001$), which displayed the lowest overall survivorship. Mixed populations were used initially in experiments (Figure 3.2) but extensive literature searches demonstrate numerous differences between males and females throughout the lifecycle (Hansen *et al*., 2012; Austad & Fischer, 2016; Regan *et al*., 2016). To further investigate these differences between males and females and to elucidate any sex-related differences in Top2 expression with ageing, individual analysis of male and female *Drosophila* was carried out in subsequent experiments. Rather than carrying out further experiments on just young versus old *Drosophila*, it was decided that young, middle-aged and old *Drosophila* age groups would be selected based on longevity experiments to determine age-related changes in Top2 expression throughout the ageing process. To determine the age that would be selected for the oldest age group in subsequent experiments, the point at which survivorship had reduced by half (survivorship value of 0.5) was used. Males reached a survivorship value of 0.5 at ~50 days and females reached a survivorship value of 0.5 at ~63 days. Large numbers of flies were required for subsequent experiments and the ability to collect such numbers decreased rapidly after the age of 50 days due to fly deaths, hence it was decided that flies aged 50 days old would be selected to represent an aged fly for this *Drosophila* model of ageing. Flies aged 5 days old were selected to represent a 'young' group and flies at 30 days old were selected to represent a 'middle-aged' group. *Drosophila* can be aged chronologically very easily but further experiments were required alongside longevity assays to support the selected age groups as a model of ageing.

3.2.2 Locomotor activity of ageing *Drosophila*

In addition to longevity assays, another important lifespan-related assay is the assessment of locomotor activity. The relationship between ageing and locomotor activity is well established with gradual declines in locomotor activity seen in ageing across many species including humans and *Drosophila* (Sun *et al*., 2013; Kulmala *et al*., 2014). The negative geotaxis assay is a commonly used test to assess the locomotor activity of *Drosophila.* The negative geotaxis assay, otherwise known as the climbing assay, measures locomotor activity by utilising the innate escape response of *Drosophila*. When tapped to the bottom of a container *Drosophila* instinctively begin to ascend the walls. Their ability to do this has been seen to decline with age (Iliadi & Boulianne, 2010). *Drosophila* are typically added to a vial and tapped to the bottom and the ability of the flies to climb to a target height within a given time is then measured.

Traditional climbing assays typically measure the number of flies to climb up to a target height between 2-5 cm over a 10-20 second period (Orso *et al*., 2005; Chakraborty *et al*., 2011). However, Madabattula *et al*. (2015) suggested that these parameters make the traditional assay insensitive to mild locomotor defects and therefore suggested carrying out the assay over a longer period of time and measuring the climbing ability of the flies up to a greater target height. As locomotor declines are gradual in ageing, the decision was made to make alterations to the traditional climbing assay as described by Madabattula *et al*. (2015).

Climbing assays were carried out using the age groups that were selected based on longevity assays. Experiments were carried out on both male and female *Drosophila*, respectively, at the previously determined ages (5, 30 and 50 days old) and results are shown in Figure 3.3. Comparisons between male and female locomotor ability at each age group are shown in Figure 3.4.

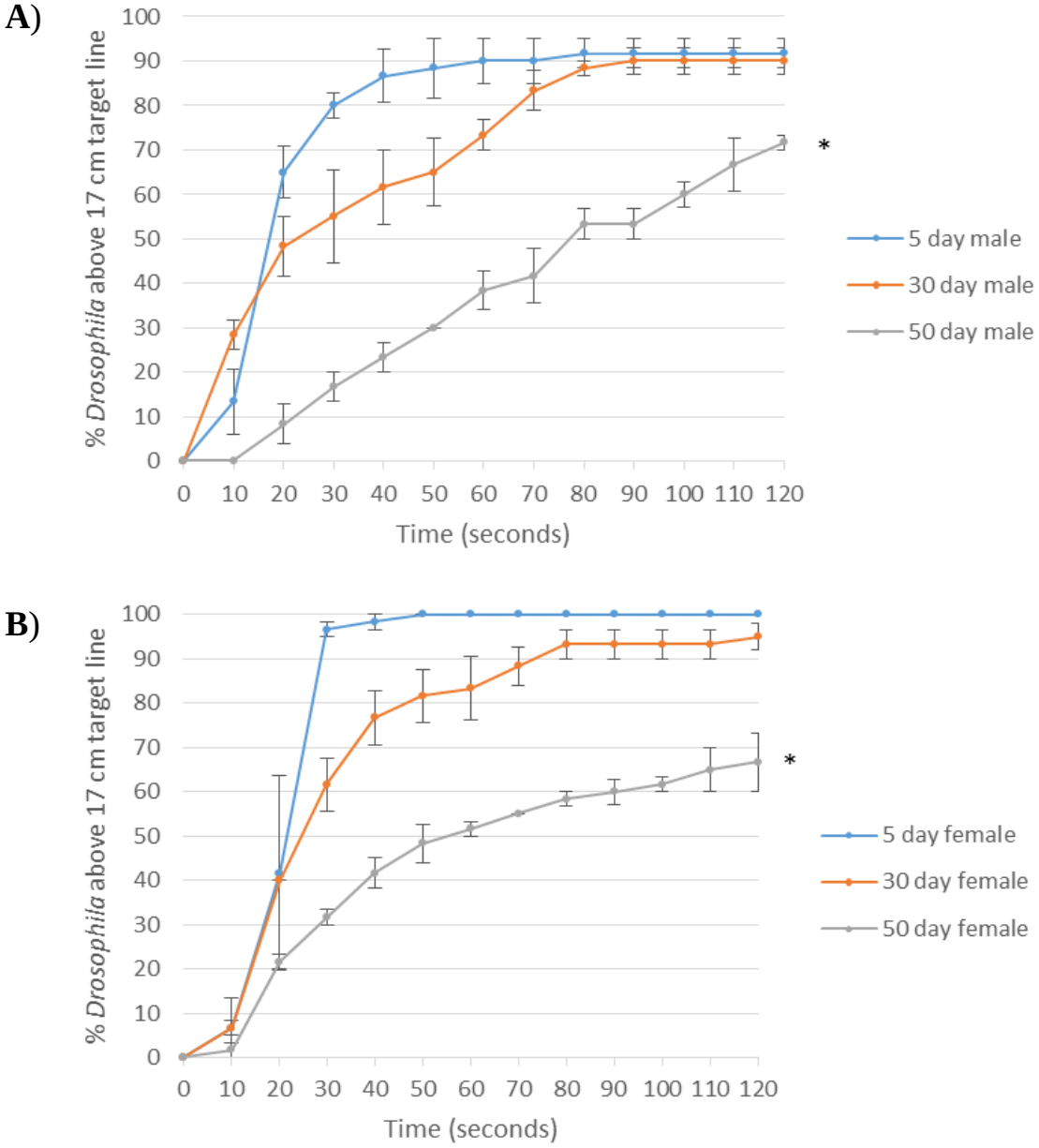

Figure 3.3 Climbing assays of male and female *Drosophila* at 5, 30 and 50 days old.

20 flies from each group were transferred to a 250 ml graduated cylinder (section 2.2.1.14). Flies were tapped to the bottom of the cylinder before starting a timer. The number of flies that crossed a 17 cm target line was recorded every 10 seconds for 2 minutes. Climbing assays were carried out in triplicate and data is shown as the mean of three biological replicates ± standard error with results for male *Drosophila* shown in (A) and results for female *Drosophila* shown in (B). Performance was analysed at 120 seconds and p values were calculated. *=P<0.05 (Student's t-test, two-tailed).

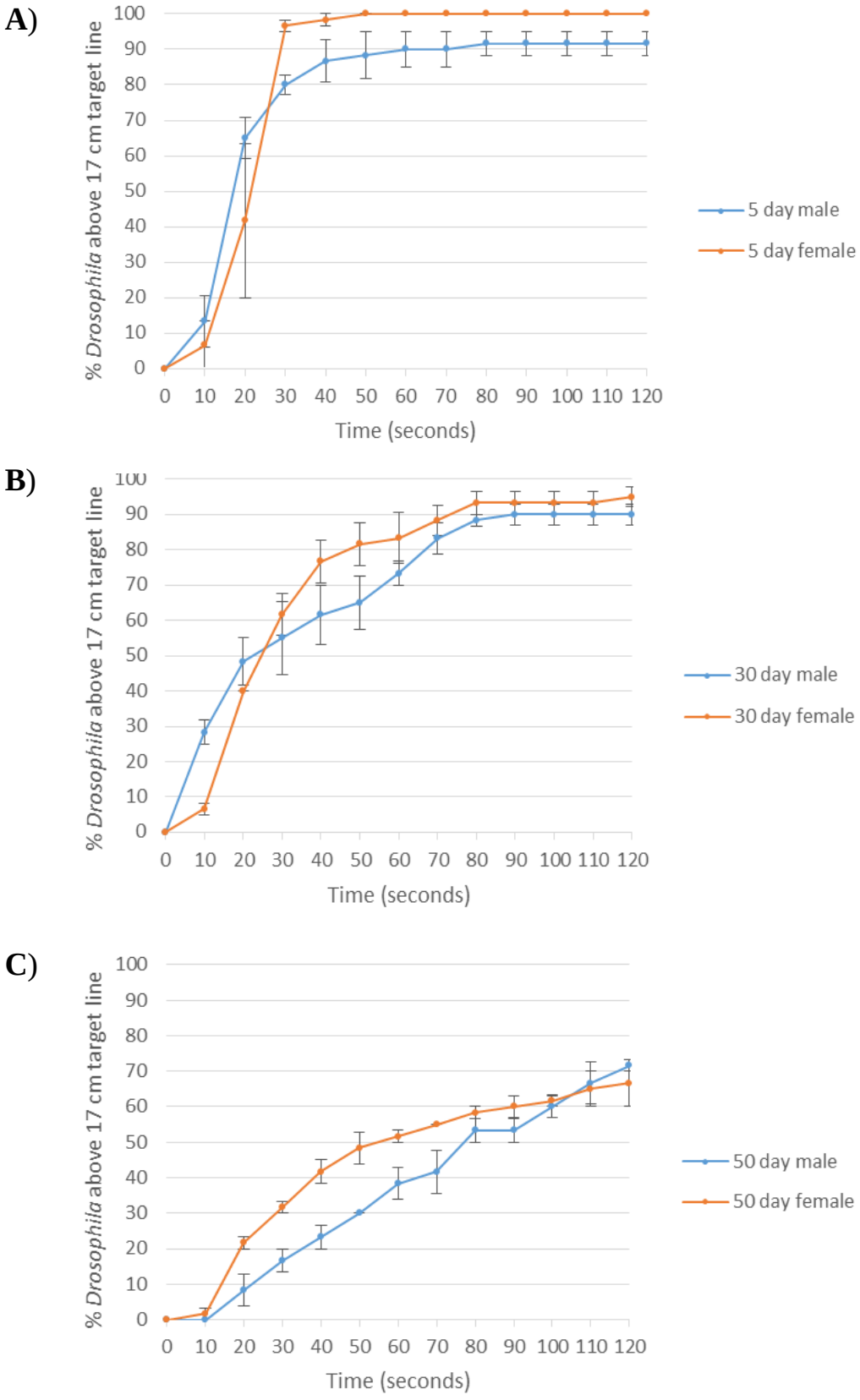

Figure 3.4 Comparison of locomotor activity between male and female *Drosophila* at 5, 30 and 50 days old.

Data from figure 3.3 displayed to show direct comparisons between male and female *Drosophila* at each age group (5, 30 and 50 days old).

Results from Figure 3.3 show significant declines in locomotor function with increasing age for both male and female *Drosophila*. These findings are in agreement with Gargano *et al*. (2005) who also reported declines in locomotor function with increasing age in both male and female *Drosophila*. Differences between 5 day old and 30 day old male and female flies over the course of the 2 minute assay were not statistically significant. However, a large decline in locomotor function can be seen in both males and females between 30 days and 50 days with data displaying statistical significance. At 50 days old, male and female locomotor ability is significantly reduced when analysing endpoint data after 120 seconds of testing compared to 5 day old (Male p= 0.012 and female p=0.008) and 30 day old flies (Male p=0.005 and female p=0.030). Endpoint analysis shows no statistical significance between male and female locomotor ability (Figure 3.4). In addition to endpoint analysis of data at 120 seconds, the time at which 50% of the flies had reached the target line was also analysed and compared. Similarly, results from this analysis showed significant differences between 50 day old *Drosophila* and the two other age groups for both males and females. The time at which 50% of males had reached the target line, 50 day old flies were significantly slower than both 5 day old flies and 30 day old flies, taking 57.4 seconds ($p=5.45x10^{-5}$) and 45.8 seconds (p=0.014) longer on average to reach the target line, respectively. Differences between 5 and 30 day old males were not significant. Similarly, female 50 day old flies were significantly slower than both 5 day old flies and 30 day old flies, taking 30.9 seconds (p=0.005) and 25.9 seconds (p=0.006) longer on average for 50% of the flies to reach the target line, respectively. Differences between 5 and 30 day old females were not significant. Although endpoint analysis between males and females shows no significant results between sexes at 120 seconds in each age group, after analysing the times at which 50% of the flies had reached the target line, 50 day old males are seen to be slower than 50 day old females. 50 day old males were 22.8 seconds slower than females on average (p=0.023). However, no other differences were seen between males and females in any other age group. Results show that although males and females demonstrate clear differences in survivorship it doesn't necessarily equate to differences in locomotor ability. A decline in locomotor function is a consequence of ageing and has previously been shown in *Drosophila* (Gargano *et al*., 2005). Results from Figure 3.3 also demonstrate a progressive decline in locomotor function with increasing age, thus suggesting age-associated changes can be observed in *Drosophila* using the age groups selected. To further support and verify that these selected age groups represent a

useful model of ageing, advanced glycation end-products (AGEs), which are a known biomarker of ageing, were analysed in each age group for both males and females.

3.2.3 Advanced Glycation End-products as a biomarker of ageing in *Drosophila*

AGEs are formed in a reaction between reducing sugars and amine residues on proteins, lipoproteins or nucleic acids and have been shown to increase and accumulate as a result of ageing and are therefore widely used as a biomarker of ageing. They are the product of multiple pathways including the Maillard reaction, Amadori rearrangements and Schiff base formation. Some AGEs display characteristic fluorescence, which can be measured at excitation wavelengths of 365 nm and emission wavelengths of 440 nm. Increases in fluorescent AGEs with progressing age have been measured in a number of organisms including *Drosophila* (Oudes *et al*., 1998; Jacobson *et al*., 2010). Jacobson *et al*. (2010) suggests accumulation of fluorescent AGEs correlates with higher mortality rates in flies maintained at higher temperatures (27°C) compared to those maintained at lower temperatures (18°C). Flies that were switched to either the higher or lower temperature acquired a rate of AGE accumulation characteristic of flies kept permanently at that temperature but carried a permanent level of accumulated damage consistent with their maintenance at the previous temperature. It was therefore suggested that non-reversible increases in mortality rate are mirrored by non-reversible increases in fluorescent AGE accumulation and supports the use of fluorescent AGEs as a biological marker of ageing in *Drosophila*.

To determine whether AGEs increase in the *Drosophila* model, male and female flies were collected at 5, 30 and 50 days old and processed as described previously (section 2.2.1.13). Results are shown in figure 3.5.

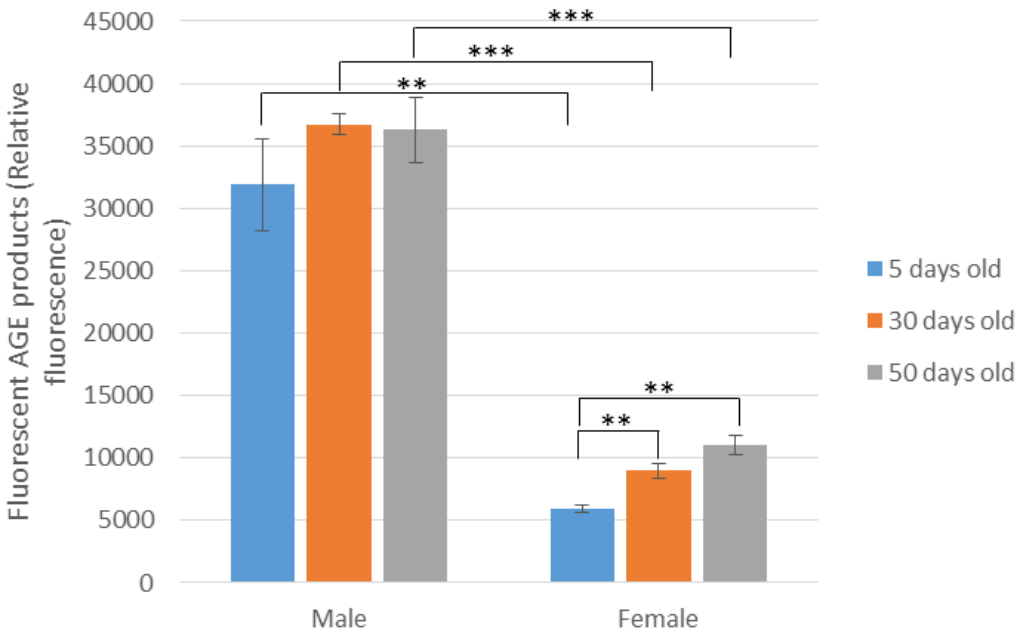

Figure 3.5 AGE products of male and female *Drosophila* aged 5, 30 and 50 days old.

20 male and female *Drosophila* aged 5, 30 and 50 days old were selected and trypsinised for 24 hours at 37°C as described in 2.2.1.13. Homogenates were then processed and aliquoted into 96-well plates. Fluorescence was measured at excitation and emission wavelengths of 365 nm and 440 nm, respectively. Results shown are the mean of four independent experiments ± standard error. **= $p<0.01$, ***= $p<0.001$ (Student's t-test, two-tailed).

Results from Figure 3.5 show an increase of AGEs in females from 5 days old up to 50 days old. However, AGEs do not change with age in male *Drosophila*. Differences in AGEs seen in females between 5-30 days old and 5-50 days old are statistically significant ($p= 0.0038$ and $p= 0.0011$) but AGEs do not change significantly between 30-50 days. An overall increase in AGE products between young and old *Drosophila* has been reported in previous studies (Oudes *et al*., 1998; Jacobson *et al*., 2010). Results for female *Drosophila* in Figure 3.5 are in agreement with this trend but results for males are not. However, previous studies have not looked at differences in AGE products between male and female *Drosophila*. Interestingly, differences in AGEs between males and females are statistically significant at every age group. Relative fluorescence of 5 day old males is >5 fold more than levels seen in 5 day old females ($p=0.0061$). Similarly, relative fluorescence of 30 and 50 day old males is >4 ($p=1.8x10^{-7}$) and >3 fold ($p=0.0008$) more than their female counterparts, respectively.

After carrying out longevity assays (Figure 3.2), climbing assays (Figure 3.3 and Figure 3.4) and analysing AGE products (Figure 3.5) in male and female *Drosophila*, a model of ageing has been established. This resulted in the selection of male and female *Drosophila* at 5, 30 and 50 days old to be used in subsequent experiments to investigate Top2 expression.

3.3 Quantification of Top2 protein in *Drosophila* brains

3.3.1 Optimising protein extraction and western blotting methods

Western blotting experiments were utilised to generate semi-quantitative data of protein levels of Top2 in male and female *Drosophila* aged 5, 30 and 50 days old. In order to carry out such experiments, protein extraction techniques needed to be optimised. To analyse Top2 expression in ageing neurons a tissue source that was predominantly composed of neurons was required. For this reason, experiments were ultimately carried out on dissected brain tissue. However, for the purposes of optimising protein extraction techniques, either whole flies or heads were utilised as dissecting *Drosophila* brains is time consuming.

Preliminary experiments attempting to extract protein from *Drosophila* tissue initially utilised *Drosophila* lysis (1) buffer as described in materials section (Table 2.8). Whole flies or heads were harvested and immediately added to a microfuge tube before adding lysis buffer. The tissue was then homogenised, centrifuged and the supernatant was collected prior to quantifying total protein using a Bradford assay. A standard curve was generated using bovine serum albumin (BSA) and *Drosophila* extracts were quantified. An example of the standard curve can be seen in Figure 3.6.

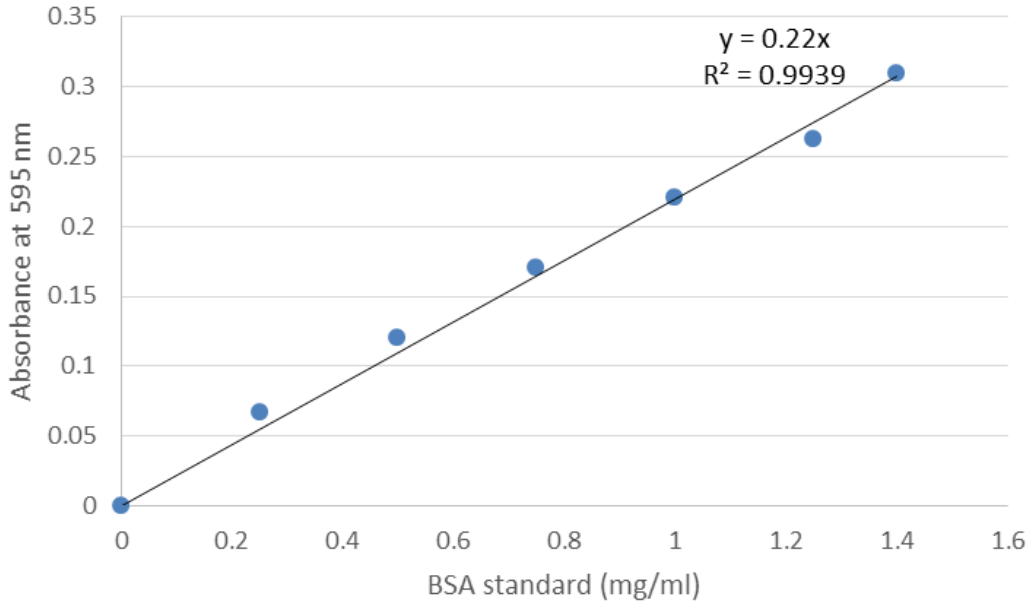

Figure 3.6 Example standard curve of BSA.

A 1.5 mg/ml stock solution of BSA was diluted to create stock solutions ranging from 0-1.4 mg/ml. Standards were added to a 96-well plate and unknown protein samples were diluted 1:5 in PBS and added in triplicate to the plate. Lysis buffer, by itself, was also diluted 1:5 and added to the 96-well plate in triplicate to act as a buffer control. Bradford reagent was added to each well and the plate was incubated at room temperature for 5 minutes before measuring absorbance at 595 nm on a plate reader. Mean absorbance of BSA standards was plotted against concentration to create a standard curve and unknown samples were quantified using y=mx+c. Final concentration of the unknown protein sample was calculated by multiplying the result by the dilution factor.

Once quantified, protein samples were processed by western blot analysis and probed for Top2. Initially, protein extracts from 20 heads, 40 heads and 20 whole flies were analysed with protein loads of 47 µg, 70 µg and 124 µg, respectively. However, this failed to yield positive results (data not shown). Subsequent experiments focussed on optimising protein extraction and western blot methods. Although total protein quantification was suggesting substantial amounts of protein after each modification to the extraction methods, subsequent western blots failed to provide positive results. Ultimately, a new antibody (anti-Top2 sc-65742) was obtained and a new lysis buffer was used (*Drosophila* lysis buffer [2] Table 2.8), as described by Tian *et al*. (2013) and extraction methods were adapted before positive results were obtained. A range of head

numbers and whole flies were used to determine optimum protein loading conditions (see methods section 2.2.1.9) and results are shown in Figure 3.7.

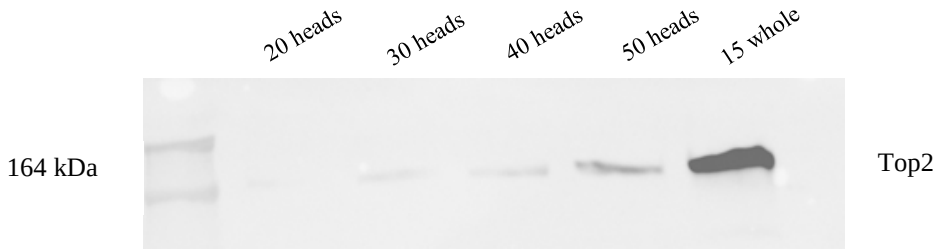

Figure 3.7 Optimisation of *Drosophila* protein extraction and western blot analysis of Top2.

Drosophila were selected (Mixed ages), processed and protein was extracted as described in 2.2.1.9 from 20 (47 µg total protein load), 30 (74 µg total protein load), 40 (70 µg total protein load), 50 (72 µg total protein load) heads and 15 whole flies (114 µg total protein load). Protein samples were loaded onto a 7.5% SDS gel and western blotting was performed.

After carrying out numerous experiments it was discovered empirically that the careful processing of *Drosophila* tissue and removal of chitin was as equally important as protein load in order to obtain successful blots. Chitin, the major constituent of a fly's exoskeleton, can interfere with protein quantification and subsequent gel electrophoresis if it is not adequately removed. After optimising extraction and western blotting techniques on whole *Drosophila* and heads, further experiments were carried out to empirically determine the number of brains that would be required to give enough protein to provide positive results. Preliminary western blot results of *Drosophila* brains used protein extracts from 20, 40, 50 and 60 dissected brains and can be seen in Appendix Figure A.2. Initial blots yielded poor results and Top2 signal was weak for all brain extracts tested. Further western blots were carried out using extracts from 100 dissected brains alongside whole heads and can be seen in Figure 3.8.

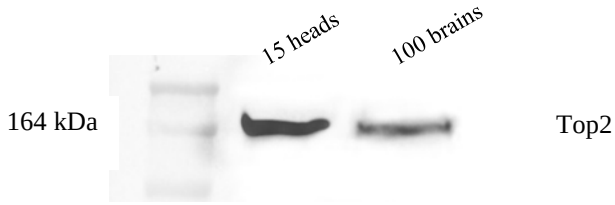

Figure 3.8 Optimisation of protein extraction and western blotting using *Drosophila* brains.

Drosophila were selected (Mixed ages), brains were dissected and protein was extracted as described in 2.2.1.9 from 100 brains (114 µg total protein load). A protein extract from 15 heads (135 µg total protein load) was run alongside the brain extract for comparison. Protein samples were loaded onto a 7.5% SDS gel and western blotting was performed.

Results from Figure 3.8 demonstrate that protein extracts from 100 brains is sufficient to achieve positive western blot results. Protein extracts from fewer than 100 brains yielded poor results, hence subsequent experiments were carried out using extracts obtained from 100 dissected brains.

Levels of Top2 protein were semi-quantified in samples from the brains of male and female *Drosophila* aged 5, 30 and 50 days old. Results are shown in Figure 3.9.

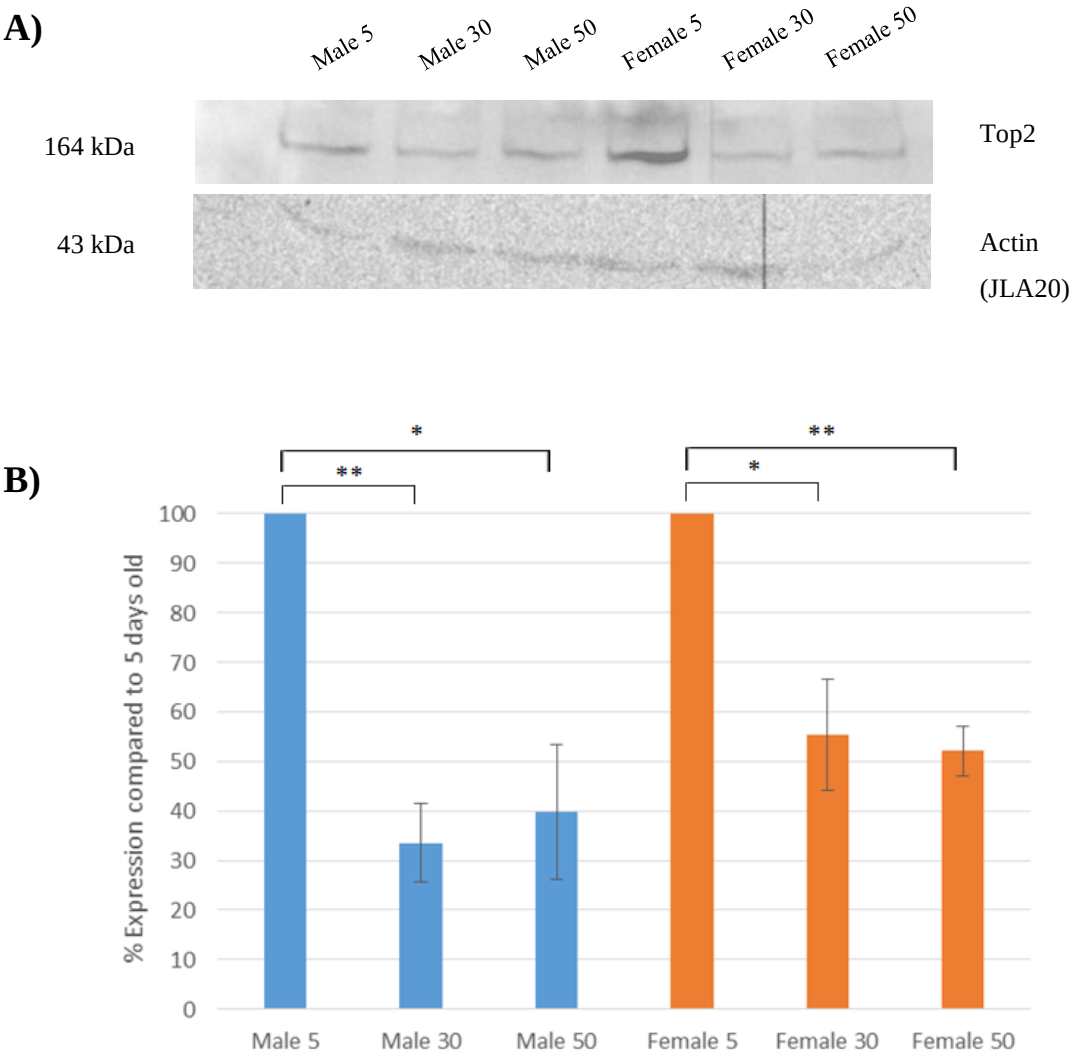

Figure 3.9 Semi-quantification of Top2 in male and female *Drosophila* aged 5, 30 and 50 days old.

Protein extracts were obtained from the brains of male and female *Drosophila* aged 5, 30 and 50 days old. Each extract consisted of 100 dissected brains. Total protein was quantified as described in section 2.2.2.10 and equal protein loads (91 µg total protein) were added to wells of a 7.5% SDS gel. SDS-PAGE was carried out and protein was transferred to nitrocellulose paper by wet western transfer. Nitrocellulose blots were probed with a Top2 (A: top blot) antibody and an Actin (JLA20) load control (A: bottom blot) antibody. Analysis of blot densitometry was carried out using GeneTools (Syngene). Top2 expression is presented as a percentage of that seen in 5 day old flies (B). Results shown are the mean of four independent experiments ± standard error. *= $p<0.05$, **= $p<0.01$ (Student's t-test, two tailed).

Declines in Top2 protein levels can be observed for both male and female *Drosophila* with increasing age in Figure 3.9. In male *Drosophila* a significant average 66.5% decrease in Top2 protein can be seen between 5 day old flies and 30 day old flies ($p=0.0035$). Similarly, a significant average decrease of 44.6% in Top2 protein can be seen between 5 day old and 30 day old females ($p=0.0284$). Significant differences between 5 and 50 day old flies can also be seen for both male and female *Drosophila* with average 60.3% ($p=0.0216$) and 47.9% ($p=0.0023$) declines in Top2 protein seen, respectively. However, differences in Top2 expression seen between 30 and 50 day old males and females are not significant. These findings are novel in *Drosophila* to the best of our knowledge but are consistent with age-related declines that have been seen in mouse brain tissue (Kondapi *et al*., 2004). Male and female *Drosophila* display very similar Top2 decreases in percentage protein expression between age groups and show no significant differences between them. Further analysis comparing the raw data also showed no significant differences between males and females at each age group (data not shown). Although differences between males and females in longevity and biomarkers of ageing can be seen, this does not appear to correlate with differences in Top2 protein expression.

3.4 Quantification of Top2 mRNA in *Drosophila* brains

3.4.1 Selection of RT-qPCR reference genes

Real-time reverse transcription quantitative polymerase chain reaction (RT-qPCR) is a widely used technique that allows rapid quantification of relative gene expression and is considered one of the prominent techniques in mRNA quantification. Numerous factors that can affect the reproducibility of a qPCR experiment such as variations in RNA extraction and reverse transcription efficiency as well as pipetting errors can have detrimental effects to the validity of results (Taylor *et al*., 2010). Therefore, the normalisation of data by incorporating internal reference genes into experimental procedure is an important step in minimising the influence of these factors. Internal reference genes are typically chosen from a set of housekeeping genes and are measured alongside target genes. These genes are abundantly and stably expressed across various experimental conditions and allow normalisation of data to be calculated. Previously, the most commonly selected reference genes for normalisation of *Drosophila* qPCR experiments were adopted from other species without verification. However, Ling &

Salvaterra (2011) measured expression stability for 20 *Drosophila* candidate reference genes in flies of different ages to be used specifically in RT-qPCR applications. Expression stability was seen to vary across sample subsets and no particular genes were seen to be stably expressed across all experimental conditions. However, suitable experiment-specific reference genes could be selected from the panel of candidate genes. Reference genes were selected based on their expression stability in age-related experiments. The reference genes cyclophilin 1 (Cyp1) and eukaryotic initiation factor 1A (eIF-1A) were the most stably expressed genes in samples that contained control, middle-aged and old-aged variables, therefore these genes were selected to be used as reference genes alongside a target gene of Top2.

3.4.2 Optimisation of Top2, Cyp1 and eIF-1A primers for RT-qPCR

Primers were designed for Top2, Cyp1 and eIF-1A to be used in RT-qPCR experiments (Materials and Methods Table 2.3). Prior to carrying out analysis of mRNA levels in aged *Drosophila* samples, the amplification efficiency of these primers was required to determine their experimental suitability. It is important for primers to work efficiently in order to be able to make valid comparisons between genes. A reaction efficiency of 90-110% is deemed acceptable (Taylor *et al*., 2010).

Amplification curves were generated for Top2, Cyp1 and eIF-1A primers, respectively, and subsequently used to calculate primer reaction efficiency (Figure 3.10). RNA was extracted from tissue of a mixed population of *Drosophila* and 0.4 µg of total RNA was reverse transcribed to cDNA. The stock solution of cDNA was used to create a 1:10 serial dilution of cDNA samples and 2 µl of each sample was incorporated into a 20 µl PCR reaction.

Primer reaction efficiencies were calculated based on equations described by Rutledge and Côté (2003). The equation for calculating reaction efficiencies is shown in Appendix Figure A.3. Calculations using the amplification curves shown in Figure 3.10 demonstrate a reaction efficiency of 103.2% for Top2, 92.1% for Cyp1 and 98.0% for eIF-1A. As the reaction efficiencies of these primers fall within the 90-110% range they were considered suitable and comparable for further RT-qPCR experiments.

In addition to analysing primer efficiency, a number of controls were also incorporated into the experimental design in order to determine whether there were any genomic DNA contaminants or primer dimer formations and to ensure only a single PCR product was being amplified. This was achieved through the inclusion of a no reverse

transcriptase control and a no template control. Melt curves were analysed in all samples to confirm the presence of a single PCR product and to confirm the absence of contaminating genomic DNA (representative melt curves are shown in Appendix Figure A.4).

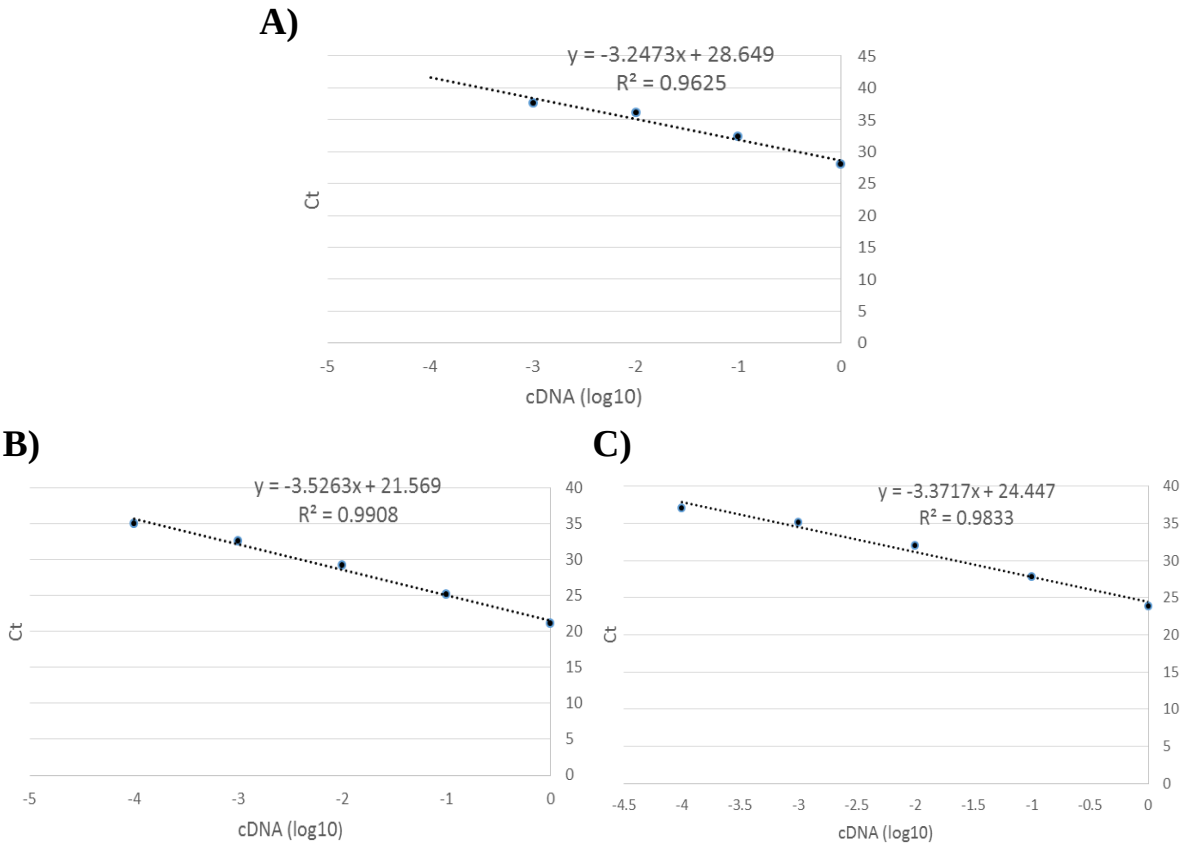

Figure 3.10 Amplification curves for primer efficiency of Top2, Cyp1 and eIF-1A.

Total RNA was extracted from a mixed population of *Drosophila* and quantified on a NanoDrop ND-1000 spectrophotometer. 0.4 µg of total RNA was reverse transcribed to cDNA using PCR Biosystems qPCRBIO cDNA synthesis kit (PB30.11) according to manufacturer instructions. The cDNA stock solution was serially diluted 1:10 to create a range of cDNA samples. This ensured the standard curve covered the dynamic range of potential template concentrations that could be encountered during further studies. cDNA concentrations were converted to logarithmic values and plotted against threshold cycle (Ct) values. Amplification curves were generated for Top2 (A), Cyp1 (B) and eIF-1A (C) and a line of best fit was added.

Statistical analysis of qPCR data can be carried out using one or numerous reference genes using the comparative ΔCt method. In order to select an appropriate method of statistical analysis, the threshold cycle (Ct) values of selected candidate housekeeping

genes under experimental conditions were analysed and evaluated for stability. Figure 3.11A displays a box and whisker diagram showing the variations in Ct values of the two candidate reference genes in male and female samples across all age groups tested. Figure 3.11B displays the coefficient of variance of the Ct values to show variability between samples. The higher the coefficient of variance, the greater the level of dispersion around the mean.

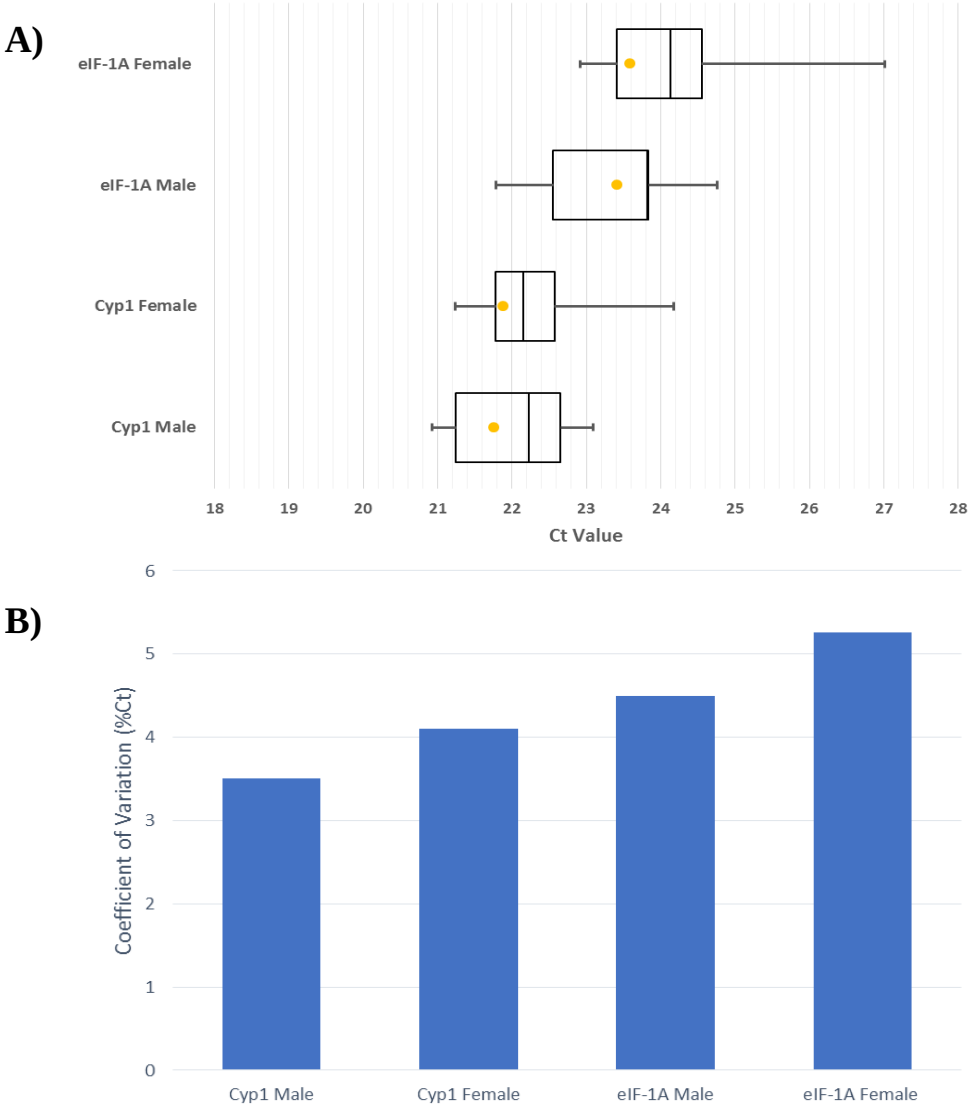

Figure 3.11 Variance of Cyp1 and eIF-1A reference genes across all *Drosophila* samples tested.

Ct values for the reference genes Cyp1 and eIF-1A from all *Drosophila* qPCR ageing study experiments were collated to observe any variations in expression. (A) Box and whisker plots showing the distribution of Ct values for the two candidate reference genes. Yellow dots indicate mean value. (B) The coefficient of variance for the data set was calculated to determine variability of Ct values for Cyp1 and eIF-1A in male and female *Drosophila* across all age groups (see Appendix Figure A.6).

Results from Figure 3.11A show that the range of Ct values differs between males and females for both Cyp1 and eIF-1A. However, mean Ct values for each gene are comparable between males and females. In addition to this, the coefficient of variance is comparable between males and females and is similar for both reference genes. Both reference genes have a greater coefficient of variance in female samples than males. As the variation between the two candidate reference genes is comparable, subsequent data analysis utilising the comparative ΔCt method utilised both reference genes.

3.4.3 Analysis of Top2 mRNA in male and female *Drosophila* aged 5, 30 and 50 days old

Following the confirmation of primer reaction efficiencies, RT-qPCR was carried out to quantify Top2 mRNA levels in the brains of male and female *Drosophila* aged 5, 30 and 50 days old. RNA was extracted from 100 brains for each experimental group. Results are shown in Figure 3.12.

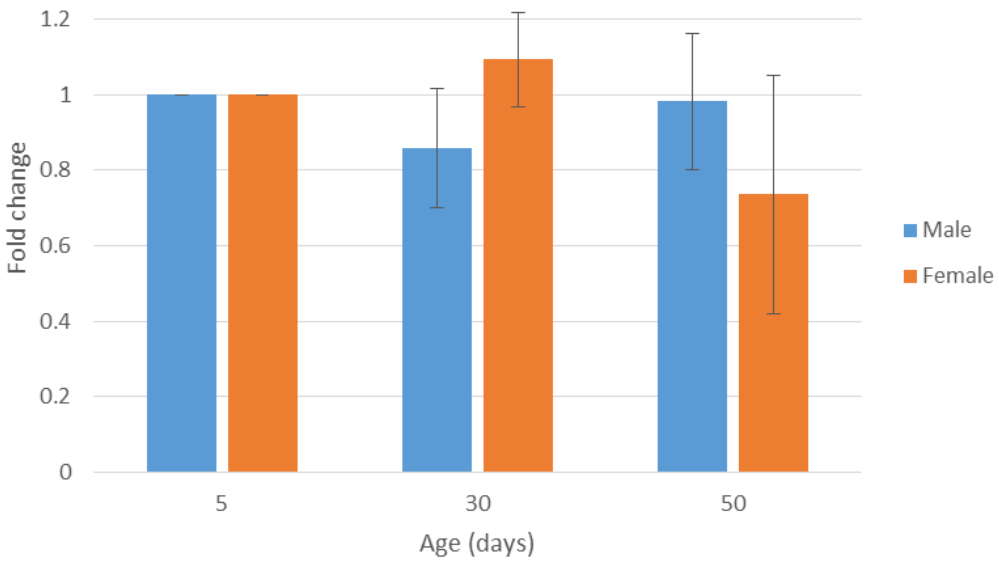

Figure 3.12 Analysis of RT-qPCR data comparing relative Top2 mRNA expression in male and female *Drosophila* aged 5, 30 and 50 days old.

Male and female *Drosophila* were aged up to 5, 30 and 50 days, respectively. 100 brains were dissected from each group and RNA was extracted as described in section 2.2.4.1. 0.4 µg of total RNA from each sample was converted to cDNA (section 2.2.4.3) and RT-qPCR was carried out (section 2.2.5) using both Cyp1 and eIF-1A as reference genes. Results were normalised by geometric averaging of both reference genes and presented as expression fold change (Vandesompele *et al*., 2002) (See Appendix Figure A.5). Samples for each individual experiment were loaded in triplicate. Results shown are presented as the mean of three biological replicates ± standard error.

Unlike protein levels of Top2, which have been shown to decrease with age (Figure 3.9), results from Figure 3.12 show no statistically significant changes in Top2 mRNA levels throughout the ageing process. Similarly, there are also no significant changes in mRNA levels between male and female *Drosophila* at each age group tested.

3.5 Immunofluorescent analysis of Top2 in *Drosophila* brains

To gain further insight into the expression of Top2 in *Drosophila* brains, immunohistochemical techniques were used to attempt to analyse regional expression patterns. Initial experiments aimed to optimise immunofluorescent staining techniques and to determine Top2 protein abundance, distribution and localisation in the *Drosophila* brain. Initial immunofluorescent staining is shown in Figure 3.13.

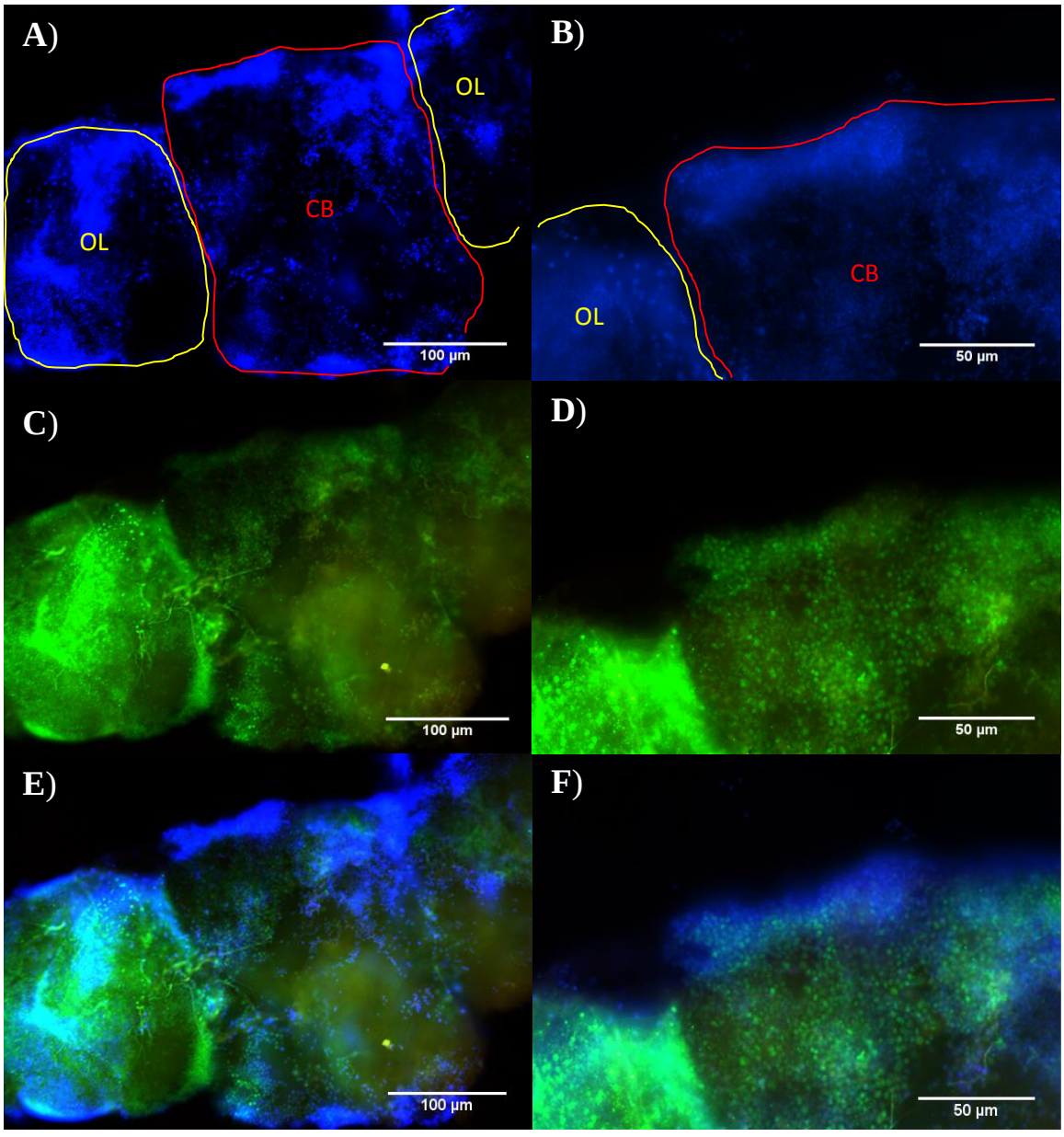

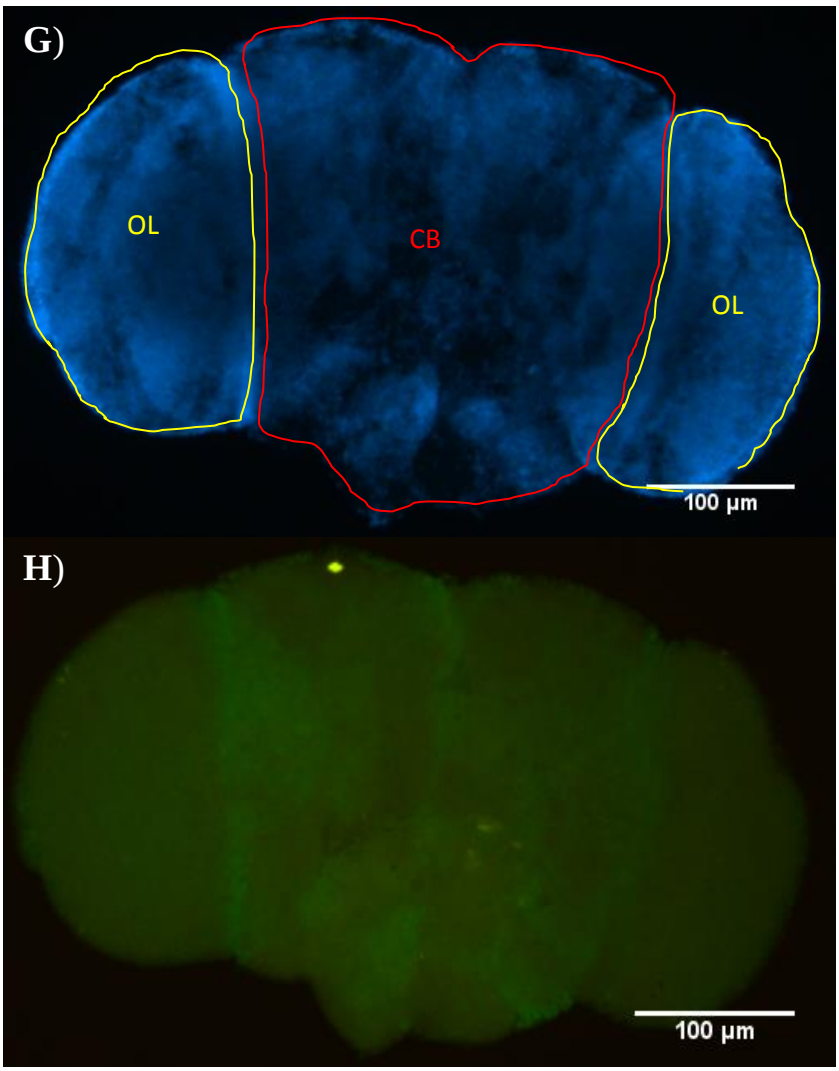

Figure 3.13 Immunofluorescent staining of Top2 in the *Drosophila* brain.

The brains of a mixed population of young *Drosophila* were dissected and processed as described in section 2.2.1.10. Brains were incubated in a Top2 antibody and a secondary FITC antibody was utilised before being mounted in mounting medium containing DAPI. Top2 staining is seen as green punctate labelling and DAPI is seen as blue staining. Images were captured using a Leica DM500 fluorescence microscope. Images A and B show DAPI staining at 20 x and 40 x objective, respectively. Images C and D show Top2 staining at 20 x and 40 x objective, respectively. Images E and F show an overlay of both DAPI and Top2 staining at 20 x and 40 x objective, respectively. Structures outlined in yellow identify the optic lobes (OL) and the structure outlined in red identifies the central brain (CB), which contains numerous structures including the mushroom bodies (not labelled). Image of control brains (staining with FITC secondary only and without primary antibody) are shown in G and H. Image G shows DAPI staining only and image H shows secondary FITC staining only at 20 x objective.

Pan-wide green punctate labelling of Top2 is expressed in the *Drosophila* brain (Figure 3.13). The use of DAPI stains nuclear DNA as a bright blue colour. DAPI staining is seen predominantly in peripheral areas of the tissue in Figure 3.13. This may be attributed to the relatively short incubation time in the mounting media containing DAPI. Brains were viewed using fluorescence microscopy 30-60 minutes after mounting, which may not have given the DAPI optimal time to penetrate and stain the entire brain. In comparison, brains were incubated in the primary Top2 antibody for 72 hours. Punctate labelling of Top2 is seen to be similar in size to that of DAPI staining when viewing peripheral areas of the brain where staining can be seen to overlap in places. As stated previously, DAPI stains nuclear DNA, so this may suggest that Top2 is predominantly nuclear in location. Results from Figure 3.13 initially provided what appeared to be positive staining for Top2. Results shown in Figure 3.13 are from a single experiment. Subsequent experiments focussed on optimising immunofluorescence techniques using both young and old *Drosophila*. However, further experiments provided no positive staining of Top2, hence further investigation would be required to determine whether any age-related/sex-related changes in Top2 occurs in *Drosophila* brains.

3.6 Discussion

Results from this chapter have revealed levels of Top2 protein decrease with age in both male and female *Drosophila* (Figure 3.9). However, no significant changes in Top2 mRNA were seen during qPCR experiments (Figure 3.12). Although male and female *Drosophila* displayed similar levels of Top2 expression from 5 day old flies to 50 day old flies, they demonstrated clear differences in longevity (Figure 3.2) and in AGE products (Figure 3.5).

3.6.1 Sex differences in lifespan

Analysis from this study revealed a shorter lifespan for male flies relative to female flies (Figure 3.2). A study of longevity in 219 inbred *Drosophila* strains showed that in 70% of these strains, virgin females lived longer than virgin males (Arya *et al*., 2010). Thus, it is known that genetic variation can influence sex differences in the longevity of flies (Pacifico *et al*., 2018). A study by Jacobson *et al*. (2010), which used wildtype files similar to this study, also reported that males are seen to be shorter-lived than females when housed separately. In the study Jacobson used Dahomey flies, the same

strain used in this chapter, and maintained them at 25°C and 65% humidity on a 12 hour light/dark cycle and fed them using a standard sugar/yeast medium. Hence, conditions were comparable to those used during this chapter.

Apart from genetic variation, other factors such as diet can affect lifespan and this can affect one sex to a higher degree than the other, which may explain the findings in this study. For example, Biteau *et al*. (2010) showed that a major cause of mortality in *Drosophila* was a loss of gut integrity, with the proliferative activity in ageing intestinal epithelia correlating with longevity over a range of genotypes. Importantly, Regan *et al*. (2016) uncovered a substantial sex difference in some genotypes of *Drosophila* in the pathology of the ageing gut with males succumbing to intestinal challenges to which females are resistant. These findings may partly explain why we see female *Drosophila* outliving males.

In addition to this, both males and females, individually, were longer lived than a mixed population of flies (Figure 3.2). The mating status of *Drosophila* has been seen to affect longevity in both male and female flies (Service, 1989) and mating-induced declines in longevity have been reported in both sexes (Service, 1989; Rogina *et al*., 2007). Mating has been seen to induce alterations in female physiology and behaviour and results in increased egg production and a shortened life span. Studies have shown that frequent mating reduces female lifespan and reproductive success and is mediated by male ejaculate accessory gland proteins (Chapman *et al*., 1995). In male *Drosophila* it has been suggested that mating directly reduces somatic lipid reserves through increased energy expenditure on courtship activities (Service, 1989). In addition to this, Gendron *et al*. (2014) reported that the sexual pheromones of one sex can directly reduce longevity in the other through interaction with insulin signalling pathways. Decreases in insulin signalling have been shown to extend lifespan in adult flies. However, sexual attractiveness in *Drosophila* is mediated by insulin/insulin-like growth factor signalling (IIS) as it regulates the transcription of genes associated with the production of cuticular hydrocarbons, many of which have been shown to function as pheromones (Kuo *et al*., 2012). Also, the perception of female sexual pheromones by males has been seen to cause them to rapidly decrease fat stores and reduce resistance to starvation, ultimately resulting in a reduced lifespan (Gendron *et al*., 2014). These studies provide reason for the differences in longevity between mixed and separated populations of *Drosophila.*

3.6.2 Advanced Glycation End-products

Under normal physiological conditions, cells ensure low intracellular concentrations of ROS are maintained. Cells are able to achieve this through a variety of mechanisms, which consist of both non-enzymatic and enzymatic processes capable of scavenging ROS. The non-enzymatic components include retinal, alpha-tocopherol, ascorbic acid, and various other molecules such as glutathione, lipoic acid and thioredoxin, which all contain thiol groups, as well as melanin (Holmgren *et al*., 2005; Covarrubias *et al*., 2008; Shay *et al*., 2008; Zhong *et al*., 2017). Enzymatic components include superoxide dismutase, catalase and glutathione peroxidases, glutathione reductase and peroxiredoxins (Snezhkina *et al*., 2019). A reduction in the ability of the cells to scavenge ROS by these mechanisms will result in the accumulation of ROS, which leads to oxidative stress (Birben *et al*., 2012; Schieber & Chandel, 2014).

Oxidative stress induces lipid peroxidation and glycoxidation reactions, which leads to an elevation in the endogenous production of aldehydes and their derivatives such as malondialdehyde (Moldogazieva *et al*., 2019). These are highly reactive and because they are electrophilic, they attack free amino groups in proteins and cause covalent modifications, resulting in the generation of advanced glycation end products (AGEs) and advanced lipoxidation end products (ALEs) (Vistoli *et al*., 2013). The formation of oxidative stress-induced ALEs and AGEs causes the formation of protein cross-links and subsequently damages protein structure, which can result in protein oligomerisation and aggregation (Fuentealba *et al*., 2009).

Oxidative stress-induced ALEs and AGEs along with lipofuscin (a highly oxidised aggregate of covalently cross-linked proteins, lipids and carbohydrates) have been found to accumulate during ageing and in several age-related diseases (Yamada *et al*., 2001). For example, Domínguez-González *et al*. (2018) measured the levels of the ALE protein adducts neuroketal (NKT) and malondialdehyde (MDA) in twelve brain regions in middle-aged and old-aged humans with no neurological deficits. Their findings show that NKT and MDA increase and decrease in a region-dependent manner. NKT protein adducts were seen to significantly increase in the frontal cortex, visual cortex and substantia nigra in old-aged individuals compared with middle-aged individuals. However, significant decreases of NKT levels were seen in the thalamus. Significant increases of MDA protein adduct levels were reported in the frontal cortex, parietal cortex, hippocampus, thalamus and putamen in old-aged individuals when compared to middle-aged individuals, whereas significant decreases of total MDA levels were found

in the temporal cortex and entorhinal cortex in the old-aged group. This suggests that particular brain regions may be more susceptible to oxidative stress than others. Significant increases in oxidative protein modification levels and lipid peroxidation has also been seen in brain homogenate, mitochondria and synaptosomes of Wistar rats studied up to 26 months of age (Babusikova *et al*., 2007).

Interestingly, Tsakiri *et al*. (2013) showed that young *Drosophila* supplied with feed enriched in AGEs or in lipofuscin resulted in an increase in the rate of AGE-modified proteins and carbonylated proteins that accumulated in their somatic tissues. This was accompanied by a reduction in locomotor performance as well as life span. Their study showed that these changes were accompanied by reduced proteasome peptidase activities suggesting that AGEs or lipofuscin can disrupt proteostasis (a complex network of mechanisms, which prevent and eliminate protein misfolding) and accelerates the functional decline that occurs with normal ageing. Indeed, natural increases in AGEs and AGE-modified proteins during the ageing process may partly explain the decreases in locomotor function that are seen in Figure 3.3 in male and female *Drosophila.* Locomotor performance, as demonstrated by climbing assays, was seen to significantly decrease over 50 days of ageing in both sexes.

In addition, the accumulation of AGEs in *Drosophila* has been shown to strongly correlate with mortality rate of flies at different temperatures but was independent of dietary restriction (Jacobson *et al*., 2010). Thus, AGEs are useful biomarkers of ageing-related damage in flies. AGE products in this current study can clearly be seen to increase throughout the ageing process in female *Drosophila*, as expected (Figure 3.5). The same cannot be said for male *Drosophila* as they do not show any significant changes in AGEs from 5 day old flies up to 50 day old flies. However, differences in AGEs between males and females are statistically significant. Male *Drosophila* display significantly higher levels of AGEs than females at each age group tested. Previous studies in other species have also reported differences in AGEs between sexes. Studies carried out in rats have shown that the AGE *N*-(Carboxyethyl)-lysine (CEL) is elevated in males compared to age-matched females (Wang *et al*., 2006). Evidence suggests that higher levels of oxidative stress are generally observed in males compared to females (Ide *et al*., 2002; Kander *et al*., 2017), which may go some way to explaining why fluorescent AGEs are considerably higher in male *Drosophila* than females. In addition to this, Jacobson *et al*. (2010) measured a number of oxidised protein adducts in male and female *Drosophila* at numerous time points from 7 days up to 45 days old

and discovered all protein adducts were higher in males than females at each time point tested. Oxidative stress can contribute to ageing and if high levels are present it can leave an organism susceptible to DNA damage. If males have a genetic predisposition to increased levels of oxidative stress it may explain why the lifespan of male *Drosophila* is lower than that of females.

3.6.3 Top2 mRNA levels in ageing

Results from this chapter have revealed no significant changes in Top2 mRNA during qPCR experiments (Figure 3.12). This is in contrast to what is shown for Top2B mRNA in mammals during ageing where Top2B is seen to decrease (Bhanu *et al*., 2010; Terzioglu-Usak *et al*., 2017). Bhanu *et al*. (2010) reported declines in mRNA levels of Top2B in cultured rat cerebellar cells that had been aged over 5 weeks *in vitro*. Top2B levels were seen to significantly decrease from 2 weeks onwards and negligible levels were reported after 4 weeks of ageing. Furthermore, models based on age-related neurodegenerative diseases, such as Alzheimer's disease, have similarly shown decreases in Top2B expression at the mRNA level (Terzioglu-Usak *et al*., 2017). Terzioglu-Usak developed an Alzheimer's disease model by incubating fibrillar amyloid-β 1-42 (Aβ1-42) for 48 hours with cultured cerebellar granule neurons (CGNs) isolated from post-natal eight-day rats and found Top2B mRNA levels to be decreased compared to control cells.

As previously stated, the chromosomes of *Drosophila* are morphologically comparable to chromosomes of vertebrates (Mengoli *et al*., 2014). In this organism Top2 has been shown to be expressed in mitotically active cells but has also been found to be stably expressed bound to chromatin in non-dividing cells. Based on this expression, indications might be made for homologous roles between *Drosophila* Top2 and mammalian Top2A and Top2B (Lee & Berger, 2019). The potential dual role for Top2 in *Drosophila* may explain why decreases of mRNA expression are not seen, whilst decreases in Top2B mRNA have been reported in some mammalian experiments (Bhanu *et al*., 2010; Terzioglu-Usak *et al*., 2017).

Pacifico *et al*. (2018) investigated age-dependent changes in the *Drosophila* whole-brain transcriptome by comparing 5, 20, 30 and 40 day old male and female flies. They reported an overall decrease in the expression of genes from the mitochondrial oxidative phosphorylation pathway during *Drosophila* ageing. Davie *et al*. (2018) also showed that genes involved in oxidative phosphorylation decline faster than the average.

However, changes in gene expression of Top2 as a function of ageing were not reported. Although Pacifico reported an overall downregulation of electron transport chain genes with age, increases in stress response genes was also seen in older flies. Interestingly, it was also observed that a number of overlapping sets of neuronal function genes, that were seen to gradually decline between young and middle-aged flies, became upregulated in the oldest group of flies. Pacifico suggested that this reversal pattern of gene expression may act as a compensatory response to an overall decline in neuronal function. As Top2 plays key roles in neuronal function, the observations by Pacifico *et al*. (2018) may explain why mRNA levels of Top2 are not decreased in 50 day old flies in Figure 3.12.

The reference genes used during this study for qPCR experiments were selected based on their expression stability in age-related experiments as described by Ling & Salvaterra (2011). The reference genes Cyp1 and eIF-1A were selected with confidence and data shown in this chapter were therefore considered valid results. However, data in this chapter presents relative levels of Top2, so it may therefore provide useful research to determine absolute levels of Top2 mRNA in future experiments to fully elucidate age-related changes of Top2 in *Drosophila*.

3.6.4 Top2 protein levels in ageing

3.6.4.1 Age-related changes in protein folding and degradation

As mentioned previously, cells possess a complex set of mechanisms, referred to as the proteostasis network, to prevent and eliminate protein misfolding. The network includes protein synthesis, folding, trafficking, disaggregation, and degradation pathways (Balch *et al*., 2008). Often misfolded proteins are caused by inherent errors in protein biosynthesis and turnover. Genetic mutations and polymorphisms, genomic instability, mistranslation and incorporation of amino-acid analogues are all processes capable of causing variations in amino acid sequence and have the potential to affect folding pathways and the stability of the native state of a protein (Kikis *et al*., 2010). Nevertheless, older cells contain more proteins with oxidative damage such as ALEs and AGEs as shown in this study, as well as oxidised methionine and accumulations of cross-linked and aggregated proteins, and less catalytically active enzyme populations (Soskic *et al*., 2008).

Damaged proteins and those that have reached the end of their lifespan are degraded by the proteasomal and autophagic systems (Lilienbaum, 2013). However, these systems

have been seen to deteriorate with age. For example, during ageing the assembly of the proteasome has been shown to become imbalanced, resulting in alterations in ubiquitin ligation machinery and an overall reduction in protein ubiquitination (David, 2012). Berke & Paulson (2003) suggested that disturbances or impairments of the ubiquitin proteasome system can lead to an altered function of this pathway, which can positively affect the accumulation of protein aggregates in a cell. These disturbances and impairments are thought to be induced by an accumulation of misfolded proteins in the endoplasmic reticulum or a loss of function to key enzymes involved in the ubiquitin conjugation and deconjugation pathways. The formation of aggregated proteins occurs in a cell when a critical concentration of misfolded protein has been reached. These aggregated proteins often lead to the formation of amyloid-like structures and can eventually cause numerous types of degenerative disorders leading to cell death (Berke & Paulson, 2003). Indeed, large numbers of neurodegenerative diseases have been shown to occur as a result of misfolded and aggregated proteins (Sweeney *et al*., 2017). Autophagy, a process that is known to play a housekeeping role in removing misfolded or aggregated proteins (Glick *et al*., 2010), has also been shown to be impaired at both the stage of induction and fusion of autophagosomes with lysosomes during ageing (Basisty *et al*., 2018). The comprehensive proteome profiling in *C. elegans* shows an imbalance of these components of proteostasis with age along with increased protein aggregation and an overload of chaperone machinery (Walther *et al*., 2015). In addition, the processes by which cells degrade these misfolded proteins are, in part, influenced by the energy status of the cell. During ageing, deterioration of cellular energetics is seen with alterations in glucose and fatty acid metabolism occurring. This reduces the amount of available ATP and alters chaperone activity, which results in the accumulation of misfolded protein (Calderwood *et al*., 2009).

Age-related changes in the rate of translation may also explain differences in the abundance of proteins. However, Toyama *et al*. (2013) analysed translation levels in more than 11,000 genes in 6 month and 24 month old liver and brain tissue in rats and showed that 98% of these genes displayed an age-dependent change in translation level of less than 2-fold. This illustrated the stability of protein translation levels during ageing, which has previously been shown (Walther & Mann, 2011). However, the process of translation is only the first step in the production of functional proteins and most require assistance to correctly fold, which occurs either co-translationally or post-translationally and is facilitated by chaperones and other partner proteins, such as

disulphide isomerases (McLaughlin & Bulleid, 1998). Decreased chaperone capacity, response and activity with age has been shown in several studies (Soti & Csermely, 2003) and could lead to misfolding and subsequent degradation of Top2, resulting in reduced protein levels in the aged *Drosophila* brain seen in this present study. This may also explain why low levels of Top2 protein may be seen despite maintenance of mRNA levels.

3.6.4.2 Modification of Top2 structure by oxidative stress

It is conceivable that structural modifications to Top2 via oxidative stress may result in subsequent changes such as alterations to the active site, blockage of phosphorylation sites, or disruption to the binding sites for DNA, magnesium ions or partner proteins. This may lead to dysfunction of Top2 and could potentially lead to an increase in abortive catalytic cycles of the enzyme (Morimoto *et al*., 2019). Spontaneously occurring stabilised Top2 cleavage complexes have not been considered a serious threat to genome stability as they are normally rapidly repaired (Gómez-Herreros *et al*., 2014; Rao *et al*., 2016; Lee *et al*., 2018). However, during ageing there is a decrease in the efficiency of the DNA damage response (Gorbunova *et al*., 2007), which may result in increased abortive catalytic cycles.

As the majority of cells in the adult fly brain are non-cycling, the major role of Top2 will be in supporting transcription. A number of studies have shown that Top2B binding is enriched within the promoters and gene bodies of transcribed genes, suggesting that it is involved in transcriptional initiation and elongation (Kouzine *et al*, 2013; Manville *et al*., 2015; Madabhushi *et al*, 2015). Top2B is known to contribute to neuronal development by facilitating the transcriptional elongation of neuronal genes that are longer than 200 kb (King *et al*., 2013). Top2B has also been reported to be involved in RNA polymerase II promoter pause release and productive transcription. It is speculated that the catalytic activity of Top2B is needed for this process (Bunch, 2018). As stated previously, *Drosophila* possess only a single isoform of Top2. However, its involvement in transcriptional activities has previously been reported (Gemkow *et al*., 2001; Cugusi *et al*., 2013), which suggests that correlations between *Drosophila* and mammalian type 2 topoisomerase isoforms can be made.

A study by Ban *et al*. (2013) showed that persistent Top2B cleavage complexes arrested elongating RNA polymerase II during transcription. In addition, they showed that Top2B cleavage complexes are removed from the DNA by the 20S proteasome and 19S

ATPases. This process required 19S ATPase ring assembly but was independent of ubiquitination of Top2B. Thus, it is plausible that modified Top2 structure induced by age-related oxidative stress in *Drosophila* brains may generate more endogenous stabilised Top2 cleavage complexes that are removed by an analogous process in this species and could account for the decrease in Top2 protein seen with increasing age during this study.

It is important to consider the possibility that modification of Top2 by oxidative stress may have masked epitopes important for antibody recognition. Certainly, the opposite has been shown to occur in which modifications of self-proteins have unmasked epitopes, resulting in the triggering of an immune response, which may induce autoimmune disorders (Abello *et al*., 2009). Again, future experiments to elucidate the binding epitope of the antibody used in this study would rule out this possibility.

3.6.5 Consequences of declining Top2 levels

Previous studies have shown dramatic declines in the transcription of long genes when Top2 becomes inactivated. As previously stated mammalian Top2B is known to contribute to neuronal development by facilitating the transcriptional elongation of long neuronal genes (King *et al*., 2013), with inhibition of Top2B shown to cause reductions in expression of these long genes. In organisms that possess just a single isoform of Top2, such as yeast, the expression of long genes has also been seen to be impaired without the presence of Top2, irrespective of their function (Joshi *et al*., 2012). This reduction in expression was seen to produce a stall in the progression of RNA polymerase II during elongation but did not alter transcription initiation of long genes. As *Drosophila* Top2 and each of the human topoisomerase isoforms, Top2A and Top2B, can rescue the phenotype of yeast Top2 mutants, it highlights the strong functional conservation of type II topoisomerases between species and suggests that Top2 in *Drosophila* also plays important roles in the transcription of long genes (Wyckoff & Hsieh, 1988; Jensen *et al*., 1996). Indeed, increases of positive supercoils and subsequent torsional stress can also inhibit RNA polymerase activities and disrupt transcription in mammalian cells, with the roles of topoisomerase in relieving torsional stress shown to be crucial in maintaining DNA templates in a transcriptionally competent state (Gilbert & Allan, 2014). Previous studies have shown that a number of genes that are required for proper neuronal function are downregulated with age. Hall *et al*. (2017) reported a downregulation of genes including *Sh*, *Csp*, *Hdc*, *Shal* and *Sap47* in *Drosophila* over 40 days of ageing. These genes have been reported to be required for

proper neuronal synaptic function. As discussed by Gabel *et al*. (2015), on average, neuronal genes tend to be longer, which implies that elongation during transcription is crucial for proper expression of these genes. As Top2 is a key player in the expression of long genes it is conceivable that decreases in Top2 may affect the normal function of neuronal cells. Not only is the expression of long genes dependent on topoisomerases for proper expression but they also rely heavily on DNA repair pathways as long genes typically accumulate more DNA damage compared to shorter genes (Vermeij *et al*., 2016). Defects to DNA repair pathways have previously been associated with reduced lifespan in *Drosophila* (Garschall *et al*., 2017). As discussed previously, Top2B has been associated with DNA repair pathways in mammals as reported by Gupta *et al*. (2012) and Morotomi-Yano *et al*. (2018). It is possible that Top2 also plays a role in the DNA repair pathways of *Drosophila*, although further work would need to be carried out to elucidate this. Nevertheless, reductions of Top2 with age may have profound effects on the ability of cells to repair DNA and may result in increased vulnerability to oxidative stress, ultimately having detrimental effects on longevity.

It is important to remember that Top2 in the *Drosophila* brain may also be involved in DNA replication as Top2 has been shown to be expressed in mitotically active cells (Gemkow *et al*., 2001). A study by Von Trotha *et al*. (2009) showed that proliferating cells can be found in the adult brain of *Drosophila*, specifically around the antennal nerve. It was hypothesised that these may be adult stem cells with the potential to generate glial and/or non-glial cell types. In addition, neurogenesis has been shown to occur in the medulla cortex of the adult *Drosophila* optic lobes (Fernandez-hernandez *et al*., 2013). Thus, the consequence of declining levels of Top2 may also lead to detrimental effects in this physiological context too.

A number of questions remain to be answered from this study, including; (1) Is Top2 structure damaged with ageing? (2) Do higher levels of endogenous Top2 cleavage complexes form in aged cells? (3) Is the proteasome system involved in removal and degradation of these endogenous Top2 cleavage complexes?

Experiments aiming to answer these questions may provide useful future research. For example, immunoprecipitation experiments may reveal whether structural damage to epitopes of Top2 occur during ageing. Furthermore, the use of the trapped in agarose DNA immunostaining assay (TARDIS) would allow quantification of topoisomerase–DNA complexes to be made. Unlike the alkaline comet assay, the TARDIS assay can detect these specific modifications rather than the general presence of DNA breaks

(Cowell *et al*., 2010). This may answer whether higher levels of endogenous Top2 cleavage complexes form in aged cells. Alongside TARDIS assays, the use of proteasome inhibitors in future experiments may help to determine whether the proteasome system has any involvement in the degradation of Top2 cleavage complexes. As stated previously, this system is known to be responsible for the degradation and removal of damaged proteins. As protein levels of Top2 have been shown to decrease in this study but mRNA levels have been shown to be constant, analysis of the rate of transcription may provide insightful research. It may be that mRNA levels become upregulated to compensate for a loss of protein.

It may also be useful to look deeper into the expression of Top2 in *Drosophila*. In this study, relative levels of Top2 were investigated from extracts of whole brain tissue. However, brain tissue is made up of numerous cell types and not just neurons. Experiments carried out on whole brains alone will result in a loss of cellular information and may be hiding cell-specific roles of Top2. Thomas *et al*. (2010) developed and adapted the translating ribosome affinity purification (TRAP) method to allow the unique translatome profiles of different cell-types to be determined under various physiological, pharmacological and pathological conditions in *Drosophila*. Thomas suggested that translatome profiling using these methods allows questions regarding the life-cycle of mRNA molecules in *Drosophila* to be answered. Future work using these methods may help to determine tissue specific expression of Top2.

In conclusion, Top2 protein levels have been shown to decrease during ageing in male and female *Drosophila*. Alongside decreases in Top2 protein levels, declines in locomotor function were also seen in males and females during ageing with significant increases of AGEs seen in female flies.

4. Development of a cell line model of ageing using the human neuroblastoma cell line SH-SY5Y to investigate changes in Top2B expression

4.1 Introduction

To explore the expression of Top2B in aged neurons, the development of a suitable cell line model was required. The neuroblastoma cell line SH-SY5Y is widely used in the field of neuroscience research due to the ability of the cell line to be differentiated into a cell with a more mature neuronal-like phenotype. This cell line is derived from the SK-N-SH cell line, which was cultured from the biopsy of a metastatic tumour in a four year old female neuroblastoma patient in 1970 (Kovalevich & Langford, 2013). In an undifferentiated state, SH-SY5Y continuously rapidly proliferate (Påhlman *et al*., 1984) and so provide an unlimited supply of material, which is cost effective and also bypasses the ethical concerns associated with using human tissue. SH-SY5Y are morphologically characterised as neuroblast-like cells possessing only a few short neuronal processes with tendencies to grow in clusters (Kovalevich & Langford, 2013) and express immature neuronal markers (Påhlman *et al*., 1984). After induction of differentiation SH-SY5Y morphologically become more comparable to mature neurons. Cells no longer grow in clusters and they develop long neurite processes forming networks with neighbouring cells with reductions in proliferation also seen. In addition, mature neuronal markers are expressed such as neuronal nuclei (NeuN), synaptophysin (SYN), growth-associated protein (GAP-43), microtubule associated protein (MAP), neuron specific enolase (NSE) and synaptic vesicle protein II (SV2) (Shipley *et al*., 2016). The SH-SY5Y cell line is known to produce different cellular phenotypes: N-type cells and S-type cells. N-type cells are neuroblastic and are characterised by neurite processes, whereas S-type cells are substrate adherent multipotent precursors to a number of non-neuronal cells including glial cells, melanocytes and Schwann cells (Bell *et al*., 2013). The SH-SY5Y cell line is predominantly composed of N-type cells having derived from three successive subclone selections of N-type cells. However, a small proportion of S-type cells remain in the SH-SY5Y cell line (Forster *et al*., 2016). SH-SY5Y have been commonly used to investigate neurodegenerative diseases such as Parkinson's disease and Alzheimer's disease (Agholme *et al*., 2010; Xie *et al*., 2010) but its use as a model of ageing has also been reported (Heidari *et al*., 2018; Rahimi *et al*., 2018). In ageing studies SH-SY5Y cell are most commonly 'aged' through oxidative stress. Cells are typically stressed until ROS generation occurs to produce a

senescence-associated secretory phenotype (SASP), rather than chronologically aged to produce the same features of an aged cell (Liu *et al*., 2013; Heidari *et al*., 2018). ROS generation and subsequent oxidative stress is known to cause mitochondrial dysfunction, which is one of the leading triggers of senescence (Chapman *et al*., 2019). Dysfunction of mitochondria alters cell signalling and subsequently SASP is produced (section 1.2) (Vizioli *et al*., 2020). Sub-lethal concentrations of H_2O_2 can increase oxidative stress, cause DNA cleavage and induce a hyperactivation of poly (ADP-ribose) polymerase (PARP) and subsequent depletion of NAD+. A decrease in SIRT1 function follows this with an accumulation of acetylated p53 and transcription of p53 target genes, such as p21, that bind to cyclin E/Cyclin dependent kinase 2 and cyclin D/Cyclin dependent kinase 4 complexes to cause G_1 arrest in the cell cycle (Chen, 2016). It is likely that this pathway plays an important role in oxidative stress induced cellular senescence (Han *et al*., 2014).

As stated previously, SH-SY5Y cells are frequently used because of their ability to be differentiated into more neuronal-like cells. The addition of all-trans retinoic acid (RA) to the culture medium is one of the most commonly employed methods to induce differentiation in the SH-SY5Y cell line. As a vitamin A derivative, RA has been shown to induce cellular differentiation and inhibit cell growth (Xicoy *et al*., 2017). Various studies have shown SH-SY5Y can become differentiated into cells with cholinergic phenotypes, whereas as others have shown a shift towards a dopaminergic phenotype in response to the addition of RA to the culture medium (Xie *et al*., 2010; Kovalevich & Langford, 2013). RA controls a number of aspects associated with cell differentiation, proliferation and apoptosis (Gudas & Wagner, 2011). The actions of the two transcription factor families, retinoic acid receptors (RAR) and retinoid X receptors (RXR) are responsible for the mediation of most RA activities. Once inside a cell, RA binds to cellular RA-binding protein II (CRABPII) or FABP5 and is relocated to the nucleus (Conserva *et al*., 2019). In the nucleus, RA binds to RAR, which subsequently binds to RXR. This RXR/RAR complex can bind to RA response elements (RAREs) in the promoter regions of target genes. Association of the receptor with RA brings about a conformational change in its ligand-binding domain such that instead of binding transcriptional corepressors, such as nuclear receptor corepressor (NCoR) or silencing mediator of retinoic acid and thyroid hormone receptor (SMRT), it can bind to and recruit coactivators of expression such as histone acetyl transferases (HATs), including, nuclear receptor coactivator 3 (NCoA3). This triggers the transcription of a number of

key genes required for neuronal differentiation (Das *et al*., 2014). Many other co-factors are involved in these processes too. For example, interaction of the zinc-finger protein Zfp42 with RXR/RAR complexes at some RAREs has been shown to be required for RA-induced cell cycle arrest and differentiation of neuroblastoma cells (Huang *et al*., 2009).

It should also be noted that there are exceptions to this model. For example, RXR/RAR complexes bound to RA can lead to the recruitment of PRC2 and histone deacetylase (HDAC) to repress the expression of genes including homeobox B1 (*Hoxb1*) and fibroblast growth factor 8 (*Fgf8*) (Cunningham & Duester, 2015).

In addition to the classical genomic effects briefly described above, RA has a number of nongenomic effects, which it elicits by rapidly and transiently activating several kinase cascades (Al Tanoury *et al*., 2013). For example, the addition of RA has been shown to activate the phosphatidylinositol 3-kinase (PI3K)/protein kinase B (Akt) signalling pathway as well as extracellular signal-regulated kinase 1 and 2 (ERK1/2) pathways. PI3K/Akt has shown to be a regulator of both neuronal differentiation and survival of RA-treated neuroblastoma cells with inhibition of PI3K by LY294002 causing impairments in RA-induced neuronal differentiation (López-Carballo *et al*., 2002). The PI3K/Akt and ERK1/2 pathways have been seen to regulate RA-induced RXR transcriptional activity in neuroblastoma cells (Qiao *et al*., 2012).

A number of studies have previously investigated Top2B in the SH-SY5Y cell line. However, these studies have predominantly focussed on the regulation of Top2B expression during differentiation and development. As stated previously, studies have demonstrated increases in Top2B expression at both the mRNA and protein level during retinoic acid-induced neuronal differentiation of SH-SY5Y cells, alongside increases in the transcription factor Sp1, which also increased at the mRNA and protein level, suggesting that Sp1 might regulate Top2B expression by binding to its GC box in the promoter region (section 1.5.4) (Guo *et al*., 2014). In addition to this, the transcription factor NURR1 has been implicated in axonal development of dopaminergic neurons through interaction with Top2B. Reports have identified two functional NURR1 binding sites in the proximal Top2B promoter and propose that NURR1 may influence axon genesis in dopaminergic neurons by recruiting Top2B (section 1.5.4) (Heng *et al*., 2012). However, to the best of our knowledge no studies have looked into the expression of Top2B in an ageing model of the SH-SY5Y cell line.

The purpose of this research was to create senescence within the SH-SY5Y cell line to provide a model that gives a representation of an aged-like neuron. This chapter presents the results found from the development of this model.

4.2 Hydrogen peroxide induced cellular senescence of undifferentiated SH-SY5Y cells

In order to create a cell line model of ageing, a number of approaches were taken to induce senescence in SH-SY5Y cells. Methods of cellular senescence induction using oxidative stress caused by hydrogen peroxide (H_2O_2) have been reported in a number of studies using various cell types, such as fibroblasts and mesenchymal stem cells (Kiyoshima *et al*., 2012; Choo *et al*., 2014). In addition, Nopparat *et al*. (2017) demonstrated that senescence can be induced in undifferentiated SH-SY5Y cells through exposure to H_2O_2. Hydroxyl radicals, superoxide anions and H_2O_2 are all examples of reactive oxygen species (ROS) that are generated during redox reactions in the human body. Oxidative stress is induced by high levels of these ROS, which can cause mitochondria, protein, DNA and lipid membrane dysfunction and can lead to losses in cellular function and integrity, ultimately causing cellular senescence (Chapman *et al*., 2019).

Cell cycle arrest is one of the predominant features of senescence, hence initial experiments focussed on creating senescence in undifferentiated SH-SY5Y cells by exposing them to a range of H_2O_2 concentrations and analysing relative proliferation using the WST-1 assay. Cells were exposed to a range of concentrations of H_2O_2 (0.1 to 2 mM) for 1 hour and then grown over a range of incubation times following exposure (24, 48 and 72 hours) to examine the effect on proliferation (figure 4.1).

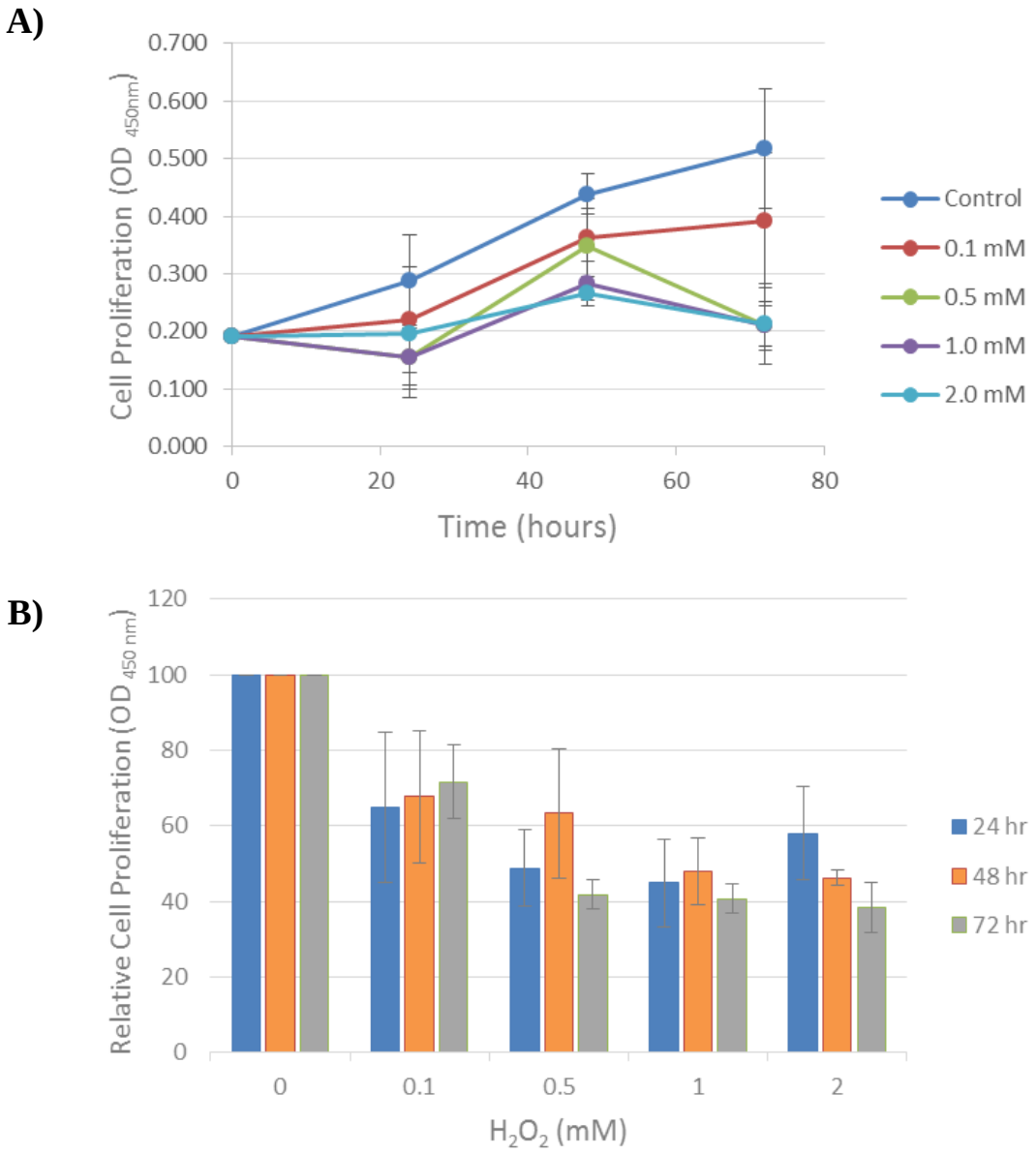

Figure 4.1 Proliferation of SH-SY5Y cells treated with a 1 hour pulse of a range of H_2O_2 concentrations and grown for 24, 48 or 72 hours.

Cells were seeded in three 96-well plates in culture media at a density of 1 x 10^5 cells/ml with 100 µl added to each well. The cells were then incubated for 48 hours at 37°C to allow cells to adhere. SH-SY5Y cells were exposed to H_2O_2 concentrations of 0.1, 0.5, 1.0 and 2.0 mM for 1 hour. Supernatant was removed and wells were rinsed in 100 µl culture media. 100 µl fresh culture media was added to wells and incubated. WST-1 assays were performed after 24, 48 and 72 hours (section 2.2.2.11) and an H_2O drug vehicle control was analysed alongside treated cells. At each time point WST-1 reagent (Roche- 05015944001) was added to a plate and incubated for 2 hours. The absorbance of the samples was measured at 450 nm on a plate reader. Proliferation data is presented as a measurement of OD at 450 nm (A) and relative cell proliferation compared to an untreated control (B). Data is presented as the mean of three biological replicates ± standard error.

Results from Figure 4.1 show that 0.1 mM H_2O_2 reduces proliferation at all post-exposure times but not significantly (see Appendix table B.1 for p values). However, 1-hour pulses of 0.5, 1.0 and 2.0 mM reduced relative proliferation to approximately 50% with all results significant apart from 0.5 mM after 48 hours (p=0.15) and 2.0 mM after 24 hours (p=0.0505 Student's t-test, two-tailed) (see Appendix table B.1 for p values). Interestingly, longer post exposure times did not always reduce proliferation further as seen in cells treated with 0.1, 0.5 and 1.0 mM H_2O_2. So although proliferation rates are reduced compared to controls they are not inhibited completely as hoped for.

Previously it has been shown that SH-SY5Y cells treated with 0.1 mM H_2O_2 for 2 hours and then grown for a further 24 hours showed a decrease in ki67 immunoreactivity using fluorescence microscopy compared to controls (Nopparat *et al*., 2017). Ki67 is strongly associated with proliferative activity of cells and is expressed in the nuclei in all phases of the cell cycle, whereas activity of Ki67 is not seen in quiescent or resting differentiated cells in the G0 phase (Juríková *et al*., 2016). However, in the Nopparat study no quantification of Ki67 immunoreactivity was performed, so it is difficult to compare with the reduction in proliferation after exposure to 0.1 mM H_2O_2 for 1 hour in this study.

Alongside WST-1 assays SH-SY5Y cells were exposed to the same range of H_2O_2 concentrations and viewed under a light microscope 24, 48 and 72 hours after a 1 hour H_2O_2 exposure. It was found that cells exposed to 0.5, 1.0 and 2.0 mM H_2O_2 were no longer adherent to the culture flask and began to clump together. Trypan blue analysis of cells treated with higher concentrations of H_2O_2 confirmed that a large proportion of cells were dead (looked at a flask of leftover cells. No data recorded). Work by Nopparat *et al*. (2017) supports this finding. Following 24 hours post exposure to 2 hours of H_2O_2, SH-SY5Y viability decreased significantly at 0.1, 0.2, and 0.4 mM to ~84%, ~67%, and ~38%, respectively.

Interestingly, cells exposed to 0.1 mM H_2O_2 for 1 hour displayed a limited loss of adherence and viability compared to the 2 hour exposure in the Nopparat study, indicating the length of exposure as well as the dose of H_2O_2 used can affect the viability of the cells.

Thus, it was decided to treat SH-SY5Y cells with lower doses of H_2O_2 to determine if this could induce senescence in the cells and this was initially assessed by observing proliferation. Cells were exposed to a range of concentrations of H_2O_2 ranging from 0.1

µM up to 10 µM for a 1 hour pulse and incubated for 24 hours or 48 hours (Figure 4.2). It was decided that WST1 assay would not be used as it does not specifically measure the number of viable cells in a culture or their growth but rather an integrated set of enzyme activities that are related in a number of ways to cell metabolism (Berridge *et al*., 2005). As such, oxidative stress may significantly affect the results due to perturbations in the activity of many mitochondrial and non-mitochondrial enzymes involved in reduction of WST1 and may result in under/over estimation of proliferation (Stepanenko & Dmitrenko, 2015). Instead, it was decided to quantify the number of viable cells using trypan exclusion to measure proliferation.

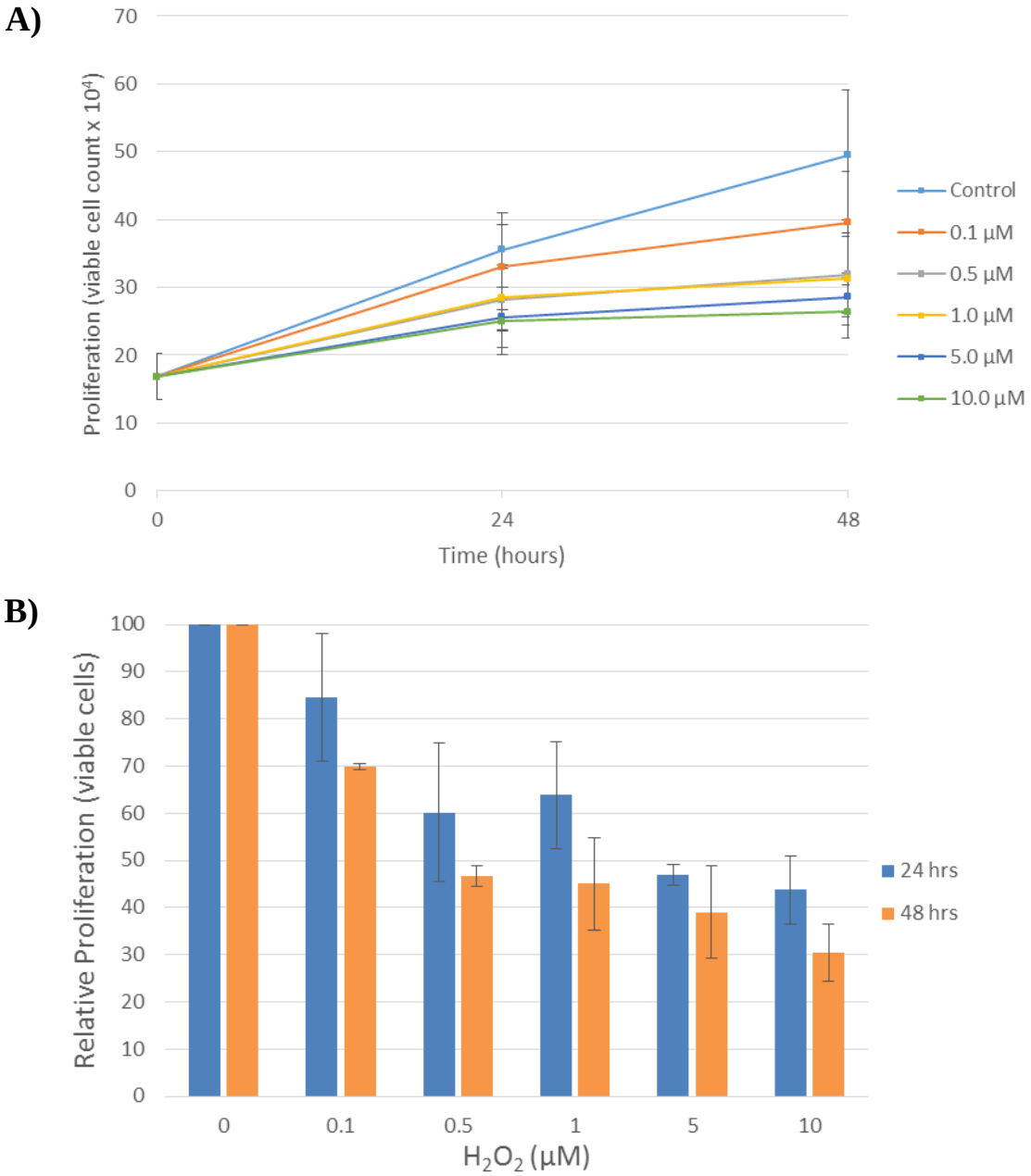

Figure 4.2 Proliferation of SH-SY5Y cells over 24 and 48 hours after a 1 hour pulse with a range of H_2O_2 concentrations.

6-well plates were seeded at 1 x 10^5 cells/ml (2ml per well) and incubated for 48 hours at 37°C. Cells were exposed to working concentrations of H_2O_2 for 1 hour (2 ml per well). SH-SY5Y cells were exposed to a range of H_2O_2 concentrations (0.1, 0.5, 1.0, 5.0 and 10.0 µM) alongside an H_2O drug vehicle control. Supernatant was removed and cells were rinsed in 1 ml DMEM. 2 ml of fresh DMEM was added to each well and plates were incubated for 24 or 48 hours. Cell counts were performed using trypan blue exclusion assay. To detach the cells from the bottom of the 6-well plate, a cell scraper was used. Proliferation data is presented as a measurement of viable cell counts (A) and relative cell proliferation compared to an untreated control (B). Data is presented as the mean of three biological replicates ± standard error.

Results from Figure 4.2B demonstrate no significant reduction in proliferation with 0.1 µM H_2O_2 after 24 hours (p=0.31). However, after 48 hours this dose reduced proliferation significantly to ~70% of the control ($p=1.5x10^{-6}$). Increasing doses of H_2O_2 also show further reductions in relative proliferation compared to the control with all remaining results, apart from 0.5 µM H_2O_2 after 24 hours, demonstrating significant reductions in relative proliferation (see Appendix table B.2 for p values).

From the data above, exposure to a 1 hour pulse of 10 µM H_2O_2 was most effective, reducing relative proliferation to ~30% after 48 hours ($p=3.2x10^{-4}$). Bearing in mind the potential toxicity of H_2O_2 to SH-SY5Y cells discussed above and shown by Nopparat *et al*. (2017), it was decided to test for senescence using the β-galactosidase (β-gal) assay on cells exposed to a 1 hour pulse of 10 µM H_2O_2 and grown for a further 48 hours. Senescence-associated β-gal is a lysosomal enzyme most commonly used as a senescence biomarker and can be detected by means of a cytochemical assay (Dimri *et al*., 1995). Reports have shown that senescent cells have large and numerous lysosomes and as a result have high levels of β-gal (Kurz *et al*., 2000). Results for the β-gal assay of SH-SY5Y cells treated with 10 µM H_2O_2 can be seen in Figure 4.3.

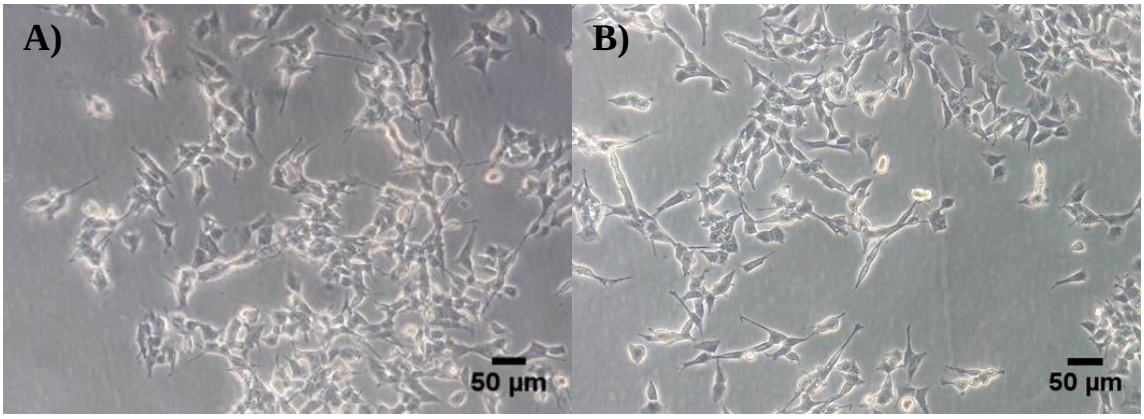

Figure 4.3 β-gal assay of SH-SY5Y cells 48 hours after a 1 hour exposure to 10 µM H_2O_2.

SH-SY5Y cells were seeded in a 6-well plate at 1 x 10^5 cells/ml (2 ml per well) and incubated for 48 hours at 37°C. 2 ml working concentrations of H_2O_2 (B) or a H_2O control (A) were added to each well and incubated for one hour. Supernatant was removed and plates were rinsed in 1 ml DMEM. Fresh DMEM was added and then incubated for 24 hours. β-gal assays were carried out using Sigma Aldrich Senescence Cells Histochemical Staining Kit (catalogue Number CS0030) according to manufacturer instructions. Cells were observed under a light microscope and images were obtained. Any cells expressing β-gal should appear bright blue in colour. Experiments were carried out in triplicate.

Results from Figure 4.3B show that no blue β-gal staining was observable in H_2O_2 treated undifferentiated SH-SY5Y cells treated with 10 µM H_2O_2. Results seen in the control cells (Figure 4.3A) are comparable to those treated with H_2O_2. This assay was carried out in triplicate and staining was not observed in any of the experiments (data not shown). In addition to this, attempts were made to induce senescence in undifferentiated SH-SY5Y by exposing cells to 10 µM H_2O_2 for 1 hour on 3 consecutive days before carrying out β-gal assays. This also provided negative results (data not shown). In contrast, Nopparat *et al*. (2017) showed that treatment with a 2 hour pulse of 100 µM H_2O_2 significantly increased the number of SA- β-gal-positive cells by ~195% compared to control cells.

In conclusion, although proliferation could be significantly reduced to ~30% of control cells using 10 µM H_2O_2 without compromising cellular viability, this treatment did not bring about senescence as measured by the β-gal assay.

4.3 Hydrogen peroxide induced cellular senescence of retinoic acid treated SH-SY5Y cells

Following unsuccessful attempts to induce senescence in undifferentiated SH-SY5Y cells it was decided that further investigations would be made in differentiated-like SH-SY5Y cells. As stated previously the addition of all-trans retinoic acid (RA) to culture medium is one of the most commonly employed methods to induce the differentiation-like phenotype in the SH-SY5Y cell line. In addition to this, utilising cells that phenotypically display mature neuronal-like characteristics may provide a more suitable model for further investigations as they are more similar to adult neurons (Shipley *et al*., 2016).

4.3.1 Retinoic acid-induced differentiation-like phenotype in SH-SY5Y cells

SH-SY5Y are derived from cancerous neuroblastoma cell lines and, as a result of this, possess dysregulated cell cycles and display a continued up-regulation of cell proliferation. This does not represent a mature neuron, which typically does not divide (Fishel *et al*., 2007). As RA has been shown to induce a differentiated-like phenotype in which cell growth is inhibited (Xicoy *et al*., 2017), SH-SY5Y cells were exposed to 1 µM and 10 µM RA in culture media. This range of concentrations was chosen but 10 µM RA has been most commonly used in previous studies to differentiate SH-SY5Y

(Kovalevich & Langford, 2013; Shipley *et al*., 2016). The effect of these concentrations of RA on proliferation was monitored and the results are shown in Figure 4.4. Cuende *et al*. (2008) showed that exposure to 10 µM RA causes SH-SY5Y cells to progressively develop phenotypic changes compatible with neuronal-like morphology, characterised by neurite outgrowth and a reduction in proliferation after 2 days. The expression of neuronal markers including Gap43, Map2 and Tau was seen at day 2 and progressively increased up to day 5. In addition, a decline in proliferating cell nuclear antigen (PCNA) protein was seen, whereas cyclin-dependent kinase inhibitors p27 and p21 were increased. This data suggested that treatment of SH-SY5Y cells with RA was suitable to differentiate these cells. Similarly, Maruyama *et al*. (1997) also differentiated SH-SY5Y cells for 3 days with 10 µM RA, which caused morphological changes and arrest of proliferation.

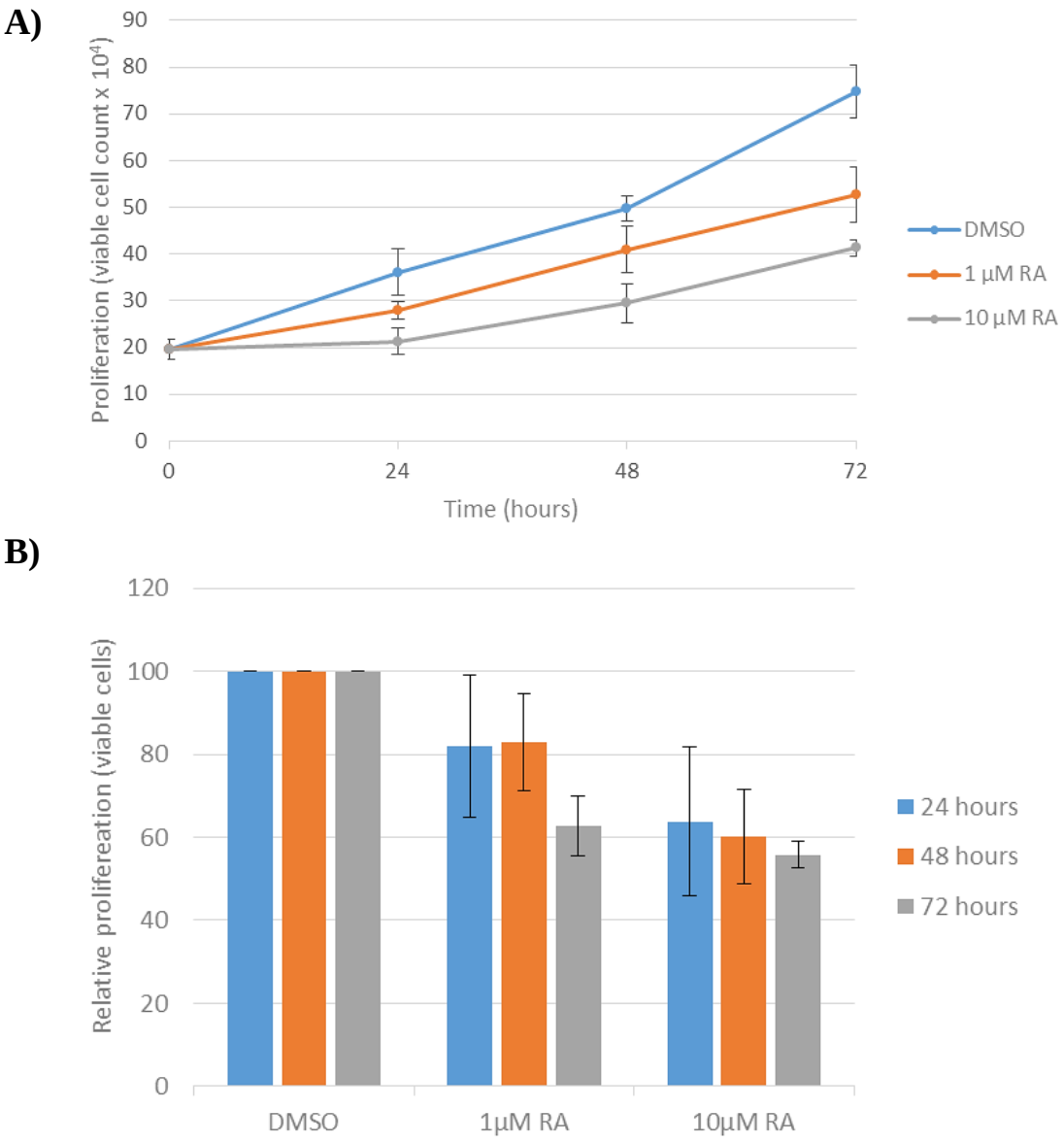

Figure 4.4 The effects of all-trans retinoic acid on SH-SY5Y proliferation.

6-well plates were seeded at 1 x 10^5 cells/ml (2 ml per well) and incubated for 24 hours at 37°C. Supernatant was removed and cells were exposed to working concentrations of RA at 1.0 µM or 10 µM for 24, 48 and 72 hours. A 0.1% DMSO (v/v) control was analysed alongside RA-treated cells. Cells were detached from the bottom of the 6-well flask at 24, 48 and 72 hours using a cell scraper and viable cells were counted using trypan blue exclusion. Proliferation data is presented as a measurement of viable cell counts (A) and relative cell proliferation compared to an untreated control (B). Data is presented as the mean of three biological replicates ± standard error.

Results from Figure 4.4A shows significant reductions of cell growth in SH-SY5Y cells treated with 10 µM RA after 48 and 72 hours compared to the DMSO control with p values of 0.027 and 0.005, respectively. However, these cells still continue to proliferate, albeit at a much slower rate than the control cells. For example, SH-SY5Y cell numbers after 72 hours of 10 µM RA treatment is significantly higher than T_0 (p=0.002), which suggests that some of the cells are not entering cell cycle arrest. Differences between the DMSO control and cells treated with 1.0 µM RA are not significant, therefore no further experiments were carried out using this concentration of RA.

Alongside proliferation assays, morphological comparisons between undifferentiated and 10 µM RA treated cells were made. Cells were monitored for any changes in neurite outgrowth and cell shape. Results can be seen in Figure 4.5.

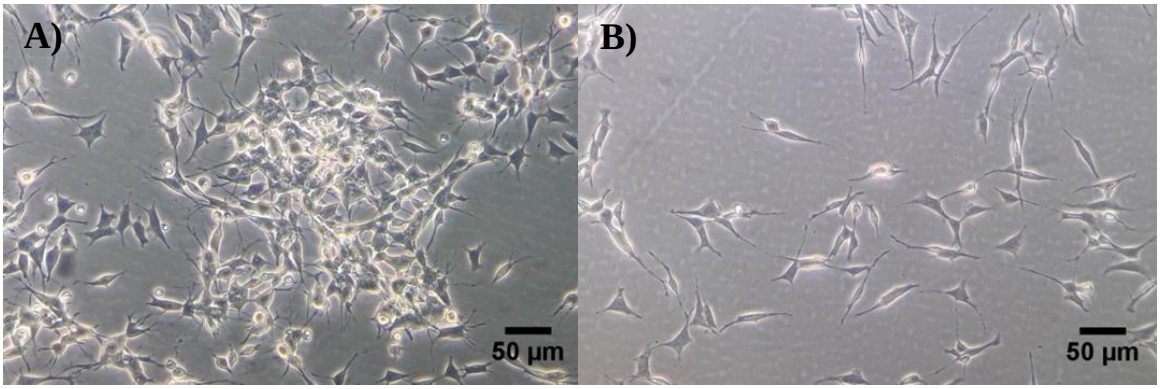

Figure 4.5 Morphological changes of SH-SY5Y after 10 µM RA treatment.

6-well plates were seeded at 1 x 10^5 cells/ml (2 ml per well) and incubated for 24 hours at 37°C. Supernatant was removed and plates were treated with 10 µM RA or a 0.1% DMSO (v/v) control. Cells were observed under a light microscope after 24, 48 and 72 hours and images were obtained. Image (A) shows cells treated with DMSO and image (B) shows cells treated with 10 µM RA after 72 hours.

Images seen in Figure 4.5 clearly show morphological changes in SH-SY5Y cells treated with 10 µM RA for 72 hours (Figure 4.5B) compared to the DMSO control (Figure 4.5A). Untreated cells can be seen to grow in clumps and possess short neurites. A neurite is an elongated cylindrical process that extends from the cell body and serves as a precursor of axons and dendrites to allow polarisation of the neuron to occur (Clagett-Dame *et al.*, 2006). In comparison, RA-treated cells tend to spread out and

develop longer neuronal projections. These morphological changes suggest the development of a differentiated-like phenotype in the RA treated cells.

Although these morphological changes were accompanied by some reduction in proliferation, results from figure 4.4 show that proliferation failed to continually decrease with time but instead remained stable from 24 to 72 hours. Further molecular analysis was needed to determine if differentiated-like cells had developed.

4.3.2 Quantification of Topoisomerase II protein during SH-SY5Y differentiation

Previous studies have shown that Top2B is expressed throughout the cell cycle in all mammalian cells. However, it is reported to be significantly upregulated when cells enter a state of terminal differentiation (Tsutsui *et al*., 1993; Tiwari *et al*., 2012; Guo *et al*., 2014; Harkin *et al*., 2015; Austin *et al*., 2018). In contrast, Top2A is seen to be highly expressed in proliferating cells but not in terminally differentiated tissue. Tsutsui *et al*. (1993) reported that Top2A was present in embryonic rat brains and in the cerebellum two days after birth but levels were undetectable after 4 weeks. If a differentiation-like phenotype has been achieved in RA-treated SH-SY5Y cells, Top2B protein levels should be seen to increase while Top2A levels should be seen to decrease. Indeed, Top2A has been used as a marker for proliferation in many other studies (Turley *et al*., 1997; Hong *et al*., 2012; Şahin *et al*., 2016). Thus, it was decided to semi-quantify the levels of Top2A and Top2B in RA treated cells.

SH-SY5Y cells were treated with 10 µM RA and protein extracts taken at time zero (T0) and after 24, 48 and 72 hours. Western blot analysis of Top2A and Top2B was carried out on these samples alongside untreated SH-SY5Y cells. Results can be seen in Figure 4.6 and Figure 4.7.

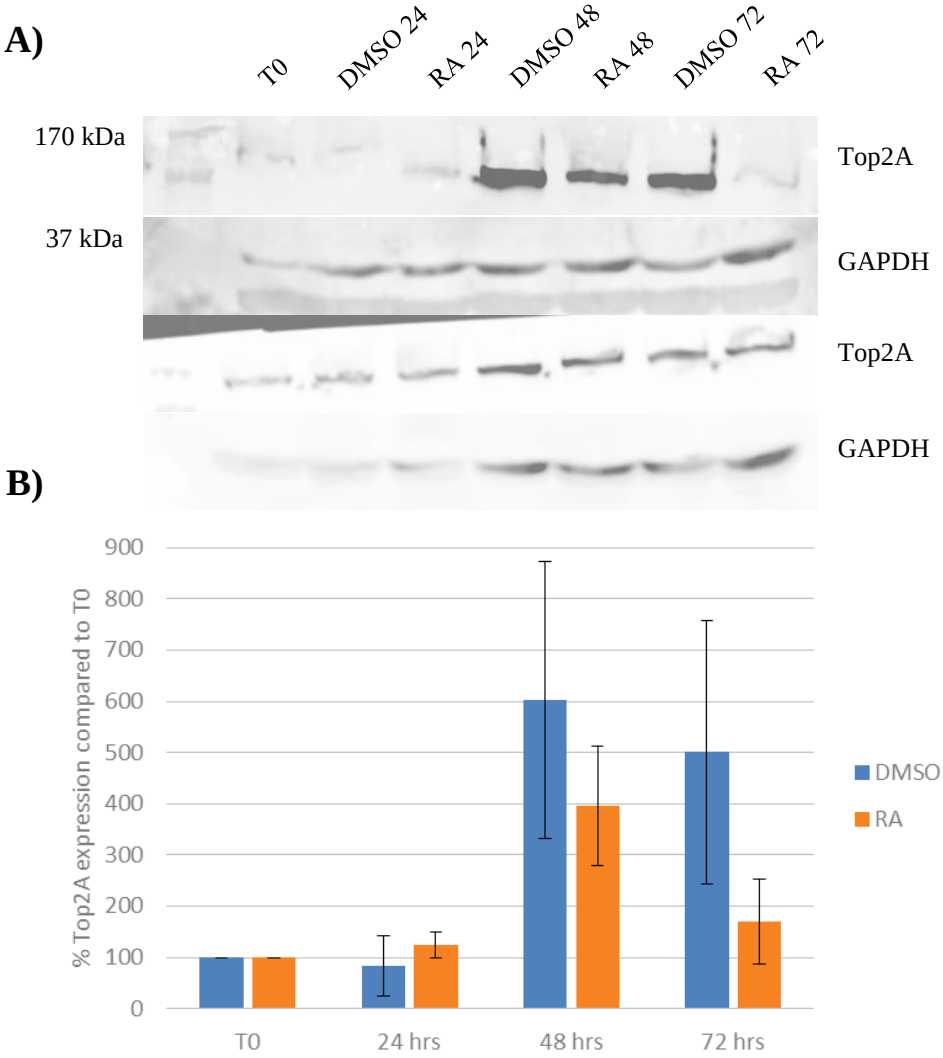

Figure 4.6 Semi-quantification of Top2A over 72 hours of RA-induced differentiation of the SH-SY5Y cell line.

T25 culture flasks were seeded at 1 x 10^5 cells/ml (5 ml per flask) and incubated for 48 hours at 37°C. Supernatant was removed and flasks were treated with 10 µM RA or a 0.1% DMSO (v/v) control and incubated. Whole cell extraction was carried out at T0 and after 24, 48 and 72 hours as described in section 2.2.2.9 and quantified as described in section 2.2.2.10. Equal protein loads (56.4 µg) were added to wells of a 7.5% SDS gel. SDS-PAGE was carried out and protein was transferred to nitrocellulose paper by wet western transfer. (A) Nitrocellulose blots were probed with a Top2A antibody and a GAPDH load control antibody. Analysis of blot densitometry was carried out using GeneTools (Syngene). (B) TopA expression is presented as a percentage of that seen in T0 cells. The results shown for Top2A are the mean of two independent experiments ± standard error.

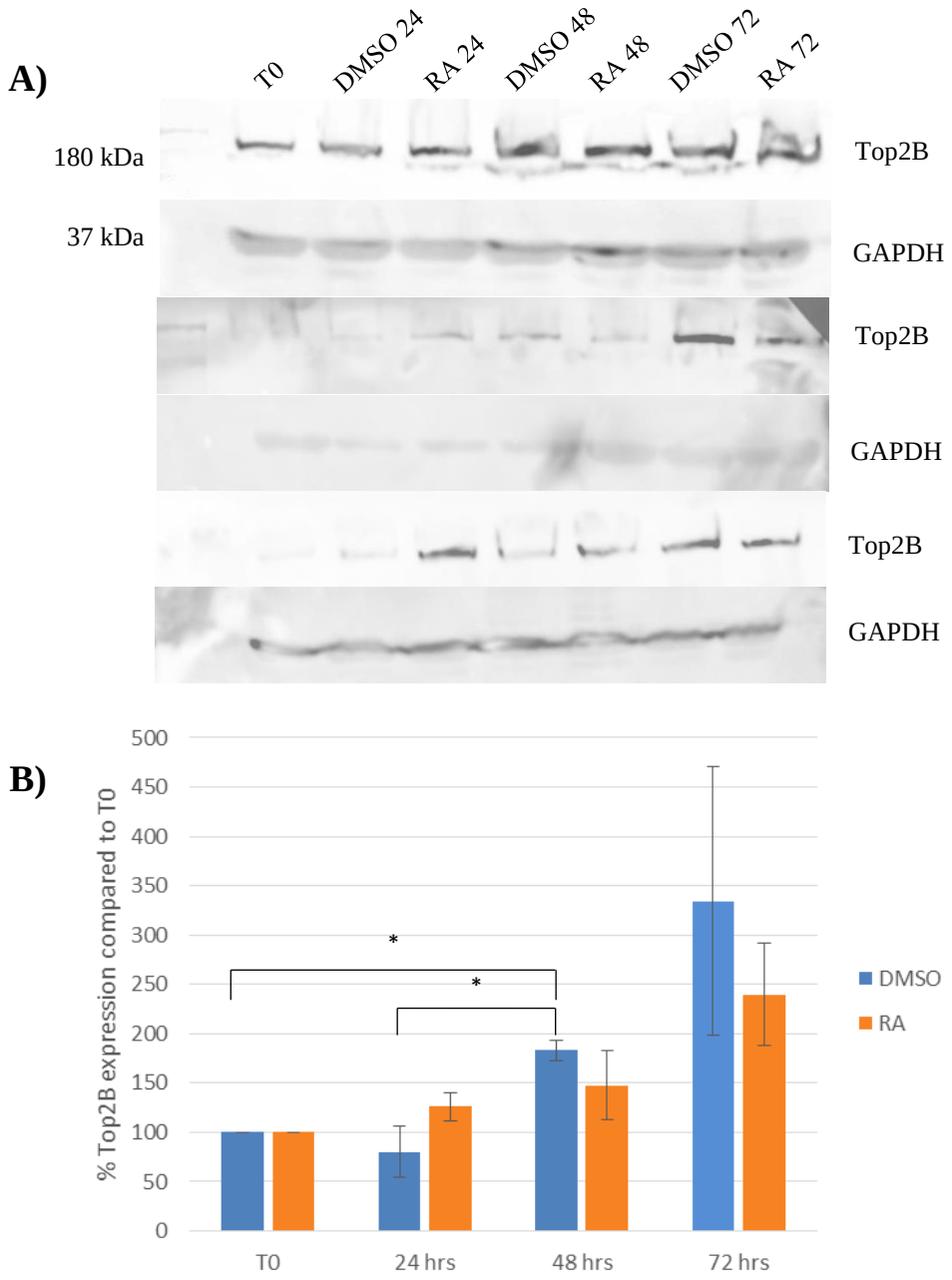

Figure 4.7 Semi-quantification of Top2B over 72 hours of RA-induced differentiation of the SH-SY5Y cell line.

T25 culture flasks were seeded at 1 x 10^5 cells/ml (5 ml per flask) and incubated for 48 hours at 37°C (5% CO_2). Supernatant was removed and flasks were treated with 10 µM RA or a 0.1% DMSO (v/v) control and incubated. Whole cell extraction was carried out after 24, 48 and 72 hours as described in section 2.2.2.9 and quantified as described in section 2.2.2.10. Equal protein loads (56.4 µg) were added to wells of a 7.5% SDS gel. SDS-PAGE was carried out and protein was transferred to nitrocellulose paper by wet western transfer. (A) Nitrocellulose blots were probed with a Top2B antibody and a GAPDH load control antibody. Analysis of blot densitometry was carried out using GeneTools (Syngene). (B) Top2B expression is presented as a percentage of that seen in T0 cells. Results shown for Top2B are the mean of three independent experiments ± standard error. * = $p < 0.05$ (Student's t-test, two-tailed).

Results shown in Figure 4.6 yielded no significant changes in protein levels of Top2A in RA-treated SH-SY5Y cells over 72 hours. In addition, treatment with 10 µM RA at all time points investigated did not show any significant differences in Top2B protein levels (Figure 4.7), although the high inter-experiment variability should be noted. This is unlike previous studies that have shown Top2A decreases during differentiation (Thakurela *et al*., 2013) and Top2B increases in terminally differentiated neurons (Guo *et al*., 2014).

These findings suggest that a differentiated-like phenotype had not been achieved despite some reduction in proliferation and morphological changes characteristic with differentiation being noted.

Interestingly, significant increases were seen in Top2B protein levels between T0-48 hours and 24-48 hours in the DMSO control with p values of 0.017 and 0.034, respectively. Many papers have reported that Top2B protein levels remain stable throughout the cell cycle (Woessner *et al*., 1991; Turley *et al*., 1997). However, Top2B protein levels are shown to increase with increasing proliferation. As equal protein loads from extracts were analysed on the gels, it would suggest that Top2B levels increase throughout the cell cycle. However, further experiments would be needed to confirm this. Nevertheless, this has also been reported in previous studies. For example, Padget *et al*. (2000) demonstrated that both Top2A and Top2B are expressed to higher levels in exponentially growing cells than in plateau phase and G_0 peripheral blood lymphocyte cells, suggesting that there is a positive correlation between type 2 topoisomerase protein content and activity.

Despite these findings it was decided to try to induce senescence using H_2O_2 in SH-SY5Y cells pre-exposed to 10 µM RA for 72 hours.

4.3.3 Hydrogen peroxide-induced cellular senescence of RA treated SH-SY5Y cells

In order to determine whether it was possible to induce senescence in RA treated cells by H_2O_2 induced oxidative stress, cells were exposed to 100 µM H_2O_2 for 1 hour post incubation with RA. This dose was chosen as previous studies have shown that differentiated SH-SY5Y cells are more resistant to the effects of DNA damaging agents than undifferentiated cells (Schneider *et al*., 2011; Tong *et al*., 2017) with further studies showing concentrations of 100 µM H_2O_2 being used to induce oxidative stress in SH-SY5Y cells, whilst maintaining sufficient cell viability (Ramalingam & Kim, 2014).

Further proliferation assays were carried out on untreated and RA treated SH-SY5Y cells with or without H_2O_2 induced oxidative stress. Results are shown in Figure 4.8.

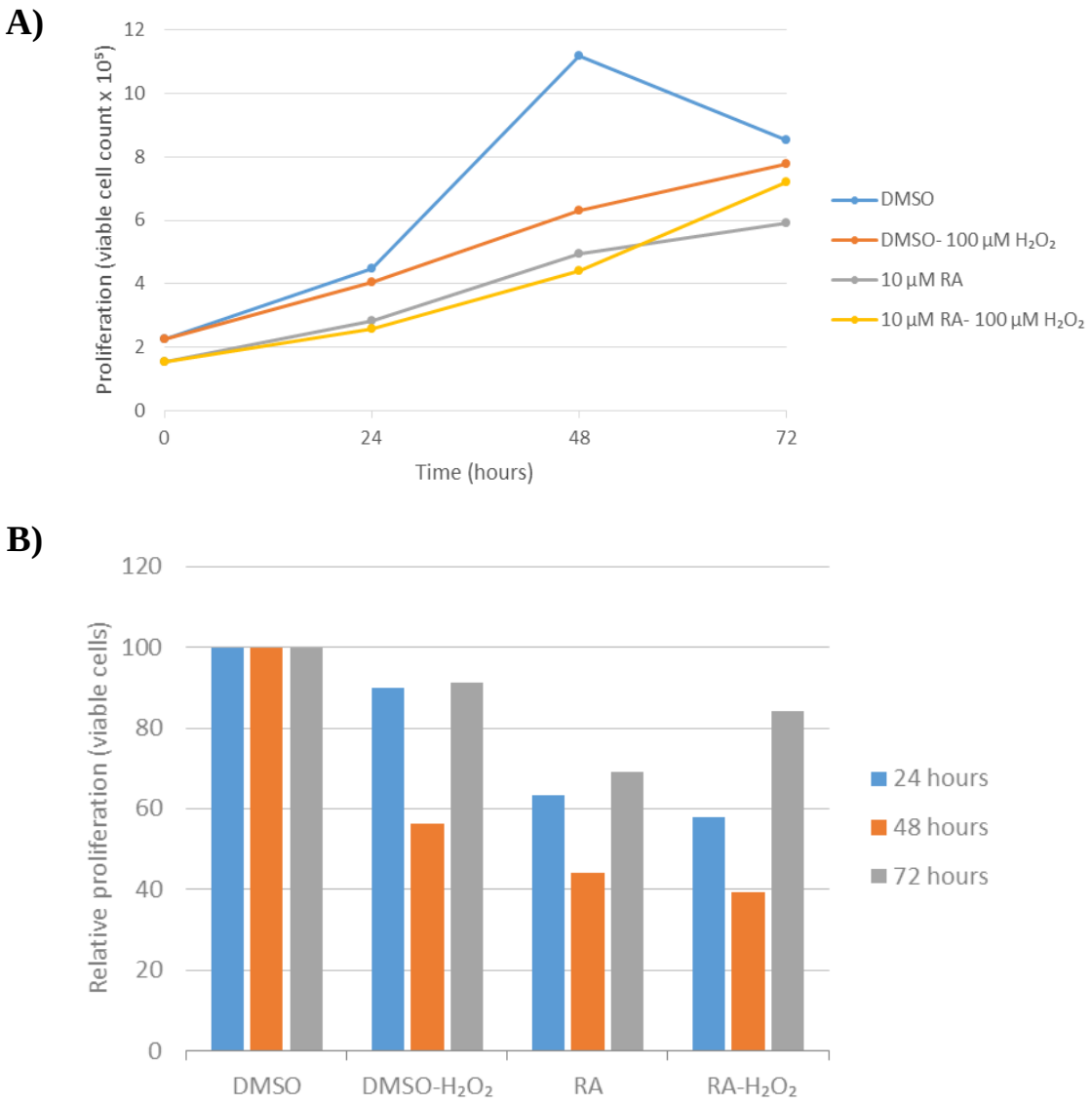

Figure 4.8 Proliferation of untreated and RA treated SH-SY5Y cells after treatment with H_2O_2.

6-well plates were seeded at 1 x 10^5 cells/ml (2 ml per well) with either DMSO and incubated for 48 hours at 37°C or 10 µM RA for 72 hours prior to collection of data. Media was removed and replaced with fresh DMSO/RA DMEM (control) or DMSO/RA DMEM containing 100 µM H_2O_2 and incubated for 1 hour at 37°C. Supernatant was removed and fresh DMSO/RA DMEM was added to the plates before incubating. Cell counts were taken at 24, 48 and 72 hours after the media change. Data is presented from one biological experiment.

Results from Figure 4.8 show a reduction in proliferation in RA treated cells and in cells treated with 100 µM H_2O_2 compared to the DMSO control. Cell numbers in the DMSO control were seen to increase during the first 48 hours and then suddenly decrease after 72 hours. The reason for this decrease was attributed to the 6-well plate becoming over-confluent and cells detaching from the surface of the plate and dying. Interestingly, during this experiment no differences in trends between cells treated with H_2O_2 can be seen. In addition to this, no trends can be seen between H_2O_2-treated and DMSO-treated RA cells and results for RA cells treated with H_2O_2 are not dissimilar to undifferentiated cells treated with H_2O_2 apart from seeing a slight reduction in relative proliferation. As results shown in Figure 4.8 are from one biological replicate, further experiments would be required to determine any statistical significance. Alongside this experiment β-gal assays were carried out to determine whether senescence had been achieved. Results from the assay can be seen in Figure 4.9.

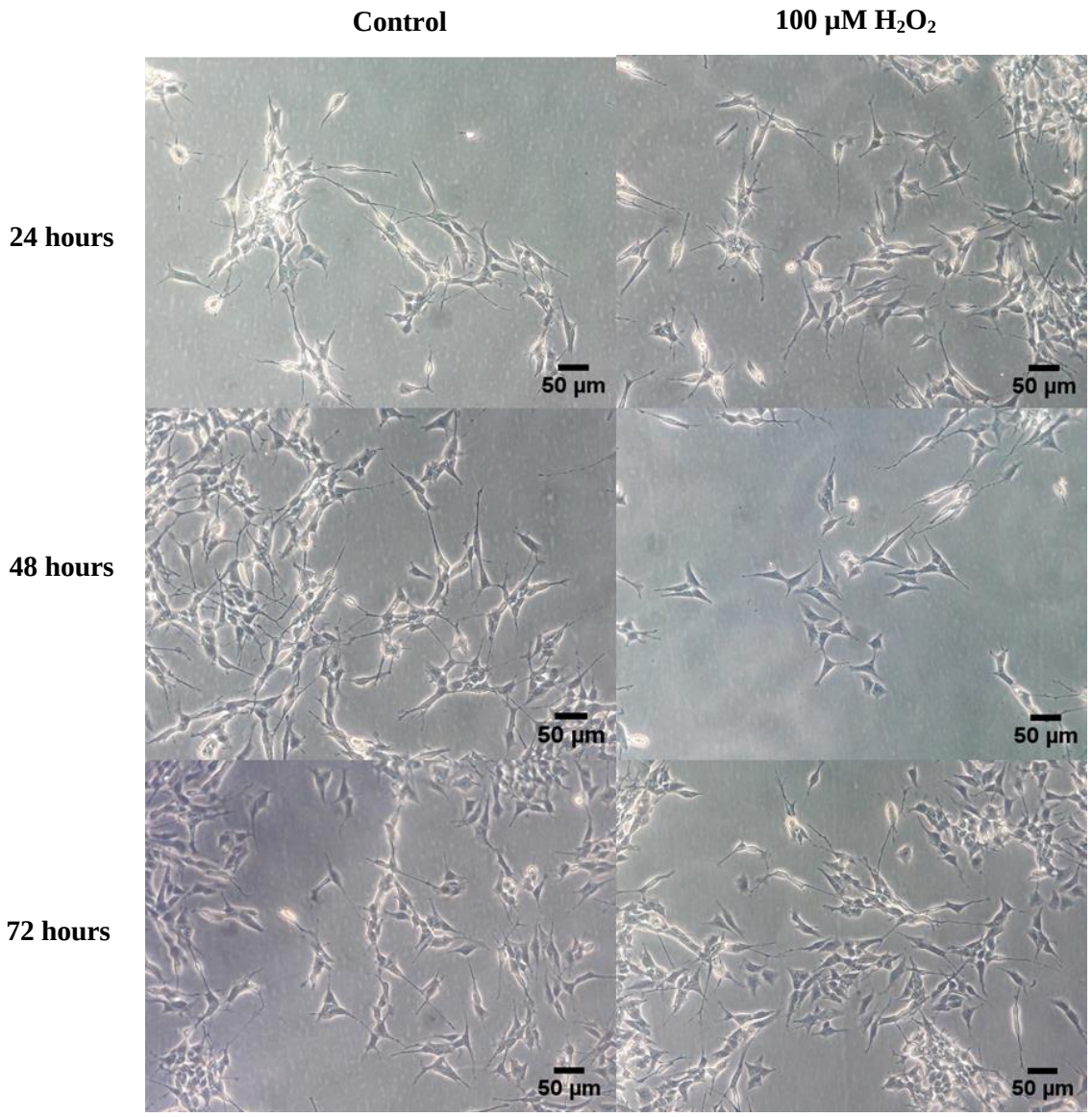

Figure 4.9 β-gal assay of RA treated SH-SY5Y cells treated with or without 100 µM H_2O_2.

6-well plates were seeded at 1 x 10^5 cells/ml (2 ml per well) in DMEM containing 10 µM RA and incubated for 72 hours. Media was removed and replaced with fresh RA DMEM containing H_2O (control) or RA DMEM containing 100 µM H_2O_2 and incubated for 1 hour at 37°C. Supernatant was removed and fresh RA DMEM was added to the plates before incubating. β-gal assays were carried out using Sigma Aldrich Senescence Cells Histochemical Staining Kit (catalogue Number CS0030) according to manufacturer instructions after 24, 48 and 72 hours. Cells were observed under a light microscope and images were obtained.

Differentiated SH-SY5Y cells treated with 100 µM H_2O_2 do not appear to have entered senescence after analysis of β-gal assay images (Figure 4.9). Senescent cells should appear blue in colour after the assay and this cannot be said for these cells. In comparison to differentiated SH-SY5Y cells that were treated with DMSO, no colour differences between the two groups can be seen. However, H_2O_2 treated cells do appear to have an altered morphology after 48 hours. A large proportion of the cells lost their long neurite processes at this time point but interestingly, cells appeared to recover after 48 hours and began to develop longer neurites again whilst continuing to proliferate.

In conclusion, pre-treating SH-SY5Y cells with RA prior to exposure to H_2O_2 did not achieve senescence in these cells as determined by the β-gal assay.

4.4 Discussion

Overall, the data in this chapter suggests that senescence was not achieved in the SH-SY5Y cell line in both untreated and RA treated cells using adapted protocols published by Lopes *et al*. (2010), Ramalingam *et al*. (2014) and Xicoy *et al*. (2017). It has previously been reported that senescence can be induced in undifferentiated SH-SY5Y cells using a single treatment of 100 µM H_2O_2 with senescence-associated β-gal staining providing positive results (Nopparat *et al*., 2017). However, this is in contrast to results shown in Figure 4.1, 4.2 and 4.3, which demonstrated that the higher doses of H_2O_2 were toxic to cells, whereas lower doses were not sufficient to induce cell cycle arrest with β-gal assays yielding negative results despite cell culture and treatments being the same as Nopparat *et al*. (2017). SH-SY5Y cells were a gift from Newcastle University UK and were at passage two upon receipt. Cells were confirmed to be mycoplasma negative and were periodically tested by technical staff throughout the duration of their use and confirmed negative using Minerva-biolabs Venor®GeM OneStep kit (Cat. No. 11-8250) (data not shown). SH-SY5Y cells are derived from the SK-N-SH cell line, which was cultured from the biopsy of a metastatic tumour and, as a result, has mutations in many genes (Krishna *et al*., 2014) including the NME1 gene, which is implicated in the repair of both SSBs and DSBs in DNA and maintaining genomic stability (Kaetzel *et al*., 2015; Puts *et al*., 2017). It is possible that a spontaneous mutation occurred in a cell within the SH-SY5Y culture and affected the remaining population of cells and altered their ability to senesce in response to H_2O_2 induced oxidative stress. It is feasible that DNA damage may be mis-repaired to generate

mutation(s) that affect cellular behaviour. Whole-genome sequencing to determine the genetic content of the cell line used in this study would be required to answer this question.

The use of a positive control during these experiments may have been able to further clarify whether senescence had been achieved or confirmed that the assay was working correctly. However, as discussed by Piechota *et al*. (2016), it appears that the use of β-gal as a marker of senescence in neurons provides varying results and may not have been the correct marker to determine whether H_2O_2 treated SH-SY5Y cells had entered a state of senescence. Other markers of senescence are commonly utilised alongside β-gal assays such as the tumour suppressor genes p16 and p21 to confirm identification of senescent cells (Ashapkin *et al*., 2019; Liu *et al*., 2019). Indeed, the use of multiple markers may have helped to identify the presence of senescent cells during this study.

Due to the cancerous nature of the SH-SY5Y cell line it was not possible to culture cells over time to cause replicative senescence. In addition to this, a sample of undifferentiated cells was taken up to a passage number of 40 without seeing any morphological changes (images not shown), i.e. they can continuously proliferate as reported previously (Pahlman *et al*., 1984). Undifferentiated SH-SY5Y also express immature neuronal markers and lack mature neuronal markers, so they are considered similar to immature catecholaminergic neurons and not a good model for dopaminergic neurons (Lopes *et al*., 2010). For this reason and the lack of success using methodology described by Nopparat *et al*. (2017), it was subsequently decided that attempts to induce senescence with H_2O_2 would be made using RA-treated SH-SY5Y cells.

Proliferation assays seen in Figure 4.4 demonstrate that SH-SY5Y cells treated with 10 μM RA for 48 hours show a significant reduction in proliferation compared to control cells. However, a further reduction in proliferation was not seen after 72 hours of incubation, suggesting that the RA was having no further effect on the cells. This is unlike findings published by Encinas *et al*. (2002), Cuende *et al*. (2009) and Lopes *et al*. (2010).

As mentioned previously, the SH-SY5Y cell line has been seen to produce different cellular phenotypes including N-type cells and S-type cells. S-type cells are substrate adherent multipotent precursors to various non-neuronal cells, including glial cells, melanocytes and Schwann cells (Bell *et al*., 2013). Although the SH-SY5Y cell line is predominantly composed of N-type cells, it is known that a small proportion of S-type

cells remain in the SH-SY5Y cell line (Forster *et al*., 2016). A study by Encinas *et al*. (2002) reported that N-type cells gain a neuronal-like phenotype more readily than S-type cells after treatment with 10 µM RA. Furthermore, S-type cells were also seen to continue proliferating and created cultures with an overgrown S-type population 10 days post RA treatment. These results could explain why cells continued to proliferate during this study, despite exposure to RA, i.e. there was continued proliferation and overgrowth of the S-type cells in culture. However, RA-treated SH-SY5Y cells in this chapter were confluent much earlier than day 10 post-treatment, which differs to results reported by Encinas *et al*. (2002). This may suggest that either the culture contained a larger proportion of cycling S-type cells or that the N-type cells present were not responding to RA in the same manner, despite the same doses of RA being used in this study. If one cell type is overgrowing the other it may explain why there were high levels of inter-experimental variability when measuring Top2A and Top2B protein after 72 hours of RA treatment. Interestingly, Encinas supplemented their culture medium with 15% FBS compared to 10% in this study, which suggests that serum content may affect cellular behaviour. Indeed, it has been shown that serum deprivation alters cellular response to DNA damage (Raffaghello *et al*., 2008). In addition, RA stability has been shown to be greatly reduced in serum-free media compared to 15% serum-supplemented media. Sharow *et al*. (2012) showed that 69% of RA could be recovered from cell-free serum-supplemented media after 24 hours compared to only 27% from cell and serum-free media. Thus, it is possible that RA was more stable for longer periods of time in media containing 15% FBS compared to 10% FBS, which could account for the differences seen.

Other differentiating protocols have also been published that utilise different serum concentrations. For example, Korecka *et al*. (2013) exposed SH-SY5Y cells to 1 µM RA for 8 days in 0.5% serum and showed that the expression profile of transcription factors involved in neuronal differentiation significantly changed. Their data showed that RAR-A and PAR-B, which control all RA-induced signalling, were significantly upregulated following treatment with RA. Some other examples that were shown to be upregulated were the neurite outgrowth initiator Rho GTPase RAC1, integrin α1 and ß1, which are cell membrane receptors involved in cell adhesion and recognition and Nrf2, a transcription factor that regulates neuronal differentiation and antioxidant homeostasis. Their data provide strong evidence for a pro-neuronal differentiation process in this cell line after treatment with RA. Interestingly, they also showed that the

transcription factor Sp1 was also increased (1.45 fold compared to control). As discussed previously, Sp1 has been shown to be implicated in the regulation of Top2B expression during neuronal differentiation, so it is possible that the increase in Sp1 expression may have also affected expression of Top2B. However, Top2B expression was not investigated during their study.

A study by Schneider *et al*. (2011) also supplemented RA differentiating media with a reduced amount of FBS using only 1% FBS to differentiate SH-SY5Y cells. Indeed, the presence of FBS has been shown to attenuate differentiation induced by RA in murine neuroblastoma N2a cells. Without FBS, RA was shown to drive N2a neuronal differentiation via protein kinase A (PKA)/phospholipase C (PLC)/protein kinase C (PKC) and MEK/ERK pathways. In media supplemented with 10% FBS, RA induced neuronal differentiation via PLC/PKC and PKA/PLC/PKC, respectively (Namsi *et al*., 2018). Although this is a mouse cell line, it highlights the different signalling pathways that can be modulated in the presence or absence of serum. However, as mentioned previously, Sharow *et al*. (2012) reported that RA was significantly more unstable in serum-free media compared to media containing 15% FBS, so the results achieved by the various differentiating protocols are a complex interplay between maintaining RA stability in the media and the effect of serum on the activation of the signalling pathways involved in neuronal differentiation.

In another report by Encinas *et al*. (2002), the addition of brain-derived neurotrophic factor (BDNF) to RA-treated cells in combination with removing serum from the media prevented replication of S-type cells in culture and was seen to be stable for up to 3 weeks. RA has been shown to induce the expression of the neurotrophin tyrosine receptor kinase B (TrkB) (Jiao *et al*., 2014), which is a receptor for BDNF, and is well known for its function during nervous system development (Minichiello, 2009). In addition, BDNF has been shown to enhance the effects of RA during differentiation (Forster *et al*., 2016).

Yet another group differentiated SH-SY5Y cells using 10 µM RA but also included the mitotic inhibitors cytosine b-D-arabinofuranoside (araC), uridine and 5-fluoro-20 -deoxyuridine (FdUr) in their long-term culture media to successfully eliminate the undifferentiated S-type cells. In this differentiation protocol cells were exposed to 10 µM RA for 14 days, which was then removed and replaced with mitotic inhibitors for a further 16 days. BrdU incorporation showed that proliferation had ceased and several

neuronal markers such as Neurogenin, tau, laminin and DRD2 were upregulated (Constantinescu *et al*., 2007).

Results from Figure 4.4 suggest that neuronal differentiation was not achieved after measuring proliferation. This was also confirmed via analysis of Top2A and Top2B. Western blot analysis of DMSO-treated SH-SY5Y and RA-treated SH-SY5Y over a 72 hour period showed no significant differences in Top2A and Top2B protein levels between the two treated groups and between the two isoforms (Figure 4.6 and Figure 4.7). If all cells had become differentiated it would be expected that a significant decrease in Top2A levels would be seen as cells stop proliferating and Top2B levels would increase as it has been shown to be upregulated during differentiation (Tsutsui *et al*., 1993; Tiwari *et al*., 2012; Harkin *et al*., 2015; Austin *et al*., 2018). If RA-treated cells maintain a proportion of proliferating S-type cells it is likely that a significant decrease in Top2A would not be seen. Equally, the presence of proliferating cells may also explain the insignificant increases in Top2B protein levels over the 72-hour period. In addition, this may account for the high inter-experiment variability seen for both Top2A and Top2B levels at later time points. Guo *et al*. (2014) reported significant increases in Top2B protein levels in SH-SY5Y cells after 3 days in media containing 10 µM RA with high levels maintained after 5 days. However, differentiating media used by Guo differed to that used in this study. Their study initially cultured SH-SY5Y in media supplemented with 10% FBS but RA differentiating media contained only 3% FBS. In addition to a reduction in FBS, Guo *et al*. (2014) also utilised a different whole cell extraction technique, incorporating a NaCl concentration of 150 mM in the lysis buffer. Previous studies have shown that salt concentration can affect the yield of Top2A and Top2B in whole cell extracts of a number of different cell lines (Padget *et al*., 2000). Furthermore, NaCl extraction techniques were also seen to yield more Top2B in the CCRF-CEM cell line in comparison to the DNase/RNase method, which was the technique used throughout this study. It appears both differentiation protocols and extraction techniques can have an effect on the levels of type 2 topoisomerases that can be obtained.

Numerous approaches could have been explored to differentiate the SH-SY5Y cell line if more time had been available. Changes to methodology, such as increasing the exposure time of RA and incorporating pulses of fresh RA as it degrades could have been investigated. Reducing the FBS concentration and incorporating BDNF into the

media or exposing cells to mitotic inhibitors following exposure to RA are also methods that could have been explored.

Unfortunately, further results from proliferation and β-gal assays showed that the treatment of cells with 10 µM RA for 72 hours prior to H_2O_2 exposure did not generate a senescent state in the cells. Thus, the generation of senescence in this cell line was unsuccessful and more experiments would be needed to achieve this. The results from this chapter highlight the difficulties in working with cell lines that are genetically damaged (Korecka *et al*., 2013). Although primary neuronal cells can be readily bought, they typically only survive three weeks in culture (Kim *et al*., 2007), which limits their usefulness for the large number of experiments that would be required to induce senescence and explore Top2B expression.

The use of a homogenous human neuronal cell line may have been preferable, such as the HCN-2 cell line. Although this cell line is fully clonal compared to SH-SY5Y cultures, these cells still must be differentiated into mature neuronal-like cells by the addition of nerve growth factor (NGF), isobutylmethylxanthine (IBMX) and the phorbol ester12-*O*-tetradecaoylphorbol-13-acetate (Ronnet *et al*., 1994). Interestingly, these cells have been shown to senesce at approximately passage 21, which may have been useful in exploring topoisomerase II expression during this process and over chronological ageing. Nevertheless, careful planning of experiments would still have been needed to empirically determine the optimal conditions to generate and verify senescence.

Improved methods of measuring proliferation could have been used in this chapter. For example, although measuring viable cell numbers using the trypan blue exclusion method gives some indication about cell proliferation, utilising assays such as the EdU proliferation assay, which directly measures DNA synthesis (Yamakoshi *et al*., 2011), may have yielded more accurate results.

In conclusion, attempts to induce senescence in both untreated and RA-treated SH-SY5Y cells using different concentrations of H_2O_2 were unsuccessful.

5. Development of murine models of ageing to investigate changes in Top2B expression

5.1. Introduction

5.1.1 CAD neuronal cell line model

Following work carried out on the neuroblastoma cell line SH-SY5Y it was decided that an alternative cell line would be utilised to investigate Top2B expression in an aged neuronal model. The murine CAD (Cath.a-differentiated) cell line is a variant of the Cath.a cell line, which was derived from catecholaminergic central nervous system neurons by targeted oncogenesis of transgenic mice carrying the wild-type Simian virus SV40 antigen oncogene (Li *et al*., 2007). The cell line is capable of being differentiated through serum starvation and displays many morphological and biochemical characteristics of mature neurons after differentiation, including cell cycle arrest and development of long neuronal processes (Qi *et al*., 1997). The CAD cell line has been shown to express specific neuronal proteins such as growth-associated protein GAP-43, synaptosomal associated protein SNAP-25, class III β-tubulin and synaptotagmin (Hashemi *et al*., 2003). CAD cells also express the rate-limiting enzyme of catecholamine biosynthesis, tyrosine hydroxylase, and are therefore considered a catecholaminergic cell line (Lazaroff *et al*., 1998). CAD cells grown in serum-containing medium possess a flattened morphology with very short neuronal processes (Lazaroff *et al*., 1998) and continuously proliferate with a doubling time of 18-22 hours (Qi *et al*., 1997). In serum-free medium CAD cells become differentiated and undergo morphological changes including the development of numerous long neuronal processes as well as exhibiting cell cycle arrest (Li *et al*., 2007).

Many neuronal cell lines cannot survive in media without serum or exogenous protein, including the parental cell line of CAD, Cath.a. The Cath.a cell line, as well as other neuronal cell lines such as ND7 and PC12, has been shown to exhibit cell cycle arrest and subsequent cell death after serum starvation (Howard *et al*., 1993; Lindenboim *et al*., 1995). However, Horton *et al*. (2008) suggests the expression of neurotrophin-3 (NT3), which is an important neurotropic factor known to play a role in the development and maintenance of the vertebrate nervous system (Zhou & Rush, 1996), and expression of tropomyosin receptor kinase (Trk) by CAD cells creates an autocrine activation loop that is capable of sustaining CAD cell survival in the absence of an exogenous protein source. Differentiated CAD cells possess a vesicular and cytoskeletal

structure typical of neuronal cells and can be maintained in serum-free medium for at least six weeks, after which small mechanical disturbances can cause the cells to detach from the surface of the tissue culture vessel (Qi *et al*., 1997). The cell line is also reversibly differentiated when serum is added to the media. Neuronal processes of differentiated cells begin to retract and within 12-24 hours 95% of differentiated cells re-enter the cell cycle after the addition of serum to the media (Qi *et al*., 1997).

In order to create a cell line model of ageing several approaches were taken to induce senescence in CAD cells. Differentiated CAD cells were produced and then exposed to either sub-cytotoxic levels of oxidative stress caused by hydrogen peroxide (H_2O_2) or chronologically aged in culture.

After carrying out extensive literature searches, there are no previous studies investigating topoisomerases in the CAD cell line to the best of our knowledge.

5.1.2 Mouse model of ageing

In addition to using a murine neuronal cell line to investigate expression of Top2B, immunohistochemical analysis of mouse hippocampus tissue was also carried out. Throughout scientific research inbred mice are the most extensively used strains for the study of ageing and age-related diseases (Mitchell *et al*., 2015). Although the use of mice as a model of ageing is expensive and time consuming, with approximately 85% of the protein-coding regions of the mouse genome identical to that of the human genome, mice are the most commonly used mammalian model in scientific research (Batzoglou *et al*., 2000). Possessing approximately 70 million neurons, the mouse brains complexity is less than that of a human. However, the nervous systems of mice and humans share many similarities at the cellular level (Vanhooren & Libert, 2013). Although mice are much longer lived than *Drosophila*, with the commonly used male C57BL/6 mouse having an average life span of ~900 days (Kunstyr & Leuenberger, 1975; Yuan *et al*., 2009), they are considered short-lived mammals relative to humans and therefore a very common model of mammalian ageing. When compared to humans and other animal models, mice similarly show phenotypic decreases in cognitive ability and memory as they age (Jucker *et al*., 1994; Matzel *et al*., 2008). One of the brain regions most affected by age is the hippocampus, with similar age-related declines in function seen in humans and numerous other mammalian species (Verbitsky *et al*., 2004). Mice and humans have evolutionarily conserved brains, which in turn also mean they share very similar brain architecture with brain tissues consisting of similar cell

types. This makes mice one of the most commonly used animal models to study ageing of the brain (Mitchell *et al*., 2015).

As mentioned previously (section 1.5.5), the number of studies investigating age-related changes in levels of Top2B in murine brains is incredibly limited with Kondapi *et al*. (2004) providing the only study focussing on Top2B levels in rat brains throughout the ageing process to the best of our knowledge. The study reported decreases of Top2B expression in the cerebellum of rats with expression seen to be high in young rats, moderate in adults and low in old rat cerebellar regions. In addition to this, Kondapi *et al*. (2004) suggested that Top2B is only expressed in cerebellar tissue.

This chapter focussed on developing a differentiated CAD cell line model to investigate changes in Top2B protein and mRNA levels during ageing, whilst also investigating Top2B expression in mouse hippocampal tissue in young and old samples using immunohistochemical techniques.

5.2 Differentiation of the CAD cell line through serum starvation

CAD cells are an immortalised cell line and, as a result of this, display a continued up-regulation of cell proliferation. Similar to the SH-SY5Y cell line, this continued proliferation is not a characteristic of mature neurons. Differentiation of CAD cells into more mature neuronal-like cells has been reported in previous studies through serum starvation (Qi *et al*., 1997; Li *et al*., 2007; Horton *et al*., 2008). In order to create a differentiated CAD cell line, cells were seeded in complete media containing serum for 24 hours before removing and replacing with media without serum. Cell proliferation was then monitored and results for serum starvation-induced differentiation of CAD cells alongside proliferation of cells in media containing serum can be seen in Figure 5.1.

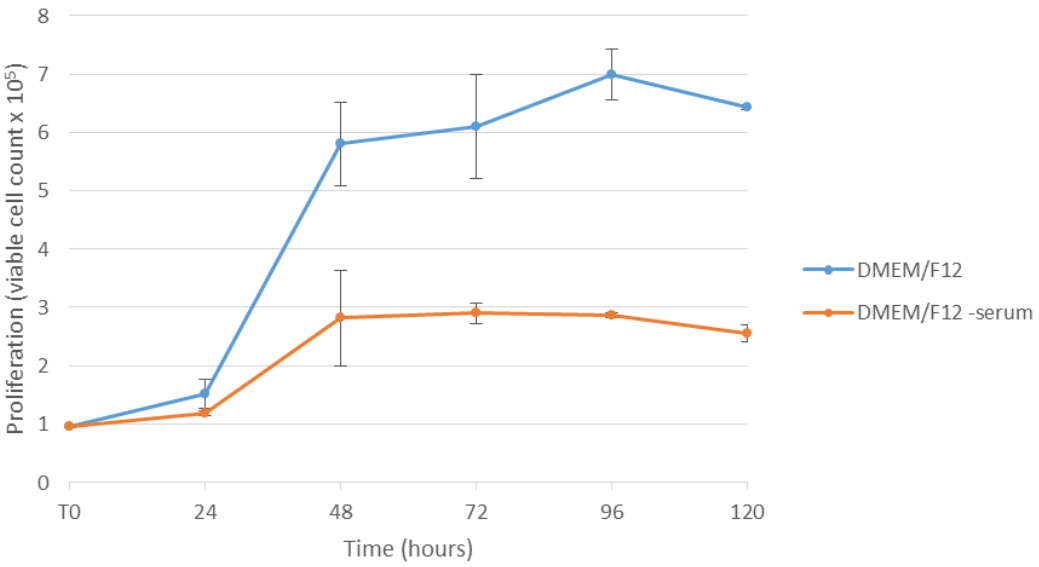

Figure 5.1 The effects of serum starvation on CAD proliferation.

6-well plates were seeded at 5 x 10^4 cells/ml (2 ml per well) and incubated for 24 hours at 37°C. Supernatant was removed and replaced with fresh complete DMEM/F12 (control) or DMEM/F12 without FBS. Viable cells were counted every 24 hours for 120 hours using trypan blue exclusion. Data is presented as the mean of three biological replicates ± standard error.

Results from Figure 5.1 show that cells grown in complete media containing serum display an initial lag period but after 24 hours cells proliferate rapidly for the next 24 hours (p=0.029 Student's t-test, two-tailed) with a doubling time of 18.39 hours. At subsequent time points cell numbers remain similar with no significant increases in number between any of the subsequent 24 hour periods. Observations of cells grown in complete media under a light microscope indicated that confluency had been reached after 96 hours, which may explain why a slight reduction in cell number is seen at 120 hours.

In comparison, cells grown in serum-free media display low but significant increases in proliferation during the first 24 hours (p=0.007) and although cell numbers generally increase between 24 and 48 hours incubation, this is not significant. Cell numbers then remain remarkably stable at the remaining time points with no significant increases in cell number between any of the subsequent 24 hour periods, indicating that cells have entered a state of cell cycle arrest. In addition, numbers of cells grown in serum-free media are significantly lower than cells grown in complete media between 72 and 120 hours with p values of 0.025 (72 hours), 0.0007 (96 hours) and 1.5 x 10^{-5} (120 hours) between the two groups.

Alongside proliferation assays, morphological comparisons between undifferentiated and differentiated cells were made. Cells were monitored for any changes in neurite outgrowth and cell shape. Results can be seen in Figure 5.2.

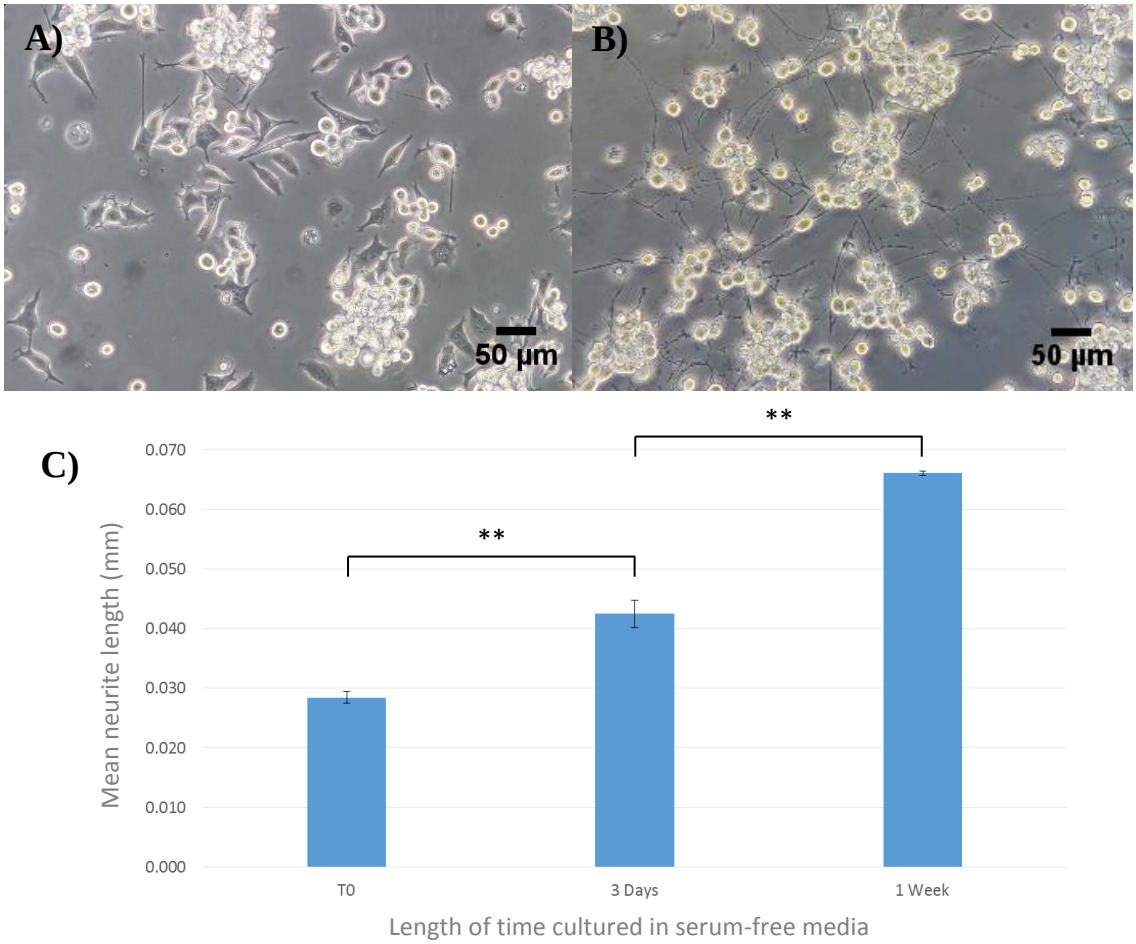

Figure 5.2 The effects of serum starvation on CAD morphology.

6-well plates were seeded at 5 x 10^4 cells/ml (2 ml per well) and incubated for 24 hours at 37°C. Supernatant was removed and replaced with fresh complete DMEM/F12 (control) or DMEM/F12 without FBS. The image of cells in (A) was taken after 1 week in complete DMEM/F12 and the image of cells in (B) were taken after 1 week in DMEM/F12 without FBS. (C) Neurite length was measured at T0, 3 days and 1 week after the addition of serum-free media. Neurite length was measured using ImageJ software and the average neurite length was calculated. **= $p<0.01$ (Student's t-test, two-tailed).

Images seen in Figure 5.2 show clear morphological changes in CAD cells grown in serum-free media (Figure 5.2B) compared to cells grown in complete media (Figure 5.2A). Cells grown in complete media have very short neuronal processes and vary in

shape. After serum starvation, cells became rounder in shape and developed long neuronal processes with varicosities. Neurite outgrowth was significant after the addition of serum-free media (Figure 5.2C). After 3 days in serum-free media neurites were significantly longer ($p=0.0048$) than T0 cells. Neurites continued to grow between day 3 and 1 week ($p=0.0094$). The development of long neuronal processes in conjunction with cell cycle arrest were the two factors used in subsequent experiments to determine whether cells had developed a differentiated-like state.

5.3 Semi-quantification of Top2B during CAD differentiation

As stated in 4.3.2, previous studies have reported that Top2B expression is upregulated significantly when cells enter a state of terminal differentiation (Tsutsui *et al*., 1993; Tiwari *et al*., 2012; Harkin *et al*., 2015). Therefore, levels of Top2B protein and mRNA could also be used to confirm terminal differentiation of CAD cells starved of serum.

5.3.1 Semi-quantification of Top2B protein during CAD differentiation

CAD cells were differentiated in serum-free media and protein extracts were taken at T0, 24, 48 and 72 hours after the addition of serum-free media. Western blot analysis of Top2B was carried out on these samples and results can be seen in Figure 5.3. In contrast to previous studies, results shown in Figure 5.3 yielded no significant changes in protein levels of Top2B in CAD cells grown in serum-free media over 72 hours with protein levels of Top2B appearing to be expressed evenly over the 72 hour period and not upregulated. It is possible that CAD cells have not become fully differentiated at 72 hours and Top2B may become upregulated at later time points, which may explain why significant increases in protein levels of Top2B are not seen in Figure 5.3. Interestingly, significant growth of neurites can be seen to continue up to 1 week in serum-free media (Figure 5.2C). However, cell proliferation was seen to stop after 48 hours in serum-free media (Figure 5.1) and was accompanied by the expected changes in morphology associated with differentiation of this cell line (Qi *et al*., 1997). Several other previous studies using differentiated CAD cells also used a 72 hour incubation period in serum-free media to characterise the effect of differentiation (Johnston *et al*., 2004; Schein *et al*., 2005). For example, Johnston *et al*. (2004) reported significant alterations in the expression and function of the cyclic adenosine monophosphate (cAMP) signalling pathway after 72 hours in serum-free media. cAMP has been shown to be critical to the

modulation of many cellular activities including differentiation. Thus, the lack of increase seen in Top2B at 72 hours may be cell line specific.

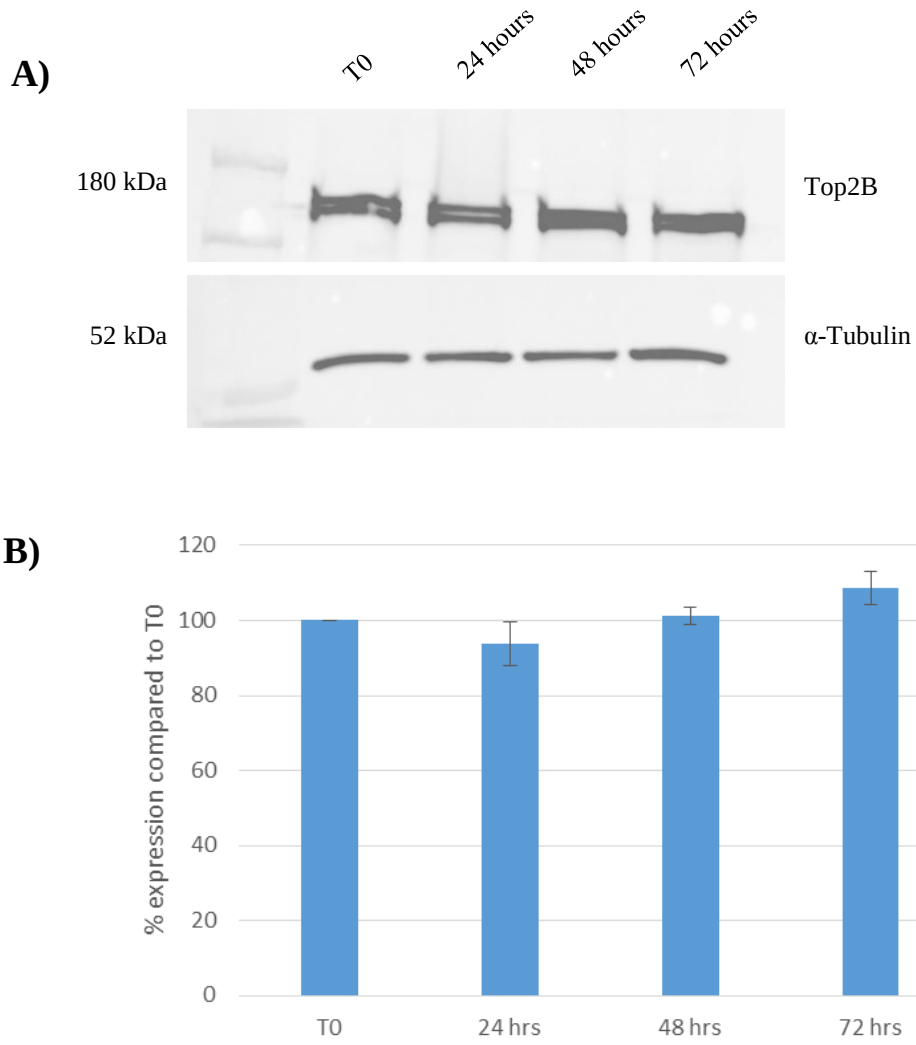

Figure 5.3 Semi-quantification of Top2B over 72 hours of serum starvation-induced differentiation in the CAD cell line.

T75 culture flasks were seeded at 5 x 10^4 cells/ml (12 ml per flask) and incubated for 24 hours at 37°C in complete media. Media was removed and replaced with serum-free media and incubated. Whole cell extraction was carried out at T0 and after 24, 48 and 72 hours as described in section 2.2.2.9 and quantified as described in section 2.2.2.10. Equal protein loads (145 µg) were added to wells of a 7.5% SDS gel. SDS-PAGE was carried out and protein was transferred to nitrocellulose paper by wet western transfer. (A) Nitrocellulose blots were probed with a Top2B antibody and an α-Tubulin load control antibody. Analysis of blot densitometry was carried out using GeneTools (Syngene). (B) Top2B expression is presented as percentage expression compared to T0 cells. Results shown are the mean of three independent experiments ± standard error.

5.3.2 Semi-quantification of Top2B mRNA during CAD differentiation

5.3.2.1 Selection of RT-qPCR reference genes

The selection of suitable internal reference genes was required for the normalisation of RT-qPCR data. Reference genes had to be suitable for neuronal tissue but also stably expressed throughout the ageing process. Bibliographic surveys carried out by Boda *et al*. (2009) reported that glyceraldehyde-3-phosphate-dehydrogenase (GAPDH) and β-actin are the most frequently used reference genes in mouse brain studies. The bibliographic survey encompassed a range of articles and studies that experimented on various tissues from mouse brains, including the cerebellum, brain stem, neocortex, septum, hippocampus and the olfactory bulb. In addition to this, work by Tanic *et al*. (2007) reported that GAPDH and β-actin were the most stably expressed reference genes in tissues from rat hippocampus and cortex during ageing when comparing the five most commonly used endogenous controls (GAPDH, β-actin, 18S rRNA, hypoxanthine phosphoribosyltransferase and cyclophilin B). However, they also reported that variation in all reference genes tested was seen under different experimental conditions. Due to potential variability in expression both GAPDH and β-actin were selected to be used as reference genes in this study and were tested for variability before carrying out statistical analysis in each experiment. Both reference genes were used alongside a target gene of Top2B.

5.3.2.2 Optimisation of Top2B, GAPDH and β-actin primers for RT-qPCR

Primers were designed for Top2B, GAPDH and β-actin to be used in RT-qPCR experiments (Materials and Methods Table 2.3). Prior to carrying out analysis of mRNA levels in CAD cells, the amplification efficiency of these primers was required to determine their experimental suitability.

Amplification curves were generated for Top2B, GAPDH and β-actin primers, respectively, and subsequently used to calculate primer reaction efficiency (Figure 5.4). RNA was extracted from differentiated CAD cells and 0.4 µg of total RNA was reverse transcribed to cDNA. Serial dilutions of stock cDNA were made as previously described (section 3.4.2).

Primer reaction efficiencies were calculated and demonstrated an efficiency of 99.6% for Top2B, 94.5% for GAPDH and 95.2% for β-actin. A reaction efficiency of 90-110% is deemed acceptable (Taylor *et al*., 2010). As the efficiencies of these primers fall

within the 90-110% range they were considered suitable and comparable for further RT-qPCR experiments.

In addition to analysing primer efficiency, a number of controls were also incorporated into the experimental design as previously described in section 3.4.2. Melt curves were also analysed in all samples to confirm the presence of a single PCR product and to confirm the absence of contaminating genomic DNA (representative melt curves are shown in Appendix Figure C.1).

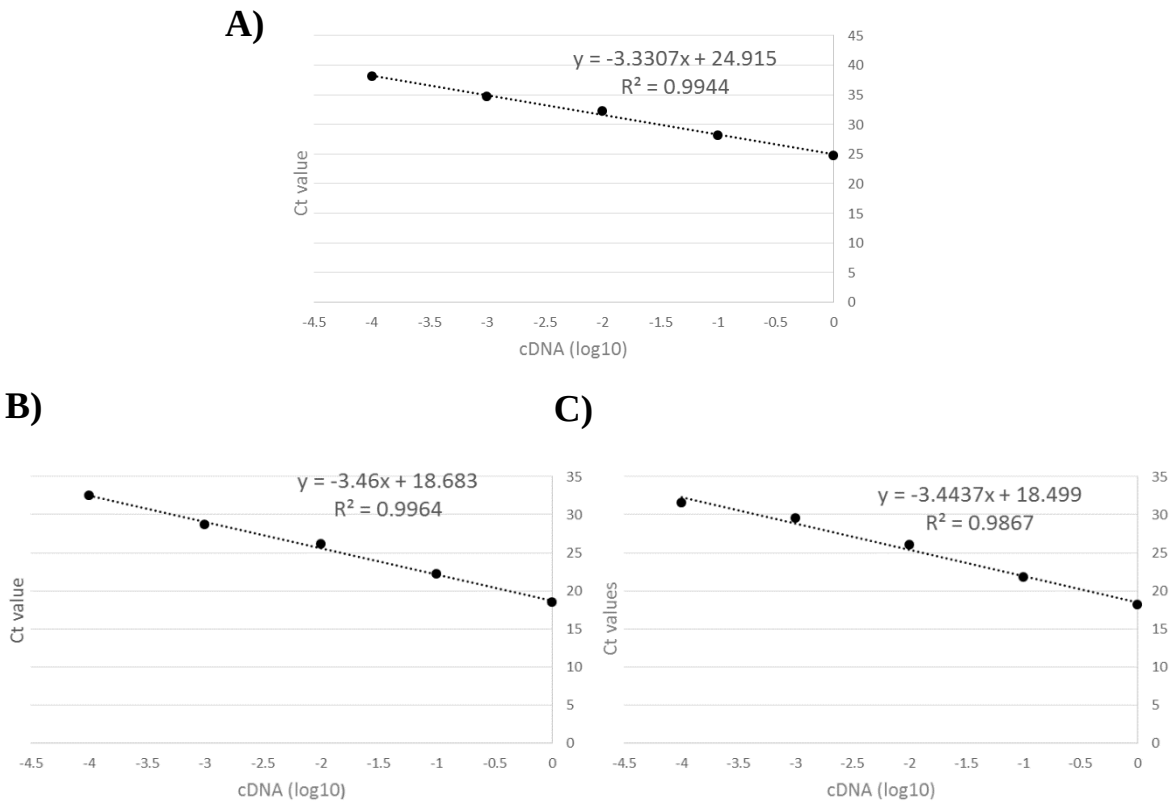

Figure 5.4 Amplification curves for primer efficiency of Top2B, GAPDH and β-actin.

Total RNA was extracted from serum-free treated CAD cells (section 2.2.4) and quantified on a NanoDrop ND-1000 spectrophotometer. 0.4 µg of total RNA was reverse transcribed to cDNA using PCR Biosystems qPCRBIO cDNA synthesis kit (PB30.11) according to manufacturer instructions. The cDNA stock solution was serially diluted 1:10 to create a range of cDNA samples. This ensured the standard curve covered the dynamic range of potential template concentrations that could be encountered during further studies. cDNA concentrations were converted to logarithmic values and plotted against threshold cycle (Ct) values. Amplification curves were generated for Top2B (A), GAPDH (B) and β-actin (C) and a line of best fit was added.

As stated in section 3.4.2, statistical analysis of qPCR data can be carried out using one or numerous reference genes using the comparative ΔCt method. In order to select an appropriate method of statistical analysis, the threshold cycle (Ct) values of β-actin and GAPDH were analysed under experimental conditions and evaluated for stability. Figure 5.5A displays a box and whisker diagram showing the variations in Ct values of β-actin and GAPDH in differentiated CAD cell samples during the first 72 hours in serum-free media. Figure 5.5B displays the coefficient of variance of the Ct values to show variability between samples.

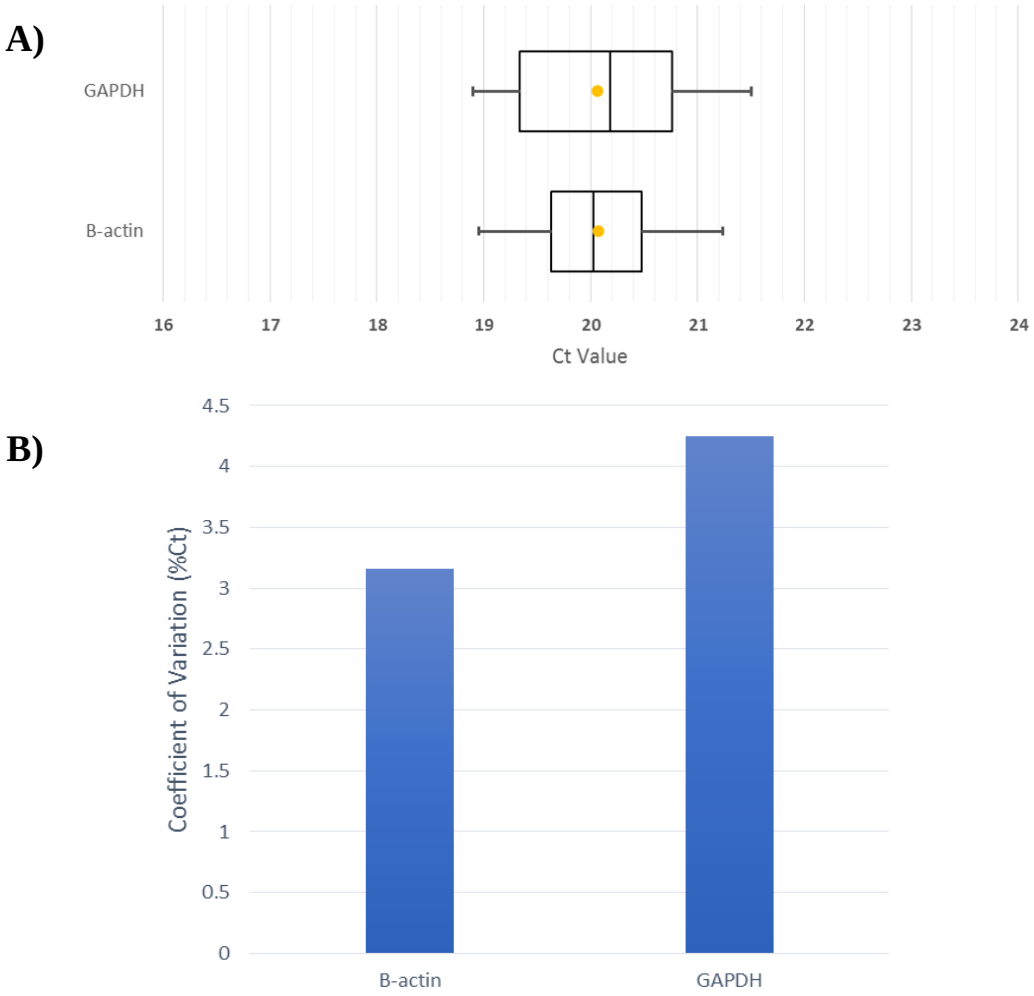

Figure 5.5 Variance of β-actin and GAPDH reference genes from all CAD 72 hour differentiation experiments.

Ct values for the reference genes β-actin and GAPDH were collated from all CAD differentiation qPCR studies to observe any variations in expression. (A) Box and whisker plots showing the distribution of Ct values for the two candidate reference genes. Yellow dots indicate mean value. (B) The coefficient of variance for the data set was calculated to determine variability of Ct values for β-actin and GAPDH over 72 hours of differentiation in CAD cells.

Results from Figure 5.5A show that the range of Ct values is comparable between β-actin and GAPDH. The mean Ct values for each gene are also comparable, hence subsequent data analysis of the following experiment (section 5.3.2.3) utilised both reference genes for normalisation.

5.3.2.3 Analysis of Top2B mRNA during CAD differentiation

Following the confirmation of primer reaction efficiencies, RT-qPCR was carried out to quantify Top2B mRNA levels in CAD cells during the first 72 hours of differentiation in serum-free media. RNA was extracted from CAD cells at T0, 24, 48 and 72 hours after the introduction of serum-free media. Ct values for Top2B were normalised against the β-actin and GAPDH reference genes. Results are shown in Figure 5.6. Similar to protein levels of Top2B, relative levels of Top2B mRNA also do not significantly change in CAD cells during 72 hours in serum-free media (Figure 5.6).

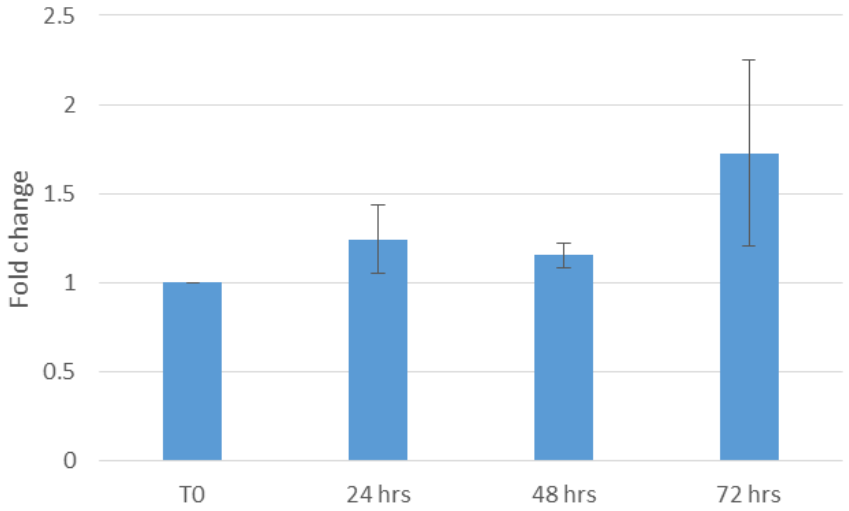

Figure 5.6 Analysis of RT-qPCR data comparing relative Top2B expression in CAD cells during the first 72 hours of differentiation in serum-free media.

T75 culture flasks were seeded at 5 x 10^4 cells/ml (12 ml per flask) and incubated for 24 hours in complete media. Media was removed and replaced with serum-free media and incubated. Cells were harvested at T0 and then every 24 hours for 72 hours and RNA was extracted as described in section 2.2.4.1 and quantified on a NanoDrop ND-1000 spectrophotometer. 0.4 µg of total RNA from each sample was converted to cDNA (section 2.2.4.3) and RT-qPCR was carried out (section 2.2.5) using β-actin and GAPDH as reference genes. Results were normalised by geometric averaging of both reference genes and presented as expression fold change (Vandesompele *et al.*, 2002) (calculation described in Appendix Figure A.5). Samples for each individual experiment were loaded in triplicate. Results shown are presented as the mean of three biological replicates ± standard error.

Despite CAD cells displaying a significant reduction in proliferation and changes in morphology associated with differentiation when starved of serum, levels of Top2B mRNA and protein do not change over a period of 72 hours. Nevertheless, as cell cycle arrest had been successfully induced and a mature neuronal-like morphology achieved, it was decided to use these conditions for further experiments to create a CAD cell line model of senescence using hydrogen peroxide.

5.4 Hydrogen peroxide-induced cellular senescence of serum-free treated CAD cells

After successfully inducing cell cycle arrest and developing a more mature neuronal-like phenotype in CAD cells, experiments were carried out attempting to induce senescence in serum-free treated cells using H_2O_2-induced oxidative stress. Serum-free treated CAD cells were exposed to 50 µM, 100 µM and 150 µM H_2O_2, respectively, and β-gal assays were carried out. Results are shown in Figure 5.7.

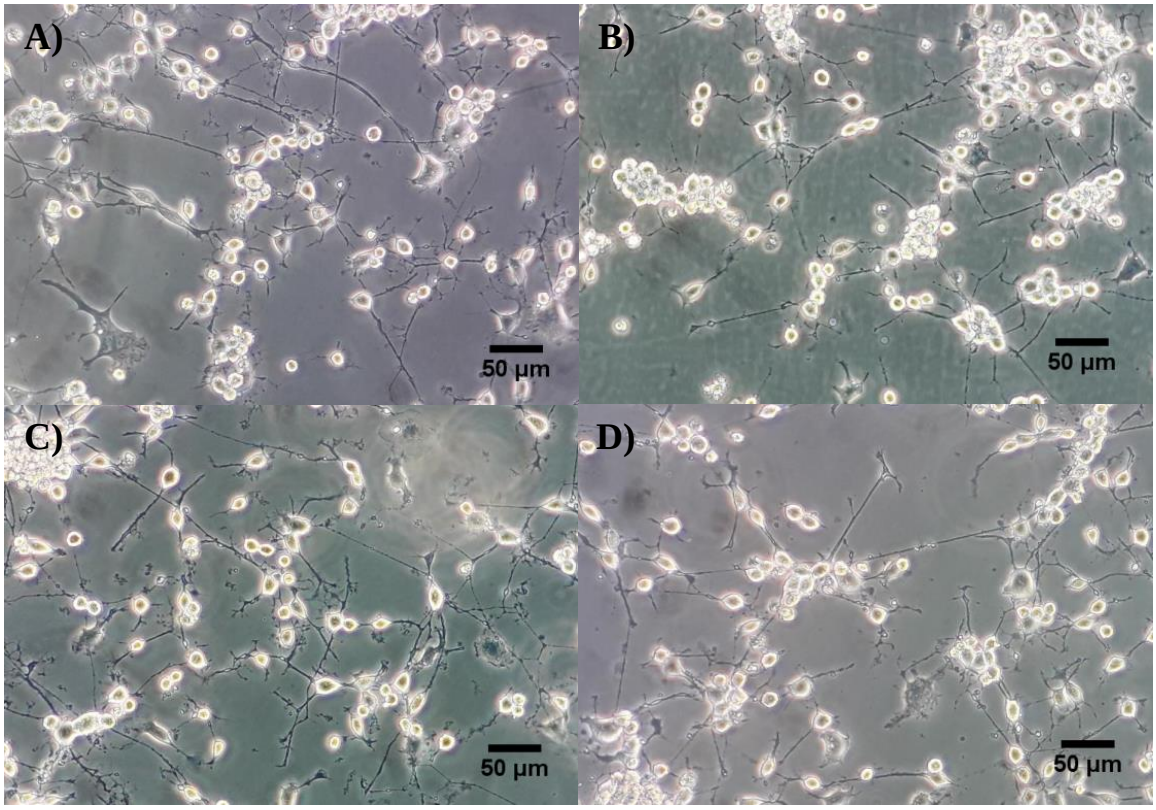

Figure 5.7 β-gal assays of serum-free treated CAD cells treated with a range of H_2O_2 concentrations.

6-well plates were seeded at 5 x 10^4 cells/ml (2 ml per well) and incubated for 24 hours. Cells were differentiated in serum-free media for 72 hours as described in section 2.2.2.7. Media was removed and replaced with fresh serum-free DMEM/F12 containing H_2O (control) (A) or serum-free DMEM/F12 containing 50 (B), 100 (C) or 150 µM (D) H_2O_2 and incubated for 24 hours. β-gal assays were carried out using Sigma Aldrich Senescence Cells Histochemical Staining Kit according to manufacturer instructions. Cells were observed using brightfield microscopy and images were obtained.

Results in Figure 5.7 show that differentiated CAD cells treated with a range of H_2O_2 concentrations did not appear to have entered a state of senescence after analysis of β-gal assay images. Cells appeared to maintain morphology with the exception of a few cells that had shorter neuronal projections. Furthermore, cells did not express the characteristic blue β-gal stain, suggesting cells had not become senescent. Further experiments were carried out utilising lab-made reagents (section 2.2.13 method 2) to determine whether the kit being used was functioning correctly. However, these experiments also yielded the same results (data not shown). In addition to this,

experiments were carried out involving the treatment of CAD cells with H_2O_2 every day for 3 days in an attempt to induce senescence but these experiments also ended with the same results (data not shown).

To further confirm that oxidative stress-induced senescence had not been achieved, p21 levels in cells exposed to H_2O_2 were explored. Previous studies in other cell lines have shown that sub-lethal ROS concentrations can induce senescence by inducing p21 leading to G1 arrest (Macip *et al*., 2002; Chakraborty *et al*., 2016). Indeed, p21 is often referred to as a senescence marker (Ashapkin *et al*., 2019). Protein levels of p21 were investigated by western blotting in CAD cells that had been grown in serum-free media for 72 hours and then treated with 0, 50 or 100 µM H_2O_2. Results are shown in Figure 5.8.

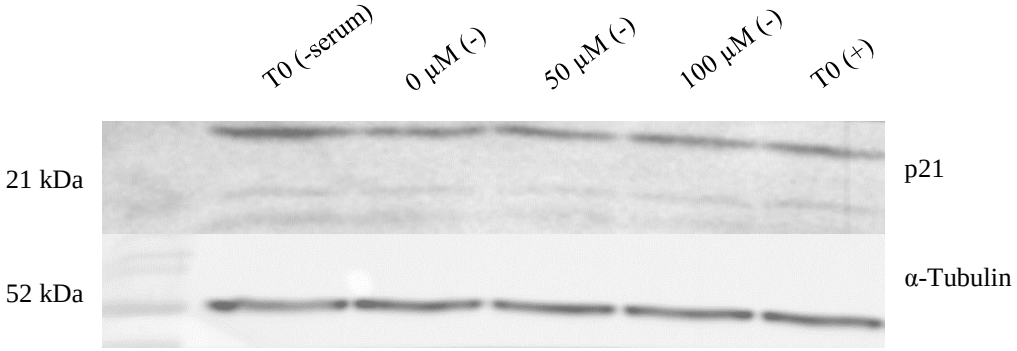

Figure 5.8 Semi-quantification of p21 in CAD cells grown in serum-free (-) or complete (+) media treated with or without a 24 hour pulse of H_2O_2.

T75 culture flasks were seeded at 5 x 10^4 cells/ml (12 ml per flask) and incubated for 24 hours at 37°C in complete media. Media was removed and replaced with serum-free media and maintained as described in section 2.2.2.7.2. Cells were harvested at T0 and then 24 hours after being exposed to 50 or 100 µM H_2O_2 alongside a 24 hour control. Cells were also harvested from cycling cells grown in complete media for 72 hours. Whole cell extractions were carried out as described in section 2.2.2.9 and quantified as described in section 2.2.2.10. Equal protein loads (195 µg) were added to wells of a 12.5% SDS gel. SDS-PAGE was carried out and protein was transferred to nitrocellulose paper by wet western transfer. Nitrocellulose blots were probed with a p21 antibody and an α-Tubulin load control antibody.

From the results seen in Figure 5.8 protein levels of p21 do not appear to appreciably change in serum-free treated CAD cells exposed to H_2O_2 suggesting that senescence had not been achieved in these cells. Interestingly, p21 expression in CAD cells grown in complete media for 72 hours is at a similar level to that seen in serum-free treated cells exposed to H_2O_2. Low basal levels of p21 have been seen to control population heterogeneity in cell cycle activity (Overton *et al*., 2014). However, as previously stated sub-lethal ROS concentrations can induce senescence by inducing p21, so it is interesting that p21 is not expressed more in cells exposed to H_2O_2.

As it was not possible to induce senescence in differentiated CAD cells by oxidative stress, it was decided to age the cells chronologically over a period of six weeks. It has previously been reported that CAD cells can be maintained in serum-free media for six weeks, hence subsequent experiments utilised a range of aged CAD cells, from newly differentiated up to six weeks old, to elucidate any age-related changes in Top2B levels.

5.5 Semi-quantification of Top2B in serum-free treated CAD cells over six weeks of ageing

5.5.1 Semi-quantification of Top2B protein in serum-free treated CAD cells over six weeks of ageing

Western blotting experiments were utilised to generate semi-quantitative data of protein levels of Top2B in serum-free treated CAD cells during ageing. CAD cells were chronologically aged between T0 and six weeks and cells were harvested at weekly time points. The seeding of flasks was staggered over a six week period to ensure that cells at each time point could be harvested and stored on the same day. This was done to prevent protein degradation of some of the samples, which would have been frozen down for long periods of time without staggering. Western blot analysis of Top2B in serum-free treated CAD cells during ageing can be seen in Figure 5.9.

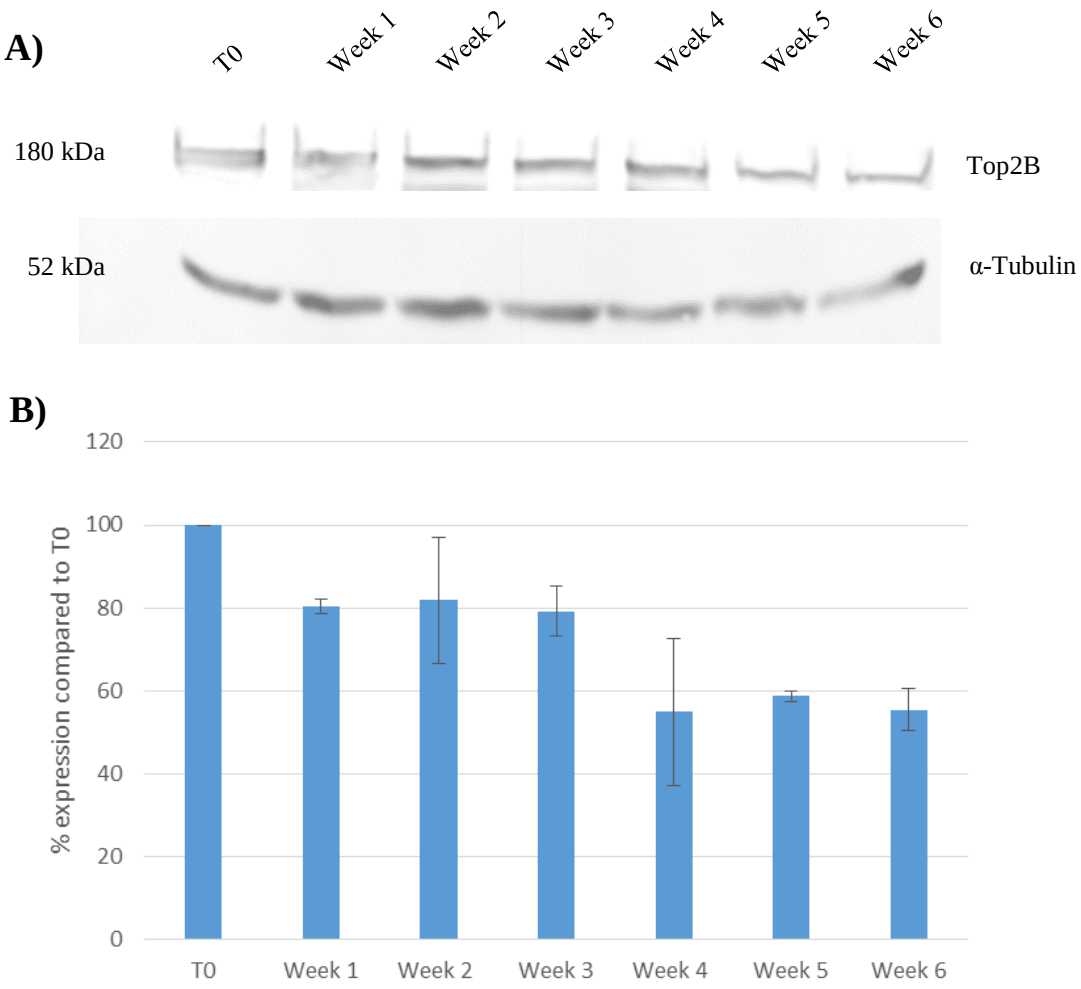

Figure 5.9 Semi-quantification of Top2B protein levels in CAD cells during six weeks of ageing in serum-free media.

T75 culture flasks were seeded at 5 x 10^4 cells/ml (12 ml per flask) and incubated for 24 hours at 37°C in complete media. Media was removed and replaced with serum-free media and maintained as described in section 2.2.2.7.2. Cells were harvested at T0 and then at weekly intervals up to six weeks. Whole cell extractions were carried out as described in section 2.2.2.9 and quantified as described in section 2.2.2.10. Equal protein loads (89 µg) were added to wells of a 7.5% SDS gel. SDS-PAGE was carried out and protein was transferred to nitrocellulose paper by wet western transfer. (A) Nitrocellulose blots were probed with a Top2B antibody and an α-Tubulin load control antibody. Analysis of blot densitometry was carried out using GeneTools (Syngene). (B) Top2B expression is presented as percentage expression compared to T0 cells. Results shown are the mean of three independent experiments ± standard error.

Results show that Top2B protein levels decline in serum-free treated CAD cells over six weeks of ageing (Figure 5.9). After one week of ageing, levels of Top2B can be seen to decrease by ~20% ($p=0.0003$ Student's t-test, two-tailed). Levels then plateau between weeks 1 and 3 before decreasing again after week 4 with levels of Top2B significantly lower in weeks 5 and 6 compared to levels seen in week 3 with p values of 0.029 and 0.040, respectively. After six weeks of ageing protein levels of Top2B are 45% lower than at T0 ($p=0.001$). These findings are novel in a neuronal cell line to the best of our knowledge.

Alongside measurements of protein levels of Top2B in serum-free treated CAD cells during ageing, the tumour suppressor gene p21 was also analysed. A study by Jurk *et al*. (2012) demonstrated that post-mitotic neurons develop a p21-dependent senescence-like phenotype driven by a DNA damage response. As increases in oxidative stress and subsequent increases in DNA damage have been reported in ageing and neurodegenerative diseases (Mattson & Magnus, 2006), the analysis of p21 in ageing CAD cells might indicate whether a senescence-like state has developed in these cells over six weeks. Results for p21 analysis are shown in Figure 5.10.

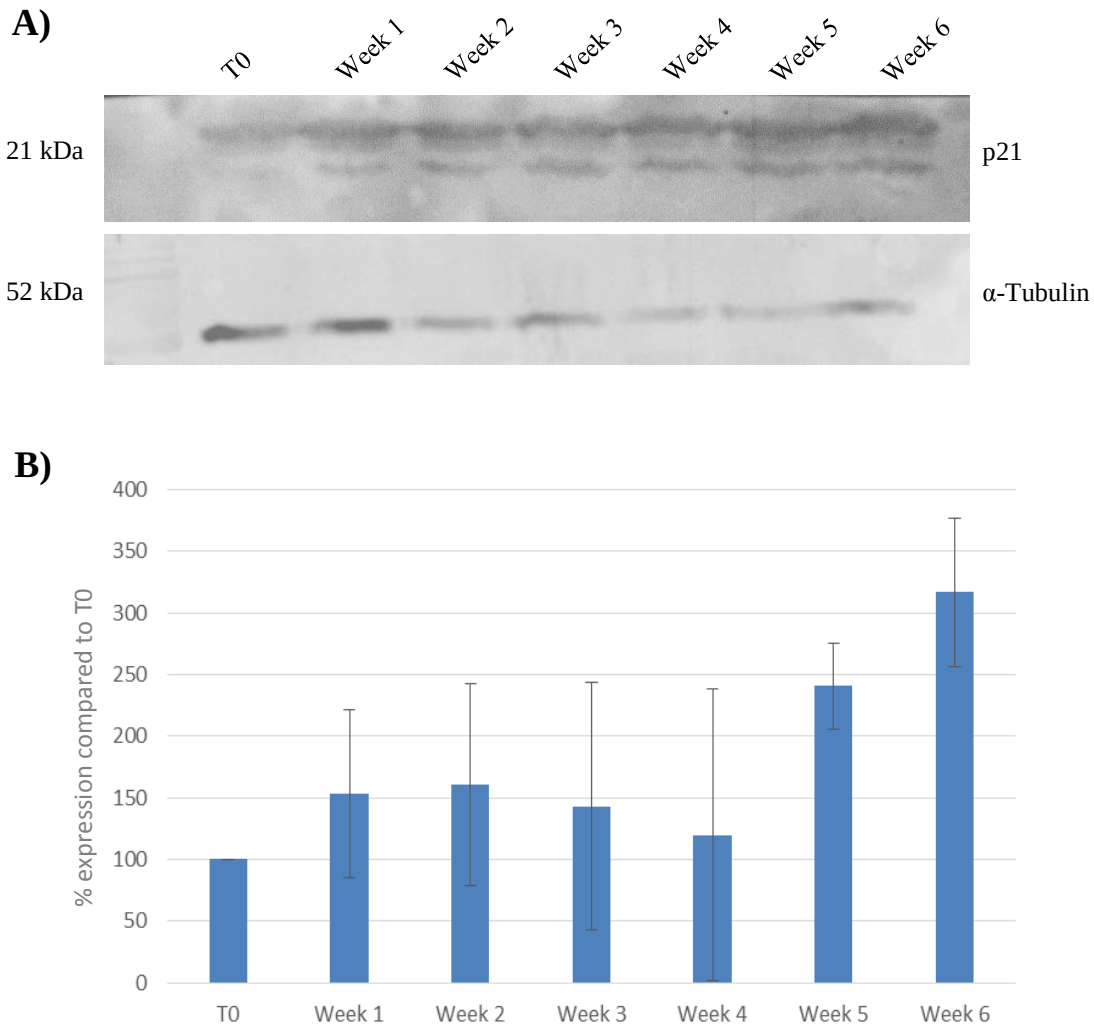

Figure 5.10 Semi-quantification of p21 in serum-free treated CAD cells during six weeks of ageing.

T75 culture flasks were seeded at 5 x 10^4 cells/ml (12 ml per flask) and incubated for 24 hours at 37°C in complete media. Media was removed and replaced with serum-free media and maintained as described in section 2.2.2.7.2. Cells were harvested at T0 and then at weekly intervals up to six weeks. Whole cell extractions were carried out as described in section 2.2.2.9 and quantified as described in section 2.2.2.10. Equal protein loads (89 µg) were added to wells of a 7.5% SDS gel. SDS-PAGE was carried out and protein was transferred to nitrocellulose paper by wet western transfer. (A) Nitrocellulose blots were probed with a p21 antibody and an α-Tubulin load control antibody. Analysis of blot densitometry was carried out using GeneTools (Syngene). (B) p21 expression is presented as percentage expression compared to T0 cells. Results shown are the mean of two independent experiments ± standard error.

In Figure 5.10A protein levels of p21 can be seen to increase over six weeks of ageing in serum-free treated CAD cells. However, results were obtained from only two biological replicates and statistical analysis of densitometry does not provide statistical significance. Further experiments would need to be carried out to confirm whether protein levels of p21 significantly increase in aged CAD cells. If p21 levels were shown to significantly increase it may support previous studies suggesting that post-mitotic neurons develop a p21-dependent senescence-like phenotype (Jurk *et al.*, 2012; Riessland *et al.*, 2019).

To confirm the non-proliferative state and differentiated-like morphology of the serum-free treated CAD cell line over the time course, cell counts were taken throughout the six week experiment and images of cells were acquired to monitor and measure any changes in neurite length. The culture flasks containing CAD cells to be used for measuring cell counts became infected ~4 weeks into the six week experiment, so proliferation results are shown up to day 30. Neurite measurements were taken for the full six weeks. Results are shown in Figure 5.11.

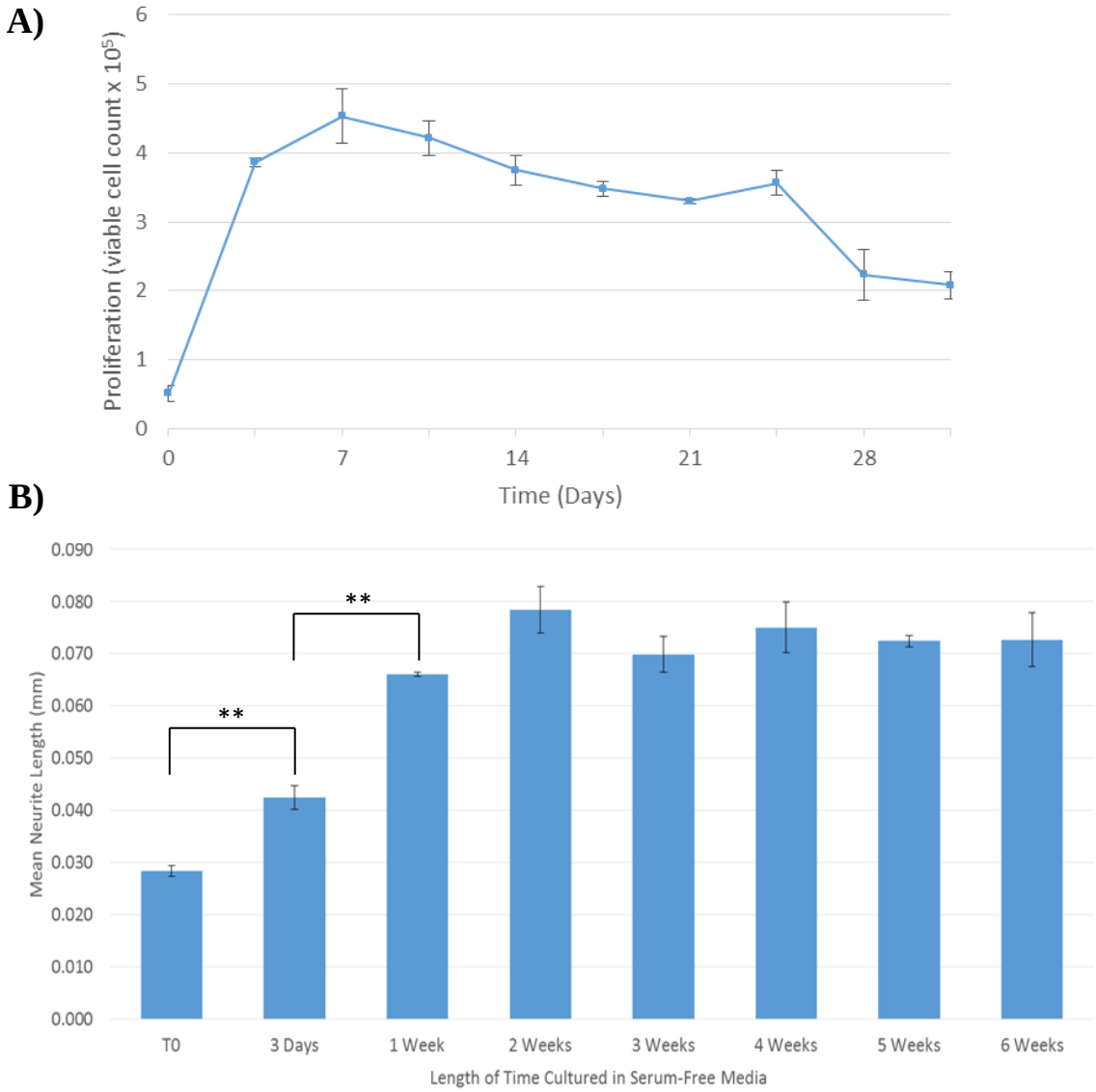

Figure 5.11 Proliferation of CAD cells over 30 days in serum-free media and neurite length over 6 weeks in serum-free media.

T25 culture flasks were seeded at 5 x 10^4 cells/ml (5 ml per flask) and incubated for 24 hours at 37°C in complete media. Media was removed and replaced with serum-free media and maintained as described in section 2.2.2.7.2. (A) Viable cell counts were obtained at T0 and then at weekly intervals up to 30 days using trypan blue exclusion. (B) Images of cells were taken at weekly intervals, neurite length was measured using ImageJ software and the average neurite length was calculated. **= $p<0.01$ (Student's t-test, two-tailed).

From the data above, proliferation of CAD cells grown in serum-free media can be seen to significantly increase up to day 7 ($p=0.0006$), after which no further increases in proliferation are seen (Figure 5.11A). These results differ slightly to the proliferation assay carried out in Figure 5.1, which displayed cell cycle arrest after 48 hours. Experimental methodology was the same for both experiments apart from the culture

vessel used. Slight differences in seeding densities may be the cause for the variations seen between experiments. Between 7 and 24 days no significant changes in viable number of cells were observed. At day 27 the number of viable cells decreased significantly ($p=0.046$) but no significant changes were observed at day 30. These results demonstrate that CAD cells can be maintained in serum-free media for prolonged periods of time without seeing any further increases in proliferation after the development of a differentiated-like phenotype, which supports the use of this cell line in these ageing studies. Neurite outgrowth was also measured alongside proliferation to determine if any morphological changes occurred during ageing. Neurite outgrowth of CAD cells can be seen to increase significantly during the first week in serum-free media (Figure 5.11B), after which neurite length does not change. These results demonstrate that the neurite morphology of CAD cells can be maintained over prolonged periods of time in serum-free media.

5.5.2 Semi-quantification of Top2B mRNA in serum-free treated CAD cells over six weeks of ageing

RT-qPCR experiments were carried out alongside western blot analysis to semi-quantify levels of Top2B mRNA in serum-free treated cells that had been aged over six weeks. CAD cells were chronologically aged between T0 and six weeks and cells were harvested at weekly time points as previously described in section 5.5.1 to allow the collection of all cells to occur on the same day. RNA was extracted and converted to cDNA before carrying out RT-qPCR experiments utilising previously optimised Top2B, GAPDH and β-actin primers (section 5.3.2.2). As discussed by Ling & Salvaterra (2011), the selection of suitable references genes is specific to each experiment and need to be validated at the post-experimental data analysis stage. In order to select an appropriate method of statistical analysis, the threshold cycle (Ct) values of β-actin and GAPDH were analysed under experimental conditions and evaluated for stability. Box and whisker diagrams showing the variations in Ct values of β-actin and GAPDH in differentiated CAD cell samples during six weeks of ageing were created and the coefficient of variance was calculated to show variability between samples (Figure 5.12).

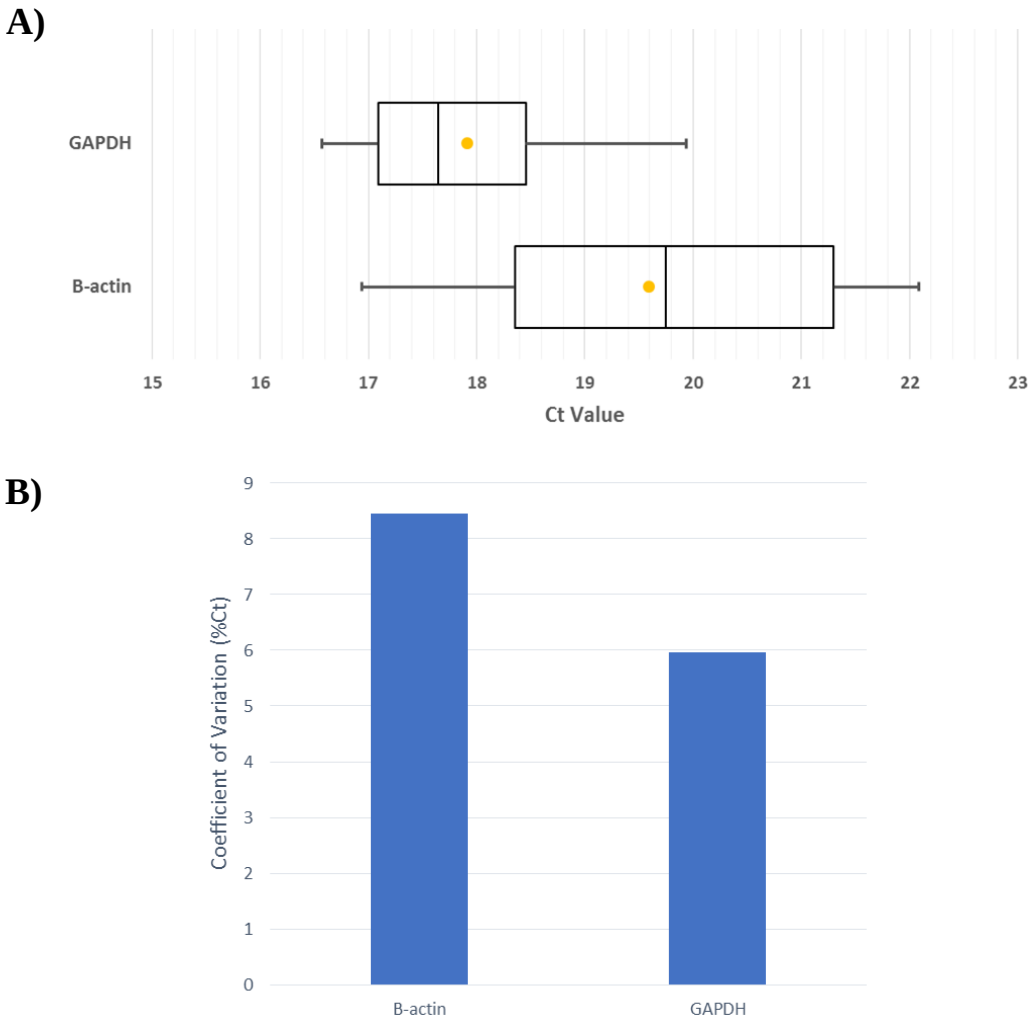

Figure 5.12 Variance of β-actin and GAPDH reference genes from all 6 week CAD experiments.

Ct values for the reference genes β-actin and GAPDH were collated from all CAD 6 week qPCR studies to observe any variations in expression. (A) Box and whisker plots showing the distribution of Ct values for the two candidate reference genes. Yellow dots indicate mean value. (B) The coefficient of variance for the data set was calculated to determine variability of Ct values for β-actin and GAPDH over 6 weeks of ageing in CAD cells.

During the previous experiment looking at Top2B expression during 72 hours of differentiation (section 5.3.2.2), both GAPDH and β-actin were stably expressed and comparable, so therefore could be used for data analysis. However, over six weeks of ageing β-actin was no longer as stably expressed and variability had increased in comparison to results seen after 72 hours of differentiation. The coefficient of variance for β-actin increased from 3.2 during the previous experiment to 8.5 after 6 weeks of ageing. The interquartile range of β-actin also increased from 0.84 to 2.94 between the

two sets of experiments. In comparison, the coefficient of variance only increased by 1.7 in GAPDH and the interquartile range of GAPDH was 1.42 in the first set of experiments and 1.36 over 6 weeks of ageing, indicating that GAPDH is more stably expressed than β-actin. Thus, subsequent analysis utilised only GAPDH for data normalisation. Results for Top2B mRNA expression over six weeks of ageing can be seen in Figure 5.13.

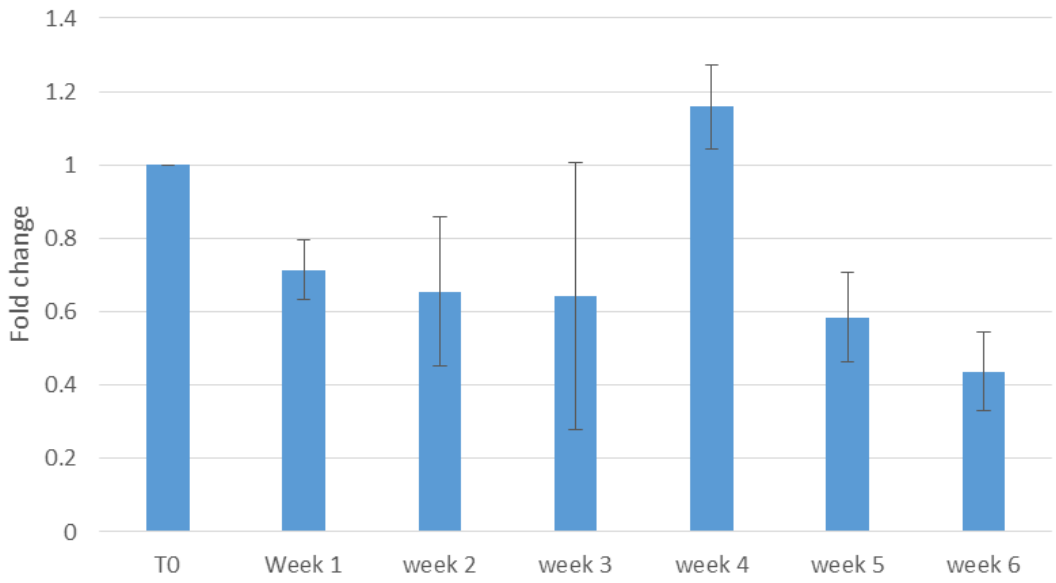

Figure 5.13 Semi-quantification of Top2B mRNA in serum-free treated CAD cells during six weeks of ageing.

T75 culture flasks were seeded at 5 x 10^4 cells/ml (12 ml per flask) and incubated for 24 hours at 37°C in complete media. Media was removed and replaced with serum-free media and maintained as described in section 2.2.2.7.2. Cells were harvested at T0 and then at weekly intervals up to six weeks and RNA was extracted as described in section 2.2.4.1 and quantified on a NanoDrop ND-1000 spectrophotometer. 0.4 µg of total RNA from each sample was converted to cDNA (section 2.2.4.3) and RT-qPCR was carried out (section 2.2.5) using GAPDH as a reference gene. Results were normalised against GAPDH and presented as expression fold change (Vandesompele *et al*., 2002) (calculation described in Appendix Figure C.2). Samples for each individual experiment were loaded in triplicate. Results shown are presented as the mean of three biological replicates ± standard error.

Results from Figure 5.13 demonstrate decreases of Top2B mRNA levels in serum-free treated CAD cells over six weeks of ageing. During the first four weeks of ageing no significant changes in Top2B expression were observed. However, levels of Top2B are significantly lower at five and six weeks of ageing compared to T0 with p values of

0.033 and 0.014, respectively. Although changes in expression at week 4 are not significant, it does appear to be an anomalous result as it is the only week that displays an increase in Top2B expression. All other weeks display a decrease in Top2B expression, which is in line with decreases in Top2B protein levels seen in Figure 5.9.

In conclusion, semi-quantitative analysis of Top2B has shown that both protein and mRNA levels decrease with age in serum-free treated CAD cells. These results are novel in a neuronal cell line to the best of our knowledge.

5.6 Immunohistochemical analysis of Top2B in mouse hippocampal tissue

Following the analysis of Top2B protein and mRNA levels in the CAD cell line, further experiments focussed on the analysis of Top2B in mouse brain tissue using immunohistochemical techniques. As previously stated, one of the brain regions most affected by age is the hippocampus, with similar age-related declines in function seen in humans and numerous other mammalian species (Verbitsky *et al*., 2004). The hippocampus is heavily involved with memory formation and age-related deterioration of the hippocampus is associated with numerous dementia-related diseases such as Alzheimer's disease (Lindberg *et al*., 2012). Hence, Top2B was analysed in mouse brain tissue from the hippocampus.

Preliminary experiments utilised immunofluorescent techniques to determine whether it was possible to identify Top2B expression in mouse hippocampal tissue. Tissue samples from a 29.5 month old C57BL/6 male mouse were sectioned using a cryostat (Bright Instrument OTF/AS Cryostat). 12 µm sections were cut sequentially and processed as described in section 2.2.6.3. Results are shown in Figure 5.14.

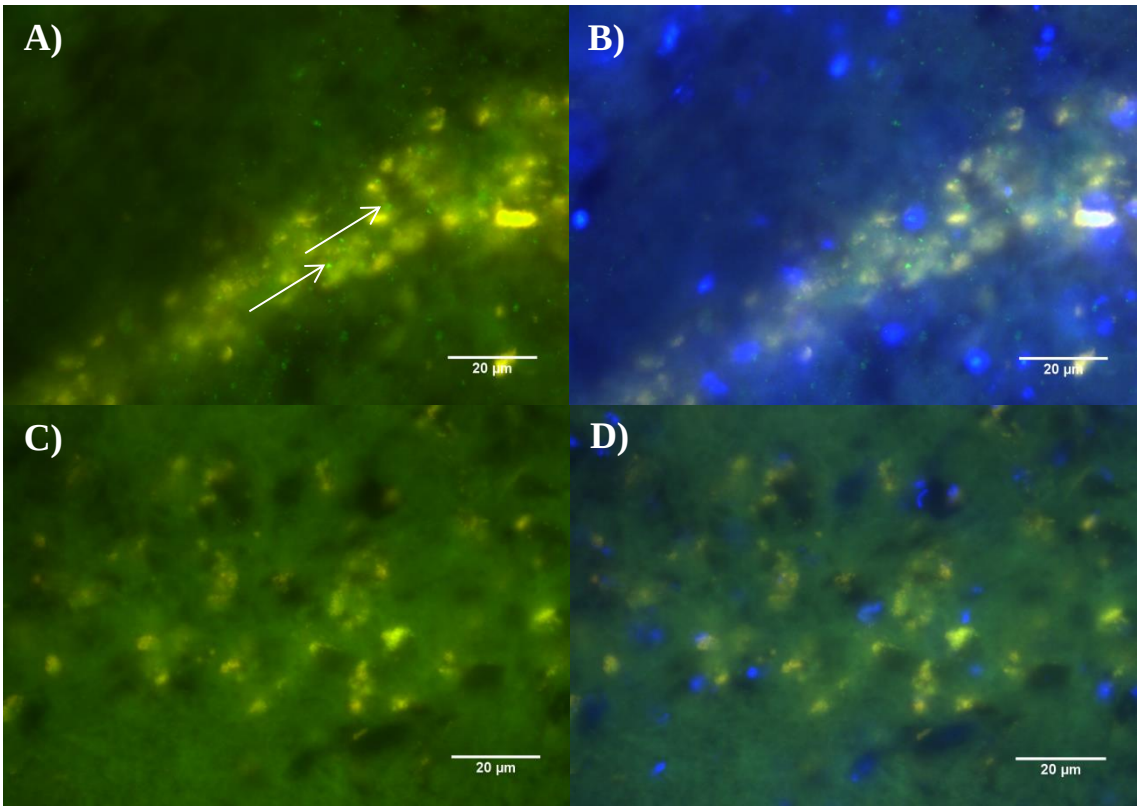

Figure 5.14 Immunofluorescent analysis of Top2B in hippocampal tissue of a 29.5 month old C57BL/6 male mouse.

The brain of a 29.5 month old C57BL/6 male mouse was sectioned using a cryostat. 12 µm sections were cut and placed sequentially on Histobond+ slides (Marienfeld Superior: 0810721). Sections were viewed under a light microscope to ensure sections of the hippocampus were being collected. Tissue was processed as described in section 2.2.6.3 and sections were incubated in a Top2B antibody or an isotype control. Sections were incubated in a secondary FITC antibody before being mounted in mounting medium containing DAPI. (A) Sections treated with Top2B antibody. (B) An overlay of Top2B and DAPI. (C) Sections treated with the isotype control. (D) An overlay of the isotype control and DAPI. Top2B staining is seen as green punctate labelling as indicated by the white arrows and DAPI is seen as blue staining in the overlay images. Images were obtained using a Leica DM500 fluorescence microscope.

Preliminary immunofluorescent analysis of Top2B in hippocampal tissue provided some encouraging results. Green punctate labelling could be seen only in sections incubated with the Top2B antibody (Figure 5.14A), although staining was not very strong, whereas punctate labelling could not be seen at all in the isotype control (Figure 5.14C). Due to poor DAPI staining it was not possible to confirm whether the punctate labelling seen in the sections incubated with the Top2B antibody was nuclear or not. To further investigate Top2B expression in mouse hippocampal tissue the highly sensitive diaminobenzidine (DAB) ABC immunoperoxidase method was utilised (Figure 5.15).

4 months 31 months

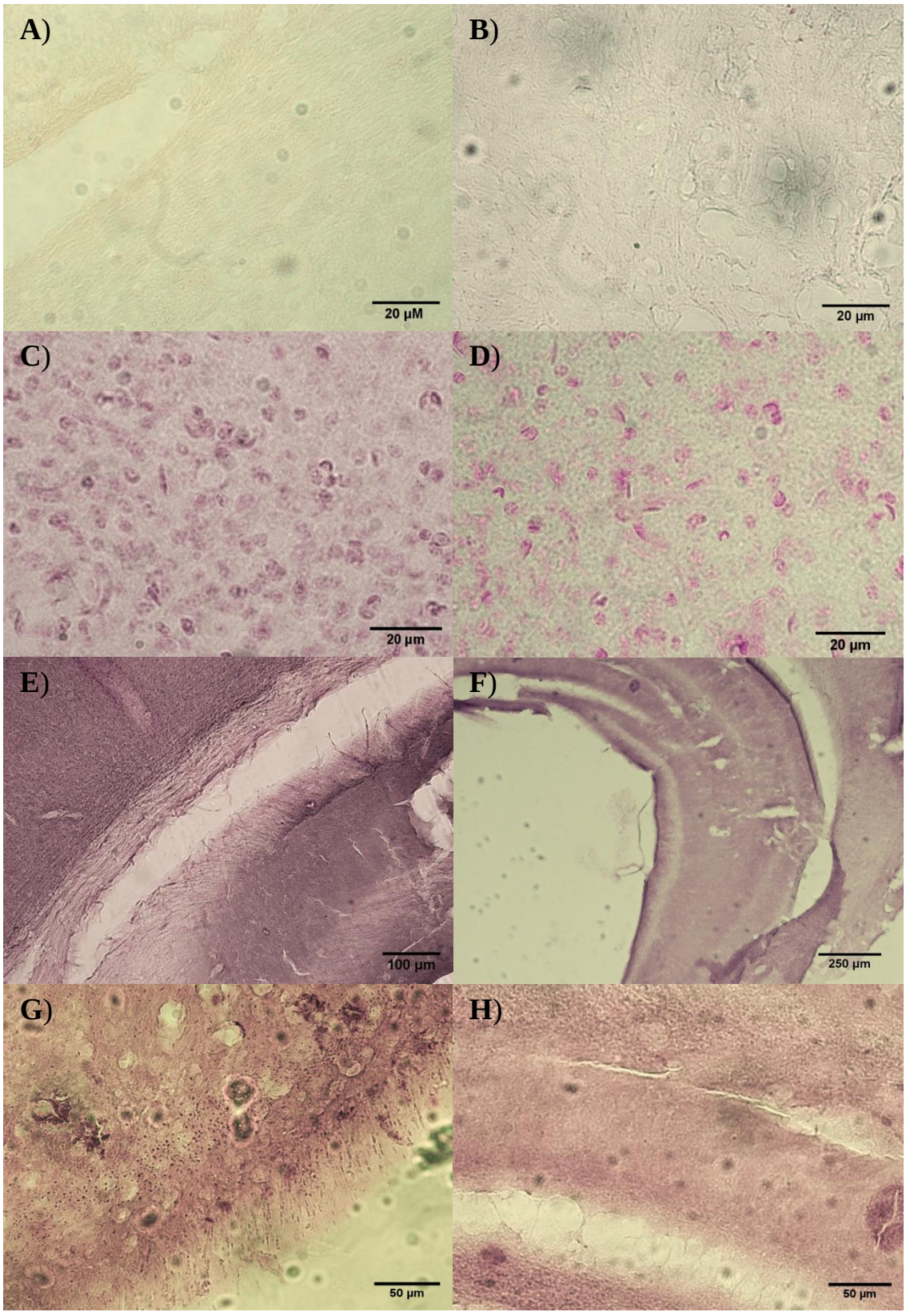

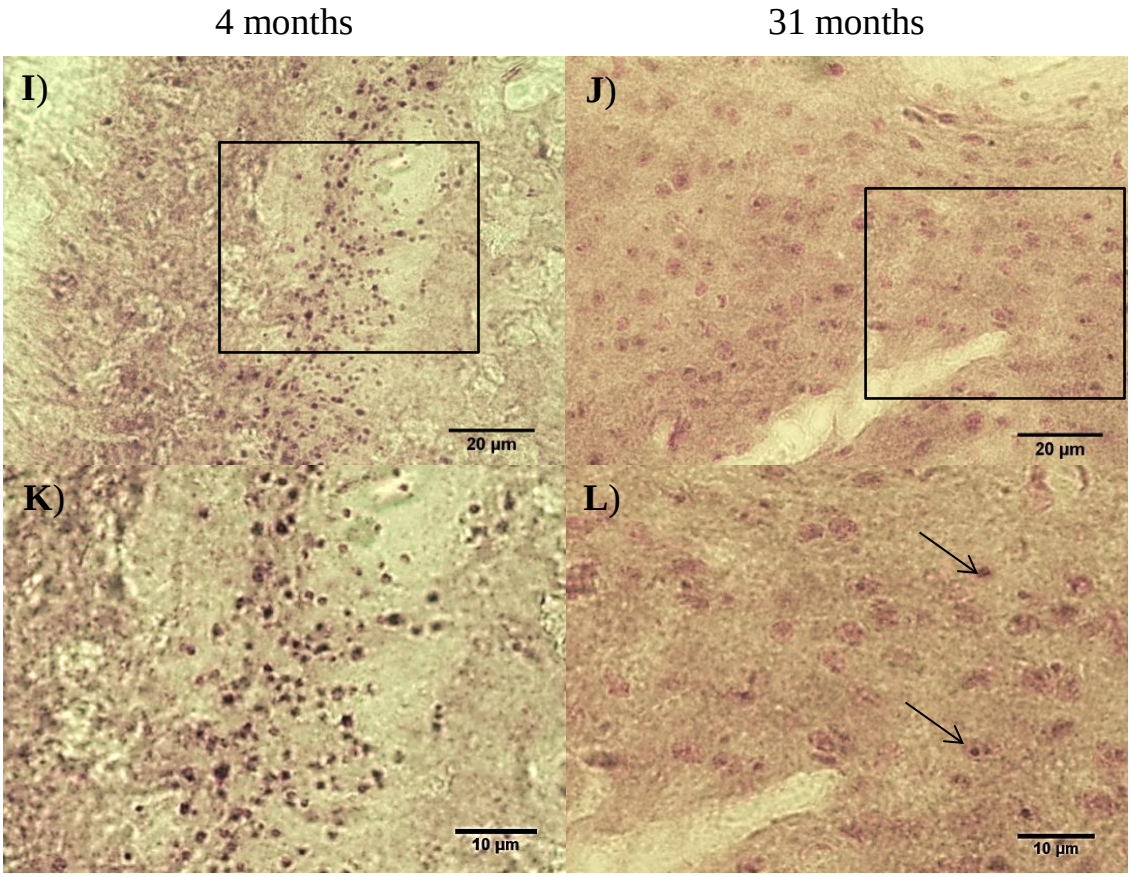

Figure 5.15 DAB immunoperoxidase staining of Top2B in the hippocampus of 4 and 31 month old C57BL/6 male mice.

30 µm sections of brain tissue from 4 and 31 month old mice were cut using a Leica VT1000S vibratome and were viewed under a light microscope to ensure sections of the hippocampus were being collected. Sections were processed as described in section 2.2.6.4.2 using Top2B antibody NBP1-89527. (A) Control section of the 4 month old mouse with secondary antibody only (no primary antibody). (B) Control section of the 31 month old mouse with secondary antibody only (no primary antibody). (C) Control section of the 4 month old mouse with secondary antibody and neutral red counterstaining (no primary antibody). (D) Control section of the 31 month old mouse with secondary antibody and neutral red counterstaining (no primary antibody). (E & G) Low magnification of Top2B labelling in the 4 month old mouse. (F & H) Low magnification of Top2B labelling in the 31 month old mouse. (I) Top2B labelling in the 4 month old mouse with a black rectangle indicating the area observed in (K) under higher magnification where punctate labelling represents Top2B. (J) Top2B labelling in a counterstained section of the 31 month old mouse with a black rectangle indicating the area observed in (L) under higher magnification. (L) Higher power magnification of a 31 month counterstained section shows nuclear labelling of Top2B as indicated by arrows.

Images from Figure 5.15 show that immunoreactivity of Top2B, in the form of punctate labelling, is much stronger in the hippocampus of the younger 4 month old mouse compared to labelling seen in the older 31 month old mouse. Analysis of a counterstained section from the 31 month old mouse (Figure 5.15F) appears to show that Top2B staining is nuclear. This is in agreement with the literature that suggests that Top2B protein is predominantly nuclear (Mirski *et al*., 1999; Onoda *et al*., 2014; Austin *et al*., 2018). Age-related declines in levels of Top2B have been reported in cerebellar tissue of rats (Kondapi *et al*., 2004). However, in that study it was reported that Top2B was not present in hippocampal tissue. Maeda *et al*. (2000) contradicted findings by Kondapi *et al*. (2004) and indicated that Top2B is present in rat hippocampal tissue. Observations of mouse hippocampal tissue in Figure 5.15 are in agreement with this. However, studies by Maeda *et al*. (2000) do not look at Top2B levels throughout the ageing process. The observations seen in mouse hippocampal tissue in Figure 5.15 are novel to the best of our knowledge. However, these preliminary observations were made from hippocampal sections of one young and one aged mouse. Further experiments utilising tissue from a number of young and old animals would be required to confirm any statistical significance.

5.7 Discussion

This chapter provides evidence that Top2B levels decrease with age as both protein and mRNA levels are seen to decrease over time in serum-free treated CAD cells with immunohistochemical sections of mouse hippocampus similarly showing decreases in expression during ageing in young versus aged animals.

As differentiated CAD cells could be maintained in culture over prolonged periods of time, this allowed age-related changes in protein and mRNA levels of Top2B to be observed. The age-related decreases in Top2B protein and mRNA seen in neuronal cells in this study are in agreement with a very limited number of studies, which have previously shown similar results in mouse cerebellum tissue and cerebellar granule neurons (Kondapi *et al*., 2004; Bhanu *et al*., 2010). This raises the important question; why do levels of Top2B decrease with age and what are the implications of this?

5.7.1 Reductions of Top2B mRNA

The activities of the transcription factor Sp1 have been observed in many cellular processes including cell differentiation, cell growth, chromatin remodelling, immune responses, responses to DNA damage and apoptosis by binding to the GC and GT box sequences of gene promoters (Gory *et al*., 1997). As discussed in section 1.5.4, Sp1 has been reported to be a regulator of Top2B expression with interference of Sp1 binding to GC-rich DNA sequences causing a decrease in Top2B expression at both the mRNA and protein level (Guo *et al*., 2014). Activity of Sp1 has been shown to decrease in aged rat brains (Ammendola *et al*., 1992) with Kim *et al*. (2012) also reporting lower levels of Sp1 in various tissues including liver, kidney and spleen from aged mice compared to young mice as well as in senescent human diploid fibroblasts. Interestingly, experiments on human diploid fibroblast cells have demonstrated that a majority of cells with depleted Sp1 also had a senescence-like phenotype and displayed increased ROS levels compared to control cells (Kim *et al*., 2012). In addition to decreases seen in Sp1 with increasing age, the transcription factor NURR1 also exhibits age-dependent decreases in neuronal tissues. Previous studies have shown that NURR1 influences the development and differentiation of mesencephalic dopaminergic neurons through axon genesis regulation (Heng *et al*., 2012). Furthermore, it has also been associated with the maintenance of function in dopaminergic neurons and provides neuroprotection (Eells *et al*., 2002). NURR1 has been shown to directly bind to a region on the Top2B promoter with NURR1 knockout models displaying significant reductions of Top2B expression in mouse brain sections. As discussed in section 1.5.4, this suggests a role for NURR1 in the regulation of Top2B expression (Terzioglu-Usak *et al*., 2017). Numerous studies have reported changes in expression of NURR1 in dopaminergic neurons with significant decreases shown in the substantia nigra of aged humans and rats (Chu *et al*., 2002; Parkinson *et al*., 2015). Further studies by Ahn *et al*. (2018) have shown NURR1 immunoreactivity to gradually decrease during normal ageing in the hippocampus of gerbils and suggest it may be associated with a decline in hippocampus-dependent cognitive function. As Top2B has been reported to be regulated by both Sp1 and NURR1, the decrease of these transcription factors throughout the ageing process will likely affect the activities of Top2B. This may prevent a number of essential processes such as neuronal maintenance from functioning correctly. Indeed, a decrease in these transcription factors may be responsible for the decreases of Top2B mRNA during this study.

Chromatin architecture has been shown to be altered by age-related epigenetic changes such as DNA methylation (Armstrong *et al*., 2019). DNA methylation is a key player in the modulation of gene expression with the activity of DNA methyltransferase enzymes typically responsible for gene silencing through the addition of a methyl group to the carbon 5 position of cytosine to produce 5-methylcytosine (Johnson *et al*., 2012). It is suggested that the methylation of cytosine prevents gene transcription by interfering with the transcriptional machinery or through interference of the recognition sequence of transcription factors. Typically, during development, DNA methylation patterns in the genome change as a result of *de novo* DNA methylation and demethylation. As a result, DNA methylation patterns that regulate tissue-specific gene transcription are stable and unique in differentiated cells. Interestingly, post-mitotic neurons are still seen to express DNA methyltransferases and some components associated with demethylation, with neuronal activity reported to modulate DNA methylation patterns in response to both physiological and environmental stimuli (Moore *et al*., 2013). This may also cause a reduction in Top2B mRNA.

Reductions in mRNA may be responsible for the declines in protein levels of Top2B that are seen in this study. However, as discussed in chapter 3 (3.6.4.1), misfolding and degradation of Top2B may also lead to a reduction in protein levels during ageing as a result of proteostasis dysfunction.

5.7.2 Implications of reductions of Top2B

Indeed, normal cognitive function relies heavily on the accurate regulation of DNA methylation with age-related changes in DNA methylation seen to alter the chromatin architecture of DNA, which has been associated with the progression of neurodegenerative diseases (Berson *et al*., 2018). The presence of DSBs in DNA is not just a deleterious event caused by exposure to DNA damaging agents but is physiologically crucial for mediating transcription of key genes. Previous work by Bunch *et al*. (2015) has shown that type II topoisomerases are crucial for RNA polymerase II (Pol II) pause release and transcriptional elongation. Pol II activities are known to initiate RNA synthesis but studies have shown that pausing of Pol II during early elongation acts as a regulatory mechanism (Adelman & Lis, 2012). The pause release of Pol II is necessary for productive RNA synthesis and topoisomerases are known to be involved in this process (Bunch *et al*., 2015). Furthermore, the action of Pol II during transcription elongation has been shown to cause axial rotation in DNA, which introduces positively supercoiled DNA in front of the enzyme (Björkegren &

Baranello, 2018). The actions of topoisomerase in relieving torsional stress in DNA are essential to maintaining DNA templates in a transcriptionally competent state (Gilbert & Allan, 2014). As Top2B is known to have key roles in the regulation of transcription and gene expression, age-related decreases in levels of Top2B may have detrimental effects on gene expression, particularly in areas with altered chromatin architecture caused by changes in DNA methylation.

The transcription factor CCCTC-binding factor (CTCF), which also acts as a transcriptional activator, has key roles in the regulation of chromatin structure and gene regulation. Top2B associates with chromatin and has also been shown to be crucial for the maintenance of chromatin architecture (Uusküla-Reimand *et al*., 2016). Chromatin architecture and organisation are considered to have a major impact on DNA topology and could be a source of topological stress. Top2B has been seen to facilitate transcription initiation through the formation of a favourable chromatin environment, with topological stress caused by chromatin looping thought to be relieved by the actions of Top2B. Therefore, Top2B is considered a key component in the maintenance of chromatin architecture (Uusküla-Reimand *et al*., 2016; Canela *et al*., 2017). CTCF has been reported to be enriched at Top2B binding sites with over half of the Top2B binding sites overlapping with CTCF suggesting an overlap of roles (Barutcu *et al*., 2017). Age-related decreases of CTCF have previously been reported (Sun *et al*., 2018). If CTCF decreases, Top2B may be relied upon more heavily to maintain chromatin architecture and vice versa. If both Top2B and CTCF decrease equally with age, this may ultimately compromise chromatin architecture and lead to age-related dysfunction of gene regulation. It is likely that age-related decreases in Top2B affect chromatin architecture and maintenance. Hence, subsequent disruptions in transcriptional regulation are possible.

Indeed, Top2B is known to be crucial in facilitating the expression of long genes with inhibition of Top2B shown to cause reductions in expression of these genes (King *et al*., 2013). Long genes such as ubiquitin protein ligase E3A (*Ube3a*) play an important role in maintaining normal neuronal function, including synaptic plasticity, and its expression is tightly regulated with increases of the gene linked to autism spectrum disorders and depletion of the gene known to cause Angelman syndrome during development (Lam *et al*., 2017). Substantial age-related decreases in *Ube3a* expression have been reported in human, monkey and cat cortex, which highlights a vulnerability during brain ageing that may be responsible for a change in cortical function and

plasticity (Williams *et al*., 2010). Top2B has been implicated in the expression of *Ube3a* and it is possible that the age-related decreases seen in Top2B may have subsequent implications in the expression of long genes such as *Ube3a* and have detrimental effects to the maintenance of neuronal function (King *et al*., 2013). Top2B has also been shown to actively repress genes through its role in chromatin architecture maintenance. It is suggested that the repression of these genes is dependent on the maintenance of DNA template integrity (Tiwari *et al*., 2012). One such repressed gene is *Ngfr* p75, which is widely expressed during development and is a key regulator of cell death but becomes downregulated and repressed after development (Nykjaer *et al*., 2005). Expression of *Ngfr* p75 is typically only seen in adults in response to injury and DNA damage, with reports showing it is responsible for cell death accompanying neurodegeneration (Miller & Kaplan, 2001). Upregulation of *Ngfr* p75 has been observed in the absence of Top2B in mouse embryonic stem cells that had been differentiated into postmitotic glutamatergic neurons and resulted in phenotypic premature cell death (Tiwari *et al*., 2012). In addition to this, Kraemer *et al*. (2014) suggested a mechanism linking oxidative stress to an upregulation of *Ngfr* p75 through ligand-independent cleavage. During the study 4-hydroxynoneal (HNE), a product of lipid peroxidation caused by oxidative stress, was seen to activate *Ngfr* p75 signalling in cells cultured from the superior cervical ganglia of mice, subsequently linking *Ngfr* p75 activation to oxidative stress. As oxidative stress is known to increase with age and subsequently cause increases in DNA damage, decreases in Top2B mRNA and protein levels with age may cause an upregulation of *Ngfr* p75 in serum-free treated CAD cells over six weeks of ageing. Indeed, the significant reduction of viable CAD cell numbers shown in Figure 5.11 after 27 days in serum-free media may indicate an increase in the activation of tumour necrosis factor receptors such as *Ngfr* p75.

Increases in neuronal activity have been shown to cause expression of early-response genes that are crucial for experience-driven changes to synapses, learning and memory. This neuronal activity can stimulate the formation of DSBs in the promotors of numerous early-response genes and is seen to induce their expression (Madabhushi *et al*., 2015). DSBs stimulated by neuronal activity are thought to be mediated by Top2B. Indeed, Top2B has been shown to be bound to the promotors of some of these genes. In particular, Top2B binding was seen to be significantly enriched within the promoter of the early-response gene Neuronal PAS domain protein 4 (*Npas4*) and Top2B knockdown models in cortical neurons from E16 Swiss-Webster mice have

demonstrated a reduction in DSBs and subsequently a reduction in the expression of early-response genes (Madabhushi *et al*., 2015). *Npas4* is a rapidly induced early-response gene that is only expressed in neurons and is selectively induced by neuronal activity. Expression of *Npas4* leads to the modification of synaptic connections and has been associated with the regulation of learning and memory formation in the hippocampus and amygdala (Sun & Lin, 2016). *Npas4* has been implicated in development, maintenance and survival of neurons and synapses, as well as regulating synaptic plasticity via downstream target genes, such as brain-derived neurotrophic factor (BDNF) (Qiu *et al*., 2016). Deletion of *Npas4* from the CA3 region of the hippocampus in *Npas4* conditional knockout mice models has been shown to result in memory formation impairments, suggesting experience-dependent changes in neural circuitry associated with memory formation are likely to occur in neurons in which *Npas4* has been induced (Ramamoorthi *et al*., 2011). As binding of Top2B to the promotor of *Npas4* has been reported, it is likely that age-related declines in Top2B may affect expression of *Npas4* and consequently lead to learning and memory impairments. Indeed, declines in *Npas4* have been observed in the ventral hippocampus of aged rats (Calabrese *et al*., 2013).

In addition to its roles in the development and maintenance of neuronal function, Top2B has also been shown to have roles in DNA repair. As discussed in section 1.5.6, the capacity of base excision repair (BER) in neurons is thought to be regulated by Top2B-mediated DNA breaks (Gupta *et al*., 2012). Gupta suggested that Top2B activity at abasic sites indicated an overlap of Top2B in BER processing regions, thus implicating it in the regulation of BER pathway intermediates. Top2B dynamically responds to DNA damage and is rapidly recruited to DSBs (Emmons *et al*., 2006). Furthermore, Top2B knockout cells display increased sensitivity to DNA damaging agents with decreases in homologous recombination (HR)-mediated DSB repair also observed, suggesting roles for Top2B in DSB repair pathways (Morotomi-Yano *et al*., 2018). The age-related declines of Top2B seen in this study may have consequences for DNA repair pathways, including HR and BER, and could result in an increase and subsequent accumulation of DNA damage in neuronal cells, which may cause dysfunction and cell death.

5.7.3 The use of the CAD cell line as a differentiated neuronal model of ageing

The ability to chronologically age CAD cells was particularly useful as H_2O_2 induced oxidative stress did not bring about senescence in serum-free treated cells with β-gal

assays providing negative results similar to the previous experiments using the neuroblastoma SH-SY5Y cell line. As discussed in the previous chapter, the use of a positive control during these experiments may have been able to further clarify whether senescence had been achieved and confirmed that the assay was working correctly or not. As previous studies have shown that other differentiated neuronal cell lines are more resistant to the effects of DNA damaging agents than undifferentiated cells (Schneider *et al*., 2011; Tong *et al*., 2017), this may have also been the case with serum-free treated CAD cells. The concentrations of H_2O_2 used in this chapter may have been too low to induce senescence in the serum-free treated CAD cells and it may have provided useful research to further investigate a greater range of H_2O_2 concentrations and exposure times to fully elucidate whether senescence could be achieved using this method. In addition to this, the β-gal assay may not be suitable to determine senescence in these experiments with studies by Piechota *et al*. (2016) suggesting that β-gal should be used with caution when identifying senescence in neurons as β-gal activity cannot be solely attributed to senescence either *in vitro* or *in vivo*. Piechota reported relatively high levels of β-gal in young 3 month old mice and suggested that this marker may be linked to non-senescent activities. In addition to this, primary cultures of cortical neurons also exhibited noticeable β-gal activity early in culture. Interestingly, treatment of these cells with low doses of doxorubicin did not increase the numbers of β-gal positive cells (Piechota *et al*., 2016). It appears that the use of β-gal as a marker of senescence in neurons provides varying results and may not have been the correct marker to determine whether H_2O_2 treated CAD cells had entered a state of senescence. Piechota *et al*. (2016) goes on to suggest the use of repressor element 1-silencing transcription factor (REST) as a marker of neuronal senescence *in vitro*. In contrast to β-gal, REST was seen to display a pattern of expression that correlated with neuronal age, thus the use of REST as a neuronal marker of senescence may have been more suitable for the set of experiments in this chapter.

Although serum-free treated CAD cells can be maintained in culture for six weeks, this is still much shorter than the length of time a mature neuronal cell survives *in vivo*, which raises the question as to how reliable serum-free treated CAD cells are as a model of ageing. p21 is used as a marker of senescence and post-mitotic neurons have been shown to develop a p21-dependent senescence-like phenotype (Jurk *et al*., 2012; Riessland *et al*., 2019). The results from Figure 5.10 shows increases in p21 over six weeks of ageing in serum-free treated CAD cells but further experiments would be

required to confirm any statistical significance as results shown are from only two biological replicates. If further experiments demonstrated that p21 does increase significantly then it may provide evidence that CAD cells are displaying a phenotypic characteristic of aged cells and are therefore suitable as a model of ageing. Nevertheless, levels of Top2B mRNA and protein were seen to decrease over six weeks of ageing (Figure 5.9 and Figure 5.13), which is also seen when comparing sections of hippocampus tissue from young and aged mice (Figure 5.15). However, as stated above, the use of more suitable markers of senescence in future experiments, such as REST, may also support the use of serum-free treated CAD cells as a model of ageing. In addition to these markers of senescence, aged cells are known to develop an accumulation of DNA damage whilst experiencing increased levels of oxidative stress, with numerous neurodegenerative diseases linked to increases in ROS (Castelli *et al*., 2019). Measuring DNA damage in serum-free treated CAD cells over a prolonged period of time would provide information on the accumulation of DNA damage with age but also may provide information on the ability of DNA repair pathways to cope with oxidative stress throughout the ageing process. This is an area of research that was investigated further in the following chapter.

Results shown in Figure 5.3 and Figure 5.6 showed that protein and mRNA levels of Top2B did not increase during the first 72 hours in serum-free media. Numerous studies have shown that Top2B becomes upregulated during differentiation, so it would be expected that Top2B mRNA and protein would increase during these experiments. These experiments were carried out based on previous proliferation experiments that showed that cells ceased proliferating at 48 hours (Figure 5.1). As cells were seen to exit the cell cycle at this point it was assumed that differentiation had taken place. However, later proliferation experiments that were carried out up to 30 days (Figure 5.11A) demonstrated that cells continued to grow during the first week in serum-free media before proliferation stopped. Furthermore, neurites were also seen to continue growing significantly during the first week in serum-free media. This indicates that terminal differentiation of CAD cells had not been reached after 72 hours in serum-free media and may explain why significant increases in Top2B mRNA and protein levels were not seen. Interestingly, chronological ageing in CAD cells did not show an increase in Top2B mRNA or protein levels after one week of ageing (Figure 5.9 and Figure 5.13). Instead, both Top2B mRNA and protein were seen to decrease after one week of ageing and continued to do so over six weeks. It is possible that Top2B mRNA

and protein levels increased between 72 hours and six days of ageing during the differentiation process before decreasing again at one week. However, that cannot be determined from this set of experiments. Further experiments using extracts from CAD cells over the first week of ageing in serum-free media may determine whether Top2B levels increase during differentiation in this cell line. Although Top2B mRNA and protein levels are typically seen to increase during differentiation, it may be possible that cell line specific changes in Top2B levels are being observed in the CAD cell line. Indeed, work by Kenig *et al*. (2016) showed that glioblastoma stem cells treated with all-trans retinoic acid to induce differentiation towards an astrocyte phenotype resulted in a decrease in Top2B expression over 120 hours, whilst results shown by Guo *et al*. (2014) report an increase in Top2B expression at both the mRNA and protein level during retinoic acid-induced neuronal differentiation of the neuroblastoma cell line SH-SY5Y over 120 hours.

Results seen in Figure 5.8 showed that protein levels of p21 were evenly expressed in serum-free treated CAD cells and in cells exposed to H_2O_2, which suggested that senescence had not been achieved in these cells. As a tumour suppressor gene it would be expected that p21 levels would increase after exposing cells to H_2O_2. However, this was not the case in CAD cells. Work by Ho *et al*. (2013) demonstrated that p21 expression and proliferative decline are not due to elevated H_2O_2 levels and are not mediated by p53 as their results suggested that the accumulation of H_2O_2 in long term cultured placenta-derived multipotent cells only made minor contributions towards p21 expression levels. They suggested that p21 increases were mediated by protein kinase C (PKC) α and β through p53- and H_2O_2-independent pathways. This may explain why p21 protein levels were not seen to significantly increase in CAD cells treated with H_2O_2. It may have also been expected that protein levels of p21 would be higher in serum-free treated cells compared those grown in complete media as these cells are entering cell cycle arrest and p21 expression is known to inhibit the cell cycle. However, a study by Morris-Hanon *et al*. (2017) reported no significant changes in levels of p21 in glioma cell lines exposed to nutrient restriction. There may be conditions that are specific to certain cell lines and this may explain why p21 protein levels were not higher in serum-free treated CAD cells compared to cells grown in complete media.

5.7.4 Declines of Top2B in hippocampal tissue

Although results in Figure 5.15 show Top2B immunoreactivity in the hippocampus from one young and one aged mouse, it does provide promising initial results and a proof of methodology that demonstrates Top2B can be identified in mouse brain tissue using these techniques. Results from Figure 5.15 show clear differences in Top2B expression with punctate labelling seen to be much stronger in tissue from the young animal compared to the aged animal. These results are also in support of previous work by Maeda *et al*. (2000), which demonstrated that Top2B expression can be seen in murine tissue of the hippocampus. This also contradicts work by Kondapi *et al*. (2004), which suggested that Top2B was predominantly expressed in cerebellar tissue and was not seen at all in hippocampal tissue. As stated previously, the hippocampus is one of the brain regions most affected by age (Verbitsky *et al*., 2004) with age-related deterioration of the hippocampus associated with numerous dementia-related diseases, such as Alzheimer's disease (Lindberg *et al*., 2012). Additional experiments would need to be carried out to determine whether levels of Top2B decrease significantly in the hippocampus of aged mice. As Top2B is a key player in neuronal development, neuronal maintenance, the transcription of long genes and has roles in DNA repair pathways, decreases in Top2B in an area such as the hippocampus may lead to numerous neurodegenerative conditions.

In conclusion, Top2B mRNA and protein were seen to decrease during ageing in serum-free treated CAD cells *in vitro* and a concomitant increase in p21 was also observed, whilst punctate labelling of Top2B was seen to be higher in young mouse hippocampal tissue compared to aged tissue. The CAD cell line would be a useful model to further examine the consequences of reductions in Top2B and the mouse model may provide more insight into Top2B expression in hippocampal tissue.

6. The DNA damage response of differentiated CAD cells during ageing

6.1 Introduction

Previous studies have demonstrated that during normal ageing brain function declines and leads to learning, memory and motor coordination impairments (Alexander *et al*., 2012; Castelli *et al*., 2019). Ageing is multifactorial in nature but it is thought that a combination of an increase in exposure to toxins such as ROS and a decline in cellular damage repair mechanisms could be at the heart of the process (Mattson & Magnus, 2006). DNA is a major target for age-related damage and is considered by some as a cause of ageing itself (Gorbunova & Seluanov, 2007).

DNA double strand breaks (DSBs) are thought to be one of the most toxic lesions that must be repaired to preserve chromosomal integrity in a cell (Mehta & Haber, 2014). DSBs can be induced spontaneously by ROS but also by exposure to ionising radiation, chemotherapeutic agents and other substances such as bioflavonoids (Negritto, 2010; Jekimovs *et al*., 2014; Goodenow *et al*., 2020). When DSBs occur, a mammalian histone variant H2AX becomes phosphorylated at serine 139, which is located in its carboxy terminal tail and is a unique site among the H2A histone family. This specific phosphorylation is denoted γH2AX (Rogakou *et al*., 1998; Podhorecka *et al*., 2010). Ataxia telangiectasia mutated (ATM) is the major kinase that controls γ-phosphorylation in human cells. However, ATR (ATM and Rad3 related) can also phosphorylate H2AX during hypoxia and replication fork collapse (Paull *et al*., 2000; McKinnon, 2004). When a DSB is generated, rapid phosphorylation of H2AX begins and spans both sites of damage on the chromatin and can range from several kilobases to a megabase in length (Rogakou *et al*., 1999; O'Hagan *et al*., 2011; Seo *et al*., 2012). γH2AX then recruits mediator of DNA damage checkpoint 1 (MDC1), which facilitates further phosphorylation of H2AX. Together, these recruit additional factors, such as p53-binding protein 1 (53BP1), C-terminal binding protein-interacting protein (CtIP) and Mre11-Rad50-Nbs1 (MRN) to the site of damage, which will carry out repair (Yuan *et al*., 2010).

In order to repair DSBs in post-mitotic neurons the error-prone NHEJ pathway is the predominant DSB repair pathway (Vyjayanti & Rao, 2006). NHEJ is a repair mechanism in which two DSB ends are directly joined by ligation (Chiruvella *et al*., 2013) and can be broken down into individual steps, which include; (1) DNA end

recognition and assembly, including NHEJ complex stabilisation at the DNA double strand break; (2) DNA end bridging and promotion of end stability; (3) Processing of the DNA end; (4) Ligation of the broken ends and subsequent termination of the NHEJ complex (Davis & Chen, 2013). The joining of the two DSB ends are characterised by having little or no homology between the two ends. Thus, NHEJ is recognised as having a high potential for making errors. The NHEJ repair pathway was considered the only pathway to be utilised in post-mitotic neurons to repair DSBs associated with oxidative damage, as HR is known to require a sister chromatid template, which is not present in non-replicating neuronal cells, in order to repair DSBs. However, recent studies have reported RNA-templated HR repair mechanisms of DSBs at active transcription sites in terminally differentiated post-mitotic neurons. It has been shown that the HR repair protein RAD52 is recruited to DSB sites and has demonstrated an HR repair mechanism in post-mitotic neurons (Welty *et al*., 2018).

After the successful repair of a DSB, γH2AX dephosphorylation occurs to restore the cell to its pre-stressed state. The phosphatases PP2A, PP4, and the p53-induced phosphatase 1 (WIP1) dephosphorylates γH2AX at serine 139 (Chowdhury *et al*., 2005; Nakada *et al*., 2008; Moon *et al*., 2010). Several reports have shown that γH2AX foci form spontaneously (Costes *et al*., 2006 & 2010; Pustovalova *et al*., 2016). In addition, further studies have reported the presence of large persistent γH2AX foci in ageing tissues, including the liver, brain and also in ageing cells, such as hematopoietic stem cells (HSCs), dermal fibroblasts and ovarian primordial follicles. It was subsequently interpreted that these foci were due to unrepairable DSBs (Rube *et al*., 2011; Hewitt *et al*., 2012; Titus *et al*., 2013). However, Mamouni *et al*. (2014) suggested that these persistent foci may reflect inadequate H2AX dephosphorylation, which may reduce with age. Nevertheless, the observed increase in persistent γH2AX foci with age correlates with evidence that shows an increase in macromolecular damage with ageing (López-Otín *et al*., 2013).

The functionality of neuronal stem cells has been shown to be directly affected by the persistent presence of DSBs. As a result, these cells either undergo premature senescence or terminally differentiate into astroglial cells, which leads to a reduction in proliferative potential and may lead to a loss of neuronal cells over time, subsequently causing neurodegeneration and cognitive impairment that is often seen in ageing. (Schneider *et al*., 2013). Thus, it is clear that unrepaired DSBs accumulate with age and are associated with major age-related cellular phenotypes, such as cellular senescence.

6.2 Do DSBs accumulate in serum-free treated CAD cells when chronologically aged *in vitro*?

This chapter explores the levels of DSBs in serum-free treated CAD cells over a 6 week period to determine whether this type of damage increases with age in this cell line. This may allow conclusions to be made about the suitability of serum-free treated CAD cells as a model of ageing and allow exploration of the DNA damage response in ageing in future experiments.

The γH2AX assay was used to measure DSBs and the alkaline Comet assay was used to measure both SSBs and DSBs in serum-free treated CAD cells that were chronologically aged. As previously stated, the quantification of γH2AX foci through immunofluorescence techniques is associated with the amount of DSBs present in a cell. Hence, the more foci that are seen in a nucleus, the more DSB damage is present (Kinner *et al*., 2008). The Comet assay, also known as single-cell gel electrophoresis, is a simple technique and is considered to be one of the gold standard techniques for measuring DNA strand breaks, which includes both SSBs and DSBs (Figueroa-González & Pérez-Plasencia, 2017). The alkaline Comet assay is sensitive to alkali labile sites and is associated with being sensitive to both SSBs and DSBs, whereas the neutral Comet assay is associated with being sensitive to only DSBs (Afanasieva & Sivolob, 2018). In the Comet assay, cells are embedded in agarose and then electrophoresed. If DNA contains breaks, chromatin supercoils become relaxed and broken ends are able to migrate to the anode due to DNA being negatively charged. Cells are described as 'comets' with the head of the comet containing a mass of undamaged DNA while the tail of the comet contains damaged DNA. The relative amount of DNA that migrates to the anode can be viewed using fluorescence microscopy and gives some indication of the relative number of DNA breaks in a cell. Undamaged DNA contains fewer broken ends, which results in larger fragments of DNA that do not migrate during electrophoresis, resulting in a comet without a tail. Comet assay results can be analysed manually or using automated software. Cells can be analysed manually and sorted into one of five classes ranging from 0-4 depending on tail intensity as described by Collins *et al*. (1995). Cells with no DNA damage are given a score of 0 and cells that are highly damaged are given a score of 4. Hence, the more damage that is seen in a population of cells, the higher the score. Automated analysis can also be carried out using software such as ImageJ with the OpenComet plugin. This software recognises cells, outlines the head and tail of the comet and measures the

percentage of DNA that is seen in the tail of the comet compared to the head. Hence, the more damage that is seen in the cell, the higher the percentage of DNA will be measured in the tail.

6.2.1 Quantification of DNA damage in serum-free treated CAD cells

6.2.1.1 γH2AX foci analysis of DNA damage

In order to quantify DNA damage during chronological ageing *in vitro*, serum-free treated CAD cells were maintained in culture for a total of 6 weeks. Samples of cells were processed each week, γH2AX assays were carried out and γH2AX foci were analysed manually. Results are shown in Figure 6.1.

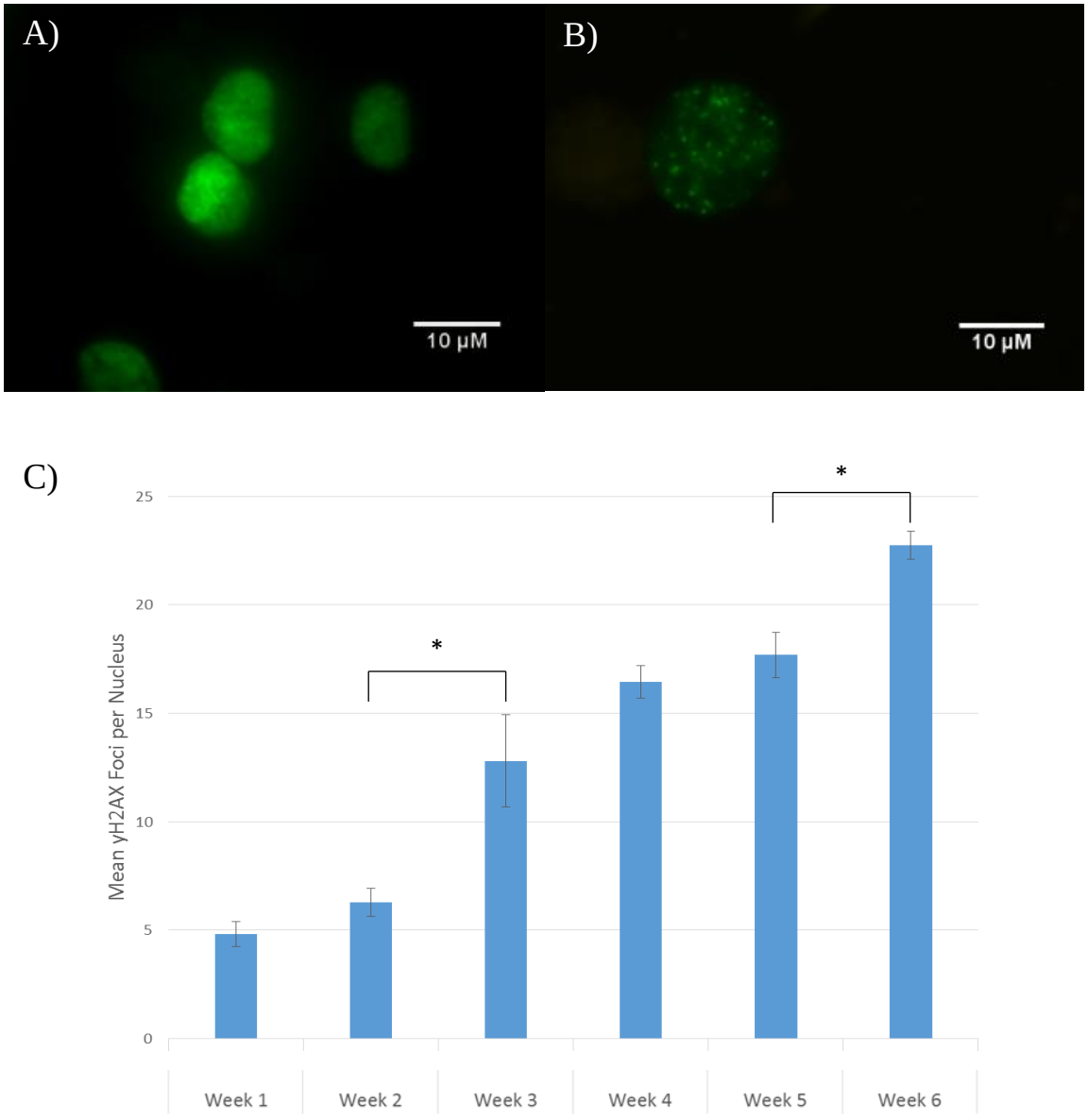

Figure 6.1 γH2AX foci analysis over 6 weeks in serum-free treated CAD cells.

T25 culture flasks were seeded at 5 x 10^4 cells/ml (5 ml per flask) and incubated for 24 hours at 37°C (5% CO_2) in complete media. Media was removed and replaced with serum-free media and maintained as described in section 2.2.2.7.2 and aged to specific time points prior to carrying out γH2AX assays. Sterilised 24 x 24 mm coverslips were placed in each well of a 6-well plate. Once CAD cells had been aged to the correct time point they were seeded into the 6-well plate at a density of 5 x 10^4 cells/ml (2 ml per well) and incubated for 24 hours. γH2AX assays were carried out as described in section 2.2.2.15 at weekly intervals for 6 weeks. (A) CAD cells at week 1. (B) CAD cells at week 6. (C) Mean number of γH2AX foci per nucleus over 6 weeks (100 cells were analysed per week). Results shown are the mean of three independent experiments ± standard error. *= $p<0.05$ (Student's t-test, two-tailed).

Results from Figure 6.1 show that the mean number of γH2AX foci per cell increases significantly over 6 weeks of ageing in serum-free treated CAD cells. During the first 2 weeks of ageing the mean number of γH2AX foci did not increase significantly in cells. However, all remaining weeks displayed a significantly increased mean number of γH2AX foci when compared to week one (see Appendix table C.1 for p values). Significant weekly increases in mean γH2AX foci are seen between weeks 2-3 ($p=0.042$) and between weeks 5-6 ($p=0.015$). Further analysis of the data shows that the number of cells displaying 25< foci per cell is significantly higher in week 6 cells compared to week one cells with a p value of 0.001.

In conclusion, DNA damage significantly increases in serum-free treated CAD cells over 6 weeks, as demonstrated by the γH2AX assay. As the γH2AX assay only shows the presence of DNA DSBs it was decided that further DNA damage assays would be carried out to explore damage throughout ageing. The alkaline Comet assay, which measures DNA damage caused by both SSBs and DSBs, was used in subsequent experiments.

6.2.1.2 Comet assay analysis of DNA damage

In order to further quantify DNA damage during the ageing process, serum-free treated CAD cells were maintained in culture for a total of 6 weeks. Samples of cells were processed at T0, week 1, week 4 and at week 6. Comet assays were carried out and cells were analysed. Cells were analysed manually and sorted into one of five classes ranging from 0-4, depending on tail intensity, as described by Collins *et al*. (1995) (section 2.2.2.15). Automated analysis using the OpenComet plugin on ImageJ was also used. However, the software was not sensitive enough to accurately identify cells on many of the images that were analysed (Figure 6.3). In addition, issues were encountered during week 4 of the experiment, which resulted in an insufficient number of cells available for processing. Hence, analysis of week 4 cells has been removed from the results. Results for manual analysis are shown in Figure 6.2.

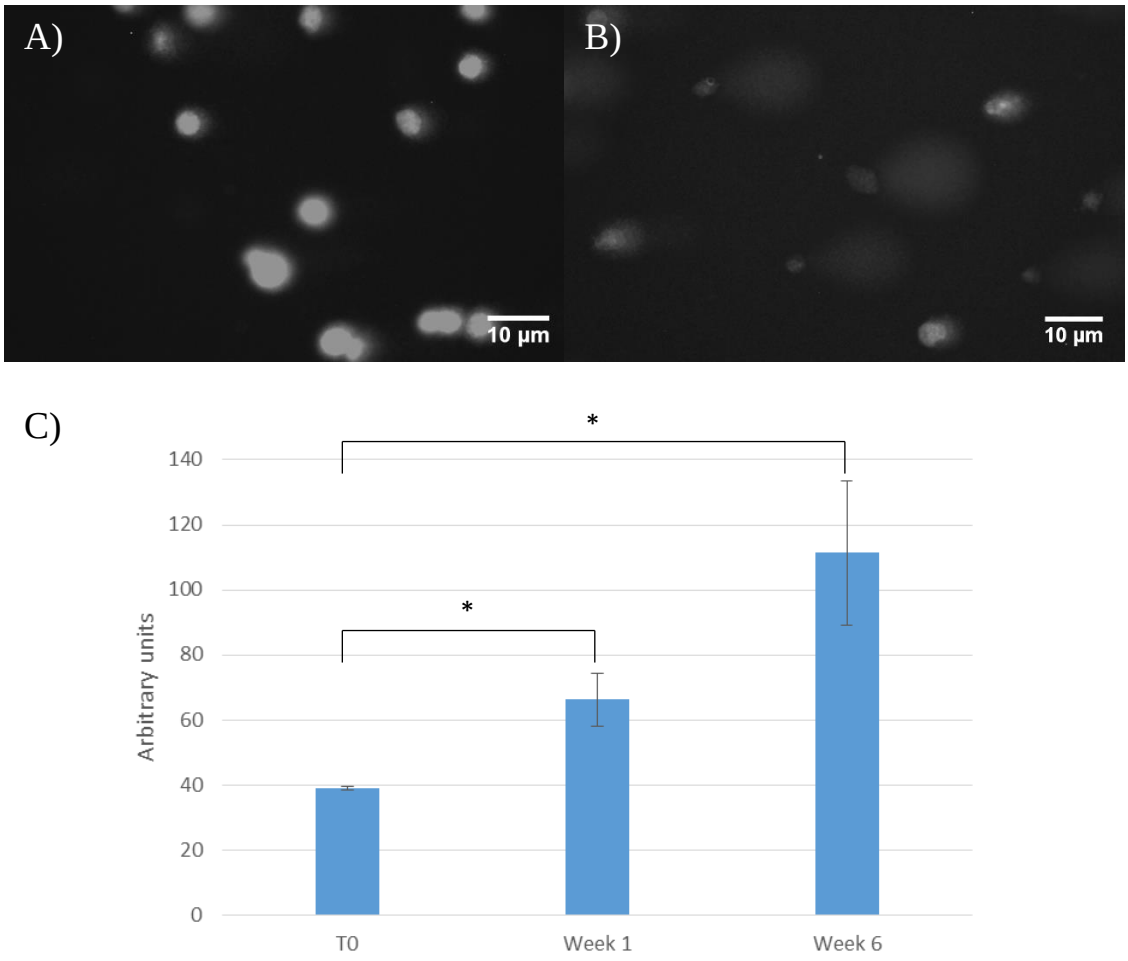

Figure 6.2 Manual scoring analysis of Comet assay over 6 weeks in serum-free treated CAD cells.

T25 culture flasks were seeded at 5 x 10^4 cells/ml (5 ml per flask) and incubated for 24 hours at 37°C (5% CO_2) in complete media. Media was removed and replaced with serum-free media and maintained as described in section 2.2.2.7.2 and aged to specific time points prior to carrying out Comet assays. Comet assays were carried out as described in section 2.2.2.16. (A) CAD cells at T0. (B) CAD cells at week 6. (C) Cells were analysed manually and were sorted into one of five classes ranging from 0-4 depending tail intensity as described by Collins *et al.* (1995). Cells with no DNA damage were given a score of 0 and cells that were highly damaged were given a score of 4. 50 cells were analysed per group. Results shown are the mean of three independent experiments ± standard error. *= $p<0.05$ (Student's t-test, two-tailed).

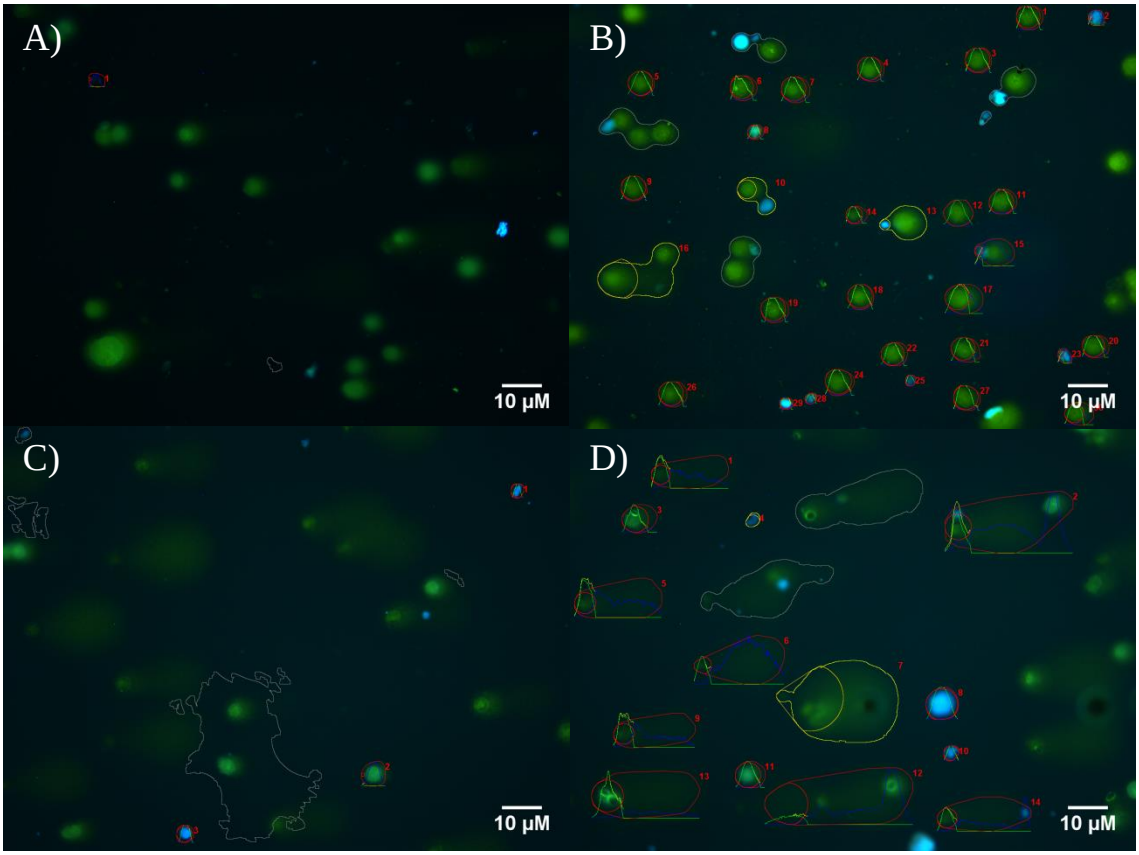

Figure 6.3 Variability of OpenComet image analysis of serum-free treated CAD cells.

OpenComet analysis of images obtained from the Comet assay described in Figure 6.2 shows variability and errors in comet head/tail identification. (A & B) Week 1 CAD cells. (C & D) Week 6 cells.

Results from Figure 6.2 show that DNA damage significantly increases in serum-free treated CAD cells over six weeks of ageing. DNA damage is significantly higher at week 1 and week 6 compared to T0 cells with p values of 0.029 and 0.031, respectively. Results from the Comet assay therefore validated results seen during the γH2AX assay in Figure 6.1.

Images from Figure 6.3 demonstrate the issues in obtaining reliable data using the OpenComet plugin on ImageJ. The software showed variability between images and was unable to successfully identify the heads and tails of each comet. Further analysis by the software, which calculated the percentage of DNA in the tail compared to the head, was not presented in this chapter due to the inconsistencies between images.

In conclusion, DNA damage, in the form of SSBs and DSBs, significantly increases in serum-free treated CAD cells over 6 weeks of ageing *in vitro* as demonstrated by the Comet assay.

6.3 Discussion

The results show that levels of DSBs significantly increase when serum-free treated CAD cells are chronologically aged *in vitro*, as shown by γH2AX assays in Figure 6.1. This is in line with previous studies such as Sedelnikova *et al*. (2004), who demonstrated that DSBs are shown to accumulate in a number of organs in ageing mice. Tissues obtained from brain, liver, testes, kidney and lung all demonstrated age-related increases in γH2AX foci between 2 to 20 month old tissue samples. In addition, Sedelnikova also reported an accumulation of DSBs in senescing human cell cultures. Normal human fibroblasts, WI38 fibroblasts and PrEC prostate epithelial cells all showed increases in γH2AX foci with increasing passage number, as well as senescence-associated β-gal staining, which suggested that during senescence and normal ageing, mammalian cells are seen to accumulate persistent DNA damage that leads to unrepairable DSBs. Increases in DSB accumulation have not only been reported in cell culture and mouse tissue during normal ageing but have also been reported in the brain tissues from patients with mild age-related cognitive impairment and Alzheimer's disease. Shandhag *et al*. (2019) showed that immunostaining for γH2AX revealed significant increases of foci in neurons and astrocytes in the frontal cortex and hippocampus of patients with mild cognitive impairment and Alzheimer's disease compared to cognitively unimpaired controls. DSBs can cause severe adverse effects on DNA, which can subsequently have detrimental effects on gene expression, chromatin stability and cellular functions (Shandhag *et al*., 2019). As DSBs are seen to increase in ageing per se and are exacerbated in certain disease states, this suggests that DSBs could be an important driver of neurodegeneration and cognitive decline. However, this raises an important question: why do DSBs accumulate during the ageing process?

6.3.1 Why do DSBs accumulate during ageing?

6.3.1.1 Decreases in DNA repair capacity

Numerous studies have demonstrated that defective DNA repair pathways, alongside an accumulation of DNA lesions and a decrease in genomic stability, underlies ageing and a number of neurodegenerative disorders (Baltanás *et al*., 2011; Borgesius *et al*., 2011; Mata-Garrido *et al*., 2016). Although the expression of repair factors is widespread in a number of different cell types, the organs of the central nervous system appear to be particularly affected by impaired DNA repair (Alt & Schwer, 2018). Several studies have looked at the ability of repair pathways to repair DSBs during ageing. As stated previously, the error-prone NHEJ pathway is the predominant DSB repair pathway in post-mitotic neurons (Vyjayanti & Rao, 2006). A study by Seluanov *et al*. (2004) showed that NHEJ efficiency decreased in aged senescent normal human fibroblasts by measuring the number of NHEJ events using a GFP reporter plasmid, which was co-transfected with a restriction enzyme (I-SceI) to induce DSBs within the construct (Seluanov *et al*., 2004). In addition, levels of ATM phosphorylation have been seen to decrease in aged mice after ionizing radiation (Feng *et al*., 2007) and reduced the expression level of genes involved in DSB processing and repair. Genes including ATM, MRE11, RAD51 and BRCA1 have been reported to decline in ageing ovarian mouse and human primordial follicles (Oktay *et al*., 2015; Titus *et al*., 2013). This suggests that the reductions in DSB processing genes with age may have detrimental outcomes for cells containing DSBs. Work by Vyjayanti & Rao (2006) demonstrated that NHEJ activity is present in isolated neurons of the rat cerebral cortex and showed that cohesive end-joining activity decreases in an age-dependent manner. Neuronal extracts from young (0-4 days), adult (6 months) and old (28 months) rats were analysed and NHEJ activity assays were carried out. NHEJ activity was seen to significantly decrease with age as adult and old extracts displayed average percentage decreases in activity of 28% and 40%, respectively, compared to young extracts. It is therefore likely that decreases in NHEJ capacity with age will cause neuronal vulnerability to ROS and lead to increases in DNA damage, particularly as it has been reported that an accumulation of DNA damage can produce dysregulation of the DNA damage response and can lead to a senescence-like phenotype in neurons (Sedelnikova *et al*., 2004). In conclusion, a reduction in DNA repair capacity may be partly responsible for the increases in DSBs seen in Figure 6.1.

6.3.1.2 Increased levels of endogenous toxins in aged cells and the response of Top2B

Concomitant with a decrease in repair capacity, there may also be an increase in the levels of endogenous toxins such as ROS, which could account for the increase of SSBs and DSBs seen in this chapter. As stated previously, excess levels of ROS have been seen to contribute to adverse modifications in cells and can amplify the development of damage to DNA, which can induce apoptosis and necrosis (Lundgren *et al*., 2018). One of the main causes of increasing ROS levels is believed to be inefficient electron transfer in the mitochondrial respiratory chain. The mitochondrial respiratory chain consists of five protein complexes. A proton gradient is created through the exchange of electrons down the respiratory chain at increasing reduction potentials from complex one through to four. This electron transfer mediated by the respiratory chain is connected to the final protein complex, ATP synthase, which drives ATP synthesis. However, premature leaking of some electrons occurs at the respiratory chain, which results in the generation of ROS (Payne & Chinnery, 2015). Modifications to mitochondria have been reported to occur during ageing and are due to changes in mitochondria-nucleus interactions and homeostatic alterations to mitochondria. Ineffective control of ROS in mitochondria can lead to ROS signalling alterations and ultimately result in a shift towards a pro-oxidant state in cells (Davalli *et al*., 2016).

ROS can damage DNA via oxidation of bases. This oxidation can lead to the formation of a DNA base lesion, which is one of the most deleterious consequences of oxidative stress. For example, guanine possesses a low redox potential and is particularly susceptible to oxidative stress with 7,8-dihydro-8-oxoguanine (8-oxoG) commonly formed under conditions of oxidative stress, which can lead to G:C to T:A transversion mutations if left unrepaired (Nakabeppu, 2014). BER is known to play a pivotal role in repairing these damaged bases. BER takes place in a number of steps, including: excision of the base, incision, end processing, repair synthesis and ligation (Krokan & Bjørås, 2013). DNA glycosylases are responsible for initiating BER by recognising and removing the damaged DNA base. The removal of a base leaves an abasic site (AP site), which is then processed by short-patch or long-patch repair to complete BER (Jacobs & Schär, 2012). Although oxidised bases are recognised and repaired by the BER pathway, when oxidised bases occur simultaneously on opposing strands of DNA, attempted BER can lead to the generation of DSBs (Cannan *et al*., 2014). As previously discussed, Top2B has been implicated in having an indirect but significant role in

regulating BER capacity in neurons (Gupta *et al*., 2012). The presence of abasic sites within the vicinity of Top2B cleavage sites have been seen to act as endogenous topoisomerase II poisons and cause subsequent Top2B-mediated cleavage. The activities of Top2B at abasic sites suggested a possible overlap of Top2B in BER processing regions, thus implicating Top2B activity in the regulation of BER pathway intermediates (Gupta *et al*., 2012). Indeed, it is possible that declines in Top2B mRNA and protein levels in serum-free treated CAD cells, shown in chapter 5, are a contributing factor towards increased unrepaired oxidised bases present on opposing DNA strands, which could lead to an increase in DSBs as shown in this chapter (Cannan *et al*., 2014).

In a study by Kenig *et al*. (2016), it was suggested that glioblastoma stem cells are more resistant to chemotherapeutic agents because of their increased efficiency of DNA repair. Kenig investigated whether increased expression of Top2B was one of the underlying reasons for the phenomenon. *In vitro* work reported that glioblastoma cells with endogenously low levels of Top2B (U251 cell line) display increased sensitivity to DNA damage-inducing drugs compared to cells with endogenously high levels of Top2B (NCH421k cell line). In addition, the down-regulation of Top2B in NCH421k cells increased their sensitivity to DNA damage-inducing drugs to the same level as detected in U251 cells. Thus, highlighting the potential role of Top2B in DNA repair mechanisms as previously discussed. Although this *in vitro* study is not a representation of biological ageing, it does provide information about a key element of cellular ageing, namely increased oxidative stress. Kenig used a range of drugs to induce stress on glioblastoma cells, including the topoisomerase II poison etoposide (VP-16). Top2A is the primary target of VP-16 with drug-stabilised Top2A complexes being detected with as little as 1 μM VP-16 in mouse and human cells. Nevertheless, Top2B is also targeted by the drug, with VP-16 stabilised Top2B complexes being induced from 10 μM in mouse and human cells (Willmore *et al*., 1998; Cowell *et al*., 2011; Atwal *et al*., 2017). These drug stabilised complexes are processed in the cell to give rise to DSBs, which then elicit the phosphorylation of histone H2AX in a dose response similar to that observed for TOP2-DNA complexes (Atwal *et al*., 2019). In addition to VP-16, the cross-linking agent cisplatin (CisPt), the alkylating agent methyl-methanesulfonate (MMS) that forms DNA adducts, as well as hydrogen peroxide (H_2O_2) that induces both single and double strand breaks, were also used. Cells treated with either MMS or CisPt were found to have increased levels of DNA damage as measured by the γH2AX assay.

In addition, checkpoint kinase 1 (CHK1) was seen to increase after downregulation of Top2B, with CHK1 known to be a key coordinator of the DNA damage response (Patil *et al*., 2013). Kenig suggested that the increased sensitivity to oxidative stress displayed by Top2B depleted NCH421k cells could be a consequence of an increased DNA damage load and less efficient repair of DNA lesions after genotoxic stress induction. As oxidative stress is known to increase with age, the results shown in this chapter may be comparable, in part, to those discussed by Kenig *et al*. (2016). The decreases in Top2B during ageing, shown in chapter 5, and the increases of DSBs shown in this chapter may point towards both an increase in oxidative stress and less efficient repair of DNA lesions with age and highlight the crucial role of Top2B in the maintenance of DNA integrity.

DSBs in neurons are repaired through pathways that are promoted by either the DNA repair subunit protein Ku70 or Poly (ADP-ribose) polymerase 1 (PARP-1). Mandraju *et al*. (2011) reported that Top2B associates with both Ku70 and PARP-1, suggesting that Top2B is associated with DSB repair in primary neurons. Results from the study showed that levels of Top2B increased during recovery in cerebellar granule neurons from rats that had been exposed to H_2O_2 alongside enhanced levels of Ku70 and PARP-1. Analysis of co-immunoprecipitation experiments revealed that Top2B strongly interacted with Ku70 and PARP-1 in neuronal extracts that had been exposed to H_2O_2, thus implicating Top2B in DSB repair in neurons. Although increases in Top2B has been associated with DNA repair, it is also important to note that the generation of Top2B-DNA cleavage complex intermediates is required to activate early response genes in neurons (Madabhushi *et al*., 2015). Early response genes have been shown to be activated in response to neuronal activity and neuronal insults. Therefore, the presence of Top2B in this context may also be due to its transcriptional activities in early response gene expression (Duclot & Kabbaj, 2017).

Recent work by Morotomi-Yano *et al*. (2018) showed that Top2B was rapidly recruited to laser-induced DSB sites. This was independent of ATM or DNA-PKcs activity but inhibitors of PARP-1 and HDAC could partially prevent this recruitment. The study also showed that catalytic inhibitors of Top2B prevented its recruitment to DSBs by reducing the enzyme's mobility. Using Top2B-knockout Nalm-6 cells they also showed an increased sensitivity to bleomycin and decreased HR-mediated repair. However, further studies are required to assess the role of Top2B on NHEJ. Nevertheless, this

raises the intriguing possibility that the decrease in Top2B shown in chapter 5 could also impact on the cells ability to carry out NHEJ.

6.3.1.3 Decreases of antioxidant system capacity in aged cells

Antioxidant systems are also known to decrease with ageing, which may also account for the increases in ROS. For example, as levels of ROS increase, nuclear factor erythroid 2-related factor (Nrf2) translocates from the cytoplasm into the nucleus and activates expression of genes including glutathione, NAD(P)H/quinone oxidoreductase 1 (NQO1) and heme oxygenase 1 (HO1), which produce antioxidant activity to counteract ROS (Zhang & Gordon, 2004). The activation of this transcription factor has been shown to decline in an age-related manner, as reported by Duan *et al*. (2009). Duan reported that expression of Nrf2 dramatically declined in aged astrocytes and in the spinal cord of mice and suggested that the reduced antioxidant effects induced by Nrf2 contributed to the increased vulnerability of the cells to oxidative stress and resulted in reduced neuroprotection. Furthermore, age-related declines in Nrf2 targets, such as glutathione, have been demonstrated in murine brain models (Sasaki *et al*., 2001; Wang *et al*., 2003). Indeed, the restoration of Nrf2 transcriptional activity through the addition of epigallocatechin gallate was seen to provide protection in aged astrocytes (Duan *et al*., 2009). Alzheimer's disease, which is associated with high levels of oxidative stress and an accumulation of oxidative damage, also exhibits dysfunction of Nrf2 (Ramsey *et al*., 2007). Ramsey reported a significant decrease in nuclear Nrf2 levels in Alzheimer's diseases cases and suggested that Nrf2-mediated transcription is not induced in the neurons of Alzheimer's disease patients, despite the abundant presence of oxidative stress. The importance of Nrf2 in the homeostatic regulation of ROS suggests that the age-related increases of DNA damage seen in serum-free treated CAD cells in Figure 6.1 and Figure 6.2 may be due, in part, to a reduction in Nrf2 activation. However, further investigation would be required to determine this.

In conclusion, there may be decreased repair, increased ROS levels and decreased antioxidants, which would account for the increase of DSBs over time, as demonstrated by the γH2AX assay in Figure 6.1.

6.3.2 DNA damage as measured by the alkaline Comet assay

As a method of validating results seen in the γH2AX assays, the alkaline Comet assay, which measures both SSBs and DSBs, was used. As shown in Figure 6.2, DNA damage can be seen to increase in serum-free treated CAD cells over six weeks of ageing using

the manual method of DNA damage quantification, detailed by Collins *et al*. (1995). This is in line with other studies such as Swain & Subba Rao (2011), who demonstrated that DNA damage increased with age using the Comet assay. They showed that isolated neurons and astrocytes from the cerebral cortex of young (7 days), adult (6 months) and old (2 years) rats display marked increases in DNA damage in terms of SSBs and DSBs between young and adult samples, with further increases seen in old samples. Swain and Subba Rao analysed Comet images using the automated Tritek CometScore^{TM} Freeware v1.5 image analysis software rather than using manual methods, as shown in Figure 6.2. Unfortunately, issues arose when trying to quantify DNA damage using the automated OpenComet plugin on ImageJ during this chapter. As previously stated, the software was unable to successfully identify the heads and tails of every comet in each image. In images where cells were considerably damaged, such as week 6 images, the head of the comet would sometimes be separated from the tail, thus giving false measurements. Future experiments may have benefitted from electrophoresing cells for a shorter length of time to avoid this problem. In addition, adjusting the image intensity threshold of the software may have allowed cells with overall weaker staining intensity to be identified. As suggested by Gyori *et al*. (2014), selecting an adaptive threshold allows the software to take into account the illumination of each Comet assay image, which can vary significantly.

In conclusion, the CAD cell line can be used as a model for ageing studies and would be a useful model for further work. Although it is an *in vitro* model of ageing and is not the same as organismal ageing, it may still provide a useful model of ageing. Results shown in serum-free treated CAD cells displaying increases in DNA damage with age are similar to those seen in studies of neurons isolated from rats throughout the ageing process (Swain & Subba Rao, 2011) and during *in vivo* experiments using mouse tissues (Sedelnikova *et al*., 2004). As DSBs have been shown to increase and Top2B has been shown to decrease during six weeks of ageing in serum-free treated CAD cells, it raises the interesting question as to whether Top2B can have an impact on DNA repair. Future work using the CAD cell line to investigate whether the epigenetic upregulation of Top2B can modulate DNA repair mechanisms may provide useful research as it may be possible to determine whether Top2B upregulation could be used as a potential strategy for cell therapy.

7. Final discussion and future work

7.1 Top2 during *Drosophila* ageing

The aim of chapter 3 was to establish a model of ageing in *Drosophila* and to carry out subsequent experiments to determine levels of mRNA and protein of the single *Drosophila* type 2 topoisomerase isoform, Top2, during ageing in brain tissue.

The analysis of longevity, locomotor function and AGEs in male and female flies allowed appropriate age ranges to be selected to establish a robust model of ageing so that further experiments could observe changes in Top2 throughout the ageing process.

Results showed that levels of Top2 protein decreased with age in both male and female *Drosophila* brain tissue (Figure 3.9). However, no significant changes in Top2 mRNA were seen during qPCR experiments (Figure 3.12). This is in contrast to previous reports in mammals that have shown decreases of mRNA in the mammalian Top2B isoform (Bhanu *et al*., 2010). There are a number of possible reasons that could explain the differences of mRNA and protein levels during ageing. For example, species-specific changes may be the cause of these differences, particularly as *Drosophila* only possess a single isoform of Top2, which has been suggested to carry out the roles of both Top2A and Top2B in this organism (Lee & Berger, 2019). Another possible reason for the maintenance of Top2 mRNA in *Drosophila* could be partially explained by a study by Pacifico *et al*. (2018). The study demonstrated that a number of overlapping sets of neuronal function genes, which are seen to decline between young and middle-aged *Drosophila*, become upregulated in the oldest group of flies. It was suggested that this reversal pattern of gene expression may be a compensatory response to an overall decline in neuronal function. Although Top2 was not discussed in the study, it has been shown to play key roles in neuronal function. Therefore, the observations by Pacifico *et al*. (2018) may explain why mRNA levels of Top2 were not decreased in 50 day old flies in Figure 3.12.

As Top2 mRNA is seen to be expressed during ageing with no significant changes, why then were protein levels seen to decrease? The process of translation is only the first step in the production of functional proteins and most require assistance to correctly fold, which occurs either co-translationally or post-translationally. This process is facilitated by chaperone proteins and other partner proteins such as disulphide isomerases (McLaughlin & Bulleid, 1998). Studies have previously shown that chaperone capacity, response and activity declines with age (Soti & Csermely, 2003)

and can lead to misfolding of proteins and subsequent degradation. It is conceivable that this could occur to Top2 during ageing and result in reduced protein levels in the *Drosophila* brain. This may be one of the reasons to suggest why low levels of Top2 protein may be seen, despite continued mRNA expression.

A lack of Top2 protein may present a number of issues for ageing *Drosophila*. In mammals, decreases in Top2B have been shown to cause reductions in the expression of long genes (King *et al*., 2016). Similarly, Joshi *et al*. (2012) reported that the inactivation of the single Top2 isoform in yeast produced a sudden decrease of RNA polymerase II transcripts greater than ~3 kb in length. Hence, it is likely that Top2 in *Drosophila* also plays important roles in the transcription of long genes. An inability to transcribe these long genes may lead to dysfunction of many key processes. As previously discussed, numerous genes that are required for proper neuronal function, including *Sh*, *Csp*, *Hdc*, *Shal* and *Sap47*, are downregulated in *Drosophila* during 40 days of ageing (Hall *et al*., 2017). It is possible that Top2 is responsible for the expression of genes like these. Reductions of Top2 could therefore lead to neuronal dysfunction and ultimately cause neurodegeneration.

The increase of oxidative stress-induced AGEs in female flies, shown in Figure 3.5, suggests that oxidative stress increases during ageing in female *Drosophila*. Interestingly, males do not display significant increases in AGEs during ageing but they do display significantly higher levels of AGEs than females at each age point, suggesting that males may have a predisposition to increased levels of oxidative stress. It is plausible that structural modifications to Top2 occurs via oxidative stress and this may result in subsequent changes, such as alterations to the active site, blockage of phosphorylation sites, or disruption to the binding sites for DNA, magnesium ions or partner proteins. These changes may lead to Top2 dysfunction and could potentially lead to an increase in abortive catalytic cycles of the enzyme (Morimoto *et al*., 2019). As males display significantly higher levels of AGEs throughout the life span compared to females, it is conceivable that modifications to proteins via oxidative stress may occur more frequently compared to females and at earlier stages in life. This could partly explain why male longevity in this study is seen to be significantly lower than females.

Drosophila have provided a useful *in vivo* model to explore Top2 levels in brain tissue during ageing and may provide useful results in future research. As discussed previously, experiments aiming to answer whether Top2 structure is damaged with

ageing or whether higher levels of endogenous cleavage complexes are formed in aged cells can be investigated using this model. It may also be interesting to carry out further experiments on males and females to fully elucidate any differences in Top2 between the sexes during ageing. Experiments focussing on determining absolute levels of Top2 mRNA, rather than relative levels, may allow such questions to be answered.

7.2 Developing senescence in the SH-SY5Y cell line

Developing a cell line model of ageing using the human neuroblastoma cell line SH-SY5Y to investigate changes in Top2B expression was the focus of chapter 4. Numerous studies have used oxidative stress-inducing agents to prematurely induce cellular senescence in cell lines to use them as *in vitro* models of ageing (Zhang *et al*., 2020). Previous studies have reported that senescence can be induced in undifferentiated SH-SY5Y cells using a single treatment of 100 µM H_2O_2 (Nopparat *et al*., 2017). Nopparat demonstrated positive senescence-associated β-gal staining in cells treated with H_2O_2. However, results shown in chapter 4 are in contrast to this. The results demonstrate that the higher doses of H_2O_2 were toxic to cells, whereas lower doses were not sufficient to induce cell cycle arrest. In addition, β-gal assays yielded negative results despite cell culture and treatments being the same as the Nopparat study.

Piechota *et al*. (2016) suggested that the β-gal assay may not be suitable to determine senescence in neuronal cells and should be used with caution as β-gal activity cannot be solely attributed to senescence, either *in vitro* or *in vivo*. Piechota reported relatively high levels of β-gal activity in young (3 month old) mice and suggested that this marker may be linked to activities outside of senescence. Indeed, primary cultures of cortical neurons also exhibited noticeable β-gal activity early in culture during this study. If further work was to be carried out using this cell line it may be worth investigating alternative markers of senescence, such as repressor element 1-silencing transcription factor (REST), as it has been shown to display a pattern of expression that is correlated with neuronal age (Piechota *et al*., 2016).

The cancerous nature of the SH-SY5Y cell line meant it was not possible to culture cells over a prolonged period of time to cause replicative senescence. However, undifferentiated SH-SY5Y also express immature neuronal markers and lack mature neuronal markers, thus, they are considered to be similar to immature catecholaminergic neurons (Lopes *et al*., 2010). Subsequent attempts were made to differentiate SH-SY5Y

cells into more neuronal-like cells (i.e. non-proliferating cells with complex dendritic processes that more closely resemble mature neurons) using 10 μM RA. Further experiments were then attempted to induce senescence in RA-treated SH-SY5Y cells using H_2O_2 to create a cell line model of neuronal ageing. Results in chapter 4 demonstrated continued proliferation of RA-treated SH-SY5Y cells, albeit at a reduced rate. The SH-SY5Y cell line has been seen to produce different cellular phenotypes, which includes N-type cells and S-type cells. These cells demonstrate clear differences, with S-type cells being substrate adherent multipotent precursors to various non-neuronal cells including glial cells, melanocytes and Schwann cells, and N-type cells being neuroblastic, characterised by neurite processes. The SH-SY5Y cell line is predominantly composed of N-type cells with only a small proportion of S-type cells remaining (Forster *et al*., 2016). However, studies have reported that S-type cells do not readily develop neuronal-like phenotypes when treated with RA and continue proliferating, unlike N-type cells (Encinas *et al*., 2002). This suggested that continually proliferating S-type cells could have been one of the reasons for the continued proliferation seen in this study.

Levels of Top2A and Top2B were semi-quantified by western blot analysis in SH-SY5Y cells over 72 hours post RA treatment. Previous studies have shown that during cell differentiation Top2A is typically seen to decline and Top2B is seen to be upregulated (Tsutsui *et al*., 1993; Tiwari *et al*., 2012; Harkin *et al*., 2015; Austin *et al*., 2018). However, changes in protein levels of Top2A and Top2B were not significant over this time period and a high level of inter-experiment variability was seen (Figure 4.6 and Figure 4.7). As S-type cells have previously been shown to continue proliferating during RA treatment, it was postulated that the high levels of inter-experimental variability seen during western blotting may be due to varying levels of S-type cell overgrowth.

Ultimately, experiments aiming to develop a human neuronal cell line model of ageing were unsuccessful in chapter 4. If more time was available, changes to the methodology utilised on the SH-SY5Y cell line, such as increasing the exposure time of RA and incorporating pulses of fresh RA as it degrades could have been investigated in an attempt to fully differentiate cells. Reducing the FBS concentration and incorporating BDNF into the media or exposing cells to mitotic inhibitors following exposure to RA are also methods that could have been explored. However, problems with ageing differentiated SH-SY5Y cells may have still persisted. Work by Shipley *et al*. (2016)

demonstrated a method of inducing terminal differentiation in SH-SY5Y cells using RA and BDNF, as previously described. However, Shipley reported that SH-SY5Y cells are only stable for up to 14 days after terminal differentiation. It is conceivable that this may not be long enough for SH-SY5Y cells to develop an aged phenotype and to observe age-related changes in Top2B expression, particularly when serum-free treated CAD cells were capable of being aged up to six weeks in culture during this study. As this is the case, it may be useful to carry out further research on an alternative human cell line, such as HCN-2, or source primary neuronal cells. However, further ethical considerations would need to be addressed prior to acquiring and utilising primary human neuronal cells.

7.3 Top2B in the CAD cell line and mouse hippocampal tissue during ageing

In chapter 5, the murine CAD cell line was utilised to create a cell line model of ageing in order to semi-quantify levels of Top2B during ageing. Results from this chapter demonstrated that mRNA and protein levels of Top2B decline during ageing *in vitro*, whilst concomitant increases in the tumour suppressor gene p21 were also seen during six weeks of ageing. Results seen for Top2B are similar with those described by Bhanu *et al*. (2010), who reported a decrease in both mRNA and protein in cerebellar granule neurons isolated from rat pups and aged over five weeks in culture. However, it is worth noting that the results seen in this chapter are the first demonstration, to the best of our knowledge, that this decrease of Top2B has been seen in a neuronal cell line that has been chronologically aged.

In contrast to results shown in *Drosophila* Top2, mRNA levels of Top2B were seen to decrease in serum-free treated CAD cells with significant reductions seen at weeks 5 and 6 (Figure 5.9 and Figure 5.13). As previously discussed, a number of transcription factors that have been reported to be regulators of Top2B expression have been shown to decline in an age-dependent manner. The transcription factor Sp1 is involved in numerous cellular processes, which includes cell differentiation, cell growth, chromatin remodelling, immune responses, responses to DNA damage and apoptosis by binding to the GC and GT box sequences of gene promoters (Gory *et al*., 1997). This particular transcription factor has been shown to decrease in aged rat brains (Ammendola *et al*., 1992). In addition, the transcription factor NURR1, which is known to influence the development, differentiation and maintenance of mesencephalic dopaminergic neurons

through axon genesis regulation, has also been shown to decrease in an age-dependent manner (Eells *et al*., 2002; Heng *et al*., 2012; Parkinson *et al*., 2015). Both Sp1 and NURR1 have been associated with the regulation of Top2B expression and as such, it is plausible that age-related decreases in these transcription factors may, in part, be responsible for the decreases of Top2B mRNA seen during ageing in chapter 5. In addition to reductions of transcription factors, epigenetic changes such as DNA methylation, which is known to be a key player in the modulation of gene expression, have been seen to occur during ageing (Armstrong *et al*., 2019). Methylation of cytosine is suggested to prevent gene transcription by interfering with the transcriptional machinery or through interference of the recognition sequence of transcription factors (Johnson *et al*., 2012). Although DNA methylation patterns that regulate tissue-specific gene transcription are typically shown to be stable in differentiated cells, post-mitotic neurons have been seen to maintain DNA methyltransferase expression and activity of neurons has been shown to modulate the methylation expression patterns in response to physiological and environmental stimuli. It is therefore plausible that changes in methylation patterns in neurons that occur during ageing could be another potential cause for the decreases of Top2B mRNA reported in this study.

As previously discussed, it is a logical assumption that decreases in Top2B mRNA may also cause the age-related reductions in Top2B protein that have been demonstrated in this study (Figure 5.9). However, other explanations for the decrease in protein levels that were seen should not be discounted. As previously discussed, the misfolding and subsequent degradation of proteins may provide a potential cause for the decline in Top2B protein shown in serum-free treated CAD cells during ageing. The proteostasis network is a complex network of mechanisms that prevent and eliminate protein misfolding (Balch *et al*., 2008). Age-related declines to elements of the proteostasis network are known to take place and can result in an increase of misfolded proteins and subsequent aggregation, resulting in a loss of function (Kikis *et al*., 2010). A decline in the mechanisms that prevent protein misfolding may be a cause for the declines in Top2B protein levels in aged CAD cells. However, it is very likely that concomitant changes in methylation patterns, transcription factor decreases, changes to mechanisms of protein homeostasis and many other processes will be responsible for the decreases of Top2B mRNA and protein levels seen in this study.

Alongside analysis of Top2B, protein levels of the tumour suppressor gene p21 were also investigated through western blot analysis (Figure 5.10). As previously stated, p21

is commonly used as a marker of senescence with post-mitotic neurons shown to develop a p21-dependent senescence-like phenotype (Jurk *et al*., 2012; Riessland *et al*., 2019). Although further experiments would need to be carried out to determine statistical significance, the results from Figure 5.10 showed increases in p21 protein levels over six weeks of ageing, particularly at weeks 5 and 6, displaying opposite trends in levels compared to Top2B at these time points. Further experiments may demonstrate that p21 protein levels do increase significantly and provide evidence that CAD cells are displaying a phenotypic characteristic of aged cells, therefore highlighting its suitability as a model of ageing.

In addition to experiments carried out in the murine CAD cell line, the preliminary study investigating Top2B levels in sections of mouse hippocampus tissue also displayed reductions in Top2B punctate labelling in a 31 month old animal compared to a 4 month old animal (Figure 5.15). Further biological replicates would need to be carried out to determine the statistical significance of this result. Nevertheless, if decreases in Top2B punctate labelling during ageing can be shown to be statistically significant, this would be the first time that this has been shown in mouse hippocampus tissue, to the best of our knowledge, and would represent an important finding using a mammalian *in vivo* model.

Declines in Top2B expression during ageing may pose numerous problems for an organism. As previously discussed, normal cognitive function relies heavily on the accurate regulation of DNA methylation, with changes in methylation patterns known to affect the chromatin architecture of DNA. The progression of neurodegenerative diseases has been associated with these changes in methylation patterns (Berson *et al*., 2018). It has been suggested that Top2B is required for the maintenance of chromatin structure (Tiwari *et al*., 2012), as well as being crucial for the development and maintenance of neurons, whilst also being involved in transcriptional roles such as RNA polymerase II pause release and elongation, which is vital for the transcription of long genes. It is likely that age-related decreases in levels of Top2B will have detrimental effects on gene expression and neuronal function, particularly in areas with altered chromatin architecture caused by changes in DNA methylation, which may subsequently lead to neurodegeneration. Top2B has also been shown to have roles in DNA repair, as discussed by Gupta *et al*. (2012), who suggested that the capacity of BER in neurons is regulated by Top2B-mediated DNA breaks. Work by Morotomi-Yano *et al*. (2018) also suggested roles for Top2B in DSB repair pathways. Indeed,

reductions of Top2B may cause neuronal dysfunction and present transcriptional issues, resulting in an accumulation of DNA damage, but it may also impair crucial pathways that are responsible for repairing this damage and ultimately lead to cell death.

7.4 Increases of DNA damage during ageing

In chapter 6, the CAD cell line was utilised to investigate levels of DNA damage during ageing *in vitro*. DNA damage, in the form of DSBs, was seen to progressively increase over six weeks of ageing in serum-free treated CAD cells, as demonstrated by the γH2AX assay (Figure 6.1). This was supported by the alkaline Comet assay, which also demonstrated increases in DNA damage (SSBs and DSBs) over the same time period (Figure 6.2). Results from this study are in line with previous studies that have also demonstrated an accumulation of DSBs in ageing mice (Sedelnikova *et al*., 2004). Sedelnikova reported age-related increases in γH2AX foci in mouse tissue obtained from brain, liver, testes, kidney and lung from 2 to 20 month old tissue samples. As CAD cells are an *in vitro* model, the fact that results are similar to *in vivo* models is an encouraging sign for the use of this cell line as a model of ageing. Higher levels of γH2AX foci in the brain tissues from patients with mild age-related cognitive impairment and Alzheimer's disease have been shown compared to unimpaired controls (Shandhag *et al*., 2019). This suggests that DNA damage increases during ageing, per se, and is exacerbated in certain disease states. Indeed, accumulations of DNA damage have been shown to be a predominant feature of numerous age-related neurodegenerative diseases, with DSBs causing severe adverse effects on DNA, which can subsequently effect gene expression, chromatin stability and cellular functions (Stein & Toiber, 2017).

Alongside increases in DNA damage during ageing, concomitant decreases in DNA repair pathway efficiency has also been reported, with organs of the central nervous system seen to be particularly affected by impaired repair (Baltanás *et al*., 2011; Borgesius *et al*., 2011; Alt & Schwer, 2018). The increases of DNA damage shown in chapter 6 may be the result of a decrease in efficiency of the NHEJ repair pathway. NHEJ is the predominant repair pathway used to repair DSBs in post-mitotic neurons and previous studies have demonstrated decreases in its efficiency during ageing (Seluanov *et al*., 2004; Vyjayanti & Rao, 2006). In addition, increases in DNA damage may also be attributed to increased levels of endogenous ROS, as they are known to

amplify the development of damage to DNA, via oxidation of bases, which can induce base lesions and lead to senescence, apoptosis and necrosis (Lundgren *et al*., 2018). The BER pathway is typically responsible for the repair of damaged bases. However, when oxidised bases occur simultaneously on opposing strands of DNA, attempted BER can lead to the generation of DSBs (Cannan *et al*., 2014). The suggested roles of Top2B in regulating BER, via BER pathway intermediates, may influence the progression of DNA damage during ageing (Gupta *et al*., 2012). Studies have shown that glioblastoma cells displaying increased levels of Top2B are more resistant to chemotherapeutic and oxidative stress-inducing agents compared to cells displaying low levels of Top2B, which highlights its potential roles in DNA repair mechanisms (Kenig *et al*., 2016). Indeed, Top2B has also been reported to associate in neuronal extracts with DNA repair protein Ku70 and PARP-1, both of which are promotors of DNA repair pathways (Mandraju *et al*., 2011). It is therefore plausible that the declines of Top2B mRNA and protein levels shown in chapter 5 contribute towards an increase of unrepaired oxidised bases on opposing DNA strands, leading to an increase in DSBs during ageing. As discussed previously, the expression of early response genes has been seen to be activated in response to neuronal activity and neuronal insults. Top2B is required for early response gene expression, so its decline during ageing may also have implications on the transcription of these genes (Madabhushi *et al*., 2015). Decreases in repair pathway efficiency, increases in ROS levels and decreases in antioxidants may all account for the increases of DSBs over time in the CAD cell line, as demonstrated by the γH2AX assay in Figure 6.1.

The CAD cell line has provided a useful model of ageing during this study and may be a suitable model for future investigations. It may be interesting to fully elucidate the roles of Top2B in DNA repair mechanisms by upregulating its expression in chronologically aged cells. By doing this it will be possible to find out whether DNA damage decreases in aged cells with increased Top2B expression and may provide future research to find a potential therapeutic use in neurodegenerative conditions.

7.5 Conclusion

To conclude, the focus of this project was to determine the expression of Top2B in aged neurons through the development of suitable models. Top2B has previously been shown to be a crucial component of neuronal differentiation and development, illustrated by

the genetic deletion of Top2B in mice, which has been seen to cause neuronal defects during development (Lyu & Wang, 2003). However, studies investigating age-related changes in Top2B expression in neuronal tissue are limited.

The body of work presented in this thesis provides evidence that during ageing Top2 decreases in the brain tissue of *Drosophila*, with decreases of Top2B in the CAD mouse neuronal cell line also seen. Decreases of Top2B in CAD cells are accompanied by an increase in DNA damage. Interestingly, preliminary experiments on mouse hippocampal tissue also revealed a decrease in Top2B during ageing. To further our understanding of Top2B, it is imperative to investigate whether these changes are observed in human brain tissues during normal ageing. It would also be extremely interesting to see if there is a difference in expression of Top2B in normally aged individuals versus those with neurodegenerative conditions. Highlighting any differences between normal and disease states may provide further scope for research into potential therapeutic targets.

Top2B has been shown to display a wide range of roles in the development and maintenance of neuronal cells in previous studies, including roles in RNA Polymerase II pause release and elongation, transcription of long genes and early response genes and roles in DNA repair pathways. It is therefore highly likely that a decrease of Top2B during ageing will have detrimental effects on a number of biological processes and potentially lead to neurodegenerative conditions. Elucidating the exact functional consequences of reductions in Top2B on transcription and repair pathways will improve our understanding of its roles in these processes. Furthermore, the cause of declining levels of Top2B also needs to be investigated. It is likely that reductions in Top2B will be caused by several mechanisms and research aiming to understand why Top2B reduces during ageing may be of great importance.

Numerous neurodegenerative diseases are linked to increases in oxidative stress and subsequent DNA damage, which includes Parkinson's disease, Alzheimer's disease, multiple sclerosis, motor neurone disease, Huntington's disease, mild cognitive impairment and cerebral ischemia (Venkataraman *et al*., 2013). As DNA damage has been shown to increase during ageing, with accompanying decreases in Top2B, as shown by our studies in the CAD cell line, future research may benefit from investigating whether an upregulation of Top2B is able to reduce the amount of DNA damage that occurs during ageing. If DNA damage is shown to decrease with Top2B upregulation it will provide further opportunities for investigation. Preliminary studies

showed that Top2B decreased during ageing in mouse hippocampal tissue. As the hippocampus is crucial for learning and memory formation and is a brain region prominently affected in Alzheimer's disease, exploring Top2B modulation in ageing may ultimately provide a potential target for future therapeutics in neurodegenerative diseases.

This work has shown that Top2 decreases in *Drosophila* during ageing and Top2B is decreased in aged mouse neuronal cells, with a concomitant increase in DNA damage. This provides solid evidence that future work is imperative to understand the impact of this in humans during the ageing process and could provide insights into mechanisms that could be pharmacologically modulated to attenuate neurodegeneration in ageing.

8. References

Abello, N., Kerstjens, H. A. M., Postma, D. S. & Bischoff, R. (2009) Protein Tyrosine Nitration: Selectivity, Physicochemical and Biological Consequences, Denitration, and Proteomics Methods for the Identification of Tyrosine-Nitrated Proteins. *Journal of Proteome Research*. **8**: 3222-3238

Ackerman, P., Glover, C. V. C. & Osheroff, N. (1985) Phosphorylation of DNA topoisomerase II by casein kinase II: Modulation of eukaryotic topoisomerase II activity in vitro. *Proceedings of the National Academy of Sciences of the United States of America.* **82**: 3164-3168

Adachi, N., Miyaike, M., Kato, S., Kanamaru, R., Koyama, H. and Kikuchi, A. (1997) Cellular distribution of mammalian DNA topoisomerase II is determined by its catalytically disepensable C-terminal domain. *Nucleic Acids Research*. **25**: 3135-3142

Adelman, K. & Lis, J. T. (2012) Promoter-proximal pausing of RNA polymerase II: emerging roles in metazoans. *Nature reviews. Genetics.* **13**: 720-731

Afanasieva, K. & Sivolob, A. (2018) Physical principles and new applications of comet assay. *Biophysical Chemistry*. **238**: 1-7

Agholme, L., Lindström, T., Kågedal, K., Marcusson, J. & Hallbeck, M. (2010) An in vitro model for neuroscience: differentiation of SH-SY5Y cells into cells with morphological and biochemical characteristics of mature neurons. *Journal of Alzheimer's Disease*. **20**: 1069-1082

Aguiar, P. H., Furtado, C., Repolês, B. M., Ribeiro, G. A., Mendes, I. C., Peloso, E. F., Gadelha, F. R., Macedo, A. M., Franco, G. R., Pena, S. D., Teixeira, S. M., Vieira, L. Q., Guarneri, A. A., Andrade, L. O. & Machado, C. R. (2013) Oxidative stress and DNA lesions: the role of 8-oxoguanine lesions in Trypanosoma cruzi cell viability. *PLoS*. **7**: e2279

Ahn, J. H., Lee, J. S., Cho, J. H., Park, J. H., Lee, T. K., Song, M., Kim, H., Kang, S. H., Won, M. H. & Lee, C. H. (2018) Age-dependent decrease of Nurr1 protein expression in the gerbil hippocampus. *Biomedical Reports*. **8**: 517-522

Akalal, D. B., Wilson, C. F., Zong, L., Tanaka, N. K., Ito, K. & Davis, R. L. (2006) Roles for Drosophila mushroom body neurons in olfactory learning and memory. *Learning & memory.* **13**: 659-668

Akimitsu, N., Adachi, N., Hirai, H., Hossain, M. S., Hamamoto, H., Kobayashi, M., Aratani, Y., Koyama, H. & Sekimizu, K. (2003) Enforced cytokinesis without complete nuclear division in embryonic cells depleting the activity of DNA topoisomerase IIα. *Genes Cells.* **8**: 393-402

Alexander, G. E., Ryan, L., Bowers, D., Foster, T. C., Bizon, J. L., Geldmacher, D. S. & Glisky, E. L. (2012) Characterizing cognitive aging in humans with links to animal models. *Frontiers in Aging Neuroscience.* **4**: 21

Alt, F. W. & Schwer, B. (2018) DNA double-strand breaks as drivers of neural genomic change, function, and disease. *DNA Repair*. **71**: 158-163

Al Tanoury, Z., Piskunov, A. & Rochette-Egly, C. (2013) Vitamin A and retinoid signaling: genomic and nongenomic effects. *Journal of Lipid Research*. **54**: 1761-1775

Ammendola, R., Mesuraca, M., Russo, T. & Cimino, F. (1992) Sp1 DNA binding efficiency is highly reduced in nuclear extracts from aged rat tissues. *The Journal of Biological Chemistry*. **267**: 17944-17948

Apte, M. S. & Meller, V. H. (2015) Sex Differences in Drosophila melanogaster Heterochromatin Are Regulated by Non-Sex Specific Factors. *PloS one*. **10**: e0128114

Aravind, L., Leipe, D. D. & Koonin, E. V. (1998) Toprim--a conserved catalytic domain in type IA and II topoisomerases, DnaG-type primases, OLD family nucleases and RecR proteins. *Nucleic Acids Research*. **26**: 4205-4213

Arcangeli, A., Rosati, B., Crociani, O., Cherubini, A., Fontana, L., Passani, B., Wanke, E. & Olivotto, M. (1991) Modulation of HERG Current and Herg Gene Expression during Retinoic Acid Treatment of Human Neuroblastoma Cells: Potentiating Effects of BDNF. *Journal of Neurobiology*. **40**: 214-225

Armstrong, M. J., Jin, Y., Allen, E. G. & Jin P. (2019) Diverse and dynamic DNA modifications in brain and diseases. *Human Molecular Genetics*. **28**: R241-R253

Arya, G. H., Weber, A. L., Wang, P., Magwire, M. M., Negron, Y. L., Mackay, T. F. & Anholt, R. R. (2010) Natural variation, functional pleiotropy and transcriptional contexts of odorant binding protein genes in Drosophila melanogaster. *Genetics*. **186**: 1475-1485

Ashapkin, V. V., Kutueva, L. I., Kurchashova, S. Y. & Kireev, I. I. (2019) Are There Common Mechanisms Between the Hutchinson-Gilford Progeria Syndrome and Natural Aging? *Frontiers in Genetics*. **10**: 455

Atamna, H., Cheung, I. & Ames, B. N. (2000) A method for detecting abasic sites in living cells: age-dependent changes in base excision repair. *Proceedings of the National Academy of Sciences of the United States of America*. **97**: 686-691

Austad, S. N. & Fischer, K. E. (2016) Sex Differences in Lifespan. *Cell Metabolism*. **23**: 1022-1033

Austad, S. N. & Hoffman, J. M. (2018) Is antagonistic pleiotropy ubiquitous in aging biology? *Evolution, Medicine, and Public Health.* **2018**: 287-294

Austin, C.A., Sng, J.H., Patel, S. & Fisher, L.M. (1993) Novel HeLa topoisomerase II is the IIβ isoform: complete coding sequence and homology with other type II topoisomerases. *Biochimica et Biophysica Acta*. **1172**: 282-291

Austin, C. A., Lee, K. C., Swan, R. L., Khazeem, M. M., Manville, C. M., Cridland, P., Treumann, A., Porter, A., Morris, N. J & Cowell, I. G. (2018) TOP2B: The First Thirty Years. *International Journal of Molecular Sciences.* **19**: 2765

Babusikova, E., Hatok, J., Dobrota, D. & Kaplan, P. (2007) Age-related oxidative modifications of proteins and lipids in rat brain. *Neurochemical Research*. **32**: 1351-1356

Balch, W. E., Morimoto, R. I., Dillin, A. & Kelly, J. W. (2008) Adapting Proteostasis for Disease Intervention. *Science*. **319**: 916-919

Baldi, S., Korber, P. & Becker, P.B. (2020) Beads on a string—nucleosome array arrangements and folding of the chromatin fiber. *Natural Structural & Molecular Biology*. **27:** 109-118

Baltanás, F. C., Casafont, I., Lafarga, V., Weruaga, E., Alonso, J. R., Berciano, M. T. & Lafarga, M. (2011) Purkinje cell degeneration in pcd mice reveals large scale chromatin reorganization and gene silencing linked to defective DNA repair. *The Journal of Biological Chemistry*. **286**: 28287-28302

Ban, Y., Ho, C. W., Lin, R. K., Lyu, Y. L. & Liu, L. F. (2013) Activation of a novel ubiquitin-independent proteasome pathway when RNA polymerase II encounters a protein roadblock. *Molecular and Cellular Biology*. **33**: 4008-4016

Barnstedt, O., Owald, D., Felsenberg, J., Brain, R., Moszynski, J. P., Talbot, C. B., Perrat, P. N. & Waddell, S. (2016) Memory-Relevant Mushroom Body Output Synapses Are Cholinergic. *Neuron*. **89**: 1237-1247

Barrera, G. (2012) Oxidative stress and lipid peroxidation products in cancer progression and therapy. *ISRN Oncology*. **2012**: 137289

Bartholomew, N. R., Burdett, J. M., VandenBrooks, J. M., Quinlan, M. C. & Call, G. B. (2015) Impaired climbing and flight behaviour in Drosophila melanogaster following carbon dioxide anaesthesia. *Scientific Report.* **5**: 15298

Barutcu, A. R., Lian, J. B., Stein, J. L., Stein, G. S. & Imbalzano, A. N. (2017) The connection between BRG1, CTCF and topoisomerases at TAD boundaries. *Nucleus.* **8**: 150-155

Barzilai, A. & Yamamoto, K.-I. (2004) DNA damage responses to oxidative stress. *DNA Repair.* **3**: 1109-1115

Basisty, N., Meyer, J. G. & Schilling, B. (2018) Protein Turnover in Aging and Longevity. *Proteomics*. **18**: 1700108

Batzoglou, S., Pachter, L., Mesirov, J. P., Berger, B. & Lander, E. S. (2000) Human and mouse gene structure: comparative analysis and application to exon prediction. *Genome Research.* **10**: 950-958

Baxter, J. & Diffley, J. F. X. (2008) Topoisomerase II inactivation prevents the completion of DNA replication in budding yeast. *Molecular Cell*. **30**: 790-802

Beauséjour, C. M., Krtolica, A., Galimi, F., Narita, M., Lowe, S. W., Yaswen, P. & Campisi, J. (2003) Reversal of human cellular senescence: roles of the p53 and p16 pathways. *The EMBO Journal. **22***: 4212-4222

Bedez, C., Lotz, C., Batisse, C., Vanden Broeck, A., Stote, R. H., Howard, E., Pradeau-Aubreton, K., Ruff, M. & Lamour, V. (2018) Post-translational modifications in DNA topoisomerase 2α highlight the role of a eukaryote-specific residue in the ATPase domain. *Scientific Reports.* **8**: 9272

Bednar, J., Furrer, P., Stasiak, A., Dubochet, J., Egelman, E. H. & Bates, A. D. (1994) The Twist, Writhe and Overall Shape of Supercoiled DNA Change During Counterion-Induced Transition From a Loosely to a Tightly Interwound Superhelix. Possible Implications for DNA Structure in Vivo. *Journal of Molecular Biology.* **235**: 825-47

Bell, N., Hann, V., Redfern, C. P. & Cheek, T. R. (2013) Store-operated Ca(2+) entry in proliferating and retinoic acid-differentiated N- and S-type neuroblastoma cells. *Biochimica et Biophysica Acta*. **1833**: 643-651

Berger, J., Gamblin, S., Harrison, S. & Wang, J. (1996) Structure and mechanism of DNA topoisomerase II. *Nature.* **379**: 225-232

Berke, S. J. S. & Paulson, H. L. (2003) Protein aggregation and the ubiquitin proteasome pathway: gaining the UPPer hand on neurodegeneration. *Current Opinion in Genetics and Development.* **13**: 253-261

Bermejo, R., Doksani, Y., Capra, T., Katou, Y. M., Tanaka, H., Shirahige, K. & Foiani, M. (2007) Top1- and Top2-mediated topological transitions at replication forks ensure fork progression and stability and prevent DNA damage checkpoint activation. *Genes & Development*. **21**: 1921-1936

Berridge, M. V., Herst, P. M. & Tan, A. S. (2005) Tetrazolium dyes as tools in cell biology: New insights into their cellular reduction. *Biotechnology Annual Review*. **11**: 127-152

Berson, A., Nativio, R., Berger, S. L. & Bonini, N. M. (2018) Epigenetic Regulation in Neurodegenerative Diseases. *Trends in Neurosciences*. **41**: 587-598

Bhanu, M. U., Mandraju, R. K., Bhaskar, C. & Kondapi, A. K. (2010) Cultured cerebellar granule neurons as an in vitro aging model: topoisomerase IIβ as an additional biomarker in DNA repair and aging. *Toxicology. In Vitro***. 24**: 1935-1945

Biedler, J. L., Roffler-Tarlov, S., Schachner, M. & Freedman, L. S. (1978) Multiple neurotransmitter synthesis by human neuroblastoma cell lines and clones. *Cancer.* **38**: 3751-3757

Birben, E., Sahiner, U. M., Sackesen, C., Erzurum, S. & Kalayci, O. (2012) Oxidative stress and antioxidant defense. *The World Allergy Organization Journal*. **5**: 9-19

Bird, C. M. & Burgess, N. (2008) The hippocampus and memory: insights from spatial processing. *Nature Reviews Neuroscience*. **9**: 182-194

Biteau, B., Karpac, J., Supoyo, S., Degennaro, M., Lehmann, R. & Jasper, H. (2010) Lifespan extension by preserving proliferative homeostasis in Drosophila. *PLoS Genetics*. **6**: e1001159

Björkegren, C. & Baranello, L. (2018) DNA Supercoiling, Topoisomerases, and Cohesin: Partners in Regulating Chromatin Architecture? *International Journal of Molecular Sciences*. **19**: 884

Boda, E., Pini, A., Hoxha, E., Parolisi, R. & Tempia, F. (2009) Selection of Reference Genes for Quantitative Real-time RT-PCR Studies in Mouse Brain. *Journal of Molecular Neuroscience*. **37**: 238-253

Borgesius, N. Z., de Waard, M. C., van der Pluijm, I., Omrani, A., Zondag, G. C., van der Horst, G. T., Melton, D. W., Hoeijmakers, J. H., Jaarsma, D. & Elgersma, Y. (2011) Accelerated age-related cognitive decline and neurodegeneration, caused by deficient DNA repair. *The Journal of Neuroscience.* **31**: 12543-12553

Bower, J. J., Karaca, G. F., Zhou, Y., Simpson, D. A., Cordeiro-Stone, M. & Kaufmann, W. K. (2010) Topoisomerase II alpha maintains genomic stability through decatenation G(2) checkpoint signaling. *Oncogene*. **29**: 4787-4799

Brandsma, I. & Gent, D. C. (2012) Pathway choice in DNA double strand break repair: observations of a balancing act. *Genome Integrity*. **3**: 9

Bunch, H., Lawney, B. P., Lin, Y. F., Asaithamby, A., Murshid, A., Wang, Y. E., Chen, B. P. & Calderwood, S. K. (2015) Transcriptional elongation requires DNA break-induced signalling. *Nature Communications*. **6**: 10191

Bunch, H. (2018) Gene regulation of mammalian long non-coding RNA. *Molecular Genetics and Genomics*. **293**: 1-15

Burden, D. A. & Osheroff, N. (1998) Mechanism of action of eukaryotic topoisomerase II and drugs targeted to the enzyme. *Biochimica et Biophysica Acta.* **1400**: 139-54

Cairns, B. R. (2009) The logic of chromatin architecture and remodelling at promoters. *Nature*. **461**: 193-198

Calabrese, F., Guidotti, G., Racagni, G. & Riva, M. A. (2013) Reduced neuroplasticity in aged rats: a role for the neurotrophin brain-derived neurotrophic factor. *Neurobiology of Aging*. **34**: 2768-2776

Calderwood, S. K., Murshid, A. & Prince, T. (2009) The shock of aging: molecular chaperones and the heat shock response in longevity and aging--a mini-review. *Gerontology*. **55**: 550-558

Caliò, A., Zamò, A., Ponzoni, M., Zanolin, M. A., Ferreri, A. J. M., Pedron, S., Montagna, L., Parolini, C., Fraifeld, V. E., Wolfson, E., Yanai, H., Pizzolo, G., Doglioni, C., Vinante, F. & Chilosi, M. (2015) Cellular Senescence Markers p16INK4a and p21CIP1/WAF Are Predictors of Hodgkin Lymphoma Outcome. *Clinical Cancer Research.* **21**: 5164-5172

Campisi, J. (1997) The biology of replicative senescence. *European Journal of Cancer.* **33**: 703-709

Canela, A., Maman, Y., Jung, S., Wong, N., Callen, E., Day, A., Kieffer-Kwon, K. R., Pekowska, A., Zhang, H., Rao, S., Huang, S. C., Mckinnon, P. J., Aplan, P. D., Pommier, Y., Aiden, E. L., Casellas, R. & Nussenzweig, A. (2017) Genome Organization Drives Chromosome Fragility. *Cell*. **170**: 507-521

Cannan, W. J., Tsang, B. P., Wallace, S. S. & Pederson, D. S. (2014) Nucleosomes suppress the formation of double-strand DNA breaks during attempted base excision repair of clustered oxidative damages. *The Journal of Biological Chemistry*. **289**: 19881-19893

Capranico, G., Tinelli, S., Austin, C.A., Fisher, M.L. & Zunino, F. (1992) Different patterns of gene expression of topoisomerase II isoforms in differentiated tissues during murine development. *Biochimica et Biophysica Acta.* **1132**: 43-48

Carpenter, A. J. & Porter, A. C. (2004) Construction, characterization, and complementation of a conditional-lethal DNA topoisomerase IIalpha mutant human cell line. *Molecular Biology of the Cell.* **15**: 5700-5711

Castelli, V., Benedetti, E., Antonosante, A., Catanesi, M., Pitari, G., Ippoliti, R., Cimini, A. & d'Angelo, M. (2019) Neuronal Cells Rearrangement During Aging and Neurodegenerative Disease: Metabolism, Oxidative Stress and Organelles Dynamic. *Frontiers in Molecular Neuroscience*. **12**: 132

Chadwick, W., Zhou, Y., Park, S.-S., Wang, L., Mitchell, N., Stone, M. D., Becker, K. G., Martin, B. & Maudsley, S. (2010) Minimal Peroxide Exposure of Neuronal Cells Induces Multifaceted Adaptive Responses. *PLoS ONE.* **5**: e14352

Chakraborty, R., Vepuri, V., Mhatre, S. D., Paddock, B. E., Miller, S., Michelson, S. J., Delvadia, R., Desai, A., Vinokur, M., Melicharek, D. J., Utreja, S., Khandelwal, P., Ansaloni, S., Goldstein, L. E., Moir, R. D., Lee, J. C., Tabb, L. P., Saunders, A. J. &

Marenda, D. R. (2011) Characterization of a Drosophila Alzheimer's disease model: pharmacological rescue of cognitive defects. *PloS one*. **6**: e20799

Chakraborty, S., Rasool, R. U., Kumar, S., Nayak, D., Rah, B., Katoch, A., Amin, H., Ali, A. & Goswami, A. (2016) Cristacarpin promotes ER stress-mediated ROS generation leading to premature senescence by activation of p21(waf-1). *Age*. **38**: 62

Chaly, N. & Brown, D. L. (1996) Is DNA topoisomerase IIβ a nucleolar protein? *Journal of Cellular Biochemistry.* **63:** 162-173

Champoux, J.J. (2001) DNA Topoisomerases: Structure, Function, and Mechanism. *Annual Review of Biochemistry*. **70**: 369-413

Chan, M. M. & Tahan, S. R. (2010) Low-affinity nerve growth factor receptor (P75 NGFR) as a marker of perineural invasion in malignant melanomas. *Journal of Cutaneous Pathology.* **37**: 336-343

Chapman, T., Liddle, L. F., Kalb, J. M., Wolfner, M. F. & Partridge, L. (1995) Cost of mating in *Drosophila melanogaster* females is mediated by male accessory-gland products. *Nature*. **373**: 241-244

Chapman, J., Fielder, E. & Passos, J. F. (2019) Mitochondrial dysfunction and cell senescence: deciphering a complex relationship. *Federation of European Biochemical Societies.* **593**: 1566-1579

Chen, H., Ruiz, P. D., McKimpson, W. M., Novikov, L., Kitsis, R. N. & Gamble, M. J. (2015) MacroH2A1 and ATM Play Opposing Roles in Paracrine Senescence and the Senescence-Associated Secretory Phenotype. *Molecular cell*. **59**: 719-731

Chen J. (2016) The Cell-Cycle Arrest and Apoptotic Functions of p53 in Tumor Initiation and Progression. Cold Spring Harbor Perspectives in Medicine. 6: a026104

Chen, Q. & Ames, B. N. (1994) Senescence-like growth arrest induced by hydrogen peroxide in human diploid fibroblast F65 cells. *Proceedings of the National Academy of Sciences*. **91**: 4130-4134

Chen, T., Sun, Y., Ji, P., Kopetz, S. & Zhang, W. (2015) Topoisomerase IIα in chromosome instability and personalized cancer therapy. *Oncogene*. **34**: 4019-4031

Chen, Y. T., Wu, J., Modrich, P. & Hsieh, T. S. (2016) The C-terminal 20 Amino Acids of Drosophila Topoisomerase 2 Are Required for Binding to a BRCA1 C Terminus

(BRCT) Domain-containing Protein, Mus101, and Fidelity of DNA Segregation. *The Journal of Biological Chemistry*. **291**: 13216-13228

Chen-Plotkin, A. S., Lee, V. M. & Trojanowski, J. Q. (2010) TAR DNA-binding protein 43 in neurodegenerative disease. *Nature reviews. Neurology*. **6**: 211-220

Chikamori, K., G. Grozav, A., Kozuki, T., Grabowski, D., Ganapathi, R. & K. Ganapathi, M. (2010) DNA Topoisomerase II Enzymes as Molecular Targets for Cancer Chemotherapy. *Current Cancer Drug Targets*. **10**: 758-771

Chiruvella, K. K., Liang, Z. & Wilson, T. E. (2013) Repair of Double-Strand Breaks by End Joining. *Cold Spring Harbor Perspectives in Biology*. **5**: a012757-a012757

Choo, K. B., Tai, L., Hymavathee, K. S., Wong, C. Y., Nguyen, P. N., Huang, C. J., Cheong, S. K. & Kamarul, T. (2014) Oxidative stress-induced premature senescence in Wharton's jelly-derived mesenchymal stem cells. *International Journal of Medical Sciences*. **11**: 1201-1207

Chowdhury, D., Keogh, M.-C., Ishii, H., Peterson, C. L., Buratowski, S. & Lieberman, J. (2005) γ-H2AX Dephosphorylation by Protein Phosphatase 2A Facilitates DNA Double-Strand Break Repair. *Molecular Cell*. **20**: 801-809

Christensen, M. O., Larsen, M. K., Barthelmes, H. U., Hock, R., Andersen, C. L., Kjeldsen, E., Knudsen, B. R., Westergaard, O., Boege, F. & Mielke, C. (2002) Dynamics of human DNA topoisomerases IIalpha and IIbeta in living cells. *The Journal of Cell Biology*. **157**:31-44

Chu, Y., Kompoliti, K., Cochran, E. J., Mufson, E. J. & Kordower, J. H. (2002) Age-related decreases in Nurr1 immunoreactivity in the human substantia nigra. *The Journal of Comparative Neurology*. **450**: 203-214

Clagett-Dame, M., McNeill, E. M. & Mulley, P. D. (2006) Role of all-trans retinoic acid in neurite outgrowth and axonal elongation. *Journal of Neurobiology*. **66**: 739-56

Cole, H. A., Cui, F., Ocampo, J., Burke, T. L., Nikitina, T., Nagarajavel, V., Kotomura, N., Zhurkin, V. B. & Clark, D. J. (2016) Novel nucleosomal particles containing core histones and linker DNA but no histone H1. *Nucleic Acids Research*. **44**: 573-581

Collins, A. R., Ai-guo, M. & Duthie, S. J. (1995) The kinetics of repair of oxidative DNA damage (strand breaks and oxidised pyrimidines) in human cells. *Mutation Research/DNA Repair*. **336**: 69-77

Conserva, M. R., Anelli, L., Zagaria, A., Specchia, G. & Albano, F. (2019) The Pleiotropic Role of Retinoic Acid/Retinoic Acid Receptors Signaling: From Vitamin A Metabolism to Gene Rearrangements in Acute Promyelocytic Leukemia. *International Journal of Molecular Sciences*. **20**: 2921

Constantinescu, R., Constantinescu, A. T., Reichmann, H. & Janetzky, B. (2007) Neuronal differentiation and long-term culture of the human neuroblastoma line SH-SY5Y. *Journal of Neural Transmission.***72**: 17-28

Coppé, J. P., Patil, C. K., Rodier, F., Sun, Y., Muñoz, D. P., Goldstein, J., Nelson, P. S., Desprez, P. Y. & Campisi, J. (2008) Senescence-associated secretory phenotypes reveal cell-nonautonomous functions of oncogenic RAS and the p53 tumor suppressor. *PLoS Biology*. **6**: 2853-2868

Coppé, J. P., Desprez, P. Y., Krtolica, A. & Campisi, J. (2010) The senescence-associated secretory phenotype: the dark side of tumor suppression. *Annual Review of Pathology*. **5:** 99-118

Corbett, K. D. & Berger, J. M. (2004) Structure, Molecular Mechanisms, and Evolutionary Relationships in DNA Topoisomerases Structure *Annual Review of Biophysics and Biomolecular Structure.* **33**: 95-118

Corless, S. & Gilbert, N. (2016) Effects of DNA supercoiling on chromatin architecture. *Biophysical Reviews.* **8**: 245-258

Cortés, F., Pastor, N., Mateos, S. & Domínguez, I. (2003) Roles of DNA topoisomerases in chromosome segregation and mitosis. *Mutation Research/Reviews in Mutation Research*. **543**: 59-66

Costes, S. V., Boissière, A., Ravani, S., Romano, R., Parvin, B. & Barcellos-Hoff, M. H. (2006) Imaging features that discriminate between foci induced by high- and low-LET radiation in human fibroblasts. *Radiation Research.* **165**: 505-515

Costes, S. V., Chiolo, I., Pluth, J. M., Barcellos-Hoff, M. H. & Jakob, B. (2010) Spatiotemporal characterization of ionizing radiation induced DNA damage foci and their relation to chromatin organization. *Mutation Research*. **704**: 78-87

Covarrubias, L., Hernández-García, D., Schnabel, D., Salas-Vidal, E. & Castro-Obregón, S. (2008) Function of reactive oxygen species during animal development: Passive or active? *Developmental Biology.* **320**: 1-11

Cowell, I. G., Tilby, M. & Austin, C. A. (2010) An overview of the visualisation and quantitation of low and high MW DNA adducts using the trapped in agarose DNA immunostaining (TARDIS) assay. *Mutagenesis*. **26**: 253-260

Cowell, I. G., Papageorgiou, N., Padget, K., Watters, G. P. & Austin, C. A. (2011) Histone deacetylase inhibition redistributes topoisomerase IIβ from heterochromatin to euchromatin. *Nucleus*. **2**: 61-71

Cuende, J., Moreno, S., Bolaños, J. P. & Almeida, A. (2008) Retinoic acid downregulates Rae1 leading to APCCdh1 activation and neuroblastoma SH-SY5Y differentiation. *Oncogene*. **27**: 3339-3344

Cugusi, S., Ramos, E., Ling, H., Yokoyama, R., Luk, K. M. & Lucchesi, J. C. (2013) Topoisomerase II plays a role in dosage compensation in Drosophila. *Transcription*. **4**: 238-250

Cunningham, T. J. & Duester, G. (2015) Mechanisms of retinoic acid signalling and its roles in organ and limb development. *Nature reviews. Molecular Cell Biology*. **16**: 110-123

Dai, D. F., Karunadharma, P. P., Chiao, Y. A., Basisty, N., Crispin, D., Hsieh, E. J., Chen, T., Gu, H., Djukovic, D., Raftery, D., Beyer, R. P., MacCoss, M. J. & Rabinovitch, P. S. (2014) Altered proteome turnover and remodeling by short-term caloric restriction or rapamycin rejuvenate the aging heart. *Aging Cell*. **13**: 529-539

Das, B. C., Thapa, P., Karki, R., Das, S., Mahapatra, S., Liu, T. C., Torregroza, I., Wallace, D. P., Kambhampati, S., Van Veldhuizen, P., Verma, A., Ray, S. K. & Evans, T. (2014) Retinoic acid signaling pathways in development and diseases. *Bioorganic & Medicinal Chemistry*. **22**: 673-683

Dash, B. C. & El-Deiry, W. S. (2005) Phosphorylation of p21 in G2/M promotes cyclin B-Cdc2 kinase activity. *Molecular and Cellular Biology*. **25**: 3364-3387

Davalli, P., Mitic, T., Caporali, A., Lauriola, A. & D'Arca, D. (2016) ROS, Cell Senescence, and Novel Molecular Mechanisms in Aging and Age-Related Diseases. *Oxidative Medicine and Cellular Longevity*. **2016**: 3565127

Davie, K., Janssens, J., Koldere, D., De Waegeneer, M., Pech, U., Kreft, Ł., Aibar, S., Makhzami, S., Christiaens, V., Bravo González-Blas, C., Poovathingal, S., Hulselmans, G., Spanier, K. I., Moerman, T., Vanspauwen, B., Geurs, S., Voet, T., Lammertyn, J.,

Thienpont, B., Liu, S., Konstantinides, N., Fiers, M., Verstreken, P. & Aerts, S. (2018) A Single-Cell Transcriptome Atlas of the Aging Drosophila Brain. *Cell*. **174**: 982-998

David, D. C. (2012) Aging and the aggregating proteome. *Frontiers in Genetics*. **3**: 247

Davis, A. J. & Chen, D. J. (2013) DNA double strand break repair via non-homologous end-joining. *Translational Cancer Research*. **2**: 130-143

Decressac, M., Volakakis, N., Björklund, A. & Perlmann, T. (2013) NURR1 in Parkinson disease—from pathogenesis to therapeutic potential. *Nature Reviews Neurology*. **9**: 629-636

Deweese, J. E. & Osheroff, N. (2009) The DNA cleavage reaction of topoisomerase II: wolf in sheep's clothing. *Nucleic Acids Research*. **37**: 738-748

Dhondt, I., Petyuk, V. A., Bauer, S., Brewer, H. M., Smith, R. D., Depuydt, G. & Braeckman, B. P. (2017) Changes of Protein Turnover in Aging Caenorhabditis elegans. *Molecular & Cellular Proteomics.* **16**: 1621-1633

Dimri, G. P., Lee, X., Basile, G., Acosta, M., Scott, G., Roskelley, C., Medrano, E. E., Linskens, M., Rubelj, I. & Pereira-Smith, O. (1995) A biomarker that identifies senescent human cells in culture and in aging skin in vivo. *Proceedings of the National Academy of Sciences of the United States of America*. **92**: 9363-9367

Domínguez-González, M., Puigpinós, M., Jové, M., Naudi, A., Portero-Otín, M., Pamplona, R. & Ferrer, I. (2018) Regional vulnerability to lipoxidative damage and inflammation in normal human brain aging. *Experimental Gerontology*. **111**: 218-228

Dovey, M., Patton, E. E., Bowman, T., North, T., Goessling, W., Zhou, Y. & Zon, L. I. (2009) Topoisomerase IIα Is Required for Embryonic Development and Liver Regeneration in Zebrafish. *Molecular and Cellular Biology*. **29**: 3746-3753

Drake, F.H., Zimmerman, J.P., McCabe, F.L., Bartus, H.F., Per, S.R., Sullivan, D.M., Ross, W.E., Mattern, M.R., Johnson, R.K., Crooke, S.T. & Mirabelli, C.K. (1987) Purification of Topoisomerase II from Amsacrine-resistant P388 Leukemia Cells. *The Journal of Biological Chemistry*. **262**: 16739-16747

Duan, W., Zhang, R., Guo, Y., Jiang, Y., Huang, Y., Jiang, H. & Li, C. (2009) Nrf2 activity is lost in the spinal cord and its astrocytes of aged mice. *In Vitro Cellular & Developmental Biology – Animal*. **45**: 388-397

Duclot, F. & Kabbaj, M. (2017) The Role of Early Growth Response 1 (EGR1) in Brain Plasticity and Neuropsychiatric Disorders. *Frontiers in Behavioral Neuroscience*. **11**: 35

Durand-Dubief, M., Svensson, J. P., Persson, J. & Ekwall, K. (2011) Topoisomerases, chromatin and transcription termination. *Transcription*. **2**: 66-70

Eells, J., Lipska, B., Yeung, S., Misler, J. & Nikodem, V. (2002) Nurr1-null heterozygous mice have reduced mesolimbic and mesocortical dopamine levels and increased stress-induced locomotor activity. *Behavioural Brain Research.* **136**: 267-275

Elfawy, H. A. & Das, B. (2019) Crosstalk Between Mitochondrial Dysfunction, Oxidative Stress, and Age Related Neurodegenerative Disease: Etiologies and Therapeutic Strategies. *Life Sciences.* **218**: 165-184

Elobeid, A., Libard, S., Leino, M., Popova, S. N. & Alafuzoff, I. (2016) Altered Proteins in the Aging Brain. *Journal of Neuropathology and Experimental Neurology*. **75**: 316-25

Emmons, M., Boulware, D., Sullivan, D. M. & Hazlehurst, L. A. (2006) Topoisomerase II beta levels are a determinant of melphalan-induced DNA crosslinks and sensitivity to cell death. *Biochemical Pharmacology*. **72**: 11-18

Encinas, M., Iglesias, M., Liu, Y., Wang, H., Muhaisen, A., Ceña, V., Gallego, C. & Comella, J. X. (2002) Sequential Treatment of SH-SY5Y Cells with Retinoic Acid and Brain-Derived Neurotrophic Factor Gives Rise to Fully Differentiated, Neurotrophic Factor-Dependent, Human Neuron-Like Cells. *Journal of Neurochemistry*. **75**: 991-1003

English, C. M., Maluf, N. K., Tripet, B., Churchill, M. E. & Tyler, J. K. (2005) ASF1 binds to a heterodimer of histones H3 and H4: a two-step mechanism for the assembly of the H3-H4 heterotetramer on DNA. *Biochemistry*. **44**: 13673-13682

Escargueil, A. E., Plisov, S. Y., Filhol, O., Cochet, C. & Larsen, A. K. (2000) Mitotic phosphorylation of DNA topoisomerase II α by protein kinase CK2 creates the MPM-2 phosphoepitope on Ser-1469. *Journal of Biological Chemistry*. **275**: 34710-34718

Faragher, R. G., McArdle, A., Willows, A. & Ostler, E. L. (2017) Senescence in the aging process. *F1000Research*. **6:** 1219

Farr, C. J., Antoniou-Kourounioti, M., Mimmack, M. L., Volkov, A. & Porter, A. C. (2014) The α isoform of topoisomerase II is required for hypercompaction of mitotic chromosomes in human cells. *Nucleic Acids Research*. **42**: 4414-4426

Feng, Z., Hu, W., Teresky, A. K., Hernando, E., Cordon-Cardo, C. & Levine, A. J. (2007). Declining p53 function in the aging process: a possible mechanism for the increased tumor incidence in older populations. *Proceedings of the National Academy of Sciences of the United States of America*. **104**: 16633-16638

Fernández-Hernández, I., Rhiner, C. & Moreno, E. (2013) Adult Neurogenesis in Drosophila. *Cell Reports*. **3**: 1857-1865

Fernández-Moreno, M. A., Farr, C. L., Kaguni, L. S. & Garesse, R. (2007) Drosophila melanogaster as a model system to study mitochondrial biology. *Methods in Molecular Biology*. **372**: 33-49

Fielder, E., von Zglinicki, T. & Jurk, D. (2017) The DNA Damage Response in Neurons: Die by Apoptosis or Survive in a Senescence-Like State? *Journal of Alzheimer's Disease.* **60**: S107-S131

Figueroa-González, G. & Pérez-Plasencia, C. (2017) Strategies for the evaluation of DNA damage and repair mechanisms in cancer (Review). *Oncology Letters*. **13**: 3982-3988

Fishel, M. L., Vasko, M. R. & Kelley, M. R. (2007) DNA repair in neurons: So if they don't divide what's to repair? *Mutation Research/Fundamental and Molecular Mechanisms of Mutagenesis*. **614**: 24-36

Fleming, A. M., Ding, Y. & Burrows, C. J. (2017) Oxidative DNA damage is epigenetic by regulating gene transcription via base excision repair. *Proceedings of the National Academy of Sciences of the United States of America.* **114**: 2604-2609

Fogg, J. M., Kolmakova, N., Rees, I., Magonov, S., Hansma, H., Perona, J. J. & Zechiedrich, E. L. (2006) Exploring writhe in supercoiled minicircle DNA. *Journal of Physics: Condensed Matter.* **18**: S145-S159

Forster, J. I., Köglsberger, S., Trefois, C., Boyd, O., Baumuratov, A. S., Buck, L., Balling, R. & Antony, P. M. (2016) Characterization of differentiated SH-SY5Y as neuronal screening model reveals increased oxidative vulnerability. *Journal of Biomolecular Screening.* **21**: 496-509

Fuentealba, D., Friguet, B. & Silva, E. (2009) Advanced glycation endproducts induce photocrosslinking and oxidation of bovine lens proteins through type-I mechanism. *Photochemistry and Photobiology*. **85**: 185-19

Gabel, H. W., Kinde, B., Stroud, H., Gilbert, C. S., Harmin, D. A., Kastan, N. R., Hemberg, M., Ebert, D. H. & Greenberg, M. E. (2015) Disruption of DNA-methylation-dependent long gene repression in Rett syndrome. *Nature*. **522**: 89-93

Gadelle, D., Krupovic, M., Raymann, K., Mayer, C. & Forterre, P. (2014) DNA topoisomerase VIII: a novel subfamily of type IIB topoisomerases encoded by free or integrated plasmids in Archaea and Bacteria. *Nucleic Acids Research*. **42**: 8578-8591

Gargano, J. W., Martin, I., Bhandari, P. & Grotewiel, M. S (2005) Rapid Iterative Negative Geotaxis (RING): A New Method for Assessing Age-Related Locomotor Decline in Drosophila. *Experimental Gerontology*. **40**: 386-389

Garschall, K., Dellago, H., Gáliková, M. Schosserer, M., Flatt, T. & Grillari, J. (2017) Ubiquitous overexpression of the DNA repair factor *dPrp19* reduces DNA damage and extends *Drosophila* life span. *Aging and Mechanisms of Disease.* **3**: 5

Gasser, S. M., Walter, R., Dang, Q. & Cardenas, M. E. (1992) Topoisomerase II: its functions and phosphorylation. *Antonie Van Leeuwenhoek*. **62**: 15-24

Gellert, M., Mizuuchi, K., O'Dea, M. H. & Nash, H. A. (1976) DNA gyrase: an enzyme that introduces superhelical turns into DNA. *Proceedings of the National Academy of Sciences of the United States of America.* **73**: 3872-3876

Gemkow, M. J., Dichter, J. & Arndt-Jovin, D. J. (2001) Developmental Regulation of DNA-Topoisomerases during Drosophila Embryogenesis. *Experimental Cell Research.* **262**: 114-121

Gendron, C. M., Kuo, T. H., Harvanek, Z. M., Chung, B. Y., Yew, J. Y., Dierick, H. A. & Pletcher, S. D. (2014) Drosophila life span and physiology are modulated by sexual perception and reward. *Science.* **343**: 544-548

Gilbert, N. & Allan, J. (2014) Supercoiling in DNA and chromatin. *Current Opinion in Genetics & Development*. **25**: 15-21

Glick, D., Barth, S. & Macleod, K. F. (2010) Autophagy: cellular and molecular mechanisms. *The Journal of Pathology*. **221**: 3-12

Gómez-Herreros, F., Schuurs-Hoeijmakers, J. H., McCormack, M., Greally, M. T., Rulten, S., Romero-Granados, R., Counihan, T. J., Chaila, E., Conroy, J., Ennis, S., Delanty, N., Cortés-Ledesma, F., de Brouwer, A. P. M., Cavalleri, G. L., El-Khamisy, S. F., de Vries, B. B. A. & Caldecott, K. W. (2014) TDP2 protects transcription from abortive topoisomerase activity and is required for normal neural function. *Nature Genetics*. **46**: 516-521

Gonzalez, R. E., Lim, C. U., Cole, K., Bianchini, C. H., Schools, G. P., Davis, B. E., Wada, I., Roninson, I. B. & Broude, E. V. (2011) Effects of conditional depletion of topoisomerase II on cell cycle progression in mammalian cells. *Cell Cycle.* **10**: 3505-3514

Goodenow, D., Emmanuel, F., Berman, C., Sahyouni, M. & Richardson, C. (2020) Bioflavonoids cause DNA double-strand breaks and chromosomal translocations through topoisomerase II-dependent and -independent mechanisms. *Mutation Research/Genetic Toxicology and Environmental Mutagenesis*. **849**: 503144

Gorbunova, V., Seluanov, A., Mao, Z. & Hine, C. (2007) Changes in DNA repair during aging. *Nucleic Acids Research*. **35**: 7466-7474

Gorbunova, V. & Seluanov, A. (2016) DNA double strand break repair, aging and the chromatin connection. *Mutation Research*. **788**: 2-6

Gory, S., Dalmon, J., Prandini, M., Kortulewski, T., Launoit, Y. & Huber, P. (1997) Requirement of a GT Box (Sp1 Site) and Two Ets Binding Sites for Vascular Endothelial Cadherin Gene Transcription. *The Journal of Biochemistry.* **273**: 6750-6755

Gudas, L. J. & Wagner, J. A. (2011) Retinoids regulate stem cell differentiation. *Journal of Cellular Physiology.* **226**: 322-330

Guo, H., Cao , C., Chi, X., Zhao, J., Liu, X., Zhou, N., Han, S., Yan, Y., Wang, Y., Xu, Y., Yan, Y., Cui, H. & Sun, H. (2014) Specificity protein 1 regulates topoisomerase IIβ expression in SH-SY5Y cells during neuronal differentiation. *Journal of Neuroscience Research.* **92**: 1374-1383

Gupta, K. P., Swain, U., Rao, K. S. & Kondapi, K. (2012) Topoisomerase IIβ regulates base excision repair capacity of neurons. *Mechanisms of Ageing and Development.* **133**: 203-213

Gyori, B. M., Venkatachalam, G., Thiagarajan, P. S., Hsu, D. & Clement, M. V. (2014) OpenComet: an automated tool for comet assay image analysis. *Redox Biology*. **2**: 457-465

Haffner, M. C., De Marzo, A. M., Meeker, A. K., Nelson, W. G. & Yegnasubramanian, S. (2011) Transcription-induced DNA double strand breaks: both oncogenic force and potential therapeutic target? *Clinical cancer research: an official journal of the American Association for Cancer Research*. **17**: 3858-3864

Haigh, R. (1993) The ageing process: a challenge for design. *Applied Ergonomics.* **24**: 9-14

Hall, H., Medina, P., Cooper, D. A., Escobedo, S. E., Rounds, J., Brennan, K. J., Vincent, C., Miura, P., Doerge, R. & Weake, V. M. (2017) Transcriptome profiling of aging Drosophila photoreceptors reveals gene expression trends that correlate with visual senescence. *BMC Genomics*. **18**: 894

Han, S. M., Kim, J. M., Park, K. K., Chang, Y. C. & Pak, S. C. (2014) Neuroprotective effects of melittin on hydrogen peroxide-induced apoptotic cell death in neuroblastoma SH-SY5Y cells. *BMC Complementary and Alternative Medicine*. **14**: 286

Hansen, T. Ø., Sarup, P., Loeschcke, V. & Rattan, S. I. S. (2012) Age-related and sex-specific differences in proteasome activity in individual Drosophila flies from wild type, longevity-selected and stress resistant strains. *Biogerontology*. **13**: 429-438

Harada, C. N., Natelson Love, M. C. & Triebel, K. L. (2013) Normal cognitive aging. *Clinics in Geriatric Medicine*. **29**: 737-752

Harkin, L. F., Gerrelli, D., Diaz, D. C. G., Santos, C., Alzu'bi, A., Austin, C. A. & Clowry, G. J. (2015) Distinct expression patterns for type II topoisomerases IIA and IIB in the early foetal human telencephalon. *Journal of Anatomy.* **228**: 452-463

Hashemi, S. H., Li, J.-Y., Faigle, R. & Dahlström, A. (2003) Adrenergic differentiation and SSR2(a) receptor expression in CAD-cells cultured in serum-free medium. *Neurochemistry International.* **42**: 9-17

Hashimoto, S., Anai, H. & Hanada, K. (2016) Mechanisms of interstrand DNA crosslink repair and human disorders. *Genes and Environment.* **38**: 9

Heck, M. M. S. & Eamshaw, W. C. (1986) Topoisomerase II: a specific marker for cell proliferation. *Journal of Cell Biology*. **103**: 2569-2581

Heidari, S., Mehri, S., Shariaty, V. & Hosseinzadeh, H. (2018) Preventive effects of crocin on neuronal damages induced by D-galactose through AGEs and oxidative stress in human neuroblastoma cells (SH-SY5Y). *Journal of Pharmacopuncture*. **21**: 18-25

Heintzman, D. R., Campos, L. V., Byl, J. W., Osheroff, N. & Dewar, J. M. (2019) Topoisomerase II Is Crucial for Fork Convergence during Vertebrate Replication Termination. *Cell Reports.* **29**: 422-436

Heng, X., Jin, G., Zhang, X., Yang, D., Zhu, M., Fu, S., Li, X. & Le, W. (2012) Nurr1 regulates Top IIβ and functions in axon genesis of mesencephalic dopaminergic neurons. *Molecular Neurodegeneration*. ***7***: 4

Herculano-Houzel, S. (2009) The human brain in numbers: a linearly scaled-up primate brain. *Frontiers in Human Neuroscience*. **3**: 31

Herranz, N. & Gil, J. (2018) Mechanisms and functions of cellular senescence. *Journal of Clinical Investigation*. **128**:1238-1246

Hewitt, G., Jurk, D., Marques, F., Correia-Melo, C., Hardy, T., Gackowska, A., Anderson, R., Taschuk, M., Mann, J. & Passos, J. F. (2012) Telomeres are favoured targets of a persistent DNA damage response in ageing and stress-induced senescence. *Nature Communications.* **3:** 708

Ho, P. J., Yen, M. L., Tang, B. C., Chen, C. T. & Yen, B. L. (2013) H2O2 accumulation mediates differentiation capacity alteration, but not proliferative decline, in senescent human fetal mesenchymal stem cells. *Antioxidants & Redox Signaling*. **18**: 1895-1905

Hohl, A. M., Thompson, M., Soshnev, A. A., Wu, J., Morris, J., Hsieh, T. S., Wu, C. T. & Geyer, P. K. (2012) Restoration of topoisomerase 2 function by complementation of defective monomers in Drosophila. *Genetics*. **192**: 843-856

Holmgren, A., Johansson, C., Berndt, C., Lönn, M. E., Hudemann, C. & Lillig, C. H. (2005) Thiol redox control via thioredoxin and glutaredoxin systems. *Biochemical Society Transactions*. **33**: 1375-1377

Hong, Y., Sang, M., Shang, C., Xue, Y. & Liu, Y. (2012) Quantitative analysis of topoisomerase II alpha and evaluation of its effects on cell proliferation and apoptosis in glioblastoma cancer stem cells. *Neuroscience Letters*. **518**: 138-143

Horton, C. D., Qi, Y., Chikaraishi, D. & Wang, J. K. T (2008) Neurotrophin-3 mediates the autocrine survival of the catecholaminergic CAD CNS neuronal cell line. *Journal of Neurochemistry*. **76**: 201-209

Houck, A. L., Seddighi, S. & Driver, J. A. (2018) At the Crossroads Between Neurodegeneration and Cancer: A Review of Overlapping Biology and Its Implications. *Current Aging Science.* **11**: 77-89

Howard, M. K., Burke, L. C., Mailhos, C., Pizzey, A., Gilbert, C. S., Lawson, W. D., Collins, M. K., Thomas, N. S. & Latchman, D.S. (1993) Cell cycle arrest of proliferating neuronal cells by serum deprivation can result in either apoptosis or differentiation. *Journal of Neurochemistry*. **60**: 1783-1791

Huang, S., Laoukili, J., Epping, M. T., Koster, J., Holzel, M., Westerman, B. A., Nijkamp, W., Hata, A., Asgharzadeh, S., Seeger, R. C., Versteeg, R., Beijersbergen, R. L. & Bernards, R. (2009) ZNF423 is critically required for retinoic acid-induced differentiation and is a marker of neuroblastoma outcome. *Cancer Cell*. **15**: 328-340

Huang, H. S., Allen, J. A., Mabb, A. M., King, I. F., Miriyala, J., Taylor-Blake, B., Sciaky, N., Dutton, J. W. Jr., Lee, H. M., Chen, X., Jin, J., Bridges, A. S., Zylka, M. J., Roth, B. L. & Philpot, B. D. (2011) Topoisomerase inhibitors unsilence the dormant allele of Ube3a in neurons. *Nature*. **481**: 185–189

Huang, Y-C., Wang, C-T., Su, T-S., Kao K-W., Lin, Y-J., Chuang, C-C., Chiang, A-S. & Lo, C-C. (2019) A Single-Cell Level and Connectome-Derived Computational Model of the Drosophila Brain. *Frontiers in Neuroinformatics.* **12**: 99

Hutchins, J. B. & Barger, S. W. (1998) Why Neurons Die: Cell Death in the Nervous System. *The Anatomical Record.* **253**: 79-90

Hyde, R. R. (1913) Inheritance of the length of life in Drosophila ampelophila. *Proceedings of the Indiana Academy of Science.* **23**: 113-123

Ide, T., Tsutsui, H., Ohashi, N., Hayashidani, S., Suematsu, N., Tsuchihashi, M., Tamai, H. & Takeshita, A. (2002) Greater oxidative stress in healthy young men compared with premenopausal women. *Arteriosclerosis Thrombosis and Vascular Biology.* **22**: 438-442

Iliadi, K. G. & Boulianne, G. L. (2010) Age-related Behavioral Changes in Drosophila. *Annals of the New York Academy of Sciences*. **1197**: 9-18

Jacobs, A. L. & Schär, P. (2012) DNA glycosylases: in DNA repair and beyond. *Chromosoma*, **121**: 1-20

Jacobson, J., Lambert, A. J., Portero-Otín, M., Pamplona, R., Magwere, T., Miwa, S., Driege, Y., Brand, M. D. & Partridge, L. (2010) Biomarkers of aging in Drosophila. *Aging Cell*. **9**: 466-477

Jain, M., Zhang, L., He, M., Zhang, Y. Q., Shen, M. & Kebebew, E. (2013) TOP2A is overexpressed and is a therapeutic target for adrenocortical carcinoma. *Endocrine-related Cancer*. **20**: 361-370

Jekimovs, C., Bolderson, E., Suraweera, A., Adams, M., O'Byrne, K. J. & Richard, D. J. (2014) Chemotherapeutic compounds targeting the DNA double-strand break repair pathways: the good, the bad, and the promising. *Frontiers in Oncology*. **4**: 86

Jennings, B. H. (2011) Drosophila – a versatile model in biology & medicine. *Materials Today*. **14**: 190-195

Jensen, S., Redwood, C. S., Jenkins, J. R., Andersen, A. H. & Hickson, I. D. (1996) Human DNA topoisomerases II alpha and II beta can functionally substitute for yeast TOP2 in chromosome segregation and recombination. *Molecular Genomics and Genetics*. **252**: 79-86

Jiao, Y., Palmgren, B., Novozhilova, E., Englund Johansson, U., Spieles-Engemann, A. L., Kale, A., Stupp, S. I. & Olivius, P. (2014) BDNF increases survival and neuronal differentiation of human neural precursor cells cotransplanted with a nanofiber gel to the auditory nerve in a rat model of neuronal damage. *BioMed Research International*. **2014**: 356415

Johnson, A. A., Akman, K., Calimport, S. R., Wuttke, D., Stolzing, A. & de Magalhães, J. P. (2012) The role of DNA methylation in aging, rejuvenation, and age-related disease. *Rejuvenation Research*, **15**: 483-494

Johnston, C. A., Beazely, M. A., Bilodeau, M. L., Andrisani, O. & Watts, V. J. (2004) Differentiation-induced alterations in cyclic AMP signaling in the Cath.a differentiated (CAD) neuronal cell line. *Journal of Neurochemistry*. **88**: 1497-1508

Jones, C. J., Rikli, R. E. & Beam, W. C. (1999) A 30-s chair-stand test as a measure of lower body strength in community-residing older adults. *Research Quarterly for Exercise and Sport.* **70**: 113-9

Joshi, R. S., Piña, B. & Roca, J. (2012) Topoisomerase II is required for the production of long Pol II gene transcripts in yeast. *Nucleic Acids Research*. **40**: 7907-7915

Ju, B.G., Lunyak, V.V., Perissi, V., Garcia-Bassets, I., Rose, D.W., Glass, C.K. & Rosenfeld, M.G. (2006) A Topoisomerase II ß-Mediated dsDNA Break Required for Regulated Transcription. *Science* **312**: 1798-1802

Jucker, M., Walker, L.C., Kuo, H., Tian, M. & Ingram, D.K. (1994) Age-related fibrillar deposits in brains of C57BL/6 mice. A review of localization, staining characteristics, and strain specificity. *Molecular Neurobiology*. **9**: 125-133

Juríková, M., Danihel, Ľ., Polák, Š. & Varga, I. (2016) Ki67, PCNA, and MCM proteins: Markers of proliferation in the diagnosis of breast cancer. *Acta Histochemica*. **118**: 544-552

Jurk, D., Wang, C., Miwa, S., Maddick, M., Korolchuk, V., Tsolou, A., Gonos, E. S., Thrasivoulou, C., Saffrey, M. J., Cameron, K. & von Zglinicki, T. (2012) Postmitotic neurons develop a p21-dependent senescence-like phenotype driven by a DNA damage response. *Aging Cell*. **11**: 996-1004

Kaetzel, D. M., Leonard, M. K., Cook, G. S., Novak, M., Jarrett, S. G., Yang, X. & Belkin, A. M. (2015) Dual functions of NME1 in suppression of cell motility and enhancement of genomic stability in melanoma. *Naunyn-Schmiedeberg's Archives of Pharmacology*. **388**: 199-206

Kander, M. C., Cui, Y. & Liu, Z. (2017) Gender difference in oxidative stress: a new look at the mechanisms for cardiovascular diseases. *Journal of Cellular and Molecular Medicine*. **21**: 1024-1032

Kanungo, J. (2012) DNA Repair Defects and DNA-PK in Neurodegeneration. *Cell & Developmental Biology*. **1**: 1000e105

Kenig, S., Faoro, V., Bourkoula, E., Podergajs, N., Ius, T., Vindigni, M., Skrap, M., Lah, T., Cesselli, D., Storici, P. & Vindigni, A. (2016) Topoisomerase IIβ mediates the resistance of glioblastoma stem cells to replication stress-inducing drugs. *Cancer Cell International*. **16**: 58

Kikis, E. A., Gidalevitz, T. & Morimoto, R. I. (2010) Protein homeostasis in models of aging and age-related conformational disease. *Advances in Experimental Medicine and Biology*. **694**: 138-159

Kim, M-J., Oh, S-J., Park, S-H., Kang, H-J., Won, M. H., Kang, T-C., Park, J-B., Kim, J-I., Kim, J. & Yong, Lee, J-Y. (2007) Neuronal loss in primary long-term cortical culture involves neurodegeneration-like cell death via calpain and p35 processing, but not developmental apoptosis or aging. *Experimental and Molecular Medicine*. **39**: 14-26

Kim, S. Y., Kang, H. T., Han, J. A. & Park, S. C (2012) The transcription factor S p1 is responsible for aging-dependent altered nucleocytoplasmic trafficking. *Aging Cell.* **11**: 1102-1109

Kimura, K., Nozaki, N., Enomoto, T., Tanaka, M. & Kikuchi, A. (1996) Analysis of M phase-specific phosphorylation of DNA topoisomerase II. *Journal of Biological Chemistry*. **271**: 21439-21445

King, I. F., Yandava, C. N., Mabb, A. M., Hsiao, J. S., Huang, H. S., Pearson, B. L., Calabrese, J. M., Starmer, J., Parker, J. S., Magnuson, T., Chamberlain, S. J., Philpot, B. D. & Zylka, M. J. (2013) Topoisomerases facilitate transcription of long genes linked to autism. *Nature* **501**: 58-62

Kinner, A., Wu, W., Staudt, C. & Iliakis, G. (2008) Gamma-H2AX in recognition and signaling of DNA double-strand breaks in the context of chromatin. *Nucleic Acids Research* **36**: 5678-5694

Kiyoshima, T., Enoki, N., Kobayashi, I., Sakai, T., Nagata, K., Wada, H., Fujiwara, H., Ookuma, Y. & Sakai, H. (2012) Oxidative stress caused by a low concentration of hydrogen peroxide induces senescence-like changes in mouse gingival fibroblasts. *International Journal of Molecular Medicine*. **30**: 1007-1012

Kondapi, A. K., Mulpuri, N., Mandraju, R., Sasikaran, B. & Subba Rao, K. (2004) Analysis of age dependent changes of Topoisomerase II α and β in rat brain. *International Journal of Developmental Neuroscience.* **22**: 19-30

Korecka, J. A., van Kesteren, R. E., Blaas, E., Spitzer, S. O., Kamstra, J. H., Smit, A. B., Swaab, D. F., Verhaagen, J. & Bossers, K. (2013) Phenotypic characterization of retinoic acid differentiated SH-SY5Y cells by transcriptional profiling. *PloS one*. **8**: e63862

Kornberg, R. D. (1977) Structure of chromatin. *Annual Review of Biochemistry*. **46**: 931-954

Koshland, D. & Strunnikov, A. (1996) Mitotic chromosome condensation. *Annual Review of Cell and Developmental Biology.* **12**: 305-333

Kouzine, F., Gupta, A., Baranello, L., Wojtowicz, D., Ben-Aissa, K., Liu, J., Przytycka, T. M. & Levens, D. (2013) Transcription-dependent dynamic supercoiling is a short-range genomic force. *Nature Structural & Molecular Biology*. **20**: 396-403

Kovalevich, J. & Langford, D. (2013) Considerations for the use of SH-SY5Y neuroblastoma cells in neurobiology. *Methods in Molecular Biology.* **1078**: 9-21

Kraemer, B. R., Snow, J. P., Vollbrecht, P., Pathak, A., Valentine, W. M., Deutch, A. Y. & Carter, B. D. (2014) A role for the p75 neurotrophin receptor in axonal degeneration and apoptosis induced by oxidative stress. *The Journal of Biological Chemistry*. **289**:21205-21216

Krishna, A., Biryukov, M., Trefois, C., Antony, P. M., Hussong, R., Lin, J., Heinäniemi, M., Glusman, G., Köglsberger, S., Boyd, O., van den Berg, B. H., Linke, D., Huang, D., Wang, K., Hood, L., Tholey, A., Schneider, R., Galas, D. J., Balling, R. & May, P. (2014) Systems genomics evaluation of the SH-SY5Y neuroblastoma cell line as a model for Parkinson's disease. *BMC Genomics*. **15**: 1154

Kritsilis, M., V Rizou, S., Koutsoudaki, P. N., Evangelou, K., Gorgoulis, V. G. & Papadopoulos, D. (2018) Ageing, Cellular Senescence and Neurodegenerative Disease. *International Journal of Molecular Sciences*. **19**: 2937

Krokan, H. E. & Bjørås, M. (2013) Base excision repair. *Cold Spring Harbor Perspectives in Biology*. **5**: a012583

Kruse, S. E., Karunadharma, P. P., Basisty, N., Johnson, R., Beyer, R. P., MacCoss, M. J., Rabinovitch, P. S. & Marcinek, D. J. (2016) Age modifies respiratory complex I and protein homeostasis in a muscle type-specific manner. *Aging Cell*. **15**: 89-99

Kubben, N. & Misteli, T. (2017) Shared molecular and cellular mechanisms of premature ageing and ageing-associated diseases. *Nature reviews. Molecular Cell Biology*, **18**: 595-609

Kuilman, T., Michaloglou, C., Mooi, W. J. & Peeper, D. S. (2010) The essence of senescence. *Genes & Development*. **24**: 2463-2479

Kulmala, J. P., Korhonen, M. T., Kuitunen, S., Suominen, H., Heinonen, A., Mikkola, A. & Avela, J. (2014) Which muscles compromise human locomotor performance with age? *Journal of the Royal Society.* **11**: 20140858

Kunstyr, I. & Leuenberger, H-G. W. (1975) Gerontological Data of C57BL/6J Mice. I. Sex Differences in Survival Curves. *Journal of Gerontology.* **30**: 157-162

Kuo, T. H., Fedina, T. Y., Hansen, I., Dreisewerd, K., Dierick, H. A., Yew, J. Y. & Pletcher, S. D. (2012) Insulin signaling mediates sexual attractiveness in Drosophila. *PLoS Genetics*. **8**: e1002684

Kurz, D. J., Decary, S., Hong, Y. & Erusalimsky, J. D. (2000) Senescence-associated β-galactosidase reflects an increase in lysosomal mass during replicative ageing of human endothelial cells. *Journal of Cell Science*. **113**: 3613-3622

Lam, C., Yeung, W. & Law, C. (2017) Global developmental delay and intellectual disability associated with a de novo TOP2B mutation. *Clinica Chimica Acta.* **469**: 63-68

Laponogov, I., Veselkov, D. A., Crevel, I. M., Pan, X. S., Fisher, L. M. & Sanderson, M. R. (2013) Structure of an 'open' clamp type II topoisomerase-DNA complex provides a mechanism for DNA capture and transport. *Nucleic Acids Research*. **41**: 9911-9923

Lazaroff, M., Qi, Y. & Chikaraishi, D. M. (1998) Differentiation of a Catecholaminergic CNS Cell Line Modifies Tyrosine Hydroxylase Transcriptional Regulation. *Journal of Neurochemistry*. **71**: 51-59

Lee, M. T. & Bachant, J. (2009) SUMO modification of DNA topoisomerase II: trying to get a CENse of it all. *DNA Repair*. **8**: 557-568

Lee, K. C., Swan, R. L., Sondka, Z., Padget, K., Cowell, I. G. & Austin, C. A. (2018) Effect of TDP2 on the Level of TOP2-DNA Complexes and SUMOylated TOP2-DNA Complexes. *International Journal of Molecular Sciences*. **19**: 2056

Lee, J. H. & Berger, J. M. (2019) Cell Cycle-Dependent Control and Roles of DNA Topoisomerase II. *Genes*. **10**: 859

Li, Y., Hou, L. X., Aktiv, A. & Dahlström, A. (2007) Studies of the Central Nervous System-Derived CAD Cell Line, a Suitable Model for Intraneuronal Transport Studies? *Journal of Neuroscience Research.* **85**: 2601-2609

Li, H., Wang, Y. & Liu, X. (2008) Plk1-dependent phosphorylation regulates functions of DNA topoisomerase IIα in cell cycle progression. *Journal of Biological Chemistry*. **283**: 6209-6221

Li, Z., Zhang, W., Chen, Y., Guo, W., Zhang, J., Tang, H., Xu, Z., Zhang, H., Tao, Y., Wang, F., Jiang, Y., Sun, F. L. & Mao, Z. (2016) Impaired DNA double-strand break repair contributes to the age-associated rise of genomic instability in humans. *Cell Death and Differentiation*. **23**:1765-1777

Liguori, I., Russo, G., Curcio, F., Bulli, G., Aran, L., Della-Morte, D., Gargiulo, G., Testa, G., Cacciatore, F., Bonaduce, D. & Abete, P. (2018) Oxidative stress, aging, and diseases. *Clinical Interventions in Aging*. **13**: 757-772

Lilienbaum, A. (2013) Relationship between the proteasomal system and autophagy. *International Journal of Biochemistry and Molecular Biology*. **4**: 1-26

Lindberg, O., Walterfang, M., Looi, J. C., Malykhin, N., Ostberg, P., Zandbelt, B., Styner, M., Paniagua, B., Velakoulis, D., Orndahl, E. & Wahlund, L. O. (2012) Hippocampal shape analysis in Alzheimer's disease and frontotemporal lobar degeneration subtypes. *Journal of Alzheimer's Disease.* **30**: 355-365

Lindenboim, L., Diamond, R., Rothenberg, E. & Stein, R.(1995) Apoptosis induced by serum deprivation of PC12 cells is not preceded by growth arrest and can occur at each phase of the cell cycle. *Cancer Research*. **55**: 1242-1247

Linford, N. J., Bilgir, C., Ro, J. & Pletcher, S. D. (2013) Measurement of lifespan in Drosophila melanogaster. *Journal of Visualized Experiments*. **71**: 50068

Ling, D. & Salvaterra, P, M. (2011) Robust RT-qPCR Data Normalization: Validation and Selection of Internal Reference Genes during Post-Experimental Data Analysis. *PloS ONE*. **6**: e17762

Linka, R. M., Porter, A. C. G., Volkov, A., Mielke, C., Boege, F. & Christensen, M. O. (2007) C-Terminal regions of topoisomerase II α and II β determine isoform-specific functioning of the enzymes in vivo. *Nucleic Acids Research* **35**: 3810-3822

Liu, L. F. & Wang, J. C. (1987) Supercoiling of the DNA template during transcription. *Proceedings of the National Academy of Sciences of the United States of America.* **84**: 7024-7027

Liu, L. P, Ni, J. Q, Shi, Y. D., Oakeley, E. J. & Sun, F. L. (2005) Sex-specific role of Drosophila melanogaster HP1 in regulating chromatin structure and gene transcription. *Nature Genetics*. **37**: 1361-1366

Liu, Y.-Y., Nagpure, B. V., Wong, P. T.-H. & Bian, J.-S. (2013) Hydrogen sulfide protects SH-SY5Y neuronal cells against d-galactose induced cell injury by suppression of advanced glycation end products formation and oxidative stress. *Neurochemistry Internationa.* **62**: 603-609

Liu, J-Y., Souroullas, G. P., Diekman, B. O., Krishnamurthy, J., Hall, B. M., Sorrentino, J. A., Parker, J. S., Sessions, G. A., Gudkov, A. V. & Sharpless, N. E (2019) Cells exhibiting strong $p16^{INK4a}$ promoter activation in vivo display features of senescence. *Proceedings of the National Academy of Sciences*. **116**: 2603-2611

Livak, K. J. & Schmittgen, T. D. (2001) Analysis of Relative Gene Expression Data Using Real-Time Quantitative PCR and the 2−ΔΔCT Method. *Methods*. **25**: 402-408

Llinas, R. (1988) The intrinsic electrophysiological properties of mammalian neurons: insights into central nervous system function. *Science.* **242**: 1654-1664

Lok, C. N., Lang, A. J., Mirski, S. E. & Cole, S. P. (2002) Characterization of the human topoisomerase IIbeta (TOP2B) promoter activity: essential roles of the nuclear factor-Y (NF-Y)- and specificity protein-1 (Sp1)-binding sites. *Biochemical Journal*. **368**: 741-751

Lopes, F. M., Schröder, F., Júnior, M. L. C. da F., Zanotto-Filho, A., Müller, C. B., Pire, A. S., Meurer, R. T. M., Colpo, G. D., Gelain, D. P., Kapczinski, F., Moreira, J. C. F., Fernandes, M. da C. & Klamt, F. (2010) Comparison between proliferative and neuron-like SH-SY5Y cells as an in vitro model for Parkinson disease studies. *Brain Research*. **1337**: 85-94

López-Carballo, G., Moreno, L., Masiá, S., Pérez, P. & Barettino, D. (2002) Activation of the Phosphatidylinositol 3-Kinase/Akt Signaling Pathway by Retinoic Acid Is Required for Neural Differentiation of SH-SY5Y Human Neuroblastoma Cells. *The Journal of Biological Chemistry.* **277**: 25297-25304

López-Otín, C., Blasco, M. A., Partridge, L., Serrano, M. & Kroemer, G. (2013) The Hallmarks of Aging. *Cell*. **153**: 1194-1217

Low, R. L., Orton, S. & Friedman, D. B. (2003) A truncated form of DNA topoisomerase IIβ associates with the mtDNA genome in mammalian mitochondria. *European Journal of Biochemistry*. **270**: 4173-4186

Lundgren, C. A. K., Sjöstrand, D., Biner, O., Bennett, M., Rudling, A., Johansson, A., Brzezinski, P., Carlsson, J., von Ballmoos, C. & Högbom, M. (2018) Scavenging of superoxide by a membrane-bound superoxide oxidase. *Nature Chemical Biology*. **14**: 788-793

Lyu, Y. L. & Wang, J. C. (2003) Aberrant lamination in the cerebral cortex of mouse embryos lacking DNA topoisomerase IIβ. *Proceedings of the National Academy of Sciences of the United States of America.* **100**: 7123-7128

Lyu, Y. L., Lin, C. P., Azarova, A. M., Cai, L., Wang, J. C. & Liu, L. F. (2006) Role of topoisomerase IIbeta in the expression of developmentally regulated genes. *Molecular and Cellular Biology*, **26**: 7929-7941

Ma, J. & Wang, M. D. (2016) DNA supercoiling during transcription. *Biophysical Reviews*. **8**: 75-87

Macip, S., Igarashi, M., Fang, L., Chen, A., Pan, Z. Q., Lee, S. W. & Aaronson, S. A. (2002) Inhibition of p21-mediated ROS accumulation can rescue p21-induced senescence. *The EMBO Journal*. **21**: 2180-2188

Madabattula, S. T., Strautman, J. C., Bysice, A. M., O'Sullivan, J. A., Androschuk, A., Rosenfelt, C., Doucet, K., Rouleau, G. & Bolduc, F. (2015) Quantitative Analysis of Climbing Defects in a Drosophila Model of Neurodegenerative Disorders. *Journal of Visualized Experiments.* **100**: e52741

Madabhushi, R., Gao, F., Pfenning, A. R., Pan, L., Yamakawa, S., Seo, J., Rueda, R., Phan, T. X., Yamakawa, H., Pao, P. C., Stott, R. T., Gjoneska, E., Nott, A., Cho, S., Kellis, M. & Tsai, L. H. (2015) Activity-Induced DNA Breaks Govern the Expression of Neuronal Early-Response Genes. *Cell*. **161**: 1592-1605

Madabhushi R. (2018) The Roles of DNA Topoisomerase IIβ in Transcription. *International Journal of Molecular Sciences*. **19**: 1917

Maeda, Y., Tsutsui, K., Tsutsui, K. & Tokunaga, A. (2000) Regional differences in the expression of DNA topoisomerase IIβ in the pyramidal neurons of the rat hippocampus. *Neuroscience Research.* **36**: 291-296

Malick, L. E. & Kidwell, J.F. (1966) The effect of mating status, sex and genotype on longevity in Drosophila melanogaster. *Genetics*. **54**: 203-9

Mamelak, M. (2018) Parkinson's Disease, the Dopaminergic Neuron and Gammahydroxybutyrate. *Neurology and Therapy*. **7**: 5-11

Mamouni, K., Cristini, A., Guirouilh-Barbat, J., Monferran, S., Lemarié, A., Faye, J.-C., Lopez, B. S., Favre, G. & Sordet, O. (2014) RhoB Promotes γH2AX Dephosphorylation and DNA Double-Strand Break Repair. *Molecular and Cellular Biology*. **34**: 3144-3155

Manville, C. M., Smith, K., Sondka, Z., Rance, H., Cockell, S., Cowell, I. G., Lee, K. C., Morris, N. J., Padget, K., Jackson, G. H. & Austin, C. A. (2015) Genome-wide ChIP-seq analysis of human TOP2B occupancy in MCF7 breast cancer epithelial cells. *Biology Open*. **4**: 1436-1447

Mao, Z. & Davis, R. L. (2009) Eight different types of dopaminergic neurons innervate the Drosophila mushroom body neuropil: anatomical and physiological heterogeneity. *Frontiers in Neural Circuits*. **3**: 5

Mao, Z., Tian, X., Van Meter, M., Ke, Z., Gorbunova, V. & Seluanov, A. (2012) Sirtuin 6 (SIRT6) rescues the decline of homologous recombination repair during replicative senescence. *Proceedings of the National Academy of Sciences of the United States of America*. **109**: 11800-11805

Marin, M., Karis, A., Visser, P., Grosveld, F. & Philipsen, S. (1997) Transcription factor Sp1 is essential for early embryonic development but dispensable for cell growth and differentiation. *Cell*. **89**: 619-628

Martínez-Cué, C. & Rueda, N. (2020) Cellular Senescence in Neurodegenerative Diseases. *Frontiers in Cellular Neuroscience.* **14**: 16

Maruyama, W., Strolin Benedetti, M., Takahashi, T. & Naoi, M. (1997) A neurotoxin N-methyl(R)salsolinol induces apoptotic cell death in differentiated human dopaminergic neuroblastoma SH-SY5Y cells. *Neuroscience Letters*. **232**: 147-150

Mata-Garrido, J., Casafont, I., Tapia, O., Berciano, M. T. & Lafarga, M. (2016) Neuronal accumulation of unrepaired DNA in a novel specific chromatin domain: structural, molecular and transcriptional characterization. *Acta Neuropathologica Communications*. **4**: 41

Mattson, M. P. & Magnus, T. (2006) Ageing and neuronal vulnerability. *Nature Reviews. Neuroscience*. **7**: 278-294

Matzel, L. D., Grossman, H., Light, K., Townsend, D. & Kolata, S. (2008) Age-related declines in general cognitive abilities of Balb/C mice are associated with disparities in working memory, body weight, and general activity. *Learning & Memory.* **15**: 733-746

Maynard, S., Schurman, S. H., Harboe, C., de Souza-Pinto, N. C. & Bohr, V. A. (2009) Base excision repair of oxidative DNA damage and association with cancer and aging. *Carcinogenesis*. **30**: 2-10

McKinnon P. J. (2004) ATM and ataxia telangiectasia. *EMBO Reports*. **5**: 772-776

McKinnon P. J. (2016) Topoisomerases and the regulation of neural function. *Nature Reviews Neuroscience*. **17**: 673-679

McClendon, A.K., Rodriguez, A.C. & Osheroff, N. (2005) Human topoisomerase IIα rapidly relaxes positively supercoiled DNA: implications for enzyme action ahead of replication forks. *The Journal of Biological Chemistry*. **280**: 39337-39345

McClendon, A. K. & Osheroff, N. (2007) DNA topoisomerase II, genotoxicity, and cancer. *Mutation Research*. **623**: 83-97

McLaughlin, S. H. & Bulleid, N. J. (1998) Thiol-independent interaction of protein disulphide isomerase with type X collagen during intra-cellular folding and assembly. *The Biochemical Journal*. **331**: 793-800

McNamara, S., Wang, H., Hanna, N. & Miller, W. H., Jr (2008) Topoisomerase IIbeta negatively modulates retinoic acid receptor alpha function: a novel mechanism of retinoic acid resistance. *Molecular and Cellular Biology*. **28**: 2066-2077

McPhee, J. S., French, D. P., Jackson, D., Nazroo, J., Pendleton, N. & Degens, H. (2016) Physical activity in older age: perspectives for healthy ageing and frailty. *Biogerontology*. **17**: 567-580

Meczes, E. L., Gilroy, K. L., West, K. L. & Austin, C. A. (2008) The impact of the human DNA topoisomerase II C-terminal domain on activity. *PloS one*. **3**: e1754

Mehta, A. & Haber, J. E. (2014) Sources of DNA double-strand breaks and models of recombinational DNA repair. *Cold Spring Harbor Perspectives in Biology*. **6**: a016428

Mengoli, V., Bucciarelli, E., Lattao, R., Piergentili, R., Gatti, M. & Bonaccorsi, S. (2014) The analysis of mutant alleles of different strength reveals multiple functions of topoisomerase 2 in regulation of Drosophila chromosome structure. *PLoS Genetics*. **10**: e1004739

Meyer, K. N., Kjeldsen, E., Straub, T., Knudsen, B. R., Hickson, I. D., Kikuchi, A., Kreipe, H. & Boege, F. (1997) Cell cycle-coupled relocation of types I and II topoisomerases and modulation of catalytic enzyme activities. *Journal of Cell Biology.* **136**: 775-88

Meyer, J. N., Boyd, W. A., Azzam, G. A., Haugen, A. C., Freedman, J. H. & Van Houten, B. (2007) Decline of nucleotide excision repair capacity in aging Caenorhabditis elegans. *Genome Biology*. **8**: R70

Miller, K. G., Liu, L. F. & Englund, P. T. (1981) A Homogeneous Type I1 DNA Topoisomerase from HeLa Cell Nuclei. *The Journal of Biological Chemistry*. **256**: 9334-9339

Miller, F. D. & Kaplan, D. R. (2001) Neurotrophin signalling pathways regulating neuronal apoptosis. *Cellular and Molecular Life Sciences*. **58**: 1045-53

Minichiello, L. (2009) TrkB signalling pathways in LTP and learning. *Nature Reviews Neuroscience.* **10:** 850-860

Mirski, S. E. L., Gerlach, J. H. & Cole, S. P. C. (1999) Sequence Determinants of Nuclear Localization in the α and β Isoforms of Human Topoisomerase II. *Experimental Cell Research*. **251**: 329-339

Mitchell, S. J., Scheibye-Knudsen, M., Longo, D. L. & Cabo, R. de (2015) Animal Models of Aging Research: Implications for Human Aging and Age-Related Diseases. *Annual Review of Animal Biosciences.* **3**: 283-303

Moldogazieva, N. T., Mokhosoev, I. M., Mel'nikova, T. I., Porozov, Y. B. & Terentiev, A. A. (2019) Oxidative Stress and Advanced Lipoxidation and Glycation End Products (ALEs and AGEs) in Aging and Age-Related Diseases. *Oxidative Medicine and Cellular Longevity.* **2019**: 3085756

Mondal, N., Zhang, Y., Jonsson, Z., Dhar, S. K., Kannapiran, M. & Parvin, J. D. (2003) Elongation by RNA polymerase II on chromatin templates requires topoisomerase activity. *Nucleic Acids Research*. **31**: 5016-5024

Monje, M. (2018) Myelin Plasticity and Nervous System Function. *Annual Review of Neuroscience*. **41**: 6176

Moon, S. H., Nguyen, T. A., Darlington, Y., Lu, X. & Donehower, L. A. (2010) Dephosphorylation of γ-H2AX by WIP1: an important homeostatic regulatory event in DNA repair and cell cycle control. *Cell Cycle*. **9**: 2092-2096

Moore, L. D., Le, T. & Fan, G. (2013) DNA methylation and its basic function. *Neuropsychopharmacology*. **38**: 23-38

Moreno-Blas, D., Gorostieta-Salas, E., Pommer-Alba, A., Muciño-Hernández, G., Gerónimo-Olvera, C., Maciel-Barón, L. A., Konigsberg, M., Massieu, L. & Castro-Obregón, S. (2019) Cortical neurons develop a senescence-like phenotype promoted by dysfunctional autophagy. *Aging*. **11**: 6175-6198

Moreno-García, A., Kun, A., Calero, O., Medina, M. & Calero, M. (2018) An Overview of the Role of Lipofuscin in Age-Related Neurodegeneration. *Frontiers in Neuroscience*. **12**: 464

Morimoto, S., Tsuda, M., Bunch, H., Sasanuma, H., Austin, C. & Takeda, S. (2019) Type II DNA Topoisomerases Cause Spontaneous Double-Strand Breaks in Genomic DNA. *Genes*. **10**: 868

Morotomi-Yano, K., Saito, S., Adachi, N. & Yano, K. (2018) Dynamic behaviour of DNA topoisomerase IIβ in response to DNA double-strand breaks. *Scientific Reports.* **8**: 10344

Morris-Hanon, O., Furmento, V. A., Rodríguez-Varela, M. S., Mucci, S., Fernandez-Espinosa, D. D., Romorini, L., Sevlever, G. E., Scassa, M. E. & Videla-Richardson, G. A. (2017) The Cell Cycle Inhibitors $p21^{Cip1}$ and $p27^{Kip1}$ Control Proliferation but Enhance DNA Damage Resistance of Glioma Stem Cells. *Neoplasia.* **19**: 519-529

Mu, Y. & Gage, F. H. (2011) Adult hippocampal neurogenesis and its role in Alzheimer's disease. *Molecular Neurodegeneration*. **6**: 85

Nakabeppu, Y. (2014) Cellular levels of 8-oxoguanine in either DNA or the nucleotide pool play pivotal roles in carcinogenesis and survival of cancer cells. *International Journal of Molecular Sciences*. **15**: 12543-12557

Nakada, S., Chen, G. I., Gingras, A. C. & Durocher, D. (2008) PP4 is a gamma H2AX phosphatase required for recovery from the DNA damage checkpoint. *EMBO Reports*. **9**: 1019-1026

Nakazawa, N., Arakawa, O., Ebe, M. & Yanagida, M. (2019) Casein kinase II-dependent phosphorylation of DNA topoisomerase II suppresses the effect of a catalytic topo II inhibitor, ICRF-193, in fission yeast. *The Journal of Biological Chemistry*. **294**: 3772-3782

Namsi, A., Nury, T., Hamdouni, H., Yammine, A., Vejux, A., Vervandier-Fasseur, D., Latruffe, N., Masmoudi-Kouki, O. & Lizard, G. (2018) Induction of Neuronal Differentiation of Murine N2a Cells by Two Polyphenols Present in the Mediterranean Diet Mimicking Neurotrophins Activities: Resveratrol and Apigenin. *Diseases*. **6**: 67

Naughton, C., Avlonitis, N., Corless, S., Prendergast, J. G., Mati, I. K., Eijk, P. P., Cockroft, S. L., Bradley, M., Ylstra, B. & Gilbert, N. (2013) Transcription forms and remodels supercoiling domains unfolding large-scale chromatin structures. *Nature Structural & Molecular Biology*. **20**: 387-395

Neale, B. M., Kou, Y., Liu, L., Ma'ayan, A., Samocha, K. E., Sabo, A., Lin, C. F., Stevens, C., Wang, L. S., Makarov, V., Polak, P., Yoon, S., Maguire, J., Crawford, E. L., Campbell, N. G., Geller, E. T., Valladares, O., Schafer, C., Liu, H., Zhao, T., Cai, G., Lihm, J., Dannenfelser, R., Jabado, O., Peralta, Z., Nagaswamy, U., Muzny, D., Reid, J. G., Newsham, I., Wu, Y., Lewis, L., Han, Y., Voight, B. F., Lim, E., Rossin, E., Kirby, A., Flannick, J., Fromer, M., Shakir, K., Fennell, T., Garimella, K., Banks, E., Poplin, R., Gabriel, S., DePristo, M., Wimbish, J. R., Boone, B. E., Levy, S. E., Betancur, C., Sunyaev, S., Boerwinkle, E., Buxbaum, J. D., Cook, E. H., Devlin, B., Gibbs, R. A., Roeder, K., Schellenberg, G. D., Sutcliffe, J. S. & Daly, M. J. (2012) Patterns and rates of exonic de novo mutations in autism spectrum disorders. *Nature*. **485**: 242-245

Negritto, M. C. (2010) Repairing Double-Strand DNA Breaks. *Nature Education.* **3**: 26

Nitiss J. L. (2009) DNA topoisomerase II and its growing repertoire of biological functions. *Nature Reviews. Cancer*. **9**: 327-337

Nopparat, C., Sinjanakhom, P. & Govitrapong, P. (2017) Melatonin reverses H2 O2 -induced senescence in SH-SY5Y cells by enhancing autophagy via sirtuin 1

deacetylation of the RelA/p65 subunit of NF-κB. *Journal of Pineal Research*. **63**: e12407

Nur-E-Kamal, A., Meiners, S., Ahmed, I., Azarova, A., Lin, C., Lyu, Y. L. & Liu, L. F. (2007) Role of DNA topoisomerase IIβ in neurite outgrowth. *Brain Research.* **1154**: 50-60

Nykjaer, A., Willnow, T. E. & Petersen, C. M. (2005) p75NTR – live or let die. *Current Opinion in Neurobiology*. **15**: 49-57

O'Hagan, H. M., Wang, W., Sen, S., Destefano Shields, C., Lee, S. S., Zhang, Y. W., Clements, E. G., Cai, Y., Van Neste, L., Easwaran, H., Casero, R. A., Sears, C. L. & Baylin, S. B. (2011) Oxidative damage targets complexes containing DNA methyltransferases, SIRT1, and polycomb members to promoter CpG Islands. *Cancer Cell*. **20**: 606-619

Oka, A., Takashima, S., Abe, M., Araki, R. & Takeshita, K. (2000) Expression of DNA-dependent protein kinase catalytic subunit and Ku80 in developing human brains: implication of DNA-repair in neurogenesis. *Neuroscience Letters.* **292**: 167-170

Oktay, K., Turan, V., Titus, S., Stobezki, R. & Liu, L. (2015) BRCA Mutations, DNA Repair Deficiency, and Ovarian Aging. *Biology of Reproduction*. **93**: 67

Onoda, A., Hosoya, O., Sano, K., Kiyama, K., Kimura, H., Kawano, S., Furuta, R., Miyaji, M., Tsutsui, K. & Tsutsui, K. M. (2014) Nuclear dynamics of topoisomerase IIβ reflects its catalytic activity that is regulated by binding of RNA to the C-terminal domain. *Nucleic Acids Research*. **42**: 9005-9020

Orso, G., Martinuzzi, A., Rossetto, M. G., Sartori, E., Feany, M. & Daga, A. (2005) Disease-related phenotypes in a Drosophila model of hereditary spastic paraplegia are ameliorated by treatment with vinblastine. *The Journal of Clinical Investigation*. **115**: 3026-3034

Oudes, A., Herr, C., Olsen, Y. & Fleming, J. (1998) Age-dependent accumulation of advanced glycation end-products in adult Drosophila melanogaster. *Mechanisms of Ageing and Development*. **100**: 221-229

Overton, K. W., Spencer, S. L., Noderer, W. L., Meyer, T. & Wang, C. L. (2014) Basal p21 controls population heterogeneity in cycling and quiescent cell cycle

states. *Proceedings of the National Academy of Sciences of the United States of America*. **111**: E4386-E4393

Pacifico, R., MacMullen, C. M., Walkinshaw, E., Zhang, X. & Davis, R. L. (2018) Brain transcriptome changes in the aging Drosophila melanogaster accompany olfactory memory performance deficits. *PloS one*. **13**: e0209405

Padget, K., Pearson, A. & Austin, C. (2000) Quantitation of DNA topoisomerase IIα and β in human leukaemia cells by immunoblotting. *Leukemia*. **14**: 1997-2005

Påhlman, S., Ruusala, A. I., Abrahamsson, L., Mattsson, M. E. & Esscher, T. (1984) Retinoic Acid-Induced Differentiation of Cultured Human Neuroblastoma Cells: A Comparison With Phorbolester-Induced Differentiation. *Cell Differentiation.* **14**: 135-44

Parkinson, G. M., Dayas, C. V. & Smith, D. W. (2015) Age-related gene expression changes in substantia nigra dopamine neurons of the rat. *Mechanisms of Ageing and Development*. **149**: 41-49

Partridge L. (2010) The new biology of ageing. *Philosophical transactions of the Royal Society of London. Series B, Biological sciences*. **365**: 147-154

Patil, M., Pabla, N. & Zheng Dong (2013) Checkpoint kinase 1 in DNA damage response and cell cycle regulation. *Cellular and Molecular Life Sciences*. **70**: 4009-4021

Paull, T. T., Rogakou, E. P., Yamazaki, V., Kirchgessner, C. U., Gellert, M. & Bonner, W. M. (2000) A critical role for histone H2AX in recruitment of repair factors to nuclear foci after DNA damage. *Current Biology*. **10**: 886-895

Payne, B. A. & Chinnery, P. F. (2015) Mitochondrial dysfunction in aging: Much progress but many unresolved questions. *Biochimica et Biophysica Acta*. **1847**: 1347-1353

Pérez-Garijo, A. & Steller, H. (2014) The benefits of aging: cellular senescence in normal development. *The EMBO Journal*. **33**: 99-100

Petrov, P., Drake, F. H., Loranger, A., Huang, W. & Hancock R. (1993) Localization of DNA topoisomerase II in Chinese hamster fibroblasts by confocal and electron microscopy. *Experimental Cell Research*. **204**: 73-78

Piechota, M., Sunderland, P., Wysocka, A., Nalberczak, M., Sliwinska, M. A., Radwanska, K. & Sikora, E. (2016) Is senescence-associated β-galactosidase a marker of neuronal senescence? *Oncotarget*. ***7***: 81099-81109

Piper, M. D. W. & Partridge, L. (2018) Drosophila as a model for ageing. *Biochimica et Biophysica Acta*. **1864**: 2707-2717

Podhorecka, M., Skladanowski, A. & Bozko, P. (2010) H2AX Phosphorylation: Its Role in DNA Damage Response and Cancer Therapy. *Journal of Nucleic Acids*. **2010**: 920161

Pommier, Y., Sun, Y., Huang, S. & Nitiss. J. (2016) Roles of eukaryotic topoisomerases in transcription, replication and genomic stability. *Nature Reviews Molecular Cell Biology*. **17**: 703-721

Postow, L., Crisona, N. J., Peter, B. J., Hardy, C. D. & Cozzarelli, N. R. (2001) Topological challenges to DNA replication: Conformations at the fork. *Proceedings of the National Academy of Sciences*. **98**: 8219-8226

Prasad, R. & Jho, E. H. (2019) A concise review of human brain methylome during aging and neurodegenerative diseases. *BMB Reports*. **52**: 577-588

Pustovalova, M., Grekhova, A., Astrelina, T., Nikitina, V., Dobrovolskaya, E., Suchkova, Y., Kobzeva, I., Usupzhanova, D., Vorobyeva, N., Samoylov, A., Bushmanov, A., Ozerov, I. V., Zhavoronkov, A., Leonov, S., Klokov, D. & Osipov, A. N. (2016) Accumulation of spontaneous γH2AX foci in long-term cultured mesenchymal stromal cells. *Aging*. **8**: 3498-3506

Puts, G. S., Leonard, M. K., Pamidimukkala, N. V., Snyder, D. E. & Kaetzel, D. M. (2017) Nuclear functions of NME proteins. *Laboratory Investigation; A Journal of Technical Methods and Pathology*. **98**: 211-218

Qi, Y., Wang, J. K., McMillian, M. & Chikaraishi, D. M. (1997) Characterization of a CNS cell line, CAD, in which morphological differentiation is initiated by serum deprivation. *The Journal of Neuroscience*. **17**: 1217-1225

Qiao, J., Paul, P., Lee, S., Qiao, L., Josifi, E., Tiao, J. R. & Chung, D. H. (2012) PI3K/AKT and ERK regulate retinoic acid-induced neuroblastoma cellular differentiation. *Biochemical and Biophysical Research Communications*. **424**: 421-426

Qiu, J., Dunbar, D. R., Noble, J., Cairns, C., Carter, R., Kelly, V., Chapman, K. E., Seckl, J. R. & Yau, J. L. (2016) Decreased Npas4 and Arc mRNA Levels in the Hippocampus of Aged Memory-Impaired Wild-Type But Not Memory Preserved 11β-HSD1 Deficient Mice. *Journal of Neuroendocrinology*. **28**: n/a

Racko, D., Benedetti, F., Dorier, J. & Stasiak, A. (2018) Transcription-induced supercoiling as the driving force of chromatin loop extrusion during formation of TADs in interphase chromosomes. *Nucleic Acids Research*. **46**: 1648-1660

Raffaghello, L., Lee, C., Safdie, F. M., Wei, M., Madia, F., Bianchi, G. & Longo, V. D. (2008) Starvation-dependent differential stress resistance protects normal but not cancer cells against high-dose chemotherapy. *Proceedings of the National Academy of Sciences.* **105**: 8215-8220

Raghuram, G. V. & Mishra, P. K. (2014) Stress induced premature senescence: a new culprit in ovarian tumorigenesis? *The Indian Journal of Medical Research*. **140**: S120-S129

Rahimi, V. B., Askari, V. R. & Mousavi, S. H. (2018) Ellagic acid reveals promising anti-aging effects against d-galactose-induced aging on human neuroblastoma cell line, SH-SY5Y: A mechanistic study. *Biomedicine & Pharmacotherapy*. **108**: 1712-1724

Ramalingam, M. & Kim, S. (2014) The role of insulin against hydrogen peroxide-induced oxidative damages in differentiated SH-SY5Y cells. *Journal of Receptors and Signal Transduction*. **34**: 212-220

Ramamoorthi, K., Fropf, R., Belfort, G. M., Fitzmaurice, H. L., McKinney, R. M., Neve, R. L., Otto, T. & Lin, Y. (2011) Npas4 regulates a transcriptional program in CA3 required for contextual memory formation. *Science.* **334**: 1669-1675

Ramocki, M. B. & Zoghbi, H. Y. (2008) Failure of neuronal homeostasis results in common neuropsychiatric phenotypes. *Nature.* **455**: 912-918

Ramsey, C. P., Glass, C. A., Montgomery, M. B., Lindl, K. A., Ritson, G. P., Chia, L. A., Hamilton, R. L., Chu, C. T. & Jordan-Sciutto, K. L. (2007) Expression of Nrf2 in neurodegenerative diseases. *Journal of Neuropathology and Experimental Neurology*. **66**: 75-85

Rando, O. J. (2012) Combinatorial complexity in chromatin structure and function: revisiting the histone code. *Current Opinion in Genetics & Development*. **22**: 148-155

Rao, T., Gao, R., Takada, S., Al Abo, M., Chen, X., Walters, K. J., Pommier, Y. & Aihara, H. (2016) Novel TDP2-ubiquitin interactions and their importance for the repair of topoisomerase II-mediated DNA damage. *Nucleic Acids Research*. **44**: 10201-10215

Ray, S., Panova, T., Miller, G., Volkov, A., Porter, A. C. G., Russell, J., Panov, K. I. & Zomerdijk, J. C. B. M. (2013) Topoisomerase IIa promotes activation of RNA polymerase I transcription by facilitating pre-initiation complex formation. *Nature Communications*. **4**: 1598

Redona, C., Pilch, D., Rogakou, E., Sedelnikova, O., Newrock, K. & Bonner, W. (2002) Histone H2A variants H2AX and H2AZ. *Current Opinion in Genetics & Development.* **12**: 162-169

Regan, J. C., Khericha, M., Dobson, A. J., Bolukbasi, E., Rattanavirotkul, N. & Partridge, L. (2016) Sex difference in pathology of the ageing gut mediates the greater response of female lifespan to dietary restriction. *eLife.* **5**: e10956

Riccio, A. A., Schellenberg, M. J. & Williams, R. S. (2019) Molecular mechanisms of topoisomerase 2 DNA–protein crosslink resolution. *Cellular and Molecular Life Sciences.* **77**:81-91

Riessland, M., Kolisnyk, B., Kim, T. W., Cheng, J., Ni, J., Pearson, J. A., Park, E. J., Dam, K., Acehan, D., Ramos-Espiritu, L. S., Wang, W., Zhang, J., Shim, J-W., Ciceri, G., Brichta, L., Studer, L. & Greengard, P. (2019) Loss of SATB1 Induces a p21 Dependent Cellular Senescence Phenotype in Dopaminergic Neurons. *Cell Stem Cell.* **25**: 514-530

Rikli, R. & Jones, C. (1998) The reliability and validity of a 6-min walk test as a measure of physical endurance in older adults. *Journal of Ageing and Physical Activity*. **6**: 363-375

Rogakou, E. P., Pilch, D. R., Orr, A. H., Ivanova, V. S. & Bonner, W. M. (1998) DNA double-stranded breaks induce histone H2AX phosphorylation on serine 139. The *Journal of Biological Chemistry.* **273**: 5858-5868

Rogakou, E. P., Boon, C., Redon, C. & Bonner, W. M. (1999) Megabase chromatin domains involved in DNA double-strand breaks in vivo. *The Journal of Cell Biology*. **146**: 905-916

Rogina, B., Wolverton, T., Bross, T. G., Chen, K., Müller, H. G. & Carey, J. R. (2007) Distinct biological epochs in the reproductive life of female Drosophila melanogaster. *Mechanisms of Ageing and Development*. **128**: 477-485

Ronnett, G. V., Hester, L. D., Nye, J. S. & Snyder, S. H. (1994) Human cerebral cortical cell lines from patients with unilateral megalencephaly and Rasmussen's encephalitis. *Neuroscience*. **63**: 1081-1099

Rübe, C. E., Fricke, A., Widmann, T. A., Fürst, T., Madry, H., Pfreundschuh, M. & Rübe, C. (2011) Accumulation of DNA damage in hematopoietic stem and progenitor cells during human aging. *PloS One*. **6**: e17487

Rutledge, R. G. & Côté, C. (2003) Mathematics of quantitative kinetic PCR and the application of standard curves. *Nucleic Acids Research*. **31**: e93

Saffer, J. D., Jackson, S. P. & Annarella, M. B. (1991) Developmental expression of Sp1 in the mouse. *Molecular and Cellular Biology*. **11**: 2189-2199

Şahin, S., Işık Gönül, İ., Çakır, A., Seçkin, S. & Uluoğlu, Ö. (2016) Clinicopathological Significance of the Proliferation Markers Ki67, RacGAP1, and Topoisomerase 2 Alpha in Breast Cancer. *International Journal of Surgical Pathology*. **24**: 607-613

Salminen, A., Kauppinen, A. & Kaarniranta, K. (2012) Emerging role of NF-κB signaling in the induction of senescence-associated secretory phenotype (SASP). *Cellular Signalling*. **24**: 835-45

Sasaki, T., Senda, M., Kim, S., Kojima, S. & Kubodera, A. (2001) Age-related changes of glutathione content, glucose transport and metabolism, and mitochondrial electron transfer function in mouse brain. *Nuclear Medicine and Biology.* **28**:25-31

Schärer, O. D. (2013) Nucleotide excision repair in eukaryotes. *Cold Spring Harbor Perspectives in Biology*. **5**: a012609

Schein, J. C., Wang, J. K. T. & Roffler-Tarlov, S. K. (2005) The effect of GIRK2wv on neurite growth, protein expression, and viability in the CNS-derived neuronal cell line, CATH.A-differentiated. *Neuroscience*. **134**: 21-32

Schieber, M. & Chandel, N. S. (2014) ROS function in redox signaling and oxidative stress. *Current Biology.* **24**: R453-R462

Schmidt, B. H., Osheroff, N. & Berger, J. M. (2012) Structure of a topoisomerase II-DNA-nucleotide complex reveals a new control mechanism for ATPase activity. *Nature Structural & Molecular Biology*. **19**: 1147-1154

Schneider, L., Giordano, S., Zelickson, B. R., S Johnson, M., A Benavides, G., Ouyang, X., Fineberg, N., Darley-Usmar, V. M. & Zhang, J. (2011) Differentiation of SH-SY5Y

cells to a neuronal phenotype changes cellular bioenergetics and the response to oxidative stress. *Free Radical Biology & Medicine*. **51**: 2007-2017

Schneider, L., Pellegatta, S., Favaro, R., Pisati, F., Roncaglia, P., Testa, G., Nicolis, S. K., Finocchiaro, G. & d'Adda di Fagagna, F. (2013) DNA damage in mammalian neural stem cells leads to astrocytic differentiation mediated by BMP2 signaling through JAK-STAT. *Stem Cell Reports*. **1**: 123-138

Schoeffler, A. J. & Berger, J. M. (2008) DNA topoisomerases: harnessing and constraining energy to govern chromosome topology. *Quarterly Reviews of Biophysics*. **41**: 41-101

Schulz, J, B., Lindenau, J., Seyfried, J. & Dichgans, J. (2001) Glutathione, oxidative stress and neurodegeneration. *European Journal of Biochemistry*. **267**: 4904-4911

Schwanhäusser, B., Busse, D., Li, N., Dittmar, G., Schuchhardt, J., Wolf, J., Chen, W. & Selbach, M. (2011) Global quantification of mammalian gene expression control. *Nature*. **473**: 337-342

Sedelnikova, O. A., Horikawa, I., Zimonjic, D. B., Popescu, N. C., Bonner, W. M. & Barrett, J. C. (2004) Senescing human cells and ageing mice accumulate DNA lesions with unrepairable double-strand breaks. *Nature Cell Biology*. **6**: 168-170

Seluanov, A., Mittelman, D., Pereira-Smith, O. M., Wilson, J. H. & Gorbunova, V. (2004) DNA end joining becomes less efficient and more error-prone during cellular senescence. *Proceedings of the National Academy of Sciences*. **101**: 7624-7629

Sengupta, T., Mukherjee, M., Mandal, C., Das, A. & Majumder, H. K. (2003) Functional dissection of the C-terminal domain of type II DNA topoisomerase from the kinetoplastid hemoflagellate Leishmania donovani. *Nucleic Acids Research*. **31:** 5305-5316

Seo, J., Kim, S. C., Lee, H. S., Kim, J. K., Shon, H. J., Salleh, N. L., Desai, K. V., Lee, J. H., Kang, E. S., Kim, J. S. & Choi, J. K. (2012) Genome-wide profiles of H2AX and γ-H2AX differentiate endogenous and exogenous DNA damage hotspots in human cells. *Nucleic Acids Research*. **40**: 5965-5974

Service, P. M. (1989) The effect of mating status on lifespan, egg laying, and starvation resistance in Drosophila melanogaster in relation to selection on longevity. *Journal of Insect Physiology*. **35**: 447-452

Shamu, C. E. & Murray, A. W. (1992) Sister chromatid separation in frog extracts requires topoisomerase II activity during anaphase. *The Journal of Cell Biology*. **117**: 921-934

Shanbhag, N. M., Evans, M. D., Mao, W., Nana, A. L., Seeley, W. W., Adame, A., Rissman, R. A., Masliah, E. & Mucke, L. (2019) Early neuronal accumulation of DNA double strand breaks in Alzheimer's disease. *Acta Neuropathologica Communications*. **7**: 77

Sharow, K. A., Temkin, B. & Asson-Batres, M. A. (2012) Retinoic acid stability in stem cell cultures. *The International Journal of Developmental Biology*. **56**: 273-278

Shay, K. P., Moreau, R. F., Smith, E. J. & Hagen, T. M. (2008) Is alpha-lipoic acid a scavenger of reactive oxygen species in vivo? Evidence for its initiation of stress signaling pathways that promote endogenous antioxidant capacity. *IUBMB Life*. **60**: 362-367

Shin, H., Kwon, H., Lee, J., Anwar, M. A. & Choi, S. (2016) Etoposide induced cytotoxicity mediated by ROS and ERK in human kidney proximal tubule cells. *Scientific Reports.* **6**: 34064

Shipley, M. M., Mangold, C. A. & Szpara, M. L. (2016) Differentiation of the SH-SY5Y Human Neuroblastoma Cell Line. *Journal of Visualized Experiments.* **108**: 53193

Singh, R., Barden, A., Mori, T. & Beilin, L. (2001) Advanced glycation end-products: a review. *Diabetologia* **44**: 129-146

Snezhkina, A. V., Kudryavtseva, A. V., Kardymon, O. L., Savvateeva, M. V., Melnikova, N. V., Krasnov, G. S. & Dmitriev, A. A. (2019) ROS Generation and Antioxidant Defense Systems in Normal and Malignant Cells. *Oxidative Medicine and Cellular Longevity*. **2019**: 1-17

Sobek, S. & Boege, F. (2014) DNA topoisomerases in mtDNA maintenance and ageing *Experimental Gerontology*. **56**: 135-141

Soskic, V., Groebe, K. & Schrattenholz, A. (2008) Nonenzymatic posttranslational protein modifications in ageing. *Experimental Gerontology*. **43**: 247-257

Soti, C. & Csermely, P. (2003) Aging and molecular chaperones. *Experimental Gerontology*. **38**: 1037-1040

Sousa, A., Meyer, K. A., Santpere, G., Gulden, F. O. & Sestan, N. (2017) Evolution of the Human Nervous System Function, Structure, and Development. *Cell*. **170**: 226-247

Srinivas, U. S., Tan, B., Vellayappan, B. A. & Jeyasekharan, A. D. (2019) ROS and the DNA damage response in cancer. *Redox Biology*. **25**: 101084

Stein, D. & Toiber, D. (2017) DNA damage and neurodegeneration: the unusual suspect. *Neural Regeneration Research*. **12**: 1441-144

Stepanenko, A. A. & Dmitrenko, V. V. (2015) Pitfalls of the MTT assay: Direct and off-target effects of inhibitors can result in over/underestimation of cell viability. *Gene*. **574**: 193-203

Sun, Y., Yolitz, J., Wang, C., Spangler, E., Zhan, M. & Zou, S. (2013) Aging studies in Drosophila melanogaster. *Methods in Molecular Biology*. **1048**: 77-93

Sun, X. & Lin, Y. (2016) Npas4: Linking Neuronal Activity to Memory. *Trends in Neurosciences*. **39**:264-275

Sun, L., Yu, R. & Dang, W. (2018) Chromatin Architectural Changes during Cellular Senescence and Aging. *Genes*. **9**: 211

Swain, U. & Subba Rao, K. (2011) Study of DNA damage via the comet assay and base excision repair activities in rat brain neurons and astrocytes during aging. *Mechanisms of Ageing and Development*. **132**: 374-381

Sweeney, P., Park, H., Baumann, M., Dunlop, J., Frydman, J., Kopito, R., McCampbell, A., Leblanc, G., Venkateswaran, A., Nurmi, A. & Hodgson, R. (2017) Protein misfolding in neurodegenerative diseases: implications and strategies. *Translational Neurodegeneration*. **6**: 6

Tan, K. B., Dorman, T. E., Falls, K. M., Chung, T. D. Y., Mirabelli, C. K., Crooke, S. T. & Mao, J. (1992) Topoisomerase IIα and Topoisomerase IIβ Genes: Characterization and Mapping to Human Chromosomes 17 and 3, Respectively. *Cancer Research* **52**: 231-234

Tanic, N., Perovic, M., Mladenovic, A., Ruzdijic, S. & Kanazir, S. (2007) Effects of aging, dietary restriction and glucocorticoid treatment on housekeeping gene expression in rat cortex and hippocampus—Evaluation by real time RT-PCR. *Journal of Molecular Neuroscience*. **32**: 38-46

Taylor, S., Wakem, M., Dijkman, G., Alsarraj, M. & Nguyen, M. (2010) A practical approach to RT-qPCR—Publishing data that conform to the MIQE guidelines. *Elsevier Methods.* **50**: S1-S5

Terzioglu-Usak, S., Negis, Y., Karabulut, D. S., Zaim, M. & Isik, S. (2017) Cellular Model of Alzheimer's Disease: Aβ1-42 Peptide Induces Amyloid Deposition and a Decrease in Topo Isomerase IIβ and Nurr1 Expression. *Current Alzheimer Research.* **14**: 636-644

Thakurela, S., Garding, A, Jung, J., Schübeler, D., Burger, L. & Tiwari, V. K. (2013) Gene regulation and priming by topoisomerase IIα in embryonic stem cells. *Nature Communications*. **4**:2478

Thomas, A., Lee, P. J., Dalton, J. E., Nomie, K. J., Stoica, L., Costa-Mattioli, M., Chang, P., Nuzhdin, S., Arbeitman, M. N. & Dierick, H. A. (2012) A versatile method for cell-specific profiling of translated mRNAs in Drosophila. *PloS one.* **7**: e40276

Tian, X., Zhu, M., Li, L. & Wu, C. (2013) Identifying protein-protein interaction in Drosophila adult heads by Tandem Affinity Purification (TAP). *Journal of Visualized Experiments.* **82**: 50968

Titus, S., Li, F., Stobezki, R., Akula, K., Unsal, E., Jeong, K., Dickler, M., Robson, M., Moy, F., Goswami, S. & Oktay, K. (2013) Impairment of BRCA1-related DNA double-strand break repair leads to ovarian aging in mice and humans. *Science Translational Medicine*. **5**: 172ra21

Tiwari, V. K., Burger, L., Nikoletopoulou, V., Deogracias, R., Thakurela, S., Wirbelauer, C., Kaut, J., Terranova, R., Hoerner, L., Mielke, C., Boege, F., Murr, R., Peters, A. H., Barde, Y. A. & Schübeler, D. (2012) Target genes of Topoisomerase IIβ regulate neuronal survival and are defined by their chromatin state. *Proceedings of the National Academy of Sciences of the United States of America.* **109**: E934-E943

Tong, Z. B., Hogberg, H., Kuo, D., Sakamuru, S., Xia, M., Smirnova, L., Hartung, T. & Gerhold, D. (2017) Characterization of three human cell line models for high-throughput neuronal cytotoxicity screening. *Journal of Applied Toxicology.* **37**: 167-180

Tonoki, A. & Davis, R. L. (2015) Aging impairs protein-synthesis-dependent long-term memory in Drosophila. *The Journal of Neuroscience*. **35**: 1173-1180

Toyama, B. H., Savas, J. N., Park, S. K., Harris, M. S., Ingolia, N. T., Yates, J. R. & Hetzer, M. W. (2013) Identification of long-lived proteins reveals exceptional stability of essential cellular structures. *Cell*. **154**: 971-982

Tsakiri, E. N., Iliaki, K. K., Höhn, A., Grimm, S., Papassideri, I. S., Grune, T. & Trougakos, I. P. (2013) Diet-derived advanced glycation end products or lipofuscin disrupts proteostasis and reduces life span in Drosophila melanogaster. *Free Radical Biology and Medicine*. **65**: 1155-1163

Tsutsui, K., Okada, S., Watanabe, M., Shohmori, T., Seki, S. & Inoue, Y. (1993) Molecular cloning of partial cDNAs for rat DNA topoisomerase II isoforms and their differential expression in brain development. *Journal of Biological Chemistry*. **268**: 19076-19083

Tsutsui, K., Tsutsui, K., Sano, K., Kikuchi, A. & Tokunaga, A. (2000) Involvement of DNA Topoisomerase II beta in Neuronal Differentiation. *The Journal of Biological Chemistry*. **276**: 5769-78

Turley, H., Comley, M., Houlbrook, S., Nozaki, N., Kikuchi, A., Hickson, I. D., Gatter, K. & Harris, A. L. (1997) The distribution and expression of the two isoforms of DNA topoisomerase II in normal and neoplastic human tissues. *British Journal of Cancer*. **75**: 1340-1346

Ungewitter, E. & Scrable, H. (2009) Antagonistic pleiotropy and p53. *Mechanisms of Ageing and Development*, **130**: 10-17

Uusküla-Reimand, L., Hou, H., Samavarchi-Tehrani, P., Rudan, M. V., Liang, M., Medina-Rivera, A., Mohammed, H., Schmidt, D., Schwalie, P., Young, E. J., Reimand, J., Hadjur, S., Gingras, A. C. & Wilson, M. D. (2016). Topoisomerase II beta interacts with cohesin and CTCF at topological domain borders. *Genome Biology*. **17**: 182

Vandesompele, J., De Preter, K., Pattyn, F., Poppe, B., Van Roy, N., De Paepe, A. & Speleman, F. (2002) Accurate normalization of real-time quantitative RT-PCR data by geometric averaging of multiple internal control genes. *Genome Biology*. **3:** RESEARCH0034

Vanhooren, V. & Libert, C. (2013). The mouse as a model organism in aging research: Usefulness, pitfalls and possibilities. *Ageing Research Reviews*. **12**: 8-21

Vávrová, A. & Šimůnek, T. (2012) DNA topoisomerase IIβ: A player in regulation of gene expression and cell differentiation. *The International Journal of Biochemistry & Cell Biology*. **44**: 834-837

Vaidya, A., Mao, Z., Tian, X., Spencer, B., Seluanov, A. & Gorbunova, V. (2014) Knock-in reporter mice demonstrate that DNA repair by non-homologous end joining declines with age. *PLoS Genetics*. **10**: e1004511

Venkataraman, K., Khurana, S. & Tai, T. C. (2013) Oxidative stress in aging-matters of the heart and mind. *International Journal of Molecular Sciences*. **14**: 17897-17925

Verbitsky, M., Yonan, A. L., Malleret, G., Kandel, E. R., Gilliam, T. C. & Pavlidis, P. (2004) Altered hippocampal transcript profile accompanies an age-related spatial memory deficit in mice. *Learning & Memory*. **11:** 253-260

Vermeij, W. P., Dollé, M. E., Reiling, E., Jaarsma, D., Payan-Gomez, C., Bombardieri, C. R., Wu, H., Roks, A. J., Botter, S. M., van der Eerden, B. C., Youssef, S. A., Kuiper, R. V., Nagarajah, B., van Oostrom, C. T., Brandt, R. M., Barnhoorn, S., Imholz, S., Pennings, J. L., de Bruin, A., Gyenis, Á., Pothof, J., Vijg, J., van Steeg, H. & Hoeijmakers, J. H. (2016) Restricted diet delays accelerated ageing and genomic stress in DNA-repair-deficient mice. *Nature*. **537**: 427-431

Vistoli, G., de Maddis, D., Cipak, A., Zarkovic, N., Carini, M. & Aldini G. (2013) Advanced glycoxidation and lipoxidation end products (AGEs and ALEs): an overview of their mechanisms of formation. *Free Radical Research*. **47**: 3-27

Vizioli, M. G., Liu, T., Miller, K. N., Robertson, N. A., Gilroy, K., Lagnado, A. B., Perez-Garcia, A., Kiourtis, C., Dasgupta, N., Lei, X., Kruger, P. J., Nixon, C., Clark, W., Jurk, D., Bird, T. G., Passos, J. F., Berger, S. L., Dou, Z. & Adams, P. D (2020) Mitochondria-to-nucleus retrograde signaling drives formation of cytoplasmic chromatin and inflammation in senescence. *Genes and Development*. **34**: 428-445

von Trotha, J. W., Egger, B. & Brand, A. H. (2009) Cell proliferation in the *Drosophila* adult brain revealed by clonal analysis and bromodeoxyuridine labelling. *Neural Development.* **4:** 9

Votyakova, T. V. & Reynolds, I. J. (2001) DeltaPsi(m)-Dependent and -Independent Production of Reactive Oxygen Species by Rat Brain Mitochondria. *Journal of Neurochemistry*. **79**: 266-77

Vyjayanti, V. N. & Rao, K. S. (2006) DNA double strand break repair in brain: reduced NHEJ activity in aging rat neurons. *Neuroscience Letters.* **393**: 18-22

Walther, D. M. & Mann, M. (2011) Accurate quantification of more than 4000 mouse tissue proteins reveals minimal proteome changes during aging. *Molecular & Cellular Proteomics.* **10**: M110.004523

Walther, D. M., Kasturi, P., Zheng, M., Pinkert, S., Vecchi, G., Ciryam, P., Morimoto, R. I., Dobson, C. M., Vendruscolo, M., Mann, M. & Hartl, F. U. (2015) Widespread Proteome Remodeling and Aggregation in Aging C. elegans. *Cell*. **161**: 919-932

Wang, J. C. (1971) Interaction between DNA and an Escherichia coli protein ω. *Journal of Molecular Biology.* **55**: 523-533

Wang, H., Liu, H. & Liu, R, M. (2003) Gender difference in glutathione metabolism during aging in mice. *Experimental Gerontology.* **38**: 507-17

Wang, X., Desai, K., Juurlink, B. H. J., de Champlain, J. & Wu, L. (2006) Gender-related differences in advanced glycation endproducts, oxidative stress markers and nitric oxide synthases in rats. *Kidney International.* **69**: 281-287

Watanabe, M., Tsutsui, K., Tsutsui, K. & Inoue, Y. (1994) Differential expressions of the topoisomerase IIα and IIβ mRNAs in developing rat brain. *Neuroscience Research.* **19**: 51-57

Welty, S., Teng, Y., Liang, Z., Zhao, W., Sanders, L. H., Greenamyre, J. T., Rubio, M. E., Thathiah, A., Kodali, R., Wetzel, R., Levine, A. S. & Lan, L. (2018) RAD52 is required for RNA-templated recombination repair in post-mitotic neurons. *The Journal of Biological Chemistry*. **293**: 1353-1362

Wendorff, T. J., Schmidt, B. H., Heslop, P., Austin, C. A. & Berger, J. M. (2012). The structure of DNA-bound human topoisomerase II alpha: conformational mechanisms for coordinating inter-subunit interactions with DNA cleavage. *Journal of Molecular Biology*. **424**: 109-124

Whalen, A. M., McConnell, M. & Fisher, P. A. (1991) Developmental regulation of Drosophila DNA topoisomerase II. *Journal of Cell Biology*. **112**: 203-213

Williams, G.C. (1957) Pleiotropy, Natural Selection, and the Evolution of Senescence. *Evolution*. **11**: 398-411

Williams, K., Irwin, D. A., Jones, D. G. & Murphy, K. M. (2010) Dramatic Loss of Ube3A Expression during Aging of the Mammalian Cortex. *Frontiers in Aging Neuroscience*. **2**: 18

Witz, G. & Stasiak, A. (2010) DNA supercoiling and its role in DNA decatenation and unknotting. *Nucleic Acids Research.* **38**: 2119-2133

Woessner, R. D., Mattern, M. R., Mirabelli, C. K., Johnson, R. K. & Drake, F. H. (1991) Proliferation- and cell cycle-dependent differences in expression of the 170 kilodalton and 180 kilodalton forms of topoisomerase II in NIH-3T3 cells. *Cell Growth and Differentiation.* **2:** 209-214

Wu, C.-C., Li, T.-K., Farh, L., Lin, L.-Y., Lin, T.-S., Yu, Y.-J., Yen, T-J., Chiang, C-W. & Chan, N.-L. (2011) Structural Basis of Type II Topoisomerase Inhibition by the Anticancer Drug Etoposide. *Science.* **333**: 459-462

Wyckoff, E. & Hsieh, T. S. (1988) Functional expression of a *Drosophila* gene in yeast: genetic complementation of DNA topoisomerase II. *Proceedings of the National Academy of Sciences of the United States of America*. **85**: 6272-6276

Wyss-Coray, T. (2016). Ageing, neurodegeneration and brain rejuvenation. *Nature*. **539:** 180-186

Xicoy, H., Wieringa, B. & Martens, G. J. (2017) The SH-SY5Y cell line in Parkinson's disease research: a systematic review. *Molecular Neurodegeneration.* **12**: 10

Xie, H., Hu, L. & Li, G. (2010) SH-SY5Y human neuroblastoma cell line: in vitro cell model of dopaminergic neurons in Parkinson's disease. *Chinese Medical Journal*. **123**: 1086-1092

Xiong, Y. & Yu, J. (2018) Modeling Parkinson's Disease in Drosophila: What Have We Learned for Dominant Traits? *Frontiers in Neurology*. **9**: 228

Yamada, S., Kumazawa, S., Ishii, T., Nakayama, T., Itakura, K., Shibata, N., Kobayashi, M., Sakai, K., Osawa, T. & Uchida, K. (2001) Immunochemical detection of a lipofuscin-like fluorophore derived from malondialdehyde and lysine. *Journal of Lipid Research.* **42**:1187-1196

Yamakoshi, H., Dodo, K., Okada, M., Ando, J., Palonpon, A., Fujita, K., Kawata, S. & Sodeoka, M. (2011) Imaging of EdU, an Alkyne-Tagged Cell Proliferation Probe, by Raman Microscopy. *Journal of the American Chemical Society*. **133**: 6102-6105

Yang, J. L., Chen, W. Y., Mukda, S., Yang, Y. R., Sun, S. F. & Chen, S. D. (2019) Oxidative DNA damage is concurrently repaired by base excision repair (BER) and apyrimidinic endonuclease 1 (APE1)-initiated nonhomologous end joining (NHEJ) in cortical neurons. *Neuropathology and Applied Neurobiology*. **00**: 1-16

Yuan, R., Tsaih, S. W., Petkova, S. B., Marin de Evsikova, C., Xing, S., Marion, M. A., Bogue, M. A., Mills, K. D., Peters, L. L., Bult, C. J., Rosen, C. J., Sundberg, J. P., Harrison, D. E., Churchill, G. A. & Paigen, B. (2009) Aging in inbred strains of mice: study design and interim report on median lifespans and circulating IGF1 levels. *Aging Cell*. **8**: 277-287

Yuan, J., Adamski, R. & Chen, J. (2010) Focus on histone variant H2AX: to be or not to be. *FEBS letters*. **584**: 3717-3724

Zandvliet, D. W. J., Hanby, A. M., Austin, C. A., Marsh, K. L., Clark, I. B. N., Wright, N. A. & Poulsom, R. (1996) Analysis of foetal expression sites of human type II DNA topoisomerase α and β mRNAs by in situ hybridisation. *Biochimica et Biophysica Acta.* **1307**: 239-247

Zhang,Y. & Gordon, G. B. A. (2004) Strategy for cancer prevention: stimulation of the Nrf2-ARE signaling pathway. *Molecular Cancer Therapeutics*. **3**: 885-893

Zhang, H., Zhang, Y.-W., Yasukawa, T., Dalla Rosa, I., Khiati, S. & Pommier, Y. (2014) Increased negative supercoiling of mtDNA in TOP1mt knockout mice and presence of topoisomerases IIα and IIβ in vertebrate mitochondria. *Nucleic Acids Research.* **42**: 7259-7267

Zhang, C., Chen, M., Zhou, N. & Qi, Y. (2020) Metformin Prevents H_2O_2-Induced Senescence in Human Lens Epithelial B3 Cells. *Medical Science Monitor Basic Research.* **26**: e923391

Zheng, Z., Lauritzen, J. S., Perlman, E., Robinson, C. G., Nichols, M., Milkie, D., Torrens, O., Price, J., Fisher, C. B., Sharifi, N., Calle-Schuler, S. A., Kmecova, L., Ali, I. J., Karsh, B., Trautman, E. T., Bogovic, J. A., Hanslovsky, P., Jefferis, G., Kazhdan, M., Khairy, K., Saalfeld, S., Fetter, R. D. & Bock, D. D. (2018) A Complete Electron Microscopy Volume of the Brain of Adult Drosophila melanogaster. *Cell*. **174**: 730-743

Zhong, X., Zeng, M., Bian, H., Zhong, C. & Xiao, F. (2017) An evaluation of the protective role of vitamin C in reactive oxygen species-induced hepatotoxicity due to

hexavalent chromium in vitro and in vivo. *Journal of Occupational Medicine and Toxicology*. **12**: 15

Zhou, X. F. & Rush, R. A. (1996) Functional Roles of Neurotrophin 3 in the Developing and Mature Sympathetic Nervous System. *Molecular Neurobiology*. **13**: 185-97

Zini, N., Martelli, A. M., Sabatelli, P., Santi, S., Negri, C., Astaldi Ricotti, G. C. & Maraldi, N. M. (1992) The 180-kDa isoform of topoisomerase II is localized in the nucleolus and belongs to the structural elements of the nucleolar remnant. *Experimental Cell Research*. **200**: 460-466

Appendix A

A)

$$\chi^2 = \Sigma \frac{(\Sigma O_{jt} - \Sigma E_{jt})^2}{\Sigma E_{jt}}$$

B)

Day	No. at risk group 1	No. at risk group 2	Total No. at risk	No. deaths group 1	No. deaths group 2	Total No. deaths	Expected No. deaths group 1	Expected No. deaths group 2
0	300	300	600	0	0	0	0	0
3	296	296	592	4	4	8	2	2
6	296	296	592	0	0	0	0	0
9	289	296	585	7	0	7	3.4581	0.506003
12	288	295	583	1	1	2	0.494	0.505155

Expected number of deaths = No. at risk x (No. deaths/Total No. at risk)

Final calculation;

$$X^2 = \frac{(\text{Sum of No. deaths group 1} - \text{expected No. deaths group 1})^2}{\text{Expected No. deaths group 1}} + \frac{(\text{Sum of No. deaths group 2} - \text{expected No. deaths group 2})^2}{\text{Expected No. deaths group 2}}$$

Figure A.1 Calculating statistical significance using the log-rank test.

(A) Equation used to perform a log-rank test as shown in Figure 3.2 to determine statistical significance of *Drosophila* longevity. ΣO_{jt} represents the sum of the observed number of events in the j^{th} group over time and ΣE_{jt} represents the sum of the expected number of events in the jth group over time. (B) Practical example of how log-rank tests were calculated in this study. The value given after the final calculation is approximately distributed as chi-square with 1 degree of freedom. Thus, the critical value for the test can be found in the table of critical values of the X^2 distribution.

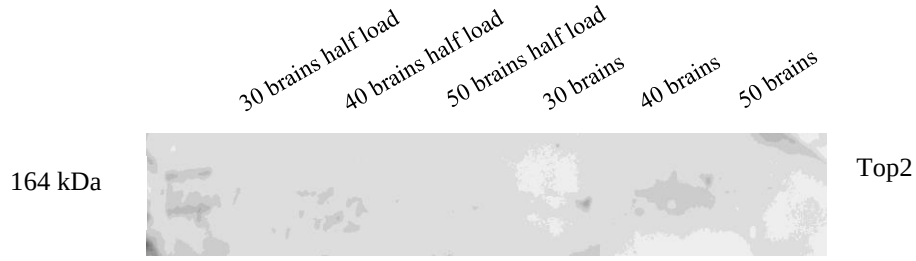

Figure A.2 Optimisation of *Drosophila* brain protein extraction and western blot analysis of Top2.

Drosophila were selected (Mixed ages), processed and protein was extracted as described in 2.2.1.9 from 30 (27.85 µg total protein load), 40 (34.47 µg total protein load) and 50 (41.63 µg total protein load) brains, respectively. Protein samples were loaded onto a 7.5% SDS gel and western blotting was performed.

Primer efficiency = $(10^{(-1/\text{slope})}-1) \times 100$

Example: Top2 primer efficiency from Figure 3.10

$= (10^{(-1/-3.2473)}-1) \times 100$

Efficiency = 103.2%

Figure A.3 Calculating the efficiency of primers.

Primer reaction efficiencies were calculated based on equations described by Rutledge and Côté (2003).

A)

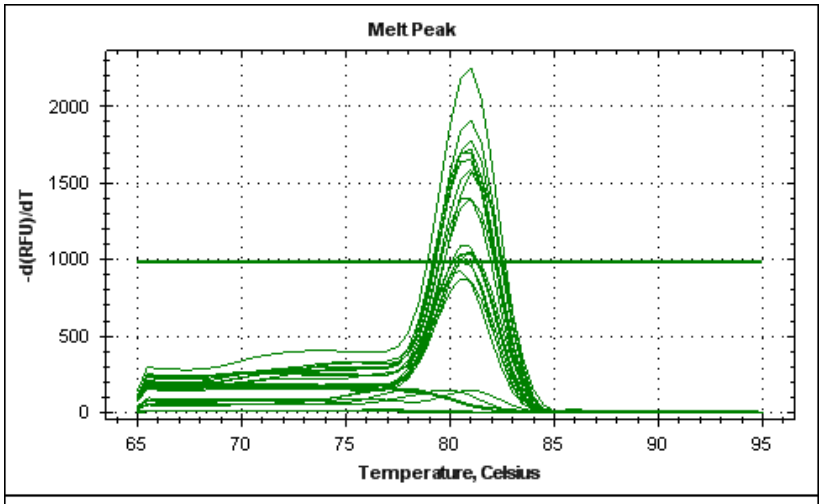

B)

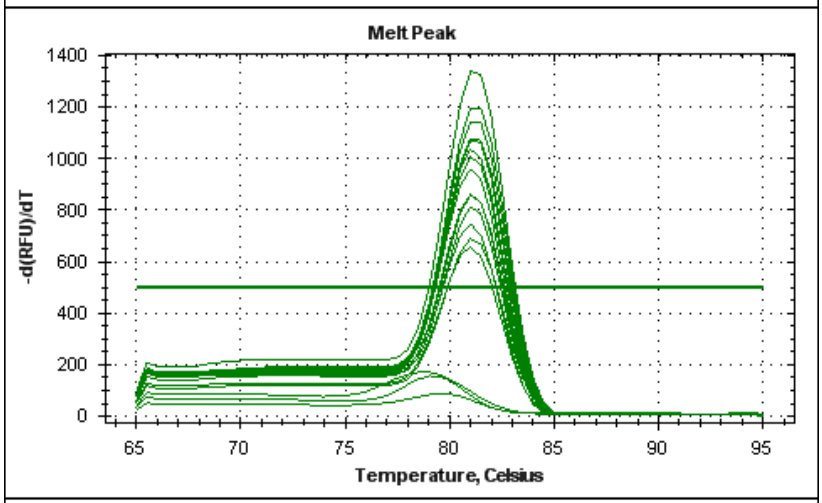

C)

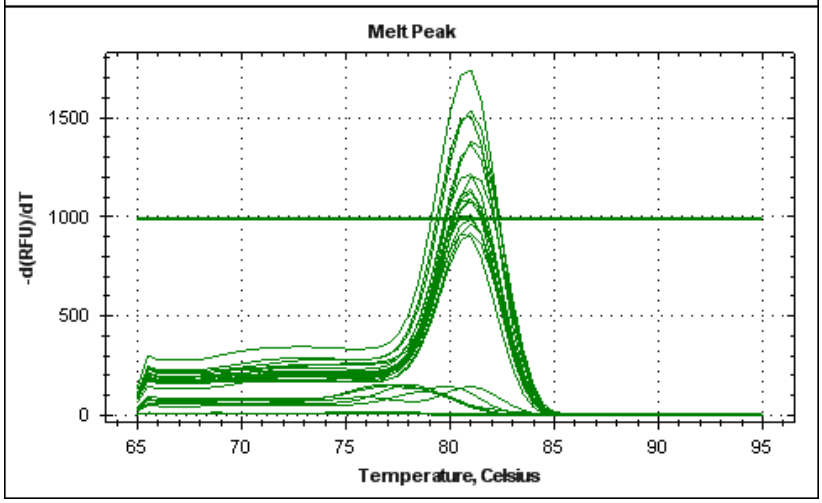

Figure A.4 Representative melt curves from RT-qPCR of primers used in *Drosophila* experiments.

Melt curves of primer optimisation experiments. (A) Melt curve for Top2. (B) Melt curve for Cyp1. (C) Melt curve for eIF-1A.

A)

$$Converted\ primer\ efficiency = \left(\frac{Primer\ efficiency\ (\%)}{100}\right) + 1$$

B)

$$RQ = E^{\Delta Ct}$$

C)

$$Relative\ gene\ expression = \frac{RQ_{GOI}}{Geomean[RQ_{REFs}]}$$

Figure A.5 Analysing qPCR results with two reference genes.

Relative gene expression using two reference genes was calculated using these equations. (A) Converted primer efficiencies were calculated by using the equation with previously calculated primer efficiencies as described in Figure A. ΔCt was calculated by subtracting the sample Ct from the control average Ct. (B) RQ was calculated. E in the equation is the base of exponential amplification (the converted primer efficiency of the reaction). (C) Relative gene expression was calculated where GOI is the gene of interest, REFs are the reference genes and GEOMEAN is a Microsoft Excel function.

	Cyp1 Males	Cyp1 Female	eIF-1A Male	eIF-1A Female
Count	9	9	9	9
Mean	21.7644444	21.8866667	23.411481	23.5951852
SD	0.76397717	0.89860849	1.0517632	1.24174621
CV1	0.03510208	0.04105735	0.0449251	0.0526271
CV2	3.51020752	4.10573481	4.4925103	5.26271015

$$\text{Coefficient of variance} = \frac{\text{Standard deviation}}{\text{Mean}} \times 100$$

Figure A.6 Example calculation of the coefficient of variance of qPCR primers using Ct data.

The coefficient of variance (CV) is calculated using the mean Ct value of the primer and the standard deviation (SD) of the Ct values. The higher the CV value, the greater the level of dispersion around the mean.

Appendix B

Table B.1 p values from Figure 4.1B

H_2O_2 concentration (mM)	Time point (hours)	p value (Test vs Control)
0.1	24	0.222
0.1	48	0.206
0.1	72	0.073
0.5	24	0.014*
0.5	48	0.154
0.5	72	0.0002**
1.0	24	0.018*
1.0	48	0.008**
1.0	72	0.0002**
2.0	24	0.0505
2.0	48	<0.0001***
2.0	72	0.0016**

Table B.2 p values from Figure 4.2B

H_2O_2 concentration (µM)	Time point (hours)	p value (Test vs Control)
0.1	24	0.314
0.1	48	<0.0001***
0.5	24	0.054
0.5	48	<0.0001***
1.0	24	0.033*
1.0	48	0.005**
5.0	24	<0.0001***
5.0	48	0.003**
10.0	24	0.0014**
10.0	48	0.0003***

Appendix C

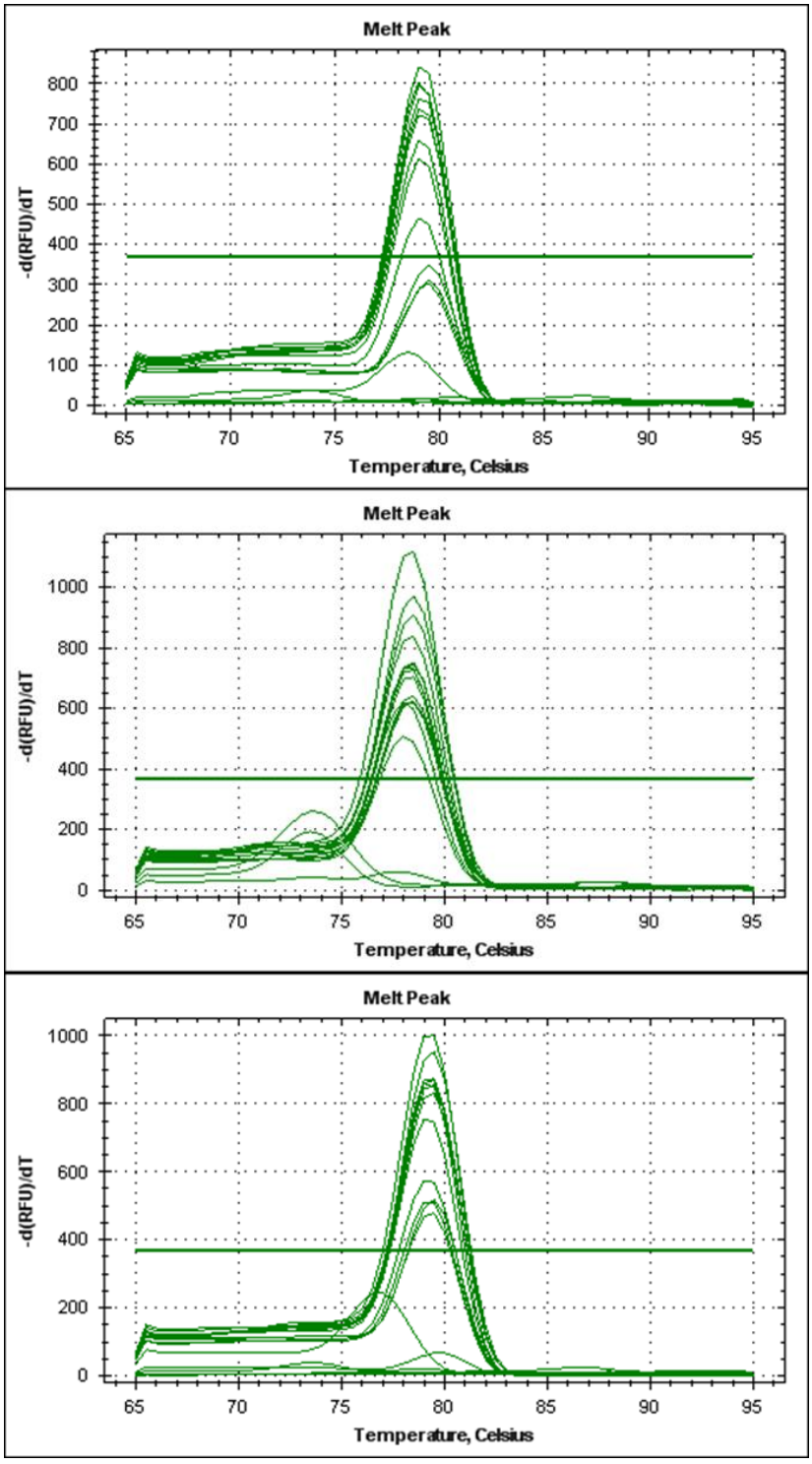

Figure C.1 Representative melt curves from RT-qPCR of primers used in CAD experiments.

Melt curves of primer optimisation experiments. (A) Melt curve for Top2B. (B) Melt curve for β-actin. (C) Melt curve for GAPDH.

ΔCte (experimental) = Average Ct (gene of interest) – Average Ct (reference gene)

ΔCtc (control) = Average Ct (gene of interest) – Average Ct (reference gene)

ΔΔCt = ΔCte – ΔCtc

Relative fold change = $2^{-\Delta\Delta Ct}$

Figure C.2 Analysing qPCR results with one reference gene

Calculations used to determine relative changes in gene expression using the ΔCt method as described by (Livak & Schmittgen, 2001)

Table C.1 p values from Figure 6.1

Time point (week)	**p value (week *n* vs week 1)**
2	0.161
3	0.022*
4	0.0002***
5	0.0004***
6	<0.0001***

Appendix D

SPRINGER NATURE LICENSE
TERMS AND CONDITIONS

Apr 15, 2020

This Agreement between Mr. Callum Bainbridge ("You") and Springer Nature ("Springer Nature") consists of your license details and the terms and conditions provided by Springer Nature and Copyright Clearance Center.

License Number	4810151119973
License date	Apr 15, 2020
Licensed Content Publisher	Springer Nature
Licensed Content Publication	Cellular and Molecular Life Sciences
Licensed Content Title	Molecular mechanisms of topoisomerase 2 DNA–protein crosslink resolution
Licensed Content Author	Amanda A. Riccio *et al*
Licensed Content Date	Nov 15, 2019
Type of Use	Thesis/Dissertation
Requestor type	academic/university or research institute
Format	print and electronic
Portion	figures/tables/illustrations
Number of figures/tables/illustrations	1
Will you be translating?	no

Circulation/distribution	1 - 29
Author of this Springer Nature content	no
Title	Investigating the Expression of Topoisomerase II Beta in Aged Neurons: development of a murine cell line and *Drosophila* model
Institution name	Northumbria University
Expected presentation date	Sep 2020
Portions	Figure 1. a
Requestor Location	Mr. Callum Bainbridge 59 Ouseburn wharf Newcastle Upon Tyne, NE6 1BY United Kingdom Attn: Mr. Callum Bainbridge
Total	0.00 GBP

Structure of an 'open' clamp type II topoisomerase-DNA complex provides a mechanism for DNA capture and transport

Publisher:

Oxford University Press

Date:

2013-08-21

SPRINGER NATURE LICENSE
TERMS AND CONDITIONS

Apr 15, 2020

This Agreement between Mr. Callum Bainbridge ("You") and Springer Nature ("Springer Nature") consists of your license details and the terms and conditions provided by Springer Nature and Copyright Clearance Center.

License Number	4810170306812
License date	Apr 15, 2020
Licensed Content Publisher	Springer Nature
Licensed Content Publication	Nature Reviews Cancer
Licensed Content Title	DNA topoisomerase II and its growing repertoire of biological functions
Licensed Content Author	John L. Nitiss
Licensed Content Date	Apr 20, 2009
Type of Use	Thesis/Dissertation
Requestor type	academic/university or research institute
Format	print and electronic
Portion	figures/tables/illustrations
Number of figures/tables/illustrations	1
High-res required	no
Will you be translating?	no

Circulation/distribution	1 - 29
Author of this Springer Nature content	no
Title	Investigating the Expression of Topoisomerase II Beta in Aged Neurons: development of a murine cell line and *Drosophila* model
Institution name	Northumbria University
Expected presentation date	Sep 2020
Portions	figure. 1
Requestor Location	Mr. Callum Bainbridge 59 Ouseburn wharf Newcastle Upon Tyne, NE6 1BY United Kingdom Attn: Mr. Callum Bainbridge
Total	0.00 GBP

SPRINGER NATURE LICENSE
TERMS AND CONDITIONS

Apr 29, 2020

This Agreement between Mr. Callum Bainbridge ("You") and Springer Nature ("Springer Nature") consists of your license details and the terms and conditions provided by Springer Nature and Copyright Clearance Center.

License Number	4818131290867
License date	Apr 29, 2020
Licensed Content Publisher	Springer Nature
Licensed Content Publication	Biophysical Reviews
Licensed Content Title	DNA supercoiling during transcription
Licensed Content Author	Jie Ma *et al*
Licensed Content Date	Jul 13, 2016
Type of Use	Thesis/Dissertation
Requestor type	academic/university or research institute
Format	print and electronic
Portion	figures/tables/illustrations
Number of figures/tables/illustrations	1
Will you be translating?	no
Circulation/distribution	1 - 29

Author of this Springer Nature content	no
Title	Investigating the Expression of Topoisomerase II Beta in Aged Neurons: development of a murine cell line and *Drosophila* model
Institution name	Northumbria University
Expected presentation date	Sep 2020
Order reference number	1
Portions	figure 1
Requestor Location	Mr. Callum Bainbridge 59 Ouseburn wharf Newcastle Upon Tyne, NE6 1BY United Kingdom Attn: Mr. Callum Bainbridge
Total	0.00 GBP

Drosophila brain image

A Complete Electron Microscopy Volume of the Brain of Adult *Drosophila melanogaster*

Publisher:

Elsevier

Date:

26 July 2018

Appendix E

Project Amendment Form

Project Title: Investigating the Expression of Topoisomerase II Beta in Aged Neurons: development of a murine cell line and *Drosophila* model	**Date original ethical approval received**: 14/12/2016
Principal Investigator: Kay Padget/Callum Bainbridge	Project ref: BMS53UNNCBKP2016
Date: 23/5/17	

Description of Amendment/Change:

To allow Callum Bainbridge to work on brain material obtained by Dr R. N. Ranson under the conditions below.

Ethical clearance is required to allow experimental work, including immunohistochemistry, to be carried out on brain tissue obtained from mice. The ethical issues that are associated with the experimentation of brain sections obtained from mice have been carefully considered for this project. Animal welfare is the predominant issue with this project and minimising animal suffering in order to acquire tissue samples is the main priority. Dr R. N. Ranson acquired the tissue samples using accepted techniques licensed under the animals (scientific procedures) act 1986. Prior to the procedures carried out by Dr Ranson, animals received terminal anaesthesia and animals were monitored for the total inhibition of reflex activity including pain reflexes.

C57BL/6 male mice (Obtained from Harlan, UK and housed at the Open University), were maintained under stable humidity (50% ± 10%) and temperature (19–23 °C) under a 12 hour light/dark cycle and fed RM1 (E) 801002 (Special Diet Services) ad libitum. Mice aged up to 30 months were euthanised using an overdose of sodium pentobarbitone prior to being exsanguinated with 50-100mls of heparinised saline and trans-cardially perfused with 200mls of fixative consisting of 4% paraformaldehyde in

0.1M PBS. Brains were dissected and removed from the skull and fixed for a further 2-4 hours on an orbital shaker at room temperature. Brains were stored in PBS at 4°C until sectioning took place. All procedures were performed under the Animals (Scientific Procedures) Act 1986.

Callum will work in conjunction with Dr Ranson under ethics licensing **BMS37UNNRNR2015**

- A programme of research to investigate the effects of ageing on Nervous and Glial cells mediating control of the bladder and bowel.

Callum has previously worked with this material on a student project with Dr Ranson and is fully aware of the ethical implications and procedures associated with working on mammalian tissues.

Reasons for Amendment/Change:

Ethical clearance for using a mouse brain model will allow immunohistochemical techniques to be used to semi-quantify levels of Top2B. Current ethical clearance only allows experimentation on drosophila, which contains a single isoform of Topoisomerase 2 (Top2), and the cell line SH-SY5Y. A mouse model will allow more direct comparisons to be made with the SH-SY5Y cell line as it also possesses the Top2B isoform.

Anticipated Implications:

None. This type of work has ethical clearance and all mammalian tissues have been obtained subject to Northumbria Ethical procedures and home office licensing.

Acceptance/Rejection: approved	Signature: Renli Ma

Date: 5 June 2017

Follow-up action passed to:

Please ensure that all workers undertaking this project, including staff, have read and are aware of the ethics forms and processes associated with this project.